

ISSN 2686-7575 (Online)

ТОНКИЕ ХИМИЧЕСКИЕ ТЕХНОЛОГИИ

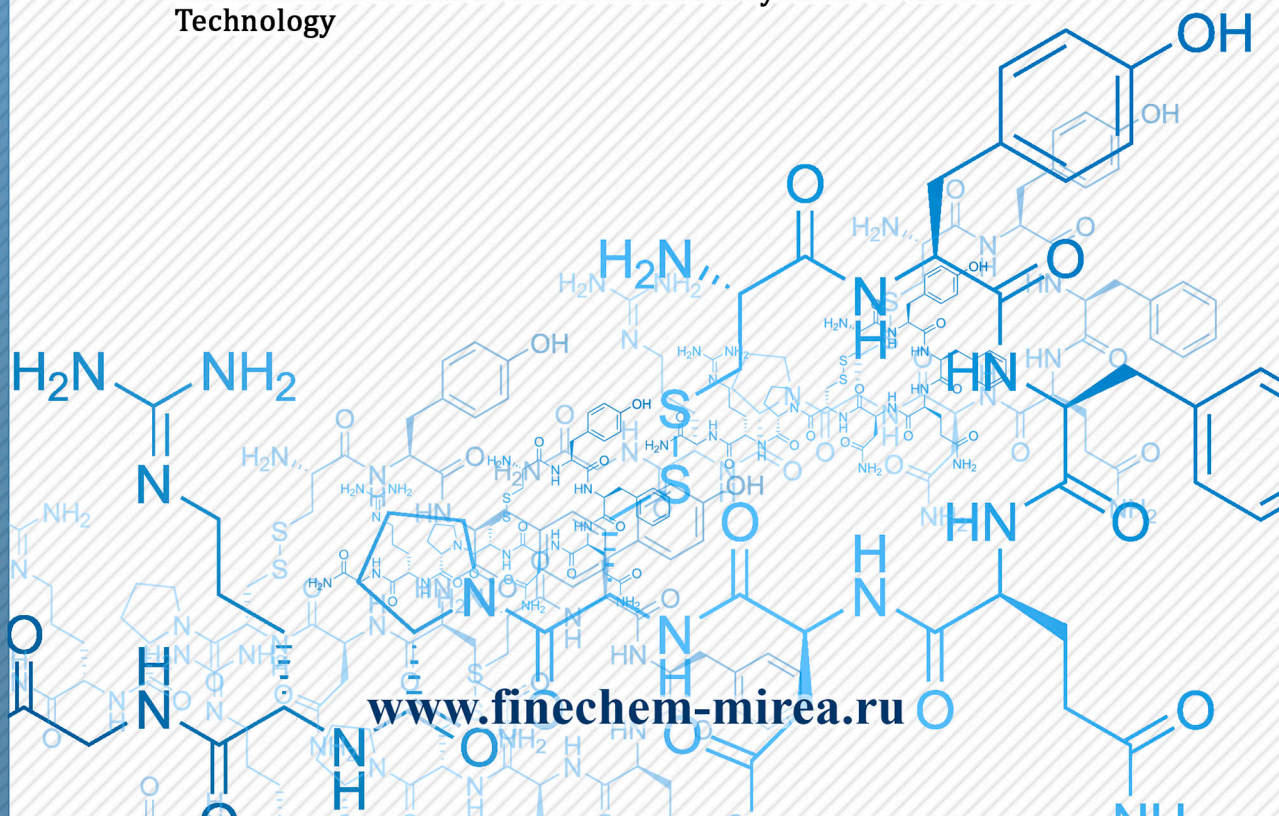
Fine Chemical Technologies

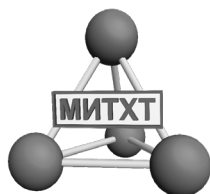
- | Theoretical Bases of Chemical Technology
- | Chemistry and Technology of Organic Substances
- | Chemistry and Technology of Medicinal Compounds and Biologically Active Substances
- | Synthesis and Processing of Polymers and Polymeric Composites
- | Chemistry and Technology of Inorganic Materials
- | Analytical Methods in Chemistry and Chemical Technology
- | Mathematical Methods and Information Systems in Chemical Technology

16(1)

2021

www.finechem-mirea.ru





ISSN 2686-7575 (Online)

ТОНКИЕ ХИМИЧЕСКИЕ ТЕХНОЛОГИИ

Fine
Chemical
Technologies

- | Theoretical Bases of Chemical Technology
- | Chemistry and Technology of Organic Substances
- | Chemistry and Technology of Medicinal Compounds and Biologically Active Substances
- | Synthesis and Processing of Polymers and Polymeric Composites
- | Chemistry and Technology of Inorganic Materials
- | Analytical Methods in Chemistry and Chemical Technology
- | Mathematical Methods and Information Systems in Chemical Technology

Tonkie Khimicheskie Tekhnologii =
Fine Chemical Technologies
Vol. 16, No. 1, 2021

Тонкие химические технологии =
Fine Chemical Technologies
Том 16, № 1, 2021

<https://doi.org/10.32362/2410-6593-2021-16-1>
www.finechem-mirea.ru

**Tonkie Khimicheskie Tekhnologii =
Fine Chemical Technologies
2021, vol. 16, no. 1**

**Тонкие химические технологии =
Fine Chemical Technologies
2021, том 16, № 1**

The peer-reviewed scientific and technical journal *Fine Chemical Technologies* highlights the modern achievements of fundamental and applied research in the field of fine chemical technologies, including theoretical bases of chemical technology, chemistry and technology of medicinal compounds and biologically active substances, organic substances and inorganic materials, synthesis and processing of polymers and polymeric composites, analytical and mathematical methods and information systems in chemistry and chemical technology.

Научно-технический рецензируемый журнал «Тонкие химические технологии» освещает современные достижения фундаментальных и прикладных исследований в области тонких химических технологий, включая теоретические основы химической технологии, химию и технологию лекарственных препаратов и биологически активных соединений, органических веществ и неорганических материалов, синтез и переработку полимеров и композитов на их основе, аналитические и математические методы и информационные системы в химии и химической технологии.

Founder and Publisher

Federal State Budget
Educational Institution
of Higher Education

“MIREA – Russian Technological University”
78, Vernadskogo pr., Moscow, 119454, Russian Federation.

Publication frequency: bimonthly.

The journal was founded in 2006. The name was *Vestnik MITHT* until 2015 (ISSN 1819-1487).

The journal is included into the List of peer-reviewed science press of the State Commission for Academic Degrees and Titles of the Russian Federation.

The journal is indexed:

DOAJ, Chemical Abstracts, Science Index, RSCI,
Ulrich's International Periodicals Directory

Editor-in-Chief:

Alla K. Frolkova – Dr. Sci. (Eng.), Professor, MIREA – Russian Technological University, Moscow, Russian Federation. Scopus Author ID 35617659200, ResearcherID G-7001-2018, <http://orcid.org/0000-0002-9763-4717>, frolkova_a@mirea.ru

Deputy Editor-in-Chief:

Valery V. Fomichev – Dr. Sci. (Chem.), Professor, MIREA – Russian Technological University, Moscow, Russian Federation. Scopus Author ID 57196028937, <http://orcid.org/0000-0003-4840-0655>, fomichev@mirea.ru

Editorial staff:

Managing Editor Cand. Sci. (Eng.) Galina D. Seredina
Science editors Dr. Sci. (Chem.), Prof. Tatyana M. Buslaeva
Dr. Sci. (Chem.), Prof. Anatolii A. Ischenko
Dr. Sci. (Eng.), Prof. Valery F. Kornyushko
Dr. Sci. (Eng.), Prof. Anatolii V. Markov
Dr. Sci. (Chem.), Prof. Yuri P. Mirosnikov
Dr. Sci. (Chem.), Prof. Vladimir A. Tverskoy
Desktop publishing Larisa G. Semernya

86, Vernadskogo pr., Moscow, 119571, Russian Federation.
Phone: +7(495) 246-05-55 (#2-88)
E-mail: seredina@mirea.ru

Registration Certificate ПИ № ФС 77–74580, issued on December 14, 2018 by the Federal Service for Supervision of Communications, Information Technology, and Mass Media of Russia

The subscription index of *Pressa Rossii*: **36924**

Учредитель и издатель

федеральное государственное бюджетное
образовательное учреждение
высшего образования

«МИРЭА – Российский технологический университет»
119454, РФ, Москва, пр-кт Вернадского, д. 78.

Периодичность: один раз в два месяца.

Журнал основан в 2006 году. До 2015 года издавался под названием «Вестник МИТХТ» (ISSN 1819-1487).

Журнал входит в Перечень ведущих рецензируемых научных журналов ВАК РФ.

Индексируется:

DOAJ, Chemical Abstracts,
РИНЦ (Science Index), RSCI,
Ulrich's International Periodicals Directory

Главный редактор:

Фролкова Алла Константиновна – д.т.н., профессор, МИРЭА – Российский технологический университет, Москва, Российская Федерация. Scopus Author ID 35617659200, ResearcherID G-7001-2018, <http://orcid.org/0000-0002-9763-4717>, frolkova_a@mirea.ru

Заместитель главного редактора:

Фомичёв Валерий Вячеславович – д.х.н., профессор, МИРЭА – Российский технологический университет, Москва, Российская Федерация. Scopus Author ID 57196028937, <http://orcid.org/0000-0003-4840-0655>, fomichev@mirea.ru

Редакция:

Зав. редакцией к.т.н. Г.Д. Середина
Научные редакторы д.х.н., проф. Т.М. Буслеева
д.х.н., проф. А.А. Ищенко
д.т.н., проф. В.Ф. Корнюшко
д.т.н., проф. А.В. Марков
д.х.н., проф. Ю.П. Миросников
д.х.н., проф. В.А. Тверской
Компьютерная верстка Л.Г. Семерня

119571, Москва, пр. Вернадского, 86, оф. Л-119.
Тел.: +7(495) 246-05-55 (#2-88)
E-mail: seredina@mirea.ru

Свидетельство о регистрации СМИ: ПИ № ФС 77-74580 от 14.12.2018 г. выдано Федеральной службой по надзору в сфере связи, информационных технологий и массовых коммуникаций (Роскомнадзор)

Индекс по Объединенному каталогу «Пресса России»: **36924**

Editorial Board

Zinesh S. Abisheva – Academician at the National Academy of Sciences of Kazakhstan, Dr. Sci. (Eng.), Professor, Institute of Metallurgy and Ore Beneficiation, K.I. Satpaev Kazakh National Research Technical University, Almaty, Kazakhstan. Scopus Author ID 6601954283, ResearcherID O-8453-2017, <http://orcid.org/0000-0002-4506-0694>, abisheva_z@mail.ru.

Sergey P. Verevkin – Dr. Sci. (Eng.), Professor, University of Rostock, Rostock, Germany. Scopus Author ID 7006607848, ResearcherID G-3243-2011, <https://orcid.org/0000-0002-0957-5594>, Sergey.verevkin@uni-rostock.de.

Konstantin Yu. Zhizhin – Corresponding Member of the Russian Academy of Sciences (RAS), Dr. Sci. (Chem.), Professor, N.S. Kurnakov Institute of General and Inorganic Chemistry of the RAS, Moscow, Russian Federation. Scopus Author ID 6701495620, ResearcherID C-5681-2013, <http://orcid.org/0000-0002-4475-124X>, kyuzhizhin@igic.ras.ru.

Igor V. Ivanov – Dr. Sci. (Chem.), Professor, MIREA – Russian Technological University, Moscow, Russian Federation. Scopus Author ID 34770109800, ResearcherID I-5606-2016, <http://orcid.org/0000-0003-0543-2067>, ivanov_i@mirea.ru.

Carlos A. Cardona – PhD (Eng.), Professor, National University of Columbia, Manizales, Colombia. Scopus Author ID 7004278560, <http://orcid.org/0000-0002-0237-2313>, ccardonaal@unal.edu.co.

Oskar I. Koifman – Corresponding Member of the RAS, Dr. Sci. (Chem.), Professor, President of the Ivanovo State University of Chemistry and Technology, Ivanovo, Russian Federation. Scopus Author ID 6602070468, ResearcherID R-1020-2016, <http://orcid.org/0000-0002-1764-0819>, president@isuct.ru.

Elvira T. Krut'ko – Dr. Sci. (Eng.), Professor, Belarusian State Technological University, Minsk, Belarus. Scopus Author ID 6602297257, ela_krutko@mail.ru.

Anatolii I. Miroshnikov – Academician at the RAS, Dr. Sci. (Chem.), Professor, M.M. Shemyakin and Yu.A. Ovchinnikov Institute of Bioorganic Chemistry of the RAS, Member of the Presidium of the RAS, Chairman of the Presidium of the RAS Pushchino Research Center, Moscow, Russian Federation. Scopus Author ID 7006592304, ResearcherID G-5017-2017, aiv@ibch.ru.

Aziz M. Muzaфарov – Academician at the RAS, Dr. Sci. (Chem.), Professor, A.N. Nesmeyanov Institute of Organoelement Compounds of the RAS, Moscow, Russian Federation. Scopus Author ID 7004472780, ResearcherID G-1644-2011, <https://orcid.org/0000-0002-3050-3253>, aziz@ineos.ac.ru.

Редакционная коллегия

Абишева Зинеш Садыровна – академик Национальной Академии Наук Республики Казахстан, д.т.н., профессор, Институт металлургии и обогащения, Казахский национальный технический университет имени К. И. Сатпаева, Алматы, Казахстан. Scopus Author ID 6601954283, ResearcherID O-8453-2017, <http://orcid.org/0000-0002-4506-0694>, abisheva_z@mail.ru.

Верёвкин Сергей Петрович – д.т.н., профессор Университета г. Росток, Росток, Германия. Scopus Author ID 7006607848, ResearcherID G-3243-2011, <https://orcid.org/0000-0002-0957-5594>, Sergey.verevkin@uni-rostock.de.

Жижин Константин Юрьевич – член-корр. Российской академии наук (РАН), д.х.н., профессор, Институт общей и неорганической химии им. Н.С. Курнакова РАН, Москва, Российская Федерация. Scopus Author ID 6701495620, ResearcherID C-5681-2013, <http://orcid.org/0000-0002-4475-124X>, kyuzhizhin@igic.ras.ru.

Иванов Игорь Владимирович – д.х.н., профессор, МИРЭА – Российский технологический университет, Москва, Российская Федерация. Scopus Author ID 34770109800, ResearcherID I-5606-2016, <http://orcid.org/0000-0003-0543-2067>, ivanov_i@mirea.ru.

Кардона Карлос Ариэль – PhD, профессор Национального университета Колумбии, Манизалес, Колумбия. Scopus Author ID 7004278560, <http://orcid.org/0000-0002-0237-2313>, ccardonaal@unal.edu.co.

Койфман Оскар Иосифович – член-корр. РАН, д.х.н., профессор, президент Ивановского государственного химико-технологического университета, Иваново, Российская Федерация. Scopus Author ID 6602070468, ResearcherID R-1020-2016, <http://orcid.org/0000-0002-1764-0819>, president@isuct.ru.

Крутько Эльвира Тихоновна – д.т.н., профессор Белорусского государственного технологического университета, Минск, Беларусь. Scopus Author ID 6602297257, ela_krutko@mail.ru.

Мирошников Анатолий Иванович – академик РАН, д.х.н., профессор, Институт биоорганической химии им. академиков М.М. Шемакина и Ю.А. Овчинникова РАН, член Президиума РАН, председатель Президиума Пушинского научного центра РАН, Москва, Российская Федерация. Scopus Author ID 7006592304, ResearcherID G-5017-2017, aiv@ibch.ru.

Музафаров Азиз Мансурович – академик РАН, д.х.н., профессор, Институт элементоорганических соединений им. А.Н. Несмеянова РАН, Москва, Российская Федерация. Scopus Author ID 7004472780, ResearcherID G-1644-2011, <https://orcid.org/0000-0002-3050-3253>, aziz@ineos.ac.ru.

Ivan A. Novakov – Academician at the RAS, Dr. Sci. (Chem.), Professor, President of the Volgograd State Technical University, Volgograd, Russian Federation. Scopus Author ID 7003436556, ResearcherID I-4668-2015, <http://orcid.org/0000-0002-0980-6591>, president@vstu.ru.

Alexander N. Ozerin – Corresponding Member of the RAS, Dr. Sci. (Chem.), Professor, Enikolopov Institute of Synthetic Polymeric Materials of the RAS, Moscow, Russian Federation. Scopus Author ID 7006188944, ResearcherID J-1866-2018, <https://orcid.org/0000-0001-7505-6090>, ozerin@ispm.ru.

Tapani A. Pakkanen – PhD, Professor, Department of Chemistry, University of Eastern Finland, Joensuu, Finland. Scopus Author ID 7102310323, tapani.pakkanen@uef.fi.

Armando J.L. Pombeiro – Academician at the Academy of Sciences of Lisbon, PhD, Professor, President of the Center for Structural Chemistry of the Higher Technical Institute of the University of Lisbon, Lisbon, Portugal. Scopus Author ID 7006067269, ResearcherID I-5945-2012, <https://orcid.org/0000-0001-8323-888X>, pombeiro@ist.utl.pt.

Dmitrii V. Pyshnyi – Corresponding Member of the RAS, Dr. Sci. (Chem.), Professor, Institute of Chemical Biology and Fundamental Medicine, Siberian Branch of the RAS, Novosibirsk, Russian Federation. Scopus Author ID 7006677629, ResearcherID F-4729-2013, <https://orcid.org/0000-0002-2587-3719>, pyshnyi@niboch.nsc.ru.

Alexander S. Sigov – Academician at the RAS, Dr. Sci. (Phys. and Math.), Professor, President of MIREA – Russian Technological University, Moscow, Russian Federation. Scopus Author ID 35557510600, ResearcherID L-4103-2017, sigov@mirea.ru.

Alexander M. Toikka – Dr. Sci. (Chem.), Professor, Institute of Chemistry, Saint Petersburg State University, St. Petersburg, Russian Federation. Scopus Author ID 6603464176, ResearcherID A-5698-2010, <http://orcid.org/0000-0002-1863-5528>, a.toikka@spbu.ru.

Andrzej W. Trochimczuk – Dr. Sci. (Chem.), Professor, Faculty of Chemistry, Wrocław University of Science and Technology, Wrocław, Poland. Scopus Author ID 7003604847, andrzej.trochimczuk@pwr.edu.pl.

Aslan Yu. Tsvadze – Academician at the RAS, Dr. Sci. (Chem.), Professor, A.N. Frumkin Institute of Physical Chemistry and Electrochemistry of the RAS, Moscow, Russian Federation. Scopus Author ID 7004245066, ResearcherID G-7422-2014, tsiv@phyche.ac.ru.

Новаков Иван Александрович – академик РАН, д.х.н., профессор, президент Волгоградского государственного технического университета, Волгоград, Российская Федерация. Scopus Author ID 7003436556, ResearcherID I-4668-2015, <http://orcid.org/0000-0002-0980-6591>, president@vstu.ru.

Озерин Александр Никифорович – член-корр. РАН, д.х.н., профессор, Институт синтетических полимерных материалов им. Н.С. Ениколопова РАН, Москва, Российская Федерация. Scopus Author ID 7006188944, ResearcherID J-1866-2018, <https://orcid.org/0000-0001-7505-6090>, ozerin@ispm.ru.

Пакканен Тапани – PhD, профессор, Департамент химии, Университет Восточной Финляндии, Йоенсуу, Финляндия. Scopus Author ID 7102310323, tapani.pakkanen@uef.fi.

Помбейро Армандо – академик Академии наук Лиссабона, PhD, профессор, президент Центра структурной химии Высшего технического института Университета Лиссабона, Португалия. Scopus Author ID 7006067269, ResearcherID I-5945-2012, <https://orcid.org/0000-0001-8323-888X>, pombeiro@ist.utl.pt.

Пышный Дмитрий Владимирович – член-корр. РАН, д.х.н., профессор, Институт химической биологии и фундаментальной медицины Сибирского отделения РАН, Новосибирск, Российская Федерация. Scopus Author ID 7006677629, ResearcherID F-4729-2013, <https://orcid.org/0000-0002-2587-3719>, pyshnyi@niboch.nsc.ru.

Сигов Александр Сергеевич – академик РАН, д.ф.-м.н., профессор, президент МИРЭА – Российского технологического университета, Москва, Российская Федерация. Scopus Author ID 35557510600, ResearcherID L-4103-2017, sigov@mirea.ru.

Тойкка Александр Матвеевич – д.х.н., профессор, Институт химии, Санкт-Петербургский государственный университет, Санкт-Петербург, Российская Федерация. Scopus Author ID 6603464176, ResearcherID A-5698-2010, <http://orcid.org/0000-0002-1863-5528>, a.toikka@spbu.ru.

Трохимчук Анджей – д.х.н., профессор, Химический факультет Вроцлавского политехнического университета, Вроцлав, Польша. Scopus Author ID 7003604847, andrzej.trochimczuk@pwr.edu.pl.

Тсвадзе Аслан Юсупович – академик РАН, д.х.н., профессор, Институт физической химии и электрохимии им. А.Н. Фрумкина РАН, Москва, Российская Федерация. Scopus Author ID 7004245066, ResearcherID G-7422-2014, tsiv@phyche.ac.ru.

CONTENTS

СОДЕРЖАНИЕ

**Theoretical Bases
of Chemical Technology**

Zakharov M.K., Egorov A.V., Podmetenny A.A.
Liquid mixtures separation and heat consumption in
the process of distillation 7

**Chemistry and Technology
of Organic Substances**

*Anashkin D.O., Raigorodskii I.M., Kirilin A.D.,
Storozhenko P.A.*
New polycarbonate siloxanes
based on siloxane-*N*-phthalimidines 16

*Yarkina E.M., Kurganova E.A., Frolov A.S.,
Koshel G.N., Nesterova T.N., Shakun V.A.,
Spiridonov S.A.*
Para-tert-butylcumene synthesis 26

**Chemistry and Technology
of Medicinal Compounds
and Biologically Active Substances**

*Lykoshin D.D., Zaitsev V.V., Kostromina M.A.,
Esipov R.S.*
New-generation osteoplastic materials
based on biological and synthetic
matrices 36

**Теоретические основы
химической технологии**

Захаров М.К., Егоров А.В., Подметенный А.А.
Разделение жидких смесей и затраты теплоты
при ректификации

**Химия и технология
органических соединений**

*Анашкин Д.О., Райгородский И.М., Кирилин А.Д.,
Стороженко П.А.*
Новые поликарбонатсилоксаны
на основе силоксан-*N*-фталимидинов

*Яркина Е.М., Курганова Е.А., Фролов А.С.,
Кошель Г.Н., Нестерова Т.Н., Шакун В.А.,
Спиридонов С.А.*
Синтез *пара-трет*-бутилкумола

**Химия и технология лекарственных
препаратов и биологически
активных соединений**

*Лыкошин Д.Д., Зайцев В.В., Костромина М.А.,
Есипов Р.С.*
Остеопластические материалы нового поколения
на основе биологических и синтетических
матриц

Chemistry and Technology of Inorganic Materials

Sarin V.A., Bush A.A.

Neutron-diffraction study of the cubic-tetragonal phase structural transition in the single crystals of the solid solutions of zirconium and yttrium oxides

55

Talanov M.V., Marakhovsky M.A.

Chemical and technological aspects of increasing the functional characteristics of hard piezoceramics

67

Analytical Methods in Chemistry and Chemical Technology

Degterev M.B., Shukurov R.R.

Comparing the original and biosimilar biotherapeutics of the monoclonal antibody eculizumab by intact mass measurement and middle-up mass spectrometry analysis

76

Shchekoldina Z.N., Bogolyubov A.A., Zakharov A.Yu., Bulgakov B.A., Babkin A.V., Kepman A.V.

Development of the technique for quality control of 1,3-bis(3,4-dicyanophenoxy)benzene by HPLC

88

Химия и технология неорганических материалов

Сарин В.А., Буш А.А.

Нейтроннографическое исследование структурного перехода кубическая–тетрагональная фаза в монокристаллах твердых растворов оксида циркония с оксидом иттрия

Таланов М.В., Мараховский М.А.

Химико-технологические аспекты повышения функциональных характеристик сегнетожесткой пьезокерамики

Аналитические методы в химии и химической технологии

Дегтерев М.Б., Шукуров Р.Р.

Сравнение оригинального и биоаналогичного препаратов моноклонального антитела экулизумаб методами масс-спектрометрии интактного белка и «с середины вверх»

Щеколдина З.Н., Боголюбов А.А., Захаров А.Ю., Булгаков Б.А., Бабкин А.В., Кепман А.В.

Разработка методики количественного анализа целевого и побочных продуктов синтеза 1,3-бис(3,4-дицианофенокси)бензола методом ВЭЖХ

THEORETICAL BASES OF CHEMICAL TECHNOLOGY
ТЕОРЕТИЧЕСКИЕ ОСНОВЫ ХИМИЧЕСКОЙ ТЕХНОЛОГИИ

ISSN 2686-7575 (Online)

<https://doi.org/10.32362/2410-6593-2021-16-1-7-15>



UDC 66.011

RESEARCH ARTICLE

Liquid mixtures separation and heat consumption in the process of distillation

Mikhail K. Zakharov[@], Alexandr V. Egorov, Alexandr A. Podmetenny

MIREA – Russian Technological University (M.V. Lomonosov Institute of Fine Chemical Technologies), Moscow, 119571 Russia

[@]Corresponding author, e-mail: mkzakharov@gmail.com

Abstract

Objectives. The aim of this study is to investigate different distillation modes of a binary ideal mixture and determine how various factors affect heat consumption in the column boilers. In addition, it intends to assess the difficulty of separating mixtures. Our research is based on analyzing the characteristics of vapor-liquid equilibrium.

Methods. To conduct our study, we used a graphic-analytical tool to calculate the distillation process of a binary mixture and mathematical models based on the Aspen Plus software package along with DSTWU, RadFrac, and the Sensitivity module. We also used the Peng-Robinson equation (PENG-ROB) to determine the liquid-vapor equilibrium.

Results. We employed the graphical method and mathematical models to obtain the operation parameters of two column variants for the distillation of binary ideal benzene-toluene mixtures. In each variant the initial mixture contained the same amount of the low- or high-boiling component. The number of plates in the column sections, reflux ratio, energy consumption, and indicators of internal energy saving were determined.

Conclusions. Study results show that using the coefficient of the component distribution between the vapor and liquid phases is a promising method for preliminary assessments of the separation difficulty and measurements of the expected heat consumption in the boilers of columns. Comparison studies showed that the heat consumption in the boiler decreases as the internal energy saving in the columns increases.

Keywords: distillation, binary mixtures, relative volatility, reflux ratio, distribution coefficient, internal energy saving in distillation

For citation: Zakharov M.K., Egorov A.V., Podmetenny A.A. Liquid mixtures separation and heat consumption in the process of distillation. *Tonk. Khim. Tekhnol. = Fine Chem. Technol.* 2021;16(1):7–15 (Russ., Eng.). <https://doi.org/10.32362/2410-6593-2021-16-1-7-15>

НАУЧНАЯ СТАТЬЯ

Разделение жидких смесей и затраты теплоты при ректификации

М.К. Захаров[®], А.В. Егоров, А.А. Подметенный

МИРЭА – Российский технологический университет (Институт тонких химических технологий им. М.В. Ломоносова), Москва, 119571 Россия

[®]Автор для переписки, e-mail: mkzakharov@gmail.com**Аннотация**

Цели. Работа посвящена изучению различных режимов ректификации бинарной идеальной смеси и установлению влияния различных факторов на затраты теплоты в кипятильниках колонн, а также оценке трудности разделения смесей на основе анализа характеристик парожидкостного равновесия.

Методы. В качестве методов исследования выбран графоаналитический расчет процесса ректификации бинарной смеси и математическое моделирование с использованием программного комплекса Aspen Plus с последовательным применением методов DSTWU, RadFrac и модуля «Sensitivity». Равновесие жидкость-пар было определено по уравнению Пенга-Робинсона (PENG-ROB).

Результаты. С использованием графического метода и метода математического моделирования получены параметры работы колонн двух вариантов ректификации бинарных идеальных смесей бензол–толуол, в каждом из которых исходная смесь содержит одинаковое количество низко(высоко)кипящего компонента. Определены числа тарелок в секциях колонны, флегмовые числа, энергозатраты и показатели внутреннего энергосбережения.

Выводы. Анализ полученных результатов показывает перспективность использования коэффициента распределения компонентов между паровой и жидкой фазами для предварительной оценки трудности разделения и ожидаемых затрат теплоты в кипятильниках колонн. Сравнение рассмотренных вариантов показало, что при увеличении внутреннего энергосбережения в колоннах затраты теплоты в кипятильнике уменьшаются.

Ключевые слова: ректификация, бинарные смеси, относительная летучесть, флегмовое число, коэффициент распределения, внутреннее энергосбережение при ректификации

Для цитирования: Захаров М.К., Егоров А.В., Подметенный А.А. Разделение жидких смесей и затраты теплоты при ректификации. *Тонкие химические технологии*. 2021;16(1):7–15. <https://doi.org/10.32362/2410-6593-2021-16-1-7-15>

INTRODUCTION

Heat consumption in the process of separating liquid mixtures by distillation results from the need of evaporating the liquid to form a vapor flow in the column. It is determined by the difficulty of separating a particular initial mixture. It is known that the still residue rather than the original mixture is evaporated in a complete distillation column. Therefore, the correct assessment of heat consumption in the boiler of a distillation column is a subject of considerable interest. This paper analyzes the main factors affecting heat consumption in the distillation process with an ideal benzene–toluene mixture as an example.

THEORY

The conventional method [1, 2] of assessing the difficulty of separating a mixture is to use the relative volatility coefficient of the starting components. For ideal systems, the coefficient is determined by the ratio of saturated vapor pressures of the pure components (P_A and P_B) at a certain temperature t : $\alpha = P_A/P_B$.

Note that even in the case of ideal binary mixtures, the value of α is not constant but rather depends on the low-boiling component (LBC) concentration in the mixture. When changing the mixture composition, its boiling temperature changes, and as a result, the value of P_A/P_B alters. This is conditional upon by the

non-linearity of saturated vapor pressure dependence on temperature. Thus, for the benzene–toluene mixture at low LBC concentrations in the mixture (less than 5%), the coefficient of relative volatility is equal to 2.30, and at high LBC concentrations (more than 80%), the coefficient is equal to 2.55. The concentration difference is about 10%. For comparison, in the benzene–*m*-xylene system, the concentration difference exceeds 20%.

Assuming that the coefficient of relative volatility is constant [1, 2], the equilibrium compositions of liquid *x* and vapor *y* for ideal binary mixtures are determined by the following relationship:

$$y = \frac{\alpha x}{\alpha x + 1 - x}. \quad (1)$$

When α is close to 1, one can take

$$y = \alpha x. \quad (2)$$

The LBC concentration in the vapor phase as compared to its concentration in the liquid is equal to

$$y - x = \alpha x - x = (\alpha - 1)x. \quad (3)$$

The value $(\alpha - 1)$ is called the enrichment factor [3]. It is clear from (3) that the enrichment factor is the relative increase in LBC concentration in the vapor phase compared to its concentration in the liquid phase. A wide range of changes in the values of α (from 1 to ∞) makes it impossible to express analytically the dependence of heat consumption and determine the influence of α and $(\alpha - 1)$ values on heat consumption in the distillation process.

To facilitate assessment of the mixture separation ability by distillation is to determine the value of P . We called it the mixture “separability,” and is determined as follows [4]:

$$P = \frac{\alpha - 1}{\alpha + 1}. \quad (4)$$

The value of P varies from 0 (at $\alpha = 1$) to 1 (at $\alpha = \infty$). From (4) it follows:

$$\alpha = \frac{1 + P}{1 - P}. \quad (5)$$

Substituting the expression of α into (1) we obtain the equilibrium dependence of the vapor composition *y* on the liquid composition *x* for mixtures obeying the Raoult’s law:

$$y = \frac{(1 + P)x}{1 - P + 2Px}. \quad (6)$$

A value comparison of the above estimates is presented in Table 1.

For any LBC concentration values in the liquid, the coefficient of relative volatility is represented as the ratio of the phase equilibrium coefficients of the components of the mixture being separated:

$$\alpha = \frac{K_A}{K_B}, \quad (7)$$

where $K_A = P_A/P_{\text{total}}$ and $K_B = P_B/P_{\text{total}}$; P_{total} is the total pressure in the column.

Table 1. Comparison of various estimates of the ability of liquid mixtures to be separated by distillation

α	P	$\alpha - 1$	α	P	$\alpha - 1$
1	0	0	3	0.5	2
1.01	0.0050	0.01	4	0.6	3
1.05	0.0244	0.05	5.6	0.7	4.6
1.1	0.0476	0.1	9	0.8	8
1.2	0.0909	0.2	19	0.9	18
1.3	0.1304	0.3	50	0.961	49
1.4	0.1667	0.4	100	0.98	99
1.5	0.2	0.5	1000	0.998	999
1.857	0.3	0.857	∞	1	∞
2.3	0.4	1.3	–	–	–

The values of the phase equilibrium constant of the components K_A and K_B at P_{total} depend on the component concentration, as the vapor pressure of the pure components is a function of their boiling point t , and the latter depends on the mixture composition. At low LBC concentrations, the constant K_B is close to 1. In this case, we assume that $\alpha = K_A$. For medium concentrations, the coefficient of relative volatility α is determined by the K_A/K_B ratio (7). This means that the coefficient α takes into account both the LBC concentration increase in the vapor phase compared to the liquid phase ($K_A = y/x$) and the high-boiling component (HBC) increase in the liquid phase compared to the vapor phase ($1/K_B = 1 - x/(1-y)$), i.e., it takes into account the same effect twice.

When the LBC concentration tends to 1, the coefficient of relative volatility becomes $\alpha = 1/K_B$. In this case, the LBC concentration in the vapor phase (y) slightly exceeds its concentration in the liquid (x). Let us take for example $x = 0.9$ and $y = 0.95$. Then

$$\alpha = \frac{1}{K_B} = \frac{1-x}{1-y} = \frac{1-0.9}{1-0.95} = \frac{0.1}{0.05} = 2 \quad (8)$$

characterizes only the increase in the HBC concentration in the liquid phase compared to the vapor phase. In this case, the value of α equal to 2 indicates a fairly the good ability of this liquid binary mixture to be separated by distillation. However, a small relative increase in the LBC concentration

$$\frac{y-x}{x} = \frac{0.95-0.90}{0.90} = 0.0556$$

testifies otherwise.

In literature [1, 2], the ratio of phase equilibrium concentrations of any component is called the distribution coefficient

$$m = \left(\frac{y}{x} \right)_{\text{eq}} \quad (9)$$

This coefficient is the tangent of the inclination angle of the secant drawn from the coordinate origin to the point with equilibrium concentrations y, x . The subscript *eq* in formula (9) indicates the equilibrium LBC concentrations in the vapor and liquid phases.

It should be emphasized that m is the tangent of the inclination angle of the secant, since m is often interpreted in a number of publications [2] as the tangent of the inclination angle of the tangent to the equilibrium line at points with equilibrium

concentrations y, x . Only at low LBC concentrations (up to 1–3%) in the mixture, the tangent of the tangent inclination angle differs slightly from the tangent of the secant inclination angle. In other cases, this difference becomes larger (Fig. 1), even for binary mixtures close to ideal. Moreover, this difference is larger in the case of real mixtures.

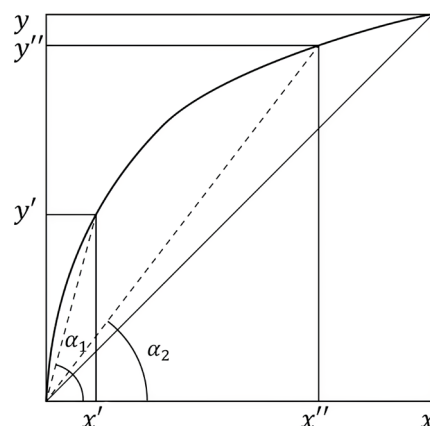


Fig. 1. Graphical determination of the components' distribution coefficient.

Figure 1 shows that the value of the distribution coefficient m at low LBC concentrations is much higher (x', y' point) than at high LBC concentrations (x'', y'' point): $\text{tg}\alpha_1 > \text{tg}\alpha_2$. When $x \rightarrow 1$, the coefficient m tends to 1, indicating a decrease in the vapor phase enrichment with the LBC compared to the liquid one. Thus, in our opinion, using the distribution coefficient, which is a measure of the absolute component volatility, is more correct when analyzing mixture separation by distillation. Yet, the relative volatility coefficient is still widely used [5–13] for assessing the ability to separate mixtures. This is partly due to the fact that, when developing energy-efficient distillation schemes for mixtures with a constant relative volatility coefficient, one of the most common methods, the Underwood method, is used to calculate the minimum reflux ratio [14]. However, the latter does not provide acceptable accuracy values. Therefore, the work [15] suggests a method for calculating the minimum reflux ratio based on the phase equilibrium constants of mixture components (distribution coefficients).

RESULTS AND DISCUSSION

We conducted a computational experiment to reveal how the distribution coefficient m affects heat consumption during distillation. We used a benzene–toluene mixture with phase behavior close to ideal. We considered two options of separating the initial

mixtures containing 0.74 mole fractions of one of the components (benzene–option 1, toluene–option 2, see Table 2). The task was to obtain a product (distillate for option 1 or still residue for option 2) containing 0.98 mole fractions of the target component and obtain the second product of separation with the equimolar composition. The column productivity L_1 with respect to the initial mixture was taken as 0.01 [kmol/s] in both cases. The excess reflux ratio σ was also assumed to be the same and equal to 1.1.

The calculation of the number of theoretical plates in the column performed graphically in the y – x diagram is qualitatively schematized in Fig. 2 for both separation options.

The values of the number of plates in the columns and the heat consumption in the boilers are listed in Table 2. In parallel, we carried out a design analysis using the Aspen Plus software along with DSTWU, RadFrac methods and the Sensitivity module. We determined the liquid–vapor equilibrium by using the Peng–Robinson equation (PENG–ROB), as this equation is the most appropriate for modeling the phase equilibrium of a mixture consisting of hydrocarbons [16–18]. The calculation results are listed in Table 2.

The DSTWU model allows for an approximate column design (minimum reflux ratio, minimum number of plates). The operating reflux ratio was

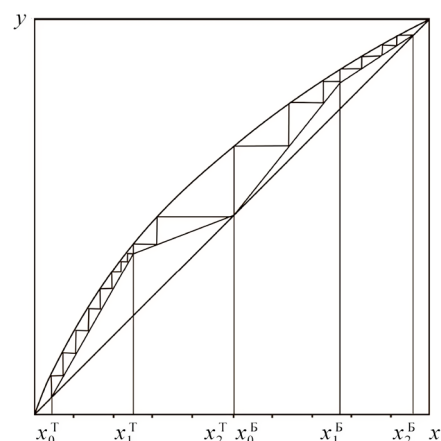


Fig. 2. Graphical determination of the number of plates in the y – x diagram.

calculated taking into account the excess reflux ratio, which is equal to 1.1. Then the RadFrac model was used for refined calculations. After selecting the total number of plates in the column closest to the previously calculated reflux ratio values the Sensitivity module was used, which allowed determine the feed plate providing the minimum heat consumption in the boiler.

When estimating the possibility of separating mixtures via a relative volatility of components we assumed that if this value is constant, it is equally

Table 2. Comparison of calculation results for two options of benzene–toluene mixture separation

Parameters	Calculation in the y – x diagram						Computer calculation in Aspen Plus software					
	Option 1			Option 2			Option 1			Option 2		
	Composition, $\left[\frac{\text{kmol LBC}}{\text{kmol mxtr}} \right]$											
	x_0	x_1	x_2	x_0	x_1	x_2	x_0	x_1	x_2	x_0	x_1	x_2
	0.50	0.74	0.98	0.02	0.26	0.50	0.50	0.74	0.98	0.02	0.26	0.50
Theoretical number of plates in the rectifying column, n_r	12.9			4.1			9			3		
Theoretical number of plates in the stripping column, n_s	3.2			15.2			3			16		
Reflux ratio, R	0.857			0.208			0.848			0.218		
Heat duty in the boiler Q_b , [kW]	283			210			284			200		
Internal energy saving, ES	0.569			0.824			0.591			0.801		
Distribution coefficient, m	1.18			1.8			1.18			1.8		

difficult to separate the mixtures. Furthermore, we expected equal heat consumptions in the boilers in the discussed distillation embodiments. However, the results in Table 2 indicate a higher heat consumption (by 26%) in the first separation option. This fully conforms to the proportionality of heat consumption to the product $D(R+1)$, where D is the distillate flow. Since the sampling ratios of the upper product in both options are equal to 0.5, the large heat consumption is due to the high reflux ratio in the first option. The question which arises is why the mixture in option 1 is more difficult to separate. The answer lies in the value of the distribution coefficient m between the vapor and liquid phases (in the range of working concentrations). In option 1, it is much lower (1.18) than in option 2 (1.80) (see Table 2). Therefore, we carried out a preliminary estimation of the possibilities of separating mixtures and of the expected heat consumption based on coefficient analyses of the component distributions between the phases in the initial mixture.

The obtained results illustrate the contribution of the internal energy saving to the heat consumption in the column boiler [19]. The internal energy saving is determined not only by the reflux ratio in the rectifying section, but also by the ratio of the number of theoretical plates in the rectifying and stripping sections of the column. When the initial mixture is fed into the column at the boiling point, the internal energy saving in the distillation column is calculated

by the following formula [19]:

$$ES = \frac{R}{R+1} \times \frac{n_r}{n_r + n_s} + \frac{n_s}{n_r + n_s}. \quad (10)$$

An example of calculation by formula (10) for option 1 is presented below. Let us calculate the value of internal energy saving at operating reflux ratio 0.857; the number of theoretical plates in the rectifying section of the column 12.9; the number of theoretical plates in the stripping section of the column 3.2:

$$ES = \frac{0.857}{0.857+1} \times \frac{12.9}{12.9+3.2} + \frac{3.2}{12.9+3.2} = 0.370 + 0.1988 = 0.569.$$

When carrying out computer calculations, the values of liquid and vapor flows along the column height become known. Then we can use a more accurate formula for calculating energy saving. The formula takes into account the counterflows of the liquid L and vapor V on each plate of the rectifying part of the column [20]:

$$ES = \frac{\sum_{n=2}^{n_y} \frac{L_{n-1}}{V_{n+1}} + n_o}{n_y + n_o}. \quad (11)$$

To perform the calculation according to formula (11)

Table 3. Flows of liquid and vapor in a distillation column during separation of a benzene–toluene mixture (option 1)

Plate number	Temperature, °C	Liquid flow, kmol/h	Vapor flow, kmol/h	$\frac{L_{n-1}}{V_{n+1}}$
1	80.1	33.27	0	–
2	80.8	15.18	33.27	0.4602
3	81.5	15.08	33.18	0.4588
4	82.2	14.99	33.08	0.4572
5	83.0	14.90	32.99	0.4556
6	83.7	14.82	32.90	0.4540
7	84.3	14.75	32.82	0.4525
8	84.8	14.69	32.75	0.4512
9	85.3	14.65	32.69	0.4500
10	85.6	50.62	32.65	0.4491
11	85.9	50.54	32.62	–
12	86.6	50.33	32.54	–
13	88.3	49.87	32.33	–
14	92.2	18.00	31.87	–

we will use the data from Table 3. It should also be considered that the first plate is a condenser, in which vapor is condensed to obtain a liquid of the same composition. Therefore, the calculation starts at the second plate and ends at the feed plate. Then:

$$ES = \frac{4.0886+3}{3+9} = 0.591.$$

The number 4.0886 in the calculation formula is the sum of the ratios of the liquid and vapor flows on the plates of the column rectifying section.

Minor discrepancies in the energy saving values calculated in the y - x diagram and in the Aspen Plus program stem from the refined computer calculation of the liquid and vapor flows through the column, and when calculating in the y - x diagram—due to the possibility of counting the fractional part of the theoretical plate.

CONCLUSIONS

The analysis of the distillation of ideal binary benzene–toluene mixtures of different composition showed that the coefficient of the distribution of components between the vapor and liquid phases is

a more accurate characteristic of the mixture, which can be used for preliminary assessments of separation difficulty and the expected heat consumption in the boilers of the columns. Using the coefficient of relative volatility α for these purposes, whose value is assumed constant for ideal mixtures, does not always yield correct results. Comparison of the considered options was carried out according to the criterion of internal energy saving. It was shown that the heat consumption in the boiler decreases with increasing internal energy saving in the columns.

Financial support

This study did not have any financial support from outside organizations.

Authors' contribution

M.K. Zakharov – developing the scientific work concept, offering consultations on methodology and research;

A.V. Egorov – collecting and processing the material, writing the text of the article;

A.A. Podmetenny – collecting and processing the material, writing the text of the article.

The authors declare no conflicts of interest.

REFERENCES

1. Ainshtein V.G., Zakharov M.K., Nosov G.A., Zakharenko V.V., Zinovkina T.V., Taran A.L., Kostanyan A.E. *Protsessy i apparaty khimicheskoi tekhnologii. Obshchii kurs: Uchebnyk v 2-kh kn. (Processes and Apparatus of Chemical Technologies. General course: Textbook in 2 books)*, 8th edition, Ainshtein V.G. (Ed.), St. Petersburg: Lan'; V. 1, 916 p., V. 2., 876 p. (in Russ.). ISBN 978-5-8114-2975-2
2. Kasatkin A.G. *Osnovnyye protsessy i apparaty khimicheskoi tekhnologii (Basic Processes and Apparatus of Chemical Technology)*. Moscow: Khimiya; 1971. 784 p.
3. Benedict M. Multistage Separation Processes. *Chem. Eng. Prog.* 1947;43(2):41–60.
4. Zakharov M.K., Martynova M.M., Prusachenkova M.I. Comparison of heat consumption in the separation of binary mixtures using distillation and rectification. *Theor. Found. Chem. Eng.* 2018;52(4):730–734. <https://doi.org/10.1134/S0040579518040322>
- [Zakharov M.K., Martynova M.M., Prusachenkova M.I. Comparison of heat consumption in case of separation of binary compositions by methods of distillation and rectification. *Khim. Tekhnologiya.* 2017;18(1):43–48 (in Russ.).]
5. Kim Y.H. Design and control of energy-efficient distillation columns. *Korean J. Chem. Eng.* 2016;33(9):2513–2521. <https://doi.org/10.1007/s11814-016-0124-4>
6. Halvorsen I.J., Skogestad S. Energy efficient distillation. *J. Nat. Gas Sci. Eng.* 2011;3(4):571–580. <https://doi.org/10.1016/j.jngse.2011.06.002>

СПИСОК ЛИТЕРАТУРЫ

1. Айнштейн В.Г., Захаров М.К., Носов Г.А., Захаренко В.В., Зиновкина Т.В., Таран А.Л., Костанян А.Е. *Процессы и аппараты химической технологии. Общий курс: Учебник в 2-х кн.*; под ред. В.Г. Айнштейна, 8-е издание. СПб.: Лань; 2019. Кн. 1. 916 с. Кн. 2. 876 с. ISBN 978-5-8114-2975-2
2. Касаткин А.Г. *Основные процессы и аппараты химической технологии*. М.: Химия; 1971. 784 с.
3. Benedict M. Multistage separation processes. *Chem. Eng. Prog.* 1947;43(2):41–60.
4. Захаров М.К., Мартынова М.М., Прусаченкова М.И. Сравнение затрат теплоты при разделении бинарных смесей методами дистилляции и ректификации. *Хим. технология.* 2017;18(1):43–47.
5. Kim Y.H. Design and control of energy-efficient distillation columns. *Korean J. Chem. Eng.* 2016;33(9):2513–2521. <https://doi.org/10.1007/s11814-016-0124-4>
6. Halvorsen I.J., Skogestad S. Energy efficient distillation. *J. Nat. Gas Sci. Eng.* 2011;3(4):571–580. <https://doi.org/10.1016/j.jngse.2011.06.002>
7. Данилов Р.Ю., Петлюк Ф.Б., Серафимов Л.А. Режим минимальной флегмы в простых ректификационных колоннах. *Теор. основы хим. технологии.* 2007;41(4):394–406.
8. Захаров М.К., Швец А.А., Бойчук А.А. Расчет минимального флегмового числа при ректификации некоторых реальных бинарных смесей. *Тонкие химические технологии.* 2015;10(6):53–57.

7. Danilov R.Yu., Petlyuk F.B., Serafimov L.A. Minimum Reflux Regime of Simple Distillation Columns. *Theor. Found. Chem. Eng.* 2007;41(4):371–383. <https://doi.org/10.1134/S0040579507040069>
- [Danilov R.Yu., Petlyuk F.B., Serafimov L.A. Minimum Reflux Regime of Simple Distillation Columns. *Teor. Osnovy Khim. Tehnologii = Theor. Found. Chem. Eng.* 2007;41(4):394–406 (in Russ.).]
8. Zakharov M.K., Shvets A.A., Boichuk A.A. Calculation of Minimal Reflux Ratio for Various Cases of Rectification of Binary Mixtures. *Tonk. Khim. Tekhnol. = Fine Chem. Technol.* 2015;10(6):53–57 (in Russ.).
9. Koehler J., Poellmann P., Blass E. A Review on Minimum Energy Calculations for Ideal and Nonideal Distillations Model. *Ind. Eng. Chem. Res.* 1995;34(4):1003–1020. <https://doi.org/10.1021/ie00043a001>
10. Wakabayashi T., Ferrari A., Hasebe S. Design and commercial operation of a discretely heat-integrated distillation column. *Chem. Eng. Res. Des.* 2019;147:214–221. <https://doi.org/10.1016/j.cherd.2019.04.036>
11. Fidkowski Z.T., Malone M.F. & Doherty M.F. Nonideal Multicomponent Distillation: Use of Bifurcation Theory for Design. *AIChE J.* 1991;37(12):1761–1779. <https://doi.org/10.1002/aic.690371202>
12. Stichlmair J.G., Offers H. & Potthoff R.W. Minimum Reflux and Reboil in Ternary Distillation. *Ind. Eng. Chem. Res.* 1993;32:2438–2445.
13. Petlyuk F.B. *Distillation Theory and its Application to Optimal Design of Separation Units*. New York: CUP; 2004. 362 p.
14. Александров И.А. *Массопередача при ректификации и абсорбции многокомпонентных смесей*. Л.: Химия; 1975. 320 с.
15. Савченко В.И., Гельперин Н.И. Метод расчета минимального флегмового числа в процессах ректификации многокомпонентных смесей. *Теор. основы хим. технологии.* 1973;7(2):160–169.
16. Martín M.M. *Introduction to Software for Chemical Engineers*. 2nd edition. CRC Press; 2019. 802 p. <https://doi.org/10.1201/9780429451010>
17. Luyben W.L. *Distillation Design and Control Using Aspen Simulation*. 2nd edition. JohnWiley & Sons, Inc.; 2013. 510 p.
18. Schefflan R. *Teach Yourself the Basic of Aspen Plus™*. 2nd edition. Hoboken, New Jersey: John Wiley & Sons, Inc.; 2016. 331 p.
19. Zakharov M.K., Boychuk A.A. Выбор оптимального варианта разделения смеси углеводородных газов методом ректификации. *Тонкие химические технологии.* 2018;13(3):23–29. <https://doi.org/10.32362/24106593-2018-13-3-23-29>
20. Zakharov M.K., Nosov G.A., Pisarenko Yu.A., Zhil'tsova L.M., Shvets A.A. Comparison of distributed heat supplies along the height of fractionating columns with conventional fractionation. *Theor. Found. Chem. Eng.* 2017;51(5):708–715. <https://doi.org/10.1134/S0040579517050402>

About the authors:

Mikhail K. Zakharov, Dr. Sci. (Eng.), Professor, N.I. Gelperin Department of Processes and Apparatus of Chemical Technology, M.V. Lomonosov Institute of Fine Chemical Technologies, MIREA – Russian Technological University (86, Vernadskogo pr., Moscow, 119571, Russia). E-mail: mkzakharov@gmail.com. <https://orcid.org/0000-0002-8595-5679>

Alexandr V. Egorov, Postgraduate Student, N.I. Gelperin Department of Processes and Apparatus of Chemical Technology, M.V. Lomonosov Institute of Fine Chemical Technologies, MIREA – Russian Technological University (86, Vernadskogo pr., Moscow, 119571, Russia). E-mail: betakiller1576@gmail.com. <https://orcid.org/0000-0002-1313-8231>

Alexandr A. Podmetenny, Postgraduate Student, N.I. Gelperin Department of Processes and apparatus of chemical technology, M. V. Lomonosov Institute of Fine Chemical Technologies, MIREA – Russian Technological University (86, Vernadskogo pr., Moscow, 119571, Russia). E-mail: sansanych08-94@yandex.ru. <https://orcid.org/0000-0001-7084-4661>

Об авторах:

Захаров Михаил Константинович, профессор кафедры процессов и аппаратов химических технологий им. Н.И. Гельперина Института тонких химических технологий им. М.В. Ломоносова ФГБОУ ВО «МИРЭА – Российский технологический университет» (119571, Россия, Москва, пр-т Вернадского, д. 86). E-mail: mkzakharov@gmail.com. <https://orcid.org/0000-0002-8595-5679>

Егоров Александр Владимирович, аспирант кафедры процессов и аппаратов химических технологий им. Н.И. Гельперина Института тонких химических технологий им. М.В. Ломоносова ФГБОУ ВО «МИРЭА – Российский технологический университет» (119571, Россия, Москва, пр-т Вернадского, д. 86). E-mail: betakiller1576@gmail.com. <https://orcid.org/0000-0002-1313-8231>

Подметенный Александр Александрович, аспирант кафедры процессов и аппаратов химических технологий им. Н.И. Гельперина Института тонких химических технологий им. М.В. Ломоносова ФГБОУ ВО «МИРЭА – Российский технологический университет» (119571, Россия, Москва, пр-т Вернадского, д. 86). E-mail: sansanych08-94@yandex.ru. <https://orcid.org/0000-0001-7084-4661>

The article was submitted: April 10, 2020; approved after reviewing: December 19, 2020; accepted for publication: February 01, 2021.

Translated from Russian into English by M. Povorin

Edited for English language and spelling by Enago, an editing brand of Crimson Interactive Inc.

ISSN 2686-7575 (Online)

<https://doi.org/10.32362/2410-6593-2021-16-1-16-25>



UDC 547.26.245

RESEARCH ARTICLE

New polycarbonate siloxanes based on siloxane-*N*-phthalimidines

Dmitrii O. Anashkin¹, Igor M. Raigorodskii^{1,@}, Aleksei D. Kirilin¹, Pavel A. Storozhenko²

¹MIREA – Russian Technological University (M.V. Lomonosov Institute of Fine Chemical Technologies), Moscow, 119571 Russia

²State Research Institute for Chemistry and Technology of Organoelement Compounds, Moscow, 105118 Russia

@Corresponding author, e-mail: imraygor@rambler.ru

Abstract

Objectives. Polymeric carbonate siloxanes containing a siloxane-*N*-phthalimidine group in the chain frame are new synthetic comb-like macromolecule systems. This work aims to study the possibility of applying them in the form of film materials for heat-resistant, high-performance gas-permeable membranes.

Methods. Comb-like polycarbonate siloxanes of the siloxane-containing polyether class were obtained using various polycondensation methods, i.e., by the polymer-analogous transformation of polycarbonate-allyl-*N*-phthalimidines, using their reaction in an alkyl hydride siloxane solution; polycondensation of *N*-(3-(pentamethyldisiloxane)-propyl)-3,3-bis-(4'-hydroxyphenyl)-phthalimidine with diphenylolpropane bis-chloroformate in a solution using triethylamine as an acceptor of hydrochloric acid; interphase polycondensation of the above reagents in a dichloromethane aqueous alkali system. The structures of the obtained initial and polymeric compounds were confirmed by proton nuclear magnetic resonance spectroscopy and elemental analysis. All of the synthesized comb-like copolymers had good solubility in several available solvents and film formations.

Results. The new comb-like polycarbonate siloxanes had high thermal stability. According to thermogravimetric analysis, the introduction of up to 20 wt % siloxane units makes it possible to increase the heat resistance of polycarbonate siloxanes by 25°C. Concurrently, their glass-transition temperature reaches 160°C. Copolymers of polycarbonate siloxanes in the form of films have a high tensile strength above 50 MPa and an elastic modulus of up to 2000 MPa. The permeability coefficients of gases through a copolymer of polycarbonate siloxanes in the form of a film for several gases surpass the permeability of industrial polycarbonate from diphenylolpropane and fluorine-containing siloxane polycarbonate.

Conclusions. The results achieved indicate the possibility of creating new polymeric comb-shaped siloxane systems with a variable structure that can contribute to obtaining the properties desired from them. Combined with high selectivity gas separation, this makes it possible to use such comb-shaped polycarbonate siloxanes as film membrane materials with an increased operating temperature range.

Keywords: polycarbonate siloxanes, comb-like polymers, polycondensation, mechanical and thermal properties, gas permeability

For citation: Anashkin D.O., Raigorodskii I.M., Kirilin A.D., Storozhenko P.A. New polycarbonate siloxanes based on siloxane-*N*-phthalimides. *Tonk. Khim. Tekhnol. = Fine Chem. Technol.* 2021;16(1):16–25 (Russ., Eng.). <https://doi.org/10.32362/2410-6593-2021-16-1-16-25>

НАУЧНАЯ СТАТЬЯ

Новые поликарбонатсилоксаны на основе силоксан-*N*-фталимиديнов

Д.О. Анашкин¹, И.М. Райгородский^{1,@}, А.Д. Кирилин¹, П.А. Стороженко²

¹МИРЭА – Российский технологический университет (Институт тонких химических технологий им. М.В. Ломоносова), Москва, 119571 Россия

²Государственный научно-исследовательский институт химии и технологии элементоорганических соединений, Москва, 111123 Россия

@Автор для переписки, e-mail: imraigor@rambler.ru

Аннотация

Цели. Полимерные карбонатсилоксаны, содержащие в обрамлении цепи силоксан-*N*-фталимидиновую группировку, являются новыми синтетическими гребнеобразными системами макромолекул. Цель работы – изучить возможность их применения в виде пленочных материалов для термостойких высокоэффективных газопроницаемых мембран.

Методы. Гребнеобразные поликарбонатсилоксаны класса силоксан-содержащих полиэфиров были получены различными поликонденсационными методами: полимераналогичным превращением поликарбонат-аллил-*N*-фталимидинов их реакцией в растворе с алкилгидридсилоксанами; поликонденсацией *N*-(3-(пентаметилдисилокси)-пропил)-3,3-бис-(4'-окси-фенил)фталимидина с бис-хлорформиатом дифенилолпропана в растворе, используя триэтиламин в качестве акцептора соляной кислоты или межфазной поликонденсацией указанных реагентов в системе метиленхлорид–водная щелочь. Структуры полученных исходных и полимерных соединений были подтверждены спектроскопией ядерного магнитного резонанса ¹H и элементным анализом. Свойством всех синтезированных гребнеобразных сополимеров является их хорошая растворимость в ряде доступных растворителях и пленкообразование.

Результаты. Показано, что новые гребнеобразные поликарбонатсилоксаны обладают высокой термической устойчивостью. По данным термогравиметрического анализа введение в сополимер до 20 масс. % силоксановых звеньев позволяет повысить термостойкость поликарбонатсилоксанов на 25°С. При этом, температура стеклования их достигает 160°С. Соплимеры поликарбонатсилоксанов в виде пленок обладают высокой прочностью на разрыв выше 50 МПа и модулем упругости до 2000 МПа. Коэффициенты проницаемости газов через сополимер поликарбонатсилоксанов в виде пленки по ряду газов превосходят проницаемость для промышленного поликарбоната из дифенилолпропана и фторсодержащего силоксанового поликарбоната.

Выводы. Достигнутые результаты свидетельствуют о возможности создания новых полимерных гребнеобразных силоксановых систем с варьируемой структурой, которая способствует для них получению заданных свойств. В сочетании с высокой селективностью разделения газов это позволяет использовать новые гребнеобразные поликарбонатсилоксаны в качестве пленочных мембранных материалов с повышенным интервалом рабочих температур.

Ключевые слова: поликарбонатсилоксаны, гребнеобразные полимеры, поликонденсация, механические и термические свойства, газопроницаемость

Для цитирования: Анашкин Д.О., Райгородский И.М., Кирилин А.Д., Стороженко П.А. Новые поликарбонатсилоксаны на основе силоксан-*N*-фталимидинов. *Тонкие химические технологии*. 2021;16(1):16–25. <https://doi.org/10.32362/2410-6593-2021-16-1-16-25>

INTRODUCTION

Polycarbonate siloxanes (PCS) have been broadly studied. Among these studies, in organosilicon copolymers, linear polycondensation polymers are important for practical purposes [1–4]. These are distinguished by high thermal stability, good mechanical properties, and high gas permeability.¹ Concurrently, the possibility of improving the service properties of PCS for their use as membrane materials may arise when changing not only their composition but also their molecular structure, i.e., when passing from linear copolymers of the $-(A-B)_n$ -type to comb-like structures of the $-[A(B)]_n$ -type.

Such a structural approach to the creation of highly efficient gas-permeable membranes was implemented using the example of comb-shaped polystyrene siloxanes [5, 6]. The authors found that the presence of siloxane groups in polystyrene suspensions broadly changed the permeability selectivity of such polymers in terms of the O_2/N_2 gas pair in a range from 2.7 to 4.0. Hence, it was concluded that the structural and chemical factors of lateral siloxane branches affecting the packing and mobility of polymer chains play a decisive role in diffusion processes.

To date, there is a lack of publications related to polyether–polysiloxanes with comb-like structures. In our opinion, silicon phenols based on

a phenolphthalein derivative with a grafted siloxane group are suitable as starting monomers for the production of comb-shaped polyesters and PCS using the polycondensation method [7, 8].

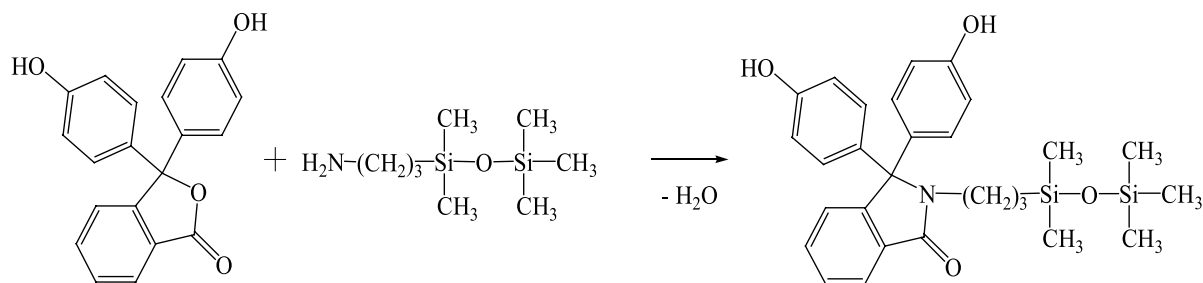
When synthesizing such bis-phenols, it was found [7] that the interaction of phenolphthalein with γ -aminopropylorganosiloxane proceeds according to the classic reaction, i.e., the preparation of siloxane-containing imidine bisphenols (Scheme 1).

However, according to gas–liquid and preparative high-performance liquid chromatography data, this reaction results in an entire range of different products (Scheme 2).

Synthesis excluding the Si–O–Si bond rearrangement, and creating only bis-phenols with a grafted siloxanephthalimidine group, was carried out according to Scheme 3 from *N*-allyl-3,3-bis-(4'-hydroxyphenyl) phthalimidine and monohydridesiloxanes [9].

MATERIALS AND METHODS

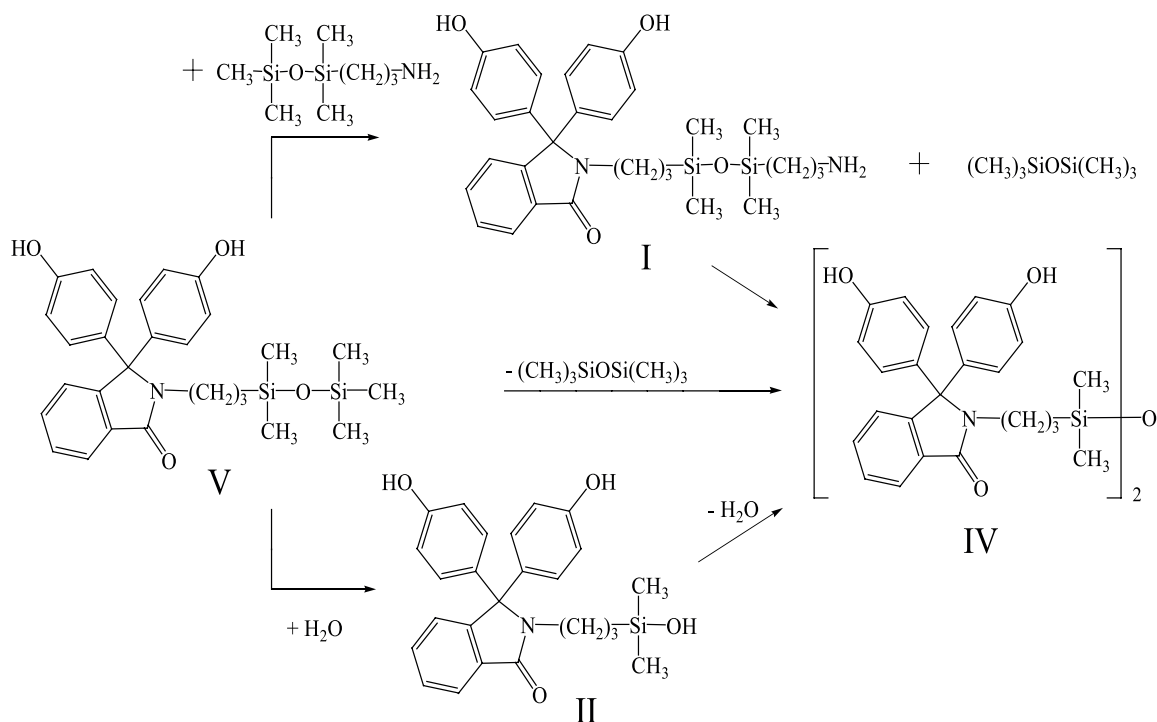
We used *N*-allyl-3,3-bis-(4'-hydroxyphenyl)-phthalimidine obtained by the method developed by S.N. Salazkin.² The chemical purity of *N*-allylphthalimidine after recrystallization (mp = 264–265°C) estimated by proton nuclear magnetic resonance (¹H NMR) was higher than 98 wt %. Monohydridesilanes: pentamethyldisiloxane hydride and heptamethyltrisiloxane hydride (98%, *Penta*, Russia); dichloromethane,



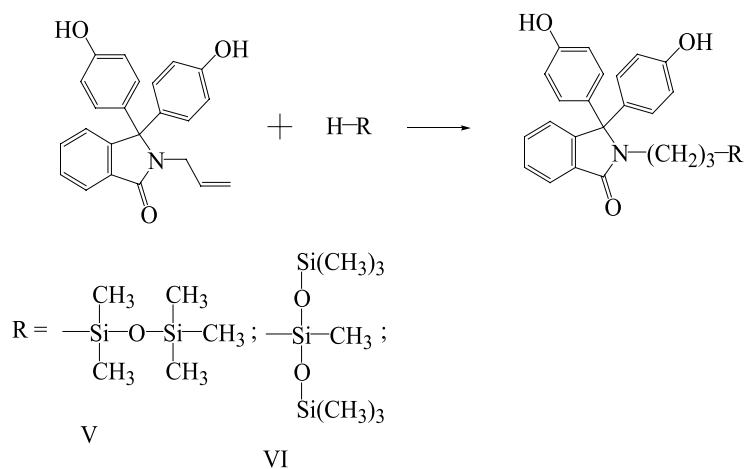
Scheme 1. Reaction of phenolphthalein with γ -aminopropylorganosiloxane.

¹ Raigorodskii I.M., Kirilin A.D. *Poliorgano-polisiloksanovye sopolimery (Polyorgano-Polysiloxanes Copolymers)*. Moscow: MIREA RTU; 2018. 192 p.

² Salazkin S.N. Research in the field of phenolphthalein polyarylates and its derivatives. Cand. Sci. Thesis, Moscow, 1965. 146 p.



Scheme 2. Products of phenolphthalein interaction with γ -aminopropylorganosiloxane.



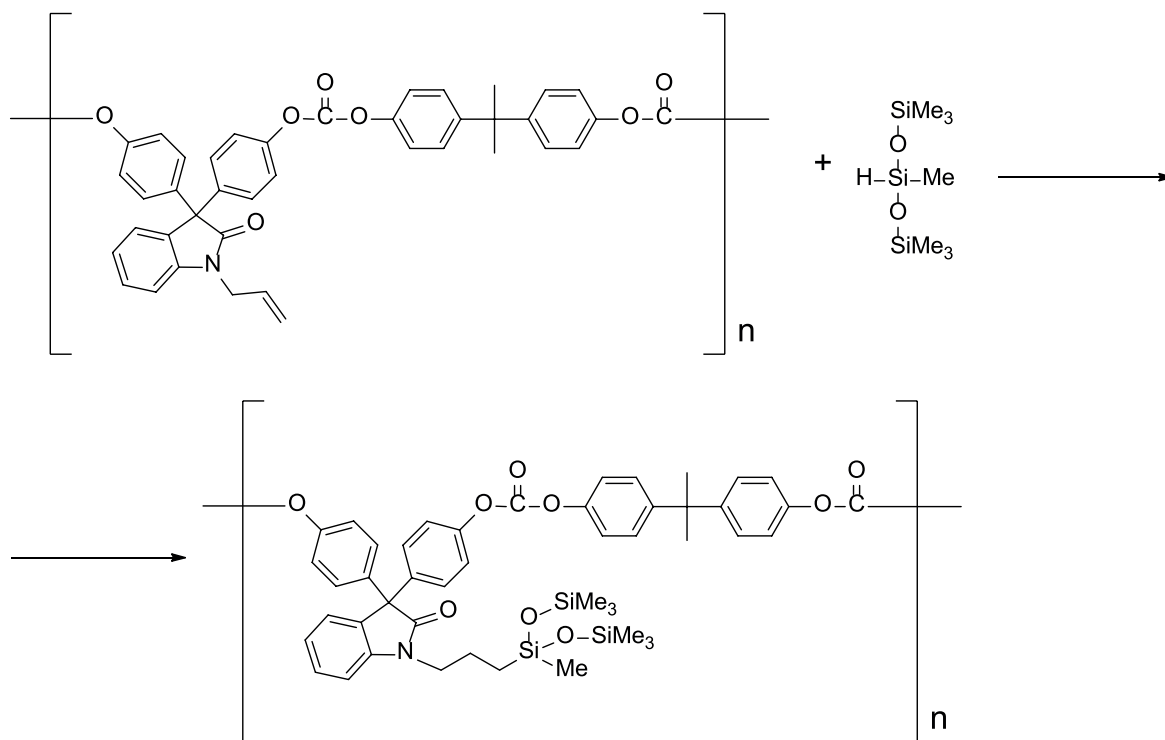
Scheme 3. Reaction excluding the rearrangement of the Si–O–Si bond and creating only bis-phenols with a grafted siloxane phthalimidine group.

dioxane, isopropyl alcohol, hexane, triethylamine (TEA), NaOH (*CHIMMED*, Russia). The ^1H NMR spectra of the products were recorded on a Bruker AT 360 MHz NMR spectrometer (*Bruker*, Germany). Deuterated chloroform, deuterated dimethyl sulfoxide (DMSO), and deuterated acetone (*Astrachem*, Russia) were used as solvents. Bis(chloroformate) diphenylolpropane (BCD) was prepared by adding dropwise liquid phosgene (*Korund*, Russia) in dichloromethane to a solution of diphenylolpropane (*VitaHim*, Russia) in dichloromethane with TEA. After recrystallization of BCD from hexane, bp = 92–94°C. Determination of the content of

chloroformate groups in BCD (solution in dioxane) after the destruction of these groups with a 5% NaOH solution was carried out by potentiometric titration.

The preparation of compounds **V** and **VI** (Scheme 3), which were selected for further syntheses of PCS copolymers, is described below.

Synthesis of phenolphthalein N-[3-(1,1,3,3,3-pentamethyldisiloxane)propyl]phthalimidine of structural formula **V**. A reaction flask was loaded with 7.148 g (0.02 mol) phenolphthalein *N*-allylphthalimidine, 3.264 (0.022 mol) 1,1,3,3,3-pentamethyldisiloxane, 20 mL dioxane, and 1.3 mg of Karstedt's catalyst (*Bayer*, Germany).



Scheme 5. Synthesis of siloxane polycarbonate (PC-SC-I).

dried at 120°C for 5 h. As a result, 9.9 g of PC-SC-I copolymer was obtained.

According to the ¹H NMR data, the ratio of the integral intensities of the proton signal of the phthalimidine ring in the region of 7.89 ppm to -Si(CH₃)₃ protons was 1 : 13.5, and the ratio to the protons of the 4.05–5.20 allyl fragment was 1 : 0.68. Thus, the hydrosilylation conversion was ~75%.

Synthesis of siloxane polycarbonate (PC-SC-II) according to Scheme 6 (option 2) was carried out from *N*-(3-(pentamethyldisiloxane)propyl)-3,3-bis-(4'-hydroxyphenyl)phthalimidine and BCD in a solution using triethylamine as an acceptor of hydrochloric acid. A four-necked flask was charged with 5.8 g (0.01 mol) *N*-(3-(pentamethyldisiloxane)propyl)-3,3-bis-(4'-hydroxyphenyl)phthalimidine, 50 mL dichloromethane, and 2.12 g (0.021 mol) trimethylamine. Additionally, 3.53 g (0.01 mol) BCD, dissolved in 50 mL of dichloromethane, was added dropwise to the mixture. The reaction was carried out at 10°C until the analytical reaction indicated the disappearance of the chloroformate groups. The reaction mixture was washed with a diluted solution of hydrochloric acid and then with water until neutral. The product was precipitated in 300 mL isopropyl alcohol and dried at 120°C for 5 h. As a result, 9.3 g of the copolymer was obtained.

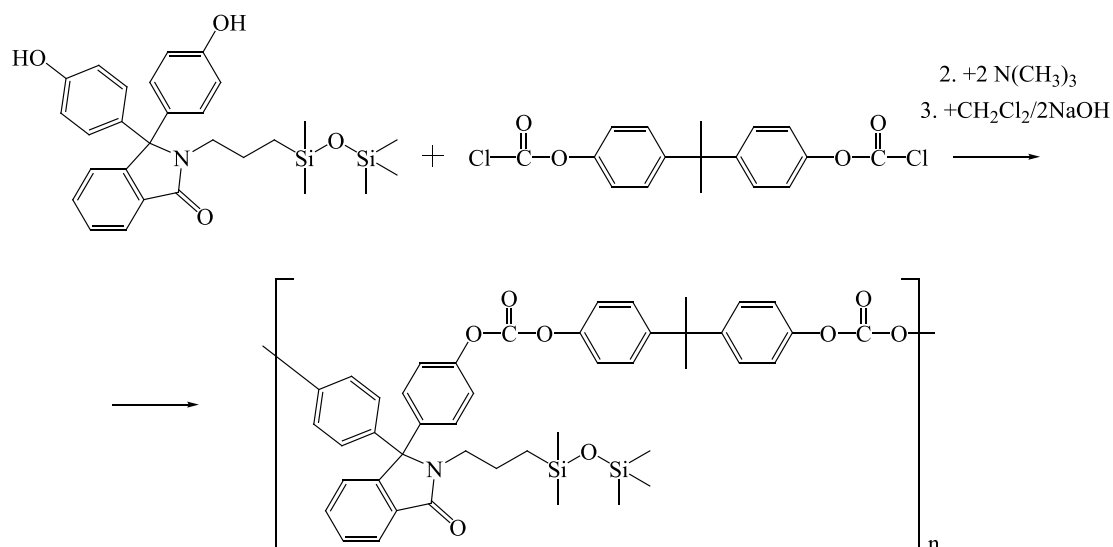
Synthesis of siloxane polycarbonate (PC-SC-III) according to Scheme 6 (option 3) from *N*-(3-(pentamethyldisiloxane)propyl)-3,3-bis-(4'-hydroxyphenyl)phthalimidine and BCD was carried out

by phase-transfer polycondensation. Here 5.8 g (0.01 mol) of *N*-(3-(pentamethyldisiloxane)propyl)-3,3-bis-(4'-hydroxyphenyl)phthalimidine was dissolved in a 1 g (0.025 mol) alkaline solution of NaOH per 100 mL of water. BCD (3.7 g, 0.0105 mol) was dissolved in 100 mL dichloromethane; 0.1 g triethylamine was used as a catalyst. The analytical reaction was carried out at 10°C until the disappearance of the chloroformate groups was indicated. The reaction mixture was washed with a diluted solution of hydrochloric acid and then with water until neutral. The product was precipitated in 300 mL isopropyl alcohol and dried at 120°C for 5 h. Subsequently, 9.5 g of the copolymer was obtained.

Figure 1 shows the NMR spectra of the PC-F and PC-SC-II polymers. Peaks at 1.67 ppm correspond to the CH₃ groups in propane; peaks at 4.1, 4.73, and 5.18 are attributed to the allyl chain; signals at 7.48 and 7.89 are attributed to protons of the phthalimidine ring; signals at 7.14–7.3 are attributed to -CH= of the phenolic fragments. The -0.16 peak is attributed to ≡Si-CH₃ and the 0.01 peak to -Si(CH₃)₃.

RESULTS AND DISCUSSION

The synthesized PCS copolymers were white powdery substances readily soluble in dichloromethane, chloroform, dioxane, tetrahydrofuran, and DMSO. The properties of PCS with lateral siloxane fragments are presented in Table 1.



Scheme 6. Synthesis of siloxane polycarbonate (PC-SC-II) (option 2) and siloxane polycarbonate (PC-SC-III) (option 3).

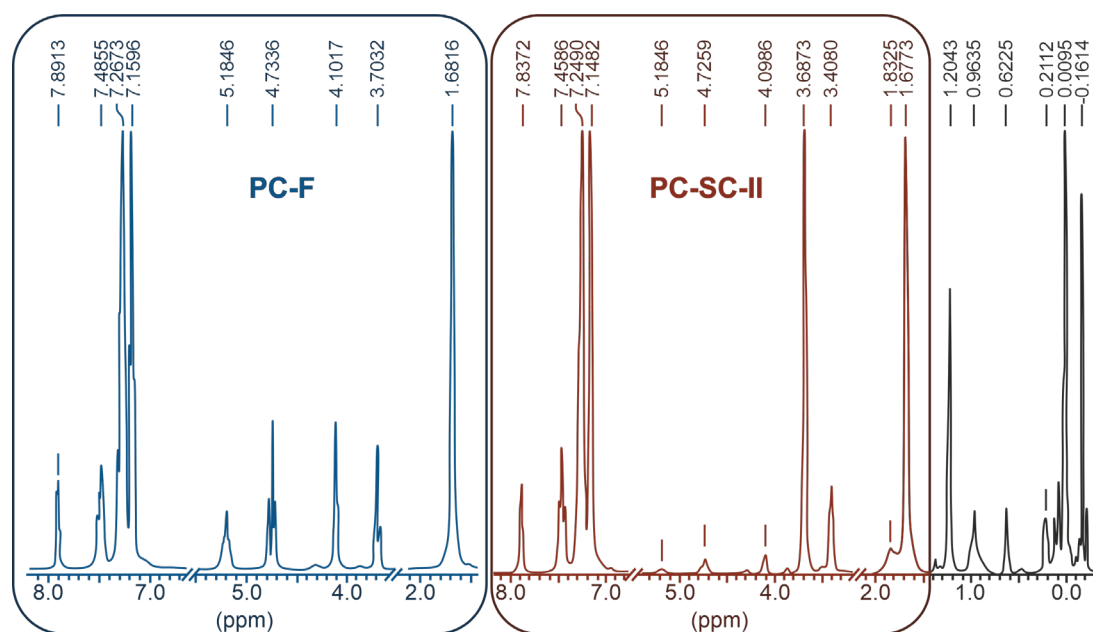


Fig. 1. ¹H NMR spectra of copolymers PC-F and PC-SC-II.

It follows from Table 1 that it is possible to obtain copolymers with maximum viscosity (molar mass) by interfacial polycondensation of product **V** with BCD (Scheme 6, option 3). Copolymers PCS I–III containing 20–23 wt % of dimethylsiloxane units had a glass-transition temperature (T_{glass}) 13°C lower compared with the PC-F copolymer without them. Concurrently, PCS copolymers in the form of films obtained from 1% solutions in dichloromethane, and dried in the air at 20–60°C for 6 h, have a high tensile strength above 50 MPa and an elastic modulus of up

to 2000 Mpa. In addition, the presence of dimethylsiloxane suspensions in PCS copolymers increased the elasticity of the films 1.5-fold.

One possible field of application for newly synthesized PCS copolymers is membrane technology. While conducting this study, it was necessary to evaluate the diffusion properties of PCS, taking into account the fact that PCS copolymers have a high glass-transition temperature, thermal stability, and good mechanical properties. The data on the coefficients of gas permeability through PC-SC-I

Table 1. Physicochemical properties of PC-F and PCS

Polymer cipher	η_{rel} , at 20°C	SiO groups' content, wt %	T_{glass} , °C	T , °C	Mechanical properties of 40- μ m films		
					E_{el} , MPa	σ , MPa	ϵ_{rel} , %
PC-F	0.9	–	175	335	2450	62.8	5.5
PC-SC-I	0.6	20	162	360	1920	58.6	9.0
PC-SC-II	0.4	23	160	355	–	–	–
PC-SC-III	1.3	23	163	358	2000	50	8.0

Note: η_{rel} – relative viscosity; T_{glass} – glass-transition temperature; E_{el} – elastic modulus; σ – tensile strength; ϵ_{rel} – elongation at room temperature, 20–25°C.

Table 2. Permeability and selectivity of PC-SC-I compared with PC and PCS-Ft-11

Sample cipher	Permeability coefficient, barrier						Selectivity of gas separation			
	N ₂	O ₂	CO ₂	He	H ₂	CH ₄	O ₂ /N ₂	CO ₂ / O ₂	CO ₂ / N ₂	H ₂ / CH ₄
PC	0.29	1.48	6.0	–	–	–	5.1	4.1	20.7	–
PCS-Ft-11	0.55	2.66	15.53	18.3	16.6	0.87	4,9	5.8	28.2	18.4
PC-SC-I	0.92	3.92	23.5	24.7	27.1	1.4	4,3	6.0	25.5	19.4

Note: PCS-Ft-11 – fluorine-containing siloxane polycarbonate.

copolymers in the form of a film for N₂, O₂, CO₂, He, H₂, and CH₄ are presented in Table 2 to serve as a comparison with the permeability coefficients for industrial polycarbonates made of diphenylolpropane (PC) and fluorine-containing siloxane polycarbonate (PCS-Ft) [1]. The table shows that the presence of 20 wt % siloxane fragments in the PC-SC-I copolymer makes it possible to obtain a three-to-four-fold increase in permeability for most of the gases under study, without a significant drop in the selectivity of their separation. Additionally, it is possible to increase the permeability up to one-and-a-half times compared with a linear copolymer containing 30 wt % fluorosiloxane blocks.

CONCLUSIONS

New comb-shaped polycarbonate siloxanes were synthesized based on monomeric *N*-phthalimidine containing siloxy units using three polycondensation methods. It was shown that these products had high levels of thermal stability, strength properties, gas

permeability, and selectivity, categories in which it outperformed linear copolymers of this class. Thus, the obtained results for the synthesis of new comb-like PCS, combined with high selectivity of gas separation, make it possible to use them as film membrane materials with an increased operating temperature range.

Financial support

This study did not have any financial support from outside organizations.

Authors' contribution

D.O. Anashkin – consultation on the planning, methodology and implementation of the study;

I.M. Raigorodskii – analysis and selection of publications, writing the text of the article, formalization of the list of references;

A.D. Kirilin – consultation on chemistry of organosilicon compounds and individual stages of research;

P.A. Storozhenko – idea and design of the study, consulting on all stages of research.

The authors declare no conflicts of interest.

REFERENCES

1. Kirilin A.D., Belova L.O., Kirilina N.I., Petrogradsky A.V., Shembel N.L. Peculiarities of isocyanates interaction with hydrazine derivatives. *Tonk. Khim. Tekhnol. = Fine Chem. Technol.* 2018;13(4):39–49 (in Russ.). <https://doi.org/10.32362/2410-6593-2018-13-4-39-49>
2. Noshay A., McGrath J.E. *Block copolymers*. New York: Academic Press; 1977. 516 p.
3. Sergeev V.A., Shitikov V.K., Abbasov G.U. Organosilicon compounds having reactive hydroxyphenyl groups and polymers synthesized from them. *Reviews. Polymer Science USSR*. 1987;29(11):2689–2708. [https://doi.org/10.1016/0032-3950\(87\)90249-8](https://doi.org/10.1016/0032-3950(87)90249-8)
[Sergeev V.A., Shitikov V.K., Abbasov G.U. Organosilicon compounds having reactive hydroxyphenyl groups and polymers synthesized from them. *Reviews. Vysokomolekul. Soed. Ser. A*. 1987;29(11):2441–2455 (in Russ.).]
4. Lim S.-C., Kim S.-W., Jung M.-H., Cho M.-K. Complete NMR spectral assignments of siloxanol based copolycarbonate including the configurational copolymer structure and the determination of each monomer conversion. *J. Mol. Struct.* 2008;886(1):166–174. <https://doi.org/10.1016/j.molstruc.2007.11.012>
5. Kawakami Y., Kamiya H., Toda H., Yamashita Y. The role of *p*-oligosiloxane substituents of polystyrene in selective oxygen permeation through the polymer film. *J. Polym. Sci., Part A: Polym. Chem.* 1987;25(12):3191–3197. <https://doi.org/10.1002/pola.1987.080251202>
6. Kawakami Y., Yamashita Y. Molecular design of polymeric systems for oxygen permeaselective membrane materials. *Mem. Fac. Eng. Nagoya Univ.* 1987;39(1):62–91.
7. Anashkin D.O., Raigorodskii I.M., Kopylov V.M. Reaction of γ -(aminopropyl)siloxanes with phenolphthalein as a route of new siloxane-containing phenols. *Russ. J. Appl. Chem.* 2014;87(2):207–213. <https://doi.org/10.1134/S1070427214020141>
[Anashkin D.O., Raigorodskii I.M., Kopylov V.M., Kovyazin V.A., Boev V.V., Sokolik V.N. Reaction of γ -(aminopropyl)siloxanes with phenolphthalein as a route of new siloxane-containing phenols. *Zhurn. prikl. khimii*. 2014;87(2):227–233 (in Russ.).]
8. Anashkin D.O., Raigorodskii I.M., Kopylov V.M. Polyorganoester polysiloxanes. *Plasticheskie massy*. 2012;12:24–35 (in Russ.).
9. Raigorodskii I.M., Anashkin D.O., Kopylov V.M., Kovyazin V.A. Phenol-organosiloxanes and method for production thereof: RF Patent RU2487901C1. 2013.
10. Zerewitinoff Th. Quantitative Bestimmung des aktiven Wasserstoffs in organischen Verbindungen. *Berichte der Deutschen Chemischen Gesellschaft*. 1908;41:2233–2243. <https://doi.org/10.1002/cber.190804102126>

About the authors:

Dmitrii O. Anashkin, Postgraduate Student, Andrianov Department of Chemistry and Technology of Organoelement Compounds, M.V. Lomonosov Institute of Fine Chemical Technologies, MIREA – Russian Technological University (78, Vernadskogo pr., Moscow, 119571, Russia). E-mail: dianol86@yandex.ru. Scopus Author ID 55956747400.

Igor M. Raigorodskii, Dr. Sci. (Chem.), Professor, Head of the Laboratory at the Andrianov Department of Chemistry and Technology of Organoelement Compounds, M.V. Lomonosov Institute of Fine Chemical Technologies, MIREA – Russian Technological University (78, Vernadskogo pr., Moscow, 119571, Russia). E-mail: imraygor@rambler.ru. Scopus Author ID 6602110677.

СПИСОК ЛИТЕРАТУРЫ

1. Кирилин А.Д., Белова Л.О., Кирилина Н.И., Петроградский А.В., Шембель Н.Л. Особенности взаимодействия изоцианатов с производными гидразина. *Тонкие химические технологии*. 2018;13(4):39–49. <https://doi.org/10.32362/2410-6593-2018-13-4-39-49>
2. Ношей А., Мак-Грат Дж. *Блок-сополимеры*. Пер с англ. М.: Мир; 1980. 487 с.
3. Сергеев В.А., Шитиков В.К., Аббасов Г.У. Кремнийорганические соединения с реакционноспособными гидроксифенильными группировками и полимеры на их основе. *Высокомолекулярные соединения. Серия А*. 1987;29(11):2441–2455.
4. Lim S.-C., Kim S.-W., Jung M.-H., Cho M.-K. Complete NMR spectral assignments of siloxanol based copolycarbonate including the configurational copolymer structure and the determination of each monomer conversion. *J. Mol. Struct.* 2008;886(1):166–174. <https://doi.org/10.1016/j.molstruc.2007.11.012>
5. Kawakami Y., Kamiya H., Toda H., Yamashita Y. The role of *p*-oligosiloxane substituents of polystyrene in selective oxygen permeation through the polymer film. *J. Polym. Sci., Part A: Polym. Chem.* 1987;25(12):3191–3197. <https://doi.org/10.1002/pola.1987.080251202>
6. Kawakami Y., Yamashita Y. Molecular design of polymeric systems for oxygen permeaselective membrane materials. *Mem. Fac. Eng. Nagoya Univ.* 1987;39(1):62–91.
7. Анашкин Д.О., Райгородский И.М., Копылов В.М. Исследование взаимодействия γ -(аминопропил)силоксанов с фенолфталеином при синтезе новых силоксансодержащих фенолов. *Журн. прикладной химии*. 2014;87(2):227–233.
8. Анашкин Д.О., Райгородский И.М., Копылов В.М. Полиорганоефир-полисилоксаны. *Пластические массы*. 2012;12:24–35.
9. Райгородский И.М., Анашкин Д.О., Копылов В.М., Ковязин В.А. Фенолорганосилоксаны и способ их получения: пат. РФ 2 487 901. Заявка № 2012129698/04; заявл. 16.07.2012; опубл. 20.07.2013.
10. Zerewitinoff Th. Quantitative Bestimmung des aktiven Wasserstoffs in organischen Verbindungen. *Berichte der Deutschen Chemischen Gesellschaft*. 1908;41:2233–2243. <https://doi.org/10.1002/cber.190804102126>

Aleksei D. Kirilin, Dr. Sci. (Chem.), Professor, Head of the Andrianov Department of Chemistry and Technology of Organoelement Compounds, M.V. Lomonosov Institute of Fine Chemical Technologies, MIREA – Russian Technological University (78, Vernadskogo pr., Moscow, 119571, Russia). E-mail: kirilinada@rambler.ru. Scopus Author ID 6603604447, ResearcherID O-9744-215.

Pavel A. Storozhenko, Academician at the Russian Academy of Sciences, Dr. Sci. (Chem.), Professor, General Director of State Scientific Research Institute of Chemistry and Technology of Organoelement Compounds (38, Entuziastov shosse, Moscow, 111123, Russia). E-mail: bigpastor@mail.ru. Scopus Author ID 9633186700, ResearcherID D-4645-214.

Об авторах:

Анашкин Дмитрий Олегович, аспирант кафедры химии и технологии элементоорганических соединений Института тонких химических технологий им. М.В. Ломоносова ФГБОУ ВО «МИРЭА – Российский технологический университет» (119571, Россия, Москва, пр-т Вернадского, д. 78). E-mail: dianol86@yandex.ru. Scopus Author ID 55956747400.

Райгородский Игорь Михайлович, д.х.н., заведующий лабораторией кафедры химии и технологии элементоорганических соединений Института тонких химических технологий им. М.В. Ломоносова ФГБОУ ВО «МИРЭА – Российский технологический университет» (119571, Россия, Москва, пр-т Вернадского, д. 78). E-mail: imraygor@rambler.ru. Scopus Author ID 6602110677.

Кирилин Алексей Дмитриевич, д.х.н., профессор, заведующий кафедрой химии и технологии элементоорганических соединений Института тонких химических технологий им. М.В. Ломоносова ФГБОУ ВО «МИРЭА – Российский технологический университет» (119571, Россия, Москва, пр-т Вернадского, д. 78). E-mail: kirilinada@rambler.ru. Scopus Author ID 6603604447, ResearcherID O-9744-215.

Стороженко Павел Аркадьевич, академик РАН, д.х.н., профессор, генеральный директор ГНЦ РФ АО «Государственный научно-исследовательский институт химии и технологии элементоорганических соединений» (111123, Россия, Москва, шоссе Энтузиастов, д. 38). E-mail: bigpastor@mail.ru. Scopus Author ID 9633186700, ResearcherID D-4645-214.

The article was submitted: August 31, 2020; approved after reviewing: October 14, 2020; accepted for publication: January 17, 2021.

Translated from Russian into English by M. Povorin

Edited for English language and spelling by Enago, an editing brand of Crimson Interactive Inc.

CHEMISTRY AND TECHNOLOGY OF ORGANIC SUBSTANCES

ХИМИЯ И ТЕХНОЛОГИЯ ОРГАНИЧЕСКИХ ВЕЩЕСТВ

ISSN 2686-7575 (Online)

<https://doi.org/10.32362/2410-6593-2020-16-1-26-35>



UDC 547.568

RESEARCH ARTICLE

Para-tert-butylcumene synthesis

Elizaveta M. Yarkina¹, Ekaterina A. Kurganova^{1,@}, Aleksandr S. Frolov¹, Georgiy N. Koshel¹, Tatyana N. Nesterova², Vladimir A. Shakun², Stanislav A. Spiridonov²

¹Yaroslavl State Technical University, Yaroslavl, 150023 Russia

²Samara State Technical University, Samara, 443100 Russia

@Corresponding author, e-mail: kurganova@ystu.ru

Abstract

Objectives. This study describes a new approach to obtain *para-tert-butylcumene* by alkylation of cumene with isobutylene in the presence of catalysts, such as Amberlyst 36 Dry, KU-2-8, aluminum chloride, and *tert-butyl alcohol* and concentrated sulfuric acid.

Methods. To determine the qualitative and quantitative composition of the compounds and reaction masses, the following analysis methods were used: gas–liquid chromatography (on the Kristall 2000M hardware-software complex), chromatomass spectrometry on an Agilent 6850 instrument equipped with an Agilent 19091S-433E capillary column (30 m × 250 μm × 0.25 μm), and nuclear magnetic resonance spectroscopy (on a Bruker DRX 400 instrument with an operating frequency of 400 MHz).

Results. A significant quantity of *meta-tert-butylcumene* was obtained by the alkylation of cumene with isobutylene using several catalysts, along with *para-tert-butylcumene*. This study also showed that the use of the catalysts Amberlyst 36 Dry and KU-2-8 during alkylation in a closed system (autoclave) led to the formation of isobutylene oligomers, often in quantity greater than the target reaction product. Simultaneously, the alkylation of cumene with *tert-butyl alcohol* in the presence of concentrated sulfuric acid enabled the obtainment of only one isomer, *para-tert-butylcumene*, which is essential for the further production of high-purity *para-tert-butyl phenol*.

Conclusions. Sulfuric acid alkylation of cumene with *tert-butyl alcohol* enabled the obtainment of an individual *para*-isomer of *tert-butylcumene* with a yield of 87–89% for the loaded *tert-butyl alcohol* with a cumene conversion of ~30%.

Keywords: *para-tert-butylcumene*, isobutylene, *tert-butyl alcohol*, alkylation

For citation: Yarkina E.M., Kurganova E.A., Frolov A.S., Koshel G.N., Nesterova T.N., Shakun V.A., Spiridonov S.A. *Para-tert-butylcumene synthesis*. *Tonk. Khim. Tekhnol. = Fine Chem. Technol.* 2021;16(1):26–35 (Russ., Eng.). <https://doi.org/10.32362/2410-6593-2021-16-1-26-35>

НАУЧНАЯ СТАТЬЯ

Синтез *пара-трет-бутилкумола*

Е.М. Яркина¹, Е.А. Курганова^{1,@}, А.С. Фролов¹, Г.Н. Кошель¹, Т.Н. Нестерова², В.А. Шакун², С.А. Спиридонов²

¹Ярославский государственный технический университет, Ярославль, 150023 Россия

²Самарский государственный технический университет, Самара, 443100 Россия

@Автор для переписки, e-mail: kurganova@yustu.ru

Аннотация

Цели. В статье рассматривается возможность получения *пара-трет-бутилкумола* алкилированием *кумола* *изобутиленом* в присутствии таких катализаторов, как Amberlyst 36 Dry, КУ-2-8, хлористый алюминий, и *трет-бутиловым спиртом* в присутствии концентрированной серной кислоты.

Методы. Для определения качественного и количественного состава веществ и реакционных масс использованы следующие методы анализа: газожидкостная хроматография (на аппаратно-программном комплексе «Кристалл 2000М»), хромато-масс-спектрометрия (на приборе Agilent 6850, оснащённом капиллярной колонкой Agilent 19091S-433E (30 м × 250 мкм × 0.25 мкм) и спектроскопия ядерного магнитного резонанса (на приборе «Bruker DRX 400» с рабочими частотами 400 МГц).

Результаты. Установлено, что в процессе алкилирования *кумола* *изобутиленом* с использованием перечисленных катализаторов наряду с *пара-трет-бутилкумолем* образуется значительное количество *мета-трет-бутилкумола*. Также исследования показали, что применение катализаторов Amberlyst 36 Dry и КУ-2-8 при алкилировании в замкнутой системе (автоклав) приводит к образованию олигомеров *изобутилена*, количество которых многократно преобладает над целевым продуктом реакции. В то же время установлено, что алкилирование *кумола* *трет-бутиловым спиртом* в присутствии концентрированной серной кислоты позволяет получать только один изомер – *пара-трет-бутилкумол*, что имеет важное практическое значение для дальнейшего получения *пара-трет-бутилфенола* с высокой степенью чистоты.

Выводы. Сернокислотное алкилирование *кумола* *трет-бутиловым спиртом* позволяет получить индивидуальный *пара-изомер трет-бутилкумола* с выходом 87–89% на загруженный *трет-бутиловый спирт* при конверсии *кумола* около 30%.

Ключевые слова: *пара-трет-бутилкумол*, *изобутилен*, *трет-бутиловый спирт*, алкилирование

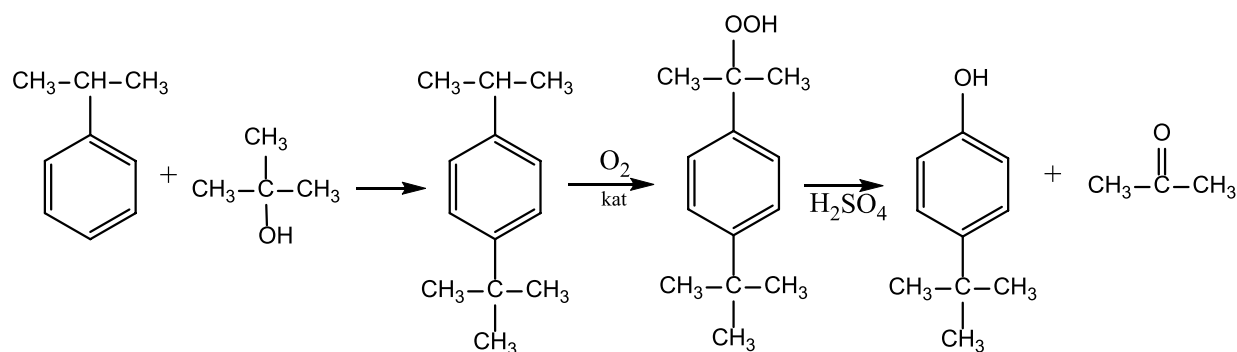
Для цитирования: Яркина Е.М., Курганова Е.А., Фролов А.С., Кошель Г.Н., Нестерова Т.Н., Шакун В.А., Спиридонов С.А. Синтез *пара-трет-бутилкумола*. Тонкие химические технологии. 2020;16(1):26–35. <https://doi.org/10.32362/2410-6593-2021-16-1-26-35>

INTRODUCTION

Alkyl- and dialkylaromatic hydrocarbons containing an isopropyl fragment in their structures are valuable products in the petrochemical synthesis. The oxidative transformations of these hydrocarbons underlie the synthesis of various (alkyl)phenols [1–6], among which *para-tert-butylphenol* is of particular interest. Its scope of application is constantly expanding, covering the production of

antioxidants, pesticides, rubbers, lacquers, paints, and pharmaceuticals [8–13]. The most promising areas of the *para-tert-butylphenol* use are the production of phenolic resin used in glued leather products, and the production of calixarenes based on it [14, 15].

Currently, *para-tert-butylphenol* is industrially obtained by the alkylation of phenol with isobutylene in the presence of ion-exchange resins or macroporous sulfocationites of the Amberlyst type [16]. However, the main limitation of this method is the low selectivity



Scheme. Method for the obtainment of *para-tert*-butylphenol.

of the *para-tert*-butylphenol formation (70–75%). Along with *para-tert*-butylphenol, *ortho*- and *meta*-isomers are also formed owing to the similar boiling points of these species, which significantly complicates the separation of *para-tert*-butylphenol from the reaction mixture with a sufficiently high degree of purity.

An alternative method for the synthesis of *para-tert*-butylphenol based on the selective preparation of *para-tert*-butylcumene (*para-TBC*) is proposed, which excludes the formation of *ortho*- and *meta*-isomers of *tert*-butylphenol [17]. The subsequent liquid-phase oxidation of *para-TBC* into tertiary hydroperoxide and its acid decomposition leads to the production of *para-tert*-butylphenol and acetone (Scheme).

In this study, the issues related to the investigation of several regularities in the synthesis of *para-TBC* by alkylation of cumene with isobutylene and *tert*-butyl alcohol in the presence of various catalysts are discussed.

MATERIALS AND METHODS

The reagents *tert*-butyl alcohol (AR, TU 2632-127-44493179-08) produced by *ECOS-I* (Russia), sulfuric acid (CP, GOST 4204-77) produced by *Sigma Tech* (Russia), cumene 99.9% extra pure produced by *Acros Organics* (USA) were used. Isobutylene (99.95% (mass), grade “A”), the sulfocationites KU-2-8 and Amberlyst 36 Dry, and the $AlCl_3$ catalyst (99.0% (mass)) were provided by *NNK* (Russia).

The main method for the reaction mixture analysis was gas–liquid chromatography. The chromatographic analysis was performed on a Kristall 2000M device (*Chromatec*, Russia) with Chromatec-Analyst hardware and software complex, equipped with a flame ionization detector, a gas flow divider, and a quartz capillary column (60 m × 250 μm × 0.25 μm) with a grafted stationary phase SE-30. Helium was used as the carrier gas. The carrier gas pressure at the column inlet was 3 atm, and the pressure stability was ensured by double reduction. The temperature profile was as follows: isotherm 333 K-10 min, temperature rise 20 K/min, isotherm 413 K-40 min. The temperatures of the evaporator and detector were 230°C and 260°C, respectively.

The components of the alkylation reaction mixtures were identified by gas chromatography combined with mass spectrometry (GC–MS). GC–MS analysis was performed on an Agilent 6850 gas chromatograph (*Agilent*, USA) equipped with an Agilent 19091S-433E capillary column (30 m × 250 μm × 0.25 μm) with a fixed phase of HP-5MS (5% diphenylpolysiloxane + 95% dimethylpolysiloxane) and an Agilent 5975C VL MSD mass-selective detector at an ionizing voltage of 70 eV. The identification of the reaction products was performed through the analysis of the mass spectra of the compounds using the rules and approaches described by Lebedev [18], and also the data from the NIST2017 library [19].

The nuclear magnetic resonance (NMR) spectra were recorded using a Bruker DRX 400 NMR spectrometer (*Bruker*, USA; 400 MHz frequency). A mixture of $DMSO-d_6-CCl_4$ was used as a solvent. Tetramethylsilane was used as the internal standard.

EXPERIMENTAL

Obtaining *para-tert*-butylcumene

Method 1. Alkylation of cumene with *tert*-butyl alcohol in the presence of concentrated sulfuric acid

The alkylation was performed in a round-bottomed three-necked flask equipped with a stirrer, a thermometer, and immersed in a water bath. The calculated quantity of concentrated sulfuric acid was slowly added to the loaded hydrocarbon. Next, *tert*-butyl alcohol was added drop by drop at a given temperature and continuous stirring (the rotation speed of the agitator was 250 rpm) using a separating funnel. After the reaction mixture was transferred to a separating funnel and sulfuric acid layer separated from the hydrocarbon layer, the latter was washed with distilled water until a neutral environment was achieved and dried over calcium chloride. The resulting alkylate was analyzed on a Crystal 2000M gas–liquid chromatograph and subjected to rectification under vacuum.

The synthesized *para-TBC* showed the following constants: $T_{boil} = 217^\circ C$ [19]. 1H NMR spectrum

(δ , ppm, J , Hz): 7.28 d (2H (arom.), H-2, H-6, $3J = 8.1$), 7.14 d (2H (arom.), H-3, H-5, $3J = 8.1$), 2.8–2.9 septet (1H, CH (isopropyl), $3J = 6.8$); 1.25 c (9H, C(CH₃)₃), 1.18 d (6H, 2CN₃ (isopropyl), $3J = 6.8$).

Method 2. Alkylation of cumene with isobutylene

The first method was a liquid-phase alkylation performed in a closed-type reactor (autoclave) using two grades of sulfocationites—KU-2-8 and Amberlyst 36 Dry (A36Dry) as catalysts.

In this method, alkylation was performed in reactors of the “glass ampoule with a screw cap” type manufactured by SamSTU glass-blowing workshop. The diagram is shown below (Fig. 1). Sealed cylindrical batch reactors were fabricated using molybdenum glass with a volume of 4–5 mL, internal diameter of 6 mm, and a wall thickness of 2 mm.

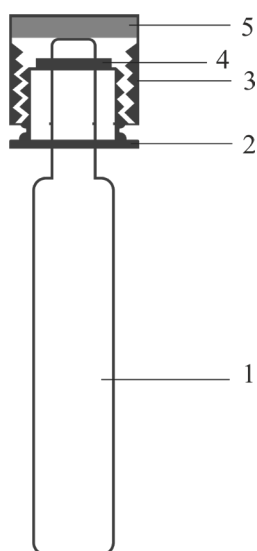


Fig. 1. Alkylation reactor:

- (1) molybdenum glass reactor, (2) metal bearing, (3) swivel nut, (4) copper ring, (5) gasket seal.

The second method was a gas-phase alkylation performed in a tubular flow-type reactor manufactured in the SamSTU glass-blowing workshop (Fig. 2). Cumene was added to the top of the reactor ($v_{\text{vol}} = 5$ mL/min) from a graduated separation funnel, and isobutylene was added to the bottom of the gas cylinder through a rheometer and a calibrated capillary ($v_{\text{vol}} = 120$ mL/min). A tank for collecting the alkylation product was also provided in the lower part of the reactor. The process was performed at atmospheric pressure, and the unreacted isobutylene was removed using a reverse refrigerator installed in the upper part of the reactor. The volume of the reaction zone filled with the A36Dry catalyst was 5 cm³.

Method 3. The third method was liquid-phase alkylation of cumene with isobutylene in the presence of aluminum chloride in a reactor containing a stirrer

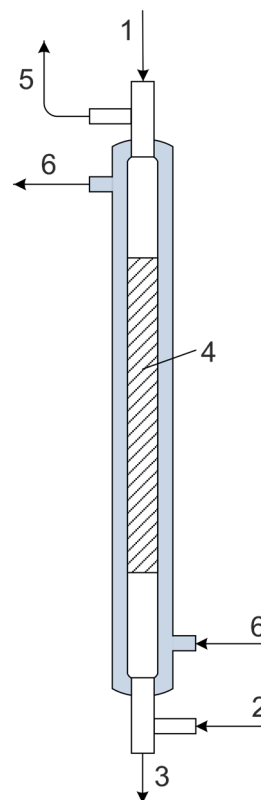


Fig. 2. Scheme of flow tubular reactor:
(1) IPB feeding, (2) isobutylene feeding, (3) alkylate to receiver, (4) catalyst bed, (5) vent gas, (6) heat carrier.

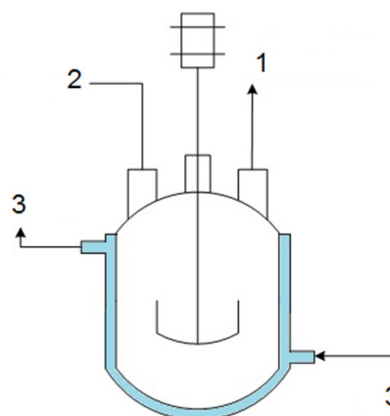


Fig. 3. Scheme of the jacketed reactor with stirrer:
(1) to reflux condenser, (2) for samples collection, (3) heat carrier.

and a jacket for the coolant, also manufactured in the SamSTU glass-blowing workshop (Fig. 3). The process was performed at atmospheric pressure, and the unreacted isobutylene was removed through a return cooler installed in the upper part of the reactor.

RESULTS AND DISCUSSION

Although extensive information is available on the regularities of the alkylation of aromatic hydrocarbons by olefins or alcohols, insufficient data on the synthesis of *para*-TBC have been reported. A method for the alkylation of cumene with isobutylene on tableted montmorillonite clay at elevated pressure and temperature of 135°C was described, and the product yield was 71.1% under these conditions [20]. An alternative method using alkylation of cumene with 1-butene or 2-butene on HZSM-12 zeolite at 200°C and pressure of 20 atm was also described, achieving 95% of selectivity for the alkylating agent in the *para*-position, the remaining 5% was alkylated in the *meta*-position [21]. The formation of a large number of by-products, (i.e., *ortho-tert-butylcumene*, *meta-tert-butylcumene*, diisopropylbenzene, isopropyltoluene, among others) along with *para*-TBC, makes necessary the use of complex systems for isolating the target product. Therefore, the search for selective methods to synthesize *para*-TBC is important, aiming for further implementation

of the technology for the joint production of *para*-TBC and acetone.

In this regard, initial attempts were made to obtain *para*-TBC by alkylation of cumene with isobutylene. As can be seen from Table 1, the alkylation of cumene with isobutylene, in open and closed systems in the presence of the A36Dry catalyst, was not selective and was accompanied by the formation of the *meta*-TBC and *para*-TBC. The ratio of *meta*- and *para*-isomers was 0.12–0.17. The use of aluminum chloride as a catalyst contributed to an even more intensive formation of *meta*-TBC and led to an increase in the ratio of *meta*- and *para*-isomers of TBC up to 0.72.

The alkylation in a closed system using A36Dry and KU-2-8 catalysts was followed by a substantial formation of isobutylene oligomers. The analysis of the reaction products demonstrated that the content of oligomers significantly exceeds the content of the *para*-TBC target product. The transition to gas-phase alkylation in a tubular flow-type reactor using an A36Dry catalyst and liquid-phase alkylation in a stirrer reactor using AlCl₃ reduced the formation of

Table 1. Alkylation of cumene with isobutylene in the presence of various catalysts

Catalyst	Temperature, K	Catalyst concentration, wt %	Reaction time, min	The ratio of <i>m</i> - and <i>p</i> -isomers of TBC
A36Dry* (closed system – autoclave)	353	5.0	60	no alkylation
	373	5.0	5/10/15/30/90	0.12–0.17
	393	5.0	15/30/60/90/120	
	393	25.0	30/60/90/120	
KY-2-8* (closed system)	393	5.0	30/60/90/120	0.12–0.15
	393	25.0	30/60/90/120	
A36Dry** (flow system)	393	–	1	0.12–0.15
	373	–	1	
AlCl ₃ ** (liquid-phase alkylation, open system)	303	0.25	90	0.41
			150	0.41
			180	0.40
	303	0.5	40	0.68
			80	0.68
	303	0.75	40	0.72
			100	0.72
			140	0.67

*active formation of isobutylene oligomers;

**oligomers of isobutylene are formed in small amounts, which is ensured by the short residence time of isobutylene in the reaction zone.

isobutylene oligomers to insignificant quantities, which can be explained by the short residence time of isobutylene in the reaction zone.

According to the conducted studies, the obtainment of an individual *para*-isomer of TBC was not possible through the alkylation of cumene with isobutylene in open and closed systems in the presence of A36Dry, KU-2-8, and AlCl₃ catalysts.

Simultaneously, the alkylation of cumene with *tert*-butyl alcohol (TBA) in the presence of concentrated sulfuric acid practically eliminated all the formation of the *meta*-isomer of TBC (Table 2). Therefore, these investigations revealed that this reaction does not follow the usual rules of orientation, despite the mild conditions of the process. This can be explained by the appearance of the steric effect associated with the size of the functional group and the resulting spatial difficulty. According to previously

reported, the ratio of *ortho*- and *para*-isomers in the alkylation of alkylphenols depends on the size of the incoming alkyl group. For example, the ratio of *o*- and *p*-isomers in the alkylation of toluene CH₃Br is 1.9 : 1; (CH₃)₂CHBr—1.2 : 1; C₆H₅CH₂Cl—0.82 : 1; no *ortho*-substitution product was detected during alkylation with *tert*-butyl bromide [22].

Accordingly, when the cumene was alkylated with *tert*-butyl alcohol in a 30 min reaction at 35°C with molar ratio cumene : TBA : H₂SO₄ 3 : 1 : 3, it was possible to synthesize *para*-TBC with a yield of 87–89% on the loaded TBA with a cumene conversion of ~30%. Table 3 shows the material balance of the process.

The *para*-TBC isolated from the reaction mixture can be oxidized to tertiary hydroperoxide, which can be decomposed to produce *para-tert*-butylphenol together with acetone [23].

Table 2. Influence of various parameters on the alkylation of cumene with *tert*-butyl alcohol (TBA) in the presence of sulfuric acid. Cumene : TBA : H₂SO₄ ratio is 3 : 1 : 3

Temperature, °C	Reaction time, h	Cumene conversion, %	<i>para</i> -TBC concentration, wt %	<i>para</i> -TBC yield for the taken <i>tert</i> -butyl alcohol, %
20	0.5	23.6	16.8	71.1
25	0.5	28.2	23.4	82.9
30	0.5	32.9	34.8	89.4
35	0.5	49.0	42.7	87.1
30*	0.5	35.5	14.4	49.0
15	0.25	19.2	12.1	63.0
15	1.0	20.1	12.5	62.0
15	2.0	21.3	13.3	62.4
15	3.0	30.4	13.7	45.0

*the ratio of cumene : TBA : H₂SO₄ is 2 : 1 : 2.

Table 3. Material balance of the process of alkylation of cumene with *tert*-butyl alcohol (TBA) in the presence of concentrated sulfuric acid

Compound	Molar mass, g/mol	Taken		Obtained	
		g	wt %	g	wt %
Cumene	120.19	49.5	49.50	35.37	35.37
TBA	74.12	10.17	10.17	0.00	0.00
H ₂ SO ₄	98.08	40.33	40.33	39.53*	39.53*
<i>para</i> -TBC	176.30	0	0.00	20.47	20.47
<i>di</i> -TBC	233.41	0	0.00	2.33	2.33
Losses	–	0	0.00	2.30	2.30
Total	–	100.00	100.00	100.00	100.00

*mass of acidic layer after reaction.

CONCLUSIONS

In summary, the regularities of the alkylation of cumene reaction with isobutylene in the presence of catalysts such as Amberlyst 36 Dry, KU-2-8, aluminum chloride, and TBA, and concentrated sulfuric acid were investigated. The sulfuric acid alkylation of cumene with TBA produced an individual *para*-isomer of *tert*-butylcumene with a yield of 87–89% on the loaded TBA with a cumene conversion of ~30%. These results confirmed that high-purity *para-tert*-butylphenol can be obtained using the hydroperoxide method based on the aerobic liquid-phase oxidation of *para*-TBC.

Financial support

This study did not have any financial support from outside organizations.

Authors' contribution

E.M. Yarkina – development of the study concepts, development and execution of the experiments, discussion of the results, writing the text of the manuscript;

E.A. Kurganova – development of the study concepts, development of the experiments, data processing, discussion of the results, writing the text of the manuscript;

A.S. Frolov – gas chromatography and mass spectrometry experiment, writing the text of the manuscript;

G.N. Koshel – development of the study concepts, development of the experiments, discussion of the results, writing the text of the manuscript;

T.N. Nesterova – development of the study concepts, development of the experiments, data processing, discussion of the results, writing of the manuscript;

V.A. Shakun – gas chromatography and mass spectrometry experiments, data processing, discussion of the results, writing the text of the manuscript;

S.A. Spiridonov – execution of the experiments, discussion of the results, writing the text of the manuscript.

The authors declare no conflicts of interest.

REFERENCES

1. Kurganova E.A., Sapunov V.N., Koshel G.N., Frolov A.S. Selective aerobic oxidation of cyclohexyl- and *sec*-alkylarenes to hydroperoxides in the presence of *N*-hydroxyphthalimide. *Russ. Chem. Bull.* 2016;65(9):2115–2128. <https://doi.org/10.1007/s11172-016-1560-3>
2. Alonso-Magdalena P., Marroquí L., Tudurí E., Quesada I., Sargis R.M., Nadal A. Toxic Effects of Common Environmental Pollutants in Pancreatic β -Cells and the Onset of Diabetes Mellitus. *Encyclopedia of Endocrine Diseases.* 2019;1:764–775. <https://doi.org/10.1016/B978-0-12-801238-3.64325-8>
3. Saha M. Alkylation of Phenol with *n*-Alcohols (C5–C7) in the Presence of Sulphuric Acid. *Dhaka Univ. J. Sci.* 2010;58(2):247–251.
4. Toor J.S., Sikka S.C. Developmental and Reproductive Disorders—Role of Endocrine Disruptors in Testicular Toxicity. In: Gupta R. (Ed.) *Reproductive and Developmental Toxicology.* Academic Press; 2017. P. 1111–1121. <https://doi.org/10.1016/B978-0-12-804239-7.00059-7>
5. Tungmunnithum D., Thongboonyou A., Pholboon A., Yangsabai A. Flavonoids and Other Phenolic Compounds from Medicinal Plants for Pharmaceutical and Medical Aspects. *Medicines.* 2018;5(3):93. <https://doi.org/10.3390/medicines5030093>
6. Flecknell P., Dyson M.C., Marini R.R., Swindle M., Wilson R.P. Preanesthesia, Anesthesia, Analgesia, and Euthanasia. In: Fox J.G., Otto G.M., Whary M.T. (Eds.). *Laboratory Animal Medicine.* Academic Press; 2015. P. 1135–1200. <https://doi.org/10.1016/B978-0-12-409527-4.00024-9>

СПИСОК ЛИТЕРАТУРЫ

1. Курганова Е.А., Сапунов В.Н., Кошель Г.Н., Фролов А.С. Селективное аэробное окисление циклогексил- и *втор*-алкиларенов до гидропероксидов в присутствии *N*-гидроксифталимида. *Изв. АН. Сер. хим.* 2016;(9):2115–2128.
2. Alonso-Magdalena P., Marroquí L., Tudurí E., Quesada I., Sargis R.M., Nadal A. Toxic Effects of Common Environmental Pollutants in Pancreatic β -Cells and the Onset of Diabetes Mellitus. *Encyclopedia of Endocrine Diseases.* 2019;1:764–775. <https://doi.org/10.1016/B978-0-12-801238-3.64325-8>
3. Saha M. Alkylation of Phenol with *n*-Alcohols (C5–C7) in the Presence of Sulphuric Acid. *Dhaka Univ. J. Sci.* 2010;58(2):247–251.
4. Toor J.S., Sikka S.C. Developmental and Reproductive Disorders—Role of Endocrine Disruptors in Testicular Toxicity. In: Gupta R. (Ed.) *Reproductive and Developmental Toxicology.* Academic Press; 2017. P. 1111–1121. <https://doi.org/10.1016/B978-0-12-804239-7.00059-7>
5. Tungmunnithum D., Thongboonyou A., Pholboon A., Yangsabai A. Flavonoids and Other Phenolic Compounds from Medicinal Plants for Pharmaceutical and Medical Aspects. *Medicines.* 2018;5(3):93. <https://doi.org/10.3390/medicines5030093>
6. Flecknell P., Dyson M.C., Marini R.R., Swindle M., Wilson R.P. Preanesthesia, Anesthesia, Analgesia, and Euthanasia. In: Fox J.G., Otto G.M., Whary M.T. (Eds.). *Laboratory Animal Medicine.* Academic Press; 2015. P. 1135–1200. <https://doi.org/10.1016/B978-0-12-409527-4.00024-9>

7. Dews T.E. 16 Analgesia and Anesthesia for Office Hysteroscopy and Hysteroscopic Procedures. *Hysteroscopy: Office Evaluation and Management of the Uterine Cavity*. 2008;1158:179–185.
8. Sokolov V.Z., Kharlampovich G.D. *Proizvodstvo i ispol'zovanie aromaticheskikh uglevodorodov (Production and use of aromatic hydrocarbons)*. Moscow: Khimiya; 1980. 336 c. (in Russ.).
9. Terekhov A.V., Zhanavskiy L.N., Khadzhiyev S.N. Selecting an Optimum Catalyst for Producing *para-tert*-Butylphenol by Phenol Alkylation with *tert*-Butanol. *Pet. Chem.* 2017;57(8):714–717. <https://doi.org/10.1134/S096554411708014X>
10. Jérôme Fr., Luque R. *Bio-Based Solvents*. Wiley Series in Renewable Resource; 2017. 183 p.
11. Kharayat Y. *Phenols & phenolic compounds*. Parivesh; 2016. 72 p. URL: https://cpcb.nic.in/uploads/News_Letter_Phenols_Phenolic_Compounds_2017.pdf
12. Wang L., Ma W., Lei D., Zhang D. Preparation and characterization of *para-tertiary*-butylphenol formaldehyde resins using dual catalytic-extraction method. *Progress in Organic Coatings*. 2015;87:1–9. <https://doi.org/10.1016/j.porgcoat.2015.04.024>
13. Saha M., Hossain M.K., Ashaduzzama M., Afroza S.T., Galib M., Sharif N. Alkylation of Phenol with Olefins in the Presence of Sulphuric Acid. *Bangladesh J. Sci. Ind. Res.* 2009;44(1):131–136. <https://doi.org/10.3329/bjsir.v44i1.2722>
14. Atwood J.L., Barbour L.J., Thallapally P.K., Wirsig T.B. A crystalline organic substrate absorbs methane under STP conditions. *Chem. Commun.* 2005;1:51–53. <https://doi.org/10.1039/B416752J>
15. Español E.S., Villamil M.M. Calixarenes: Generalities and Their Role in Improving the Solubility, Biocompatibility, Stability, Bioavailability, Detection, and Transport of Biomolecules. *Biomolecules*. 2019;9(3):90. <https://doi.org/10.3390/biom9030090>
16. Voronin I.O., Nesterova T.N., Zhuravskii E.A., Strelchik B.S. Efficiency of sulfonic cation-exchange resins used in *para-tert*-butylphenol production: a comparison based on the kinetics of transalkylation in the phenol-*tert*-butylphenols system. *Kinetics and Catalysis*. 2014;55(6):705–711. <https://doi.org/10.1134/S0023158414060147>
[In Russ.: <https://doi.org/10.7868/S045388111406015X>]
17. Yarkina E.M., Kurganova E.A., Frolov A.S., Lebedeva N.V., Koshel' G.N. Aerobic Liquid-Phase Oxidation of *Para-tert*-Butylcumene to Hydroperoxide. *Pet. Chem.* 2019;59(11):1245–1248. <https://doi.org/10.1134/S0965544119110161>
[In Russ.: <https://doi.org/10.1134/S0028242119060169>]
18. Lebedev A.T. *Mass-spektrometriya v organicheskoi khimii (Mass spectrometry in organic chemistry)*. Moscow: Tekhnosfera; 2015. 704p. ISBN 978-5-94836-409-4
19. NIST Standard Reference Database 1A. NIST/EPA/NIH EI AND NIST TANDEM LIBRARIES (NIST 17) and NIST MASS SPECTRAL SEARCH PROGRAM Version 2.3 Build May 4, 2017 for use with Microsoft(R) Windows(TM) 306,622 EI spectra for 267376 compounds.
20. Zech E.A., Okla B. Alkylation of aromatic hydrocarbons using a compacted montmorellonete clay catalyst: US Patent US3849507A, 1974.
21. Burress G.T. Alkylation of aromatic hydrocarbons: US Patent US4469908A, 1984.
22. Зефирова Н.С., Кулов Н.Н. (ред.) *Химическая энциклопедия: в 5 т. Т. 5: ТРИ-ЯТР*. М.: Большая российская энциклопедия; 1998. 783 с. ISBN 5-85270-310-9
7. Dews T.E. 16 Analgesia and Anesthesia for Office Hysteroscopy and Hysteroscopic Procedures. *Hysteroscopy: Office Evaluation and Management of the Uterine Cavity*. 2008;1158:179–185.
8. Соколов В.З., Харлампович Г.Д. *Производство и использование ароматических углеводородов*. М.: Химия; 1980. 336 с.
9. Terekhov A.V., Zhanavskiy L.N., Khadzhiyev S.N. Selecting an Optimum Catalyst for Producing *para-tert*-Butylphenol by Phenol Alkylation with *tert*-Butanol. *Pet. Chem.* 2017;57(8):714–717. <https://doi.org/10.1134/S096554411708014X>
10. Jérôme Fr., Luque R. *Bio-Based Solvents*. Wiley Series in Renewable Resource; 2017. 183 p.
11. Kharayat Y. *Phenols & phenolic compounds*. Parivesh; 2016. 72 p. URL: https://cpcb.nic.in/uploads/News_Letter_Phenols_Phenolic_Compounds_2017.pdf
12. Wang L., Ma W., Lei D., Zhang D. Preparation and characterization of *para-tertiary*-butylphenol formaldehyde resins using dual catalytic-extraction method. *Progress in Organic Coatings*. 2015;87:1–9. <https://doi.org/10.1016/j.porgcoat.2015.04.024>
13. Saha M., Hossain M.K., Ashaduzzama M., Afroza S.T., Galib M., Sharif N. Alkylation of Phenol with Olefins in the Presence of Sulphuric Acid. *Bangladesh J. Sci. Ind. Res.* 2009;44(1):131–136. <https://doi.org/10.3329/bjsir.v44i1.2722>
14. Atwood J.L., Barbour L.J., Thallapally P.K., Wirsig T.B. A crystalline organic substrate absorbs methane under STP conditions. *Chem. Commun.* 2005;1:51–53. <https://doi.org/10.1039/B416752J>
15. Español E.S., Villamil M.M. Calixarenes: Generalities and Their Role in Improving the Solubility, Biocompatibility, Stability, Bioavailability, Detection, and Transport of Biomolecules. *Biomolecules*. 2019;9(3):90. <https://doi.org/10.3390/biom9030090>
16. Воронин И.О., Нестерова Т.Н., Стрельчик Б.С., Журавский Е.А. Сравнение эффективности сульфокатионитов, применяемых в производстве *пара-tert*-бутилфенола, на основе кинетического исследования переалкилирования в системе фенол – *tert*-бутилфенолы. *Кинетика и катализ*. 2014;55(6):723–729. <https://doi.org/10.7868/S045388111406015X>
17. Яркина Е.М., Курганова Е.А., Фролов А.С., Лебедева Н.В., Кошель Г.Н. Аэробное жидкофазное окисление *пара-tert*-бутилкумола до гидропероксида. *Нефтехимия*. 2019;59(6):696–700. <https://doi.org/10.1134/S0028242119060169>
18. Лебедев А.Т. *Масс-спектрометрия в органической химии*. Изд. 2-е, перераб. и доп. М.: Техносфера; 2015. 704с. ISBN 978-5-94836-409-4
19. NIST Standard Reference Database 1A. NIST/EPA/NIH EI AND NIST TANDEM LIBRARIES (NIST 17) and NIST MASS SPECTRAL SEARCH PROGRAM Version 2.3 Build May 4, 2017 for use with Microsoft(R) Windows(TM) 306,622 EI spectra for 267376 compounds.
20. Zech E.A., Okla B. Alkylation of aromatic hydrocarbons using a compacted montmorellonete clay catalyst: US Patent US3849507A, 1974.
21. Burress G.T. Alkylation of aromatic hydrocarbons: US Patent US4469908A, 1984.
22. Зефирова Н.С., Кулов Н.Н. (ред.) *Химическая энциклопедия: в 5 т. Т. 5: ТРИ-ЯТР*. М.: Большая российская энциклопедия; 1998. 783 с. ISBN 5-85270-310-9

22. Zefirov N.S., Kulov N.N. (Eds.) *Khimicheskaya entsiklopediya: v 5 t., V. 5: TRI-YATR (Chemical Encyclopedia: in 5 v., V. 5: TRI-YATR)* Moscow: Bol'shaya Rossiiskaya Entsiklopediya; 1998. 783 p. ISBN 5-85270-310-9.

23. Yarkina E.M., Kurganova E.A., Frolov A.S., Koshel' G.N., Denisova E.M. Acid Decomposition of *p*-tert-Butylcumene Hydroperoxide to *p*-tert-Butylphenol and Acetone. *Russ. J. Appl. Chem.* 2019;92(11)1524–1530. <https://doi.org/10.1134/S1070427219110090>

[In Russ.: <https://doi.org/10.1134/S0044461819110094>]

23. Яркина Е.М., Курганова Е.А., Фролов А.С., Кошель Г.Н., Денисова Е.М. Кислотное разложение гидропероксида *пара-трет*-бутилкумола до *пара-трет*-бутилфенола и ацетона. *Журн. прикл. химии.* 2019;92(11)1427–1434. <https://doi.org/10.1134/S0044461819110094>

About the authors:

Elizaveta M. Yarkina, Postgraduate Student, Department of General and Physical Chemistry, Yaroslavl State Technical University (88, Moskovskii pr., Yaroslavl, 150023, Russia). E-mail: yarkina.elizaveta@gmail.com. <https://orcid.org/0000-0001-9719-3467>

Ekaterina A. Kurganova, Dr. Sci. (Chem.), Professor, Department of General and Physical Chemistry, Yaroslavl State Technical University (88, Moskovskii pr., Yaroslavl, 150023, Russia). E-mail: kurganova@ystu.ru. ResearcherID B-4021-2018, Scopus Author ID 24338325800, <http://orcid.org/0000-0002-0087-1784>

Aleksandr S. Frolov, Cand. Sci. (Chem.), Senior Lecturer, Department of General and Physical Chemistry, Yaroslavl State Technical University (88, Moskovskii pr., Yaroslavl, 150023, Russia). E-mail: frolovas.11@ystu.ru. ResearcherID I-8533-2018, Scopus Author ID 56412435400, <https://orcid.org/0000-0002-0491-7452>

Georgiy N. Koshel, Dr. Sci. (Chem.), Professor, Department of General and Physical Chemistry, Yaroslavl State Technical University (88, Moskovskii pr., Yaroslavl, 150023, Russia). E-mail: koshelgn@ystu.ru. ResearcherID I-7782-2017, Scopus Author ID 6506863584, <https://orcid.org/0000-0002-1020-4643>

Vladimir A. Shakun, Assistant, Department of Technology of Organic and Petrochemical Synthesis, Samara State Technical University (244, Molodogvardeiskaya ul., Samara, 443100, Russia). E-mail: shakyh@mail.ru. Scopus Author ID 56829536300, <https://orcid.org/0000-0003-2682-3024>

Tatyana N. Nesterova, Cand. Sci. (Chem.), Associate Professor, Professor, Department of Technology of Organic and Petrochemical Synthesis, Samara State Technical University (244, Molodogvardeiskaya ul., Samara, 443100, Russia). E-mail: nesterovatn@yandex.ru. Scopus Author ID 15045158000, <https://orcid.org/0000-0002-3496-1075>

Stanislav A. Spiridonov, Master Student, Department of Technology of Organic and Petrochemical Synthesis, Samara State Technical University (244, Molodogvardeiskaya ul., Samara, 443100, Russia).

Об авторах:

Яркина Елизавета Михайловна, аспирант кафедры «Общая и физическая химия» ФГБОУ ВО «Ярославский государственный технический университет» (115023, Россия, Ярославль, Московский проспект, 88). E-mail: yarkina.elizaveta@gmail.com. <https://orcid.org/0000-0001-9719-3467>

Курганова Екатерина Анатольевна, д.х.н., профессор кафедры «Общая и физическая химия» ФГБОУ ВО «Ярославский государственный технический университет» (115023, Россия, Ярославль, Московский проспект, 88). E-mail: kurganova@ystu.ru. ResearcherID B-4021-2018, Scopus Author ID 24338325800, <http://orcid.org/0000-0002-0087-1784>

Фролов Александр Сергеевич, к.х.н., старший преподаватель кафедры «Общая и физическая химия» ФГБОУ ВО «Ярославский государственный технический университет» (115023, Россия, Ярославль, Московский проспект, 88). E-mail: frolovas@ystu.ru. ResearcherID I-8533-2018, Scopus Author ID 56412435400, <https://orcid.org/0000-0002-0491-7452>

Кошель Георгий Николаевич, д.х.н., профессор, профессор кафедры «Общая и физическая химия» ФГБОУ ВО «Ярославский государственный технический университет» (115023, Россия, Ярославль, Московский проспект, 88). E-mail: koshelgn@ystu.ru. ResearcherID I-7782-2017, Scopus Author ID 6506863584, <https://orcid.org/0000-0002-1020-4643>

Шакун Владимир Андреевич, ассистент кафедры «Технология органического и нефтехимического синтеза» ФГБОУ ВО «Самарский государственный технический университет», (443100, Россия, г. Самара, ул. Молодогвардейская, 244). E-mail: shakyh@mail.ru. Scopus Author ID 56829536300, <https://orcid.org/0000-0003-2682-3024>

Нестерова Татьяна Николаевна, к.х.н., доцент, профессор кафедры «Технология органического и нефтехимического синтеза» ФГБОУ ВО «Самарский государственный технический университет», (443100, Россия, г. Самара, ул. Молодогвардейская, 244). E-mail: nesterovatn@yandex.ru. Scopus Author ID 15045158000, <https://orcid.org/0000-0002-3496-1075>

Спиридонов Станислав Андреевич, магистрант кафедры «Технология органического и нефтехимического синтеза» ФГБОУ ВО «Самарский государственный технический университет» ФГБОУ ВО «Самарский государственный технический университет», (443100, Россия, г. Самара, ул. Молодогвардейская, 244).

The article was submitted: October 12, 2020; approved after reviewing: November 06, 2020; accepted for publication: January 30, 2021.

Translated from Russian into English by N. Isaeva

Edited for English language and spelling by Enago, an editing brand of Crimson Interactive Inc.

**CHEMISTRY AND TECHNOLOGY OF MEDICINAL COMPOUNDS
AND BIOLOGICALLY ACTIVE SUBSTANCES**

**ХИМИЯ И ТЕХНОЛОГИЯ ЛЕКАРСТВЕННЫХ ПРЕПАРАТОВ
И БИОЛОГИЧЕСКИ АКТИВНЫХ СОЕДИНЕНИЙ**

ISSN 2686-7575 (Online)

<https://doi.org/10.32362/2410-6593-2021-16-1-36-54>



UDC 57.089.67

REVIEW ARTICLE

**New-generation osteoplastic materials based on biological
and synthetic matrices**

Dmitry D. Lykoshin^{1,*}, Vladimir V. Zaitsev², Maria A. Kostromina¹, Roman S. Esipov¹

¹*Shemyakin and Ovchinnikov Institute of Bioorganic Chemistry, Russian Academy of Sciences, Moscow, 117997 Russia*

²*N.N. Priorov National Medical Research Center of Traumatology and Orthopedics, Ministry of Health of the Russian Federation, Moscow, 127299 Russia*

*Corresponding author, e-mail: ldd-94@ya.ru

Abstract

Objectives. *The purpose of this analytical review is to evaluate the market for osteoplastic materials and surgical implants, as well as study the features of new-generation materials and the results of clinical applications.*

Methods. *This review summarizes the volumes of research articles presented in the electronic database PubMed and eLIBRARY. A total of 129 scientific articles related to biological systems, calcium phosphate, polymer, and biocomposite matrices as carriers of pharmaceutical substances, primary recombinant protein osteoinductors, antibiotics, and biologically active chemical reagents were analyzed and summarized. The search depth was 10 years.*

Results. *Demineralized bone matrix constitutes 26% of all types of osteoplastic matrices used globally in surgical osteology, which includes neurosurgery, traumatology and orthopedics, dentistry, and maxillofacial and pediatric surgery. Among the matrices, polymer and biocomposite matrices are outstanding. Special attention is paid to the possibility of immobilizing osteogenic factors and target pharmaceutical substances on the scaffold material to achieve controlled and prolonged release at the site of surgical implantation. Polymeric and biocomposite materials can retard the release of pharmaceutical substances at the implantation site, promoting a decrease in the toxicity and an improvement in the therapeutic effect. The use of composite scaffolds of different compositions in vivo results in high osteogenesis, promotes the initialization of biomineralization, and enables the tuning of the degradation rate of the material.*

Conclusions. Osteoplastic materials of various compositions in combination with drugs showed accelerated regeneration and mineralization of bone tissue *in vivo*, excluding systemic side reactions. Furthermore, although some materials have already been registered as commercial drugs, a plethora of unresolved problems remain. Due to the limited clinical studies of materials for use on humans, there is still an insufficient understanding of the toxicity of materials, time of their resorption, speed of drug delivery, and the possible long-term adverse effects of using implants of different compositions.

Keywords: osteosynthesis, osteoplastic materials, regenerative medicine, tissue engineering, osteogenesis, chondrogenesis, recombinant osteoinducers

For citation: Lykoshin D.D., Zaitsev V.V., Kostromina M.A., Esipov R.S. New-generation osteoplastic materials based on biological and synthetic matrices. *Tonk. Khim. Tekhnol. = Fine Chem. Technol.* 2021;16(1):36–54 (Russ., Eng.). <https://doi.org/10.32362/2410-6593-2021-16-1-36-54>

ОБЗОРНАЯ СТАТЬЯ

Остеопластические материалы нового поколения на основе биологических и синтетических матриц

Д.Д. Лыкошин^{1,@}, В.В. Зайцев², М.А. Костромина¹, Р.С. Есипов¹

¹Институт биоорганической химии им. академиков М.М. Шемякина и Ю.А. Овчинникова, Российская академия наук, Москва, 117997 Россия

²Национальный медицинский исследовательский центр травматологии и ортопедии им. Н.Н. Приорова, Министерство здравоохранения Российской Федерации, Москва, 127299 Россия

@ Автор для переписки, e-mail: ldd-94@yandex.ru

Аннотация

Цели. Цель литературного обзора – анализ остеопластических материалов и хирургических имплантатов нового поколения, изучение особенностей, характеристик и результатов их клинического применения.

Методы. Обзор суммирует объем научно-исследовательских материалов, представленных на порталах «PubMed» и «eLIBRARY». Проанализирован и обобщен материал 129 научных статей по следующим разделам: биологические, кальций-фосфатные, полимерные и биокомпозитные матрицы в качестве носителей целевых фармацевтических субстанций (рекомбинантных белковых остеоиндукторов, антибиотиков и биологически активных химических реагентов). Глубина поиска 10 лет.

Результаты. Среди всех видов остеопластических матриц, применяемых в настоящее время в мировой хирургической остеологии, куда входит нейрохирургия, травматология и ортопедия, стоматология, челюстно-лицевая и детская хирургия, деминерализованный костный матрикс (ДКМ) занимает 26%. Полимерные и биокомпозитные матрицы сегодня представляются наиболее перспективными материалами в сравнении с ДКМ. Особое внимание в разработке новых видов матриц уделяется возможности фиксации остеогенных факторов и целевых фармацевтических субстанций на материале-носителе с целью их контролируемого и пролонгированного выпуска на участке хирургической имплантации. Полимерные и биокомпозитные материалы способны замедлять время высвобождения фармсубстанций в месте имплантации, способствуя снижению токсичности и пролонгации терапевтического эффекта, являясь перспективной альтернативой аутогенной кости. Использование композитных носителей различного состава *in vivo* демонстрирует высокие показатели остеогенеза, способствует запуску биоминерализации и позволяет варьировать скорость деградации материала.

Выводы. *Остеопластические материалы различного состава в сочетании с лекарственными средствами показали ускорение регенерации и минерализации костной ткани in vivo, исключая системные побочные реакции. И, хотя некоторые материалы уже зарегистрированы в качестве коммерческих препаратов, все еще сохраняется ряд нерешенных проблем. Из-за ограниченности клинических исследований материалов на людях остаются открытыми такие вопросы как недостаточное понимание токсичности материалов, времени их резорбции, скорости доставки лекарственного средства и его высвобождения, а также возможные неблагоприятные эффекты от использования имплантатов различного состава.*

Ключевые слова: *остеосинтез, остеопластические материалы, регенеративная медицина, тканевая инженерия, остеогенез, хондроогенез, рекомбинантные остеоиндукторы*

Для цитирования: Лыкошин Д.Д., Зайцев В.В., Костромина М.А., Есипов Р.С. Остеопластические материалы нового поколения на основе биологических и синтетических матриц. *Тонкие химические технологии.* 2021;16(1):36–54. <https://doi.org/10.32362/2410-6593-2021-16-1-36-54>

Globally, ~2.2 million operations related to fractures and post-traumatic bone defects are performed annually, and this number is predicted to increase to 6 million by 2050 [1, 2]. In some cases, such as nonunion fractures of critical sizes or bone augmentation in dental implantology, the ability of the bone to self-regenerate is insufficient, and guided tissue regeneration is required, particularly when bone substitute materials are employed. The optimal osteoplastic material should have the following main biomedical characteristics:

- Biocompatibility: the material must interact with the cellular component of the bone without causing a toxic or immunological response.
- Osteoinduction: the ability of a material to induce the migration and differentiation of the recipient mesenchymal stem cells (MSCs) into osteoblasts and chondrocytes, which are the main cells of bone and cartilage tissue.
- Osteoconduction: the ability of the material to act as a supporting structure for the germination of blood vessels and structures of new tissue.
- Controlled resorption with the formation of non-toxic degradation products.
- Open bimodal porous structure (200–500 μm pores for germination into the material of the bone cells and vessels; micropores < 100 μm for interstitial fluids).
- The possibility of adhesion and chemical fixation of pharmaceutical substances on the structures of the carrier without reducing their activity.
- Preservation of biological characteristics during storage for extended periods.
- Manufacturability of the manufacturing process in commercial production [3–5].

In clinical regenerative medicine, the “gold standard” is the use of autografts. Autogenous bone grafts are osteoinductive, osteoconductive, and completely histocompatible materials [6]. However, autografts are limited to the amount of donor tissue available for transplant. The need for additional surgical intervention

to harvest bone tissue, usually from the iliac crest, carries the risk of the patient developing long-term postoperative pain syndrome [4].

The limitations associated with obtaining autogenous grafts can be overcome with allografts obtained from other donors. Today, allografts constitute 25% of the osteoplastic matrices used in surgical osteology [6]. In the United States alone, ~1 million allogeneic matrices are implanted annually [7]. Their main advantages over autogenous implants are the unlimited donor material and the ability to receive grafts of various shapes and sizes [6]. However, the risk of transmission of bacterial and viral infections is the main drawback of this material [8]. Additionally, the limited osteoinductive capacity of allografts is the main cause of recurrence or nonunion of bone tissue, which occurs in 15–20% of cases [6]. Osteoinduction activation of allogeneic bone matrices can be achieved by adding recombinant osteoinductive proteins [9]. However, the fixing of recombinant bone morphogenetic proteins (rhBMPs) on an allogeneic matrix results in uncontrolled excessive bone formation that goes beyond the field of corrected pathology, which is attributed to their uncontrolled release from the matrix framework [10].

Modern technological solutions involve the use of natural and synthetic polymers and calcium phosphates and their derivatives, including in combination with osteoinductive growth factors (Fig. 1). These materials are considered the most promising for use in osteoplasty, since they allow the setting of the required characteristics at the stage of producing the implant [3].

Even though the demand for plastic materials and surgical implants is expected to increase annually, the development of a universal osteoplastic material that could meet all the above requirements remains a major challenge.

In this review, we consider the characteristics of osteoplastic matrices that show potential in surgical osteology use and their clinical use cases.

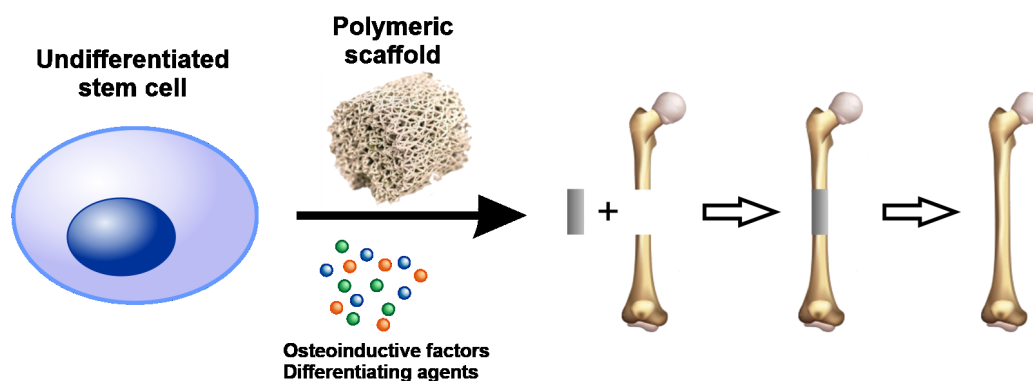


Fig. 1. Tissue engineering approach to bone treatment: undifferentiated stem cells are seeded on a polymer scaffold together with differentiating agents and growth factors, followed by implanting *in vivo*.

OSTEOPLASTIC MATRICES BASED ON BIOCERAMICS

Ceramic materials based on calcium phosphates have pronounced osteoconductive characteristics, which result in increased local interaction with the recipient's bone in corrected pathology; additionally, they are manufactured in block, granule, pasty, and injectable forms [11]. Synthetic calcium phosphates in a biological system, due to the metabolism of body cells, break down into calcium and phosphorus ions, which are further included in the structure of the regenerated bone tissue [12].

Hydroxyapatite

The most well-known calcium phosphate material is hydroxyapatite (HAP). It is the main inorganic component of bone tissue and tooth enamel, well absorbed by the human body, and widely used in orthopedics, traumatology, and dentistry to correct bone tissue defects [11].

The chemical formula of HAP is $\text{Ca}_{10}(\text{PO}_4)_6(\text{OH})_2$. In the crystal lattice, HAP molecules are distinguished by two structural frameworks. The first, the "apatite channel," is formed by OH^- groups located inside the lattice, which is bound by columns of Ca^{2+} and PO_4^{3-} ions, while the "backbone," which can accommodate F^- , Cl^- , OH^- and CO_3^{2-} ions, can isomorphically substitute PO_4^{3-} groups [12, 13].

The HAP is electrically neutral; it has a stable ionic lattice and is a stable compound. However, depending on the amount of calcium ions in the HAP structure, it can carry both positive and negative charges [13]. Further, chemical instability is a major disadvantage associated with using HAP in osteoplasty. The slow and incomplete resorption of synthetic HAP limit the formation of new bone tissue [14]. The resorption of calcium phosphate materials depends on the Ca/P

molar ratio in their composition. The lower the Ca/P ratio, the higher the rate of material resorption [15].

Due to the nonstoichiometric composition of HAP and the possibility of performing anionic or cationic substitutions in the crystal lattice, the value of the Ca/P ratio in the HAP composition can vary from 1.5 to 1.67 [12, 15]. The introduction of substituent ions into the HAP structure induces the distortion and deformation of the crystal lattice, which subsequently leads to an increase in the solubility and bioresorbability of the substituted HAP in comparison with pure HAP [14].

HAP-based materials can be modified by a covalent attachment of collagen to transfer and deliver various therapeutic agents (antibiotics, growth factors), enabling their prolonged release at the injury site [16]. The use of recombinant growth factors of bone tissue, such as bone morphogenetic proteins (BMP) immobilized on osteoplastic carriers, allows for the highly efficient and rapid correction of complex congenital and acquired pathologies of the human musculoskeletal system [10].

Covalent crosslinking using (*N*-ethyl-*N'*-(3-dimethylaminopropyl)carbodiimide) (EDC) hydrochloride and *N*-hydroxysuccinimide (NHS) hydrochloride is widely employed to obtain composite materials with increased biocompatibility, a high potential for cell differentiation [17], and increased resistance to enzymatic degradation [18]. This method allows one to obtain "zero-length" amide crosslinks between carboxylic acid groups and amino groups [19].

To modify the surface of HAP with collagen and immobilize the recombinant growth factors on it, the HAP is incubated in a solution of bovine serum albumin (BSA) and collagen, in the presence of a mixture of EDC/NHS reagents. Thereafter, the HAP–collagen

composite material is incubated in a solution with recombinant bone morphogenetic protein 2 (rhBMP-2) [20]. The protein is adsorbed on the surface of the carrier through non-covalent interactions [11, 20]. The reaction scheme for the modification of the HAP surface and the immobilization of rhBMP-2 on it is shown in Fig. 2.

Tricalcium phosphate

Another class of orthophosphate materials that have found use in osteoplasty is tricalcium phosphates. Materials based on tricalcium phosphate are characterized by a higher rate of resorption compared to the materials based on HAP [21]. They can also be used as components of composite materials together with HAP, which enables the control of the material resorption rate [22].

The osteoplastic matrix based on β -tricalcium phosphate (β -TCP) has received considerable attention in scientific clinical studies. β -TCP, with the chemical composition of $\text{Ca}_3(\text{PO}_4)_2$, unlike other polymorphic modifications of tricalcium phosphates, is stable at temperatures below 1100°C , and it has a lower Ca/P ratio than that of HAP; consequently, it exhibits increased biodegradability and biocompatibility [23].

To obtain an osteoplastic material based on β -TCP, a suspension of crystalline hydrate ($\text{CaHPO}_4 \cdot \text{H}_2\text{O}$) and calcium carbonate (CaCO_3) is mixed in the presence of zirconium dioxide (ZrO_2), dried, and subsequently calcined at $750\text{--}900^\circ\text{C}$, at which point HAP is converted into β -TCP. After sintering the preformed β -TCP at 1050°C for 1 h, a β -TCP block with a porosity of 75% is formed [24, 25]. The chemical reactions are described by Eqs. 1 and 2.

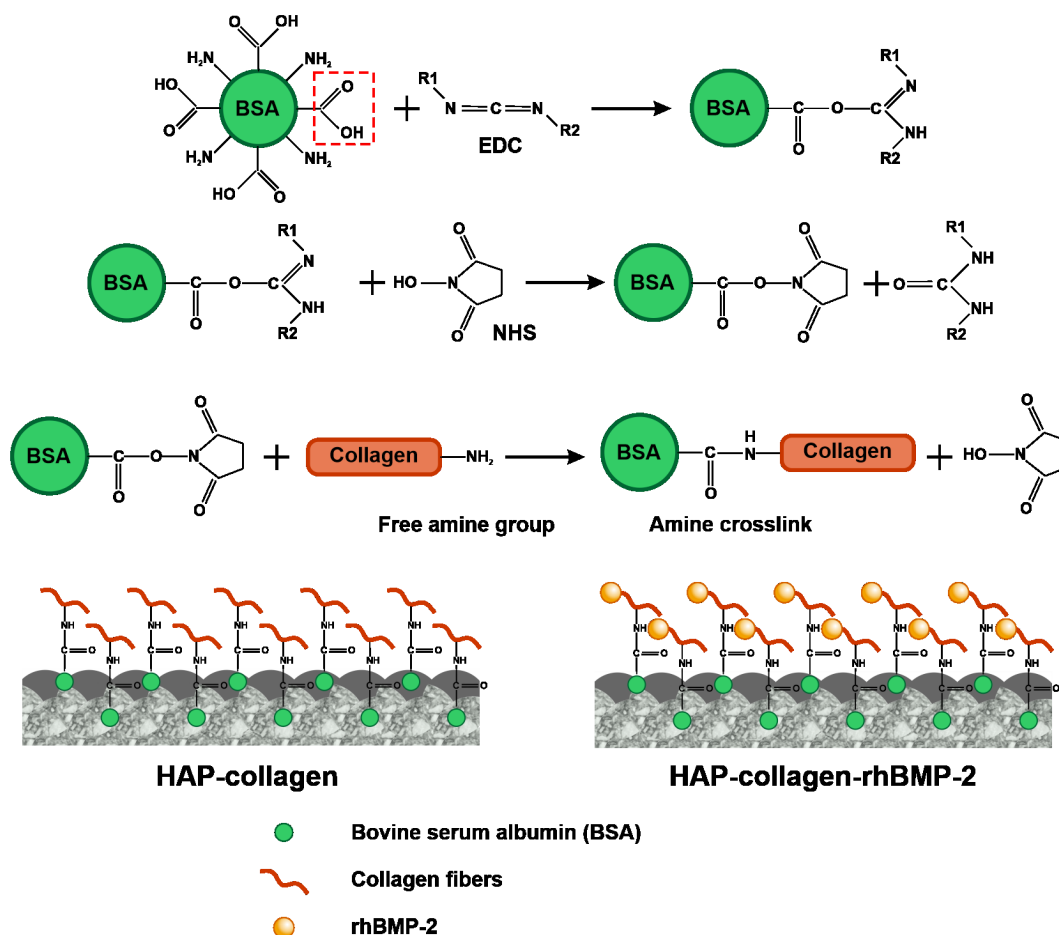
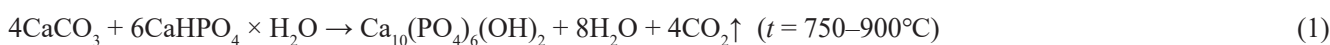


Fig. 2. Illustration of the reaction mechanism of BSA and collagen chemical crosslinking for the subsequent immobilization of the rhBMP-2 osteoinducer on a hydroxyapatite matrix;

EDC: 1-ethyl-3(3-dimethylaminopropyl)carbodiimide hydrochloride, NHS: *N*-hydroxysuccinimide.

Another common approach to obtain matrices from β -TCP involves calcining chemically synthesized calcium-deficient HAP. At temperatures of 700–800°C, it loses water and transforms into the low-temperature polymorph, β -TCP, used in osteoplasty (Eq. 3). Further heating to a temperature of ~1150°C leads to the transformation of β -TCP to a high-temperature polymorphic α -Ca₃(PO₄)₂ material, which is highly soluble in water [26].



The β -TCP structure allows one to perform isomorphous substitutions of calcium ions for ions of monovalent and divalent metals or silicate ions. Silicate ions in the β -TCP structure accelerate the differentiation of MSCs on the matrix at the implantation site [27]. Zn, Cu, and Ag metals impart antibacterial properties on the β -TCP based material. Additionally, the β -TCP matrix substituted with Zn ions retards the formation of osteoclasts (cells that destroy bone tissue) on its surface and accelerates the work of osteoblasts, contributing to the formation of the bone matrix [28].

In clinical usage, β -TCP has already demonstrated complete regeneration of bone defects over several years and replacement of the osteoplastic matrix with newly formed tissue. The partial resorption of the β -TCP implant in a clinical setting is observed 2–3 weeks after surgery, and complete degradation occurs from 1.5 to 5 years, depending on the patient's age. It was noted that in cancellous bone defects, β -TCP resorption and bone formation occurs faster than the in the case of cortical bone defects [24].

Notably, materials based on calcium phosphates have low tensile strength, and their Young's modulus is, on average, 10 times higher than that of bone tissue [3]. However, the mechanical characteristics of calcium phosphate materials can be varied during the manufacturing step. As the porosity of the material decreases, the compressive strength increases; thus, β -TCP with 60% porosity has a compressive strength of 22 MPa, which is almost seven times higher than that for β -TCP with 75% porosity. However, the resorption rate for the β -TCP with 60% porosity is lower than that for the β -TCP with 75% porosity [29].

Bioactive glass

Biologically active glasses (BGs) have gained significant interest in the fields of hard- and soft-tissue engineering. This is due to their ability to induce the expression of genes that regulate the processes of osteo- and angiogenesis, thereby enhancing the production of the corresponding growth factors [30].

The first type of these biologically active inorganic materials, known as Bioglass-1 45S5

(BG-1), was discovered by Larry Hench in the late 1960s at the University of Florida. BG-1, with the composition of 45SiO₂–24.5CaO–24.5Na₂O–6P₂O₅ (wt %), binds to living tissues, forming a stable and densely structured surface; thus, it is effectively used as a filler in bone fractures [31].

The term, “biological activity,” in the context of these special glasses indicates the ability of the bioglass surface to direct the crystallization of calcium phosphate salts toward the formation of HAP, thereby facilitating the connection between the artificial material and body tissues [32]. The biosilicate mineralization process occurs in several stages and is shown in Fig. 3. First, the surface of the bioglass turns into a silica gel with an open structure, which exchanges ions with biological body fluids (Stages 1–3, Fig. 3). Subsequently, the calcium and phosphate ions form an amorphous calcium phosphate layer (Stage 4, Fig. 3). Afterward, the Ca–P layer adds hydroxyl and carbonate ions, which facilitate the crystallization of hydroxycarbonate apatite (Stage 5, Fig. 3) [33].

Bioglass is categorized based on three different types of inorganic oxides, including structure-forming (SiO₂, B₂O₃, and P₂O₅), modifying (Na₂O, CaO, MgO, K₂O), and intermediate compounds (Al₂O₃, ZnO, ZrO₂, and TiO₂) [34]. According to the principle of the main structure-forming oxide, bioglasses are divided into glass families based on silicates, borosilicates, borates, and phosphates [35]. Additionally, BGs doped with a small amount of biologically active metal ions have been developed, and they exhibit various therapeutic effects (stimulating osteo- and angiogenesis, anti-inflammatory, and antiseptic) (Table 1) [36]. Mesoporous BGs obtained by sol–gel processes have the porosity (2–50 nm) suitable for the immobilization of various therapeutic agents in nanopores with their subsequent local release in a controlled manner [37]. Alloyed and mesoporous BGs are considered as separate classes of the bioglass family.

In vitro and *in vivo* studies have shown that such therapeutic functions of BGs, including improving the cell growth and proliferation, biomineralization, stimulation of angiogenesis, anti-inflammatory and antibacterial activity, are associated with the release of metal ions and growth factors from the glass structure, after which the bioglass itself undergoes resorption [36].

The use of biocomposite osteoplastic scaffolds based on a BG and a polymer matrix provides additional advantages, such as the launch of biomineralization, which contributes to the formation of a bond between the newly formed tissue and the material; improvement of the initial mechanical properties of the polymer phase; and the ability to fine tune the rate of material resorption [30].

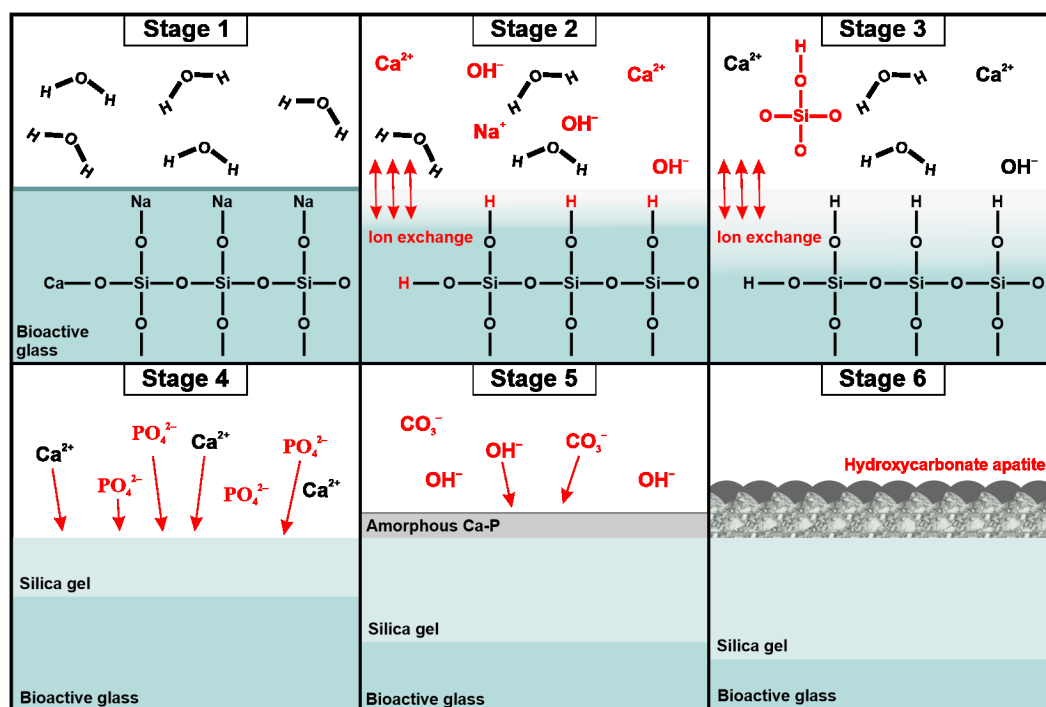


Fig. 3. Formation mechanism of hydroxycarbonate apatite on the surface of bioactive glass.

Table 1. Therapeutic effects of doped bioglass based on various biologically active ions

Therapeutic effect	Metal ions
Angiogenesis	Mg ²⁺ , Mn ²⁺ , Ca ²⁺ , Cu ²⁺ , B ³⁺ , Si ⁴⁺ , P ⁵⁺
Antibacterial	Ag ⁺ , Cu ²⁺ , Zn ²⁺ , Ga ²⁺ , Mn ²⁺ , Fe ³⁺ , Ce ³⁺
Osteogenesis	F ⁻ , Li ⁺ , Sr ²⁺ , Mg ²⁺ , Mn ²⁺ , Ca ²⁺ , Cu ²⁺ , Ga ²⁺ , Si ⁴⁺ , Nb ⁵⁺
Anti-inflammatory	Li ⁺ , Mn ²⁺ , Zn ²⁺ , B ³⁺

To date, several studies have been published on the use of BG frameworks [38] and composite carriers of the polymer/BG composition [39, 40] in the field of bone tissue engineering. Results of these studies indicate that PLA/BG scaffolds are suitable candidates for achieving optimal bonding between material and tissues, the latter being both soft and hard [41]. Therefore, several studies are actively underway that suggest the use of these systems in areas where the device must simultaneously connect to both soft and hard tissues (for example, middle ear implants or joint implants) [36].

MATRICES BASED ON SYNTHETIC POLYMERS

Synthetic biodegradable polymers appear to be promising materials for use in various tissue-engineered structures, mainly of composite composition [42].

The most used resorbable synthetic polymers for the manufacture of osteoplastic matrices are saturated poly (α -hydroxyesters), including polylactic acid (PLA) and polyglycolic acid (PGA), as well as polylactic acid glycolide copolymer (PLGA) [43].

The chemical composition of these polymers allows for hydrolytic degradation by deesterification. After resorption, the monomeric components of each polymer are excreted from the recipient's body naturally. PGA is converted to metabolites or removed via other mechanisms, and PLA can be purified through the tricarboxylic acid cycle [44].

PGA is a hydrophilic and highly crystalline polymer with a relatively high degradation rate. Although PLA is structurally very similar to PGA, it exhibits different chemical, physical, and mechanical properties due to the presence of a pendant methyl group on the α carbon (Fig. 4) [45].

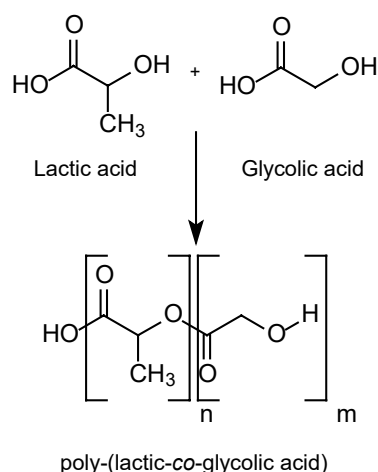


Fig. 4. Chemical structure of PLGA and monomers PLA and PGA.

The PLGA copolymer is preferred over its constituent homopolymers for the manufacture of bone implants, since the physicochemical properties of PLGA allow one to control the rate of decomposition of the material, and PLGA can be obtained in block, fiber, hydrogel, and nanoparticle forms [44].

The rate of resorption of synthetic polymer matrices is influenced by the following factors:

1) The molecular weight of the polymer: degradation rates vary from several weeks to several months.

2) The LA/GA ratio: PLGA copolymers with a high LA content are less hydrophilic; consequently, they absorb a low amount of water and degrade slowly.

3) Stereochemistry: mixtures of D- and L-lactic acid monomers are often used for the preparation of PLGA, since the rate of penetration of water molecules in the D- and L-regions is high, which leads to accelerated degradation.

4) The structure of end groups: polymers with ester residues at the ends have longer half-lives than those with free carboxylic acid [46, 47].

Furthermore, polyethylene glycol (PEG) [48, 49], polyanhydrides [50], poly- ϵ -caprolactone (PCL) [49, 51], polypropylene fumarate (PPF) [51], and poloxamers [52] are considered synthetic polymer carriers. The advantages of these resorbable polymer carriers are hydrolytic and enzymatic resorption, zero risk of bacterial and viral contamination, and the ability to regulate the mechanical strength by manipulating the polymer structure [53].

Due to their flexible design and controlled degradation rate, biodegradable synthetic polymers in the form of nanoparticles are considered as carriers for the delivery of recombinant protein osteoinducers and pharmaceutical substances. A system for delivery of the growth factor, rhBMP-2, was demonstrated

based on the PLA-PEG copolymer; a carrier in the form of a viscous liquid or polymer granules was implanted at the site of surgical correction of bone pathology [54]. According to the results of the study, the PLA-PEG complex was recognized as an effective transport matrix for the prolonged release of the recombinant osteoinducer, rhBMP-2. The efficacy of rhBMP-2 in various animal models was shown when it was immobilized on the matrices of PLA [55], PGA [56], and their copolymer, PLGA [57].

Even though the low pH of the medium created by the products of acid cleavage accelerates the degradation of PLGA due to autocatalysis, this factor is simultaneously a disadvantage of synthetic polymers [58]. This acidification of the medium and the hydrophobic nature of the polymers have a negative effect on the stability of the protein immobilized on the surface of the carrier [59] and increase the risk of inflammatory reactions and delayed clearance [60].

In bone tissue engineering, a combined approach is used, which consists of the synthesis of block copolymers to manipulate the characteristics of the polymer delivery system, e.g., the kinetics of the release of pharmaceutical compounds immobilized on an osteoplastic polymer carrier [61, 62].

Synthetic polymer matrices based on PLA and PGA can be combined in various ratios with calcium phosphate materials (CaPs) to create composite materials with or without chemical modifications of the surface [63]. When CaPs are combined with polymers to form a composite framework, the rate of their resorption is reduced in comparison with that of the pure polymer [64].

Park *et al.* demonstrated the effectiveness of using PCL composites with the addition of β -TCP under mechanical loading conditions, comparable to the modulus of compression of the human trabecular bone. The earliest differentiation of MSCs and high expression of osteogenic markers were noted in PCL/ β -TCP composites with a content of 30% β -TCP [65].

Additionally, a high level of osseointegration was demonstrated by the PLA composite containing tricalcium phosphate microspheres with a size of 60–140 μm (PLA/ β -TCP). Due to the formation of an ordered porous structure of the composite material, PLA/ β -TCP, 16 weeks after implantation into the femur of rabbits, the vascularization of the implant and growth of newly formed tissue into its pores were observed [66].

BIOCOMPOSITE FRAMEWORKS

Composite frameworks with mesoporous silicon

From the viewpoint of clinical efficacy, biocomposite carriers of various pharmaceutical substances created based on nanotechnologies are the most promising materials for tissue engineering [67].

Mesoporous silicon nanoparticles (MSNs) accelerate bone formation by increasing the osteoblast activity and decreasing the bone resorption due to a decrease in the osteoclast activity [68]. MSN-based materials can deliver pharmaceutical molecules of various structures and masses to the injury site due to their pore size and morphology, as well as the possibility of modifying the MSN surface [67]. The variability and flexibility in the design of silicon nanoparticles allow one to choose the dosage of a pharmaceutical substance and control the kinetics of its release in accordance with the functional groups of the molecule that will be adsorbed on the MSN surface [69, 70].

Take the delivery of ibuprofen, which has a –COOH group in its composition, as an example. There is an increase in the adsorption of ibuprofen on the surface of MSN modified with polar molecules as compared to silicon nanoparticles with nonpolar modifications [70]. Consequently, prolonged release of the pharmaceutical substance and a lasting therapeutic effect are observed [70].

The efficacy of doxorubicin delivery using MSNs surface-modified with PEG has been demonstrated in a mouse malignant tumor model [71]. On the 12th day, the animals were withdrawn from the experiment, and the comparable growth rates of tumor volumes were evaluated. The effect of doxorubicin, expressed as the degree of inhibition of the tumor growth rate, was 68.7% for the MSN–PEG loaded particles, compared to 42.5% for pure silicon nanoparticles [71]. This result is due to the improved stability of the doxorubicin molecule on the MSN–PEG surface and the prolonged circulation of the nanoparticles with the pharmaceutical substance in the blood.

In recent studies, significant attention has been paid to composite frameworks based on MSN nanoparticles crosslinked with methacrylate gelatin as part of hydrogel membranes [72]. A recombinant osteoinducer, rhBMP-2, is immobilized on the surface of the mesoporous bioglass through an amide bond. It was shown *in vitro* that the release of rhBMP-2 from the matrix during the first 4 weeks of the experiment significantly stimulated the osteogenic differentiation of cells, and the resorption of the composite carrier to calcium and silicon ions promoted cell adhesion and osteogenic differentiation over a long period [73]. *In vivo* hydrogel membranes based on mesoporous bioglass crosslinked with gelatin demonstrated high rates of bone tissue osteogenesis in a defect in a rat's skull of critical size [72, 73].

Composite frameworks with carbon nanotubes

Biodegradable composite scaffolds based on PLA and PGA polymers in combination with carbon nanotubes (CNTs) are a promising development for a

wide range of applications in bone tissue engineering, particularly in cases where the implanted material mainly handles high loads [74]. This combination of composites is particularly effective, since it allows one to achieve self-assembly of CNT fibers and create a network structure in the polymer matrix, and it improves the mechanical strength, thermal stability, and electrical conductivity of the material at low CNT concentrations [75].

Mikael *et al.* presented an efficient method for the preparation of composite frameworks from PLGA microspheres and multi-walled carbon nanotubes (MWCNTs) with various surface modifications [76]. Such scaffolds showed high *in vitro* cell adhesion, cell proliferation, and mineralization, as well as signs of a connection with soft tissues.

A similar approach was tested on composite frameworks with single-walled carbon nanotubes (SWCNTs). It was shown that the PLGA/SWCNT combination led to an even higher gene expression and cell proliferation for the formation of new muscle tissue, compared with that for the composite carrier of PLGA and MWCNTs [77]. It is assumed that such a cellular activity is a consequence of the increased expression of transmembrane cellular receptors, integrins, which may be caused by the topographic features of SWCNTs. This activity is essential for achieving enhanced interaction of the polymer framework with biological components [77].

Another quality of CNTs in composite materials is their ability to change the thermal and electrical properties of PLA [76, 78]. This approach can be used to increase the reactivity of stem cells seeded on the polymer through electrical stimulation, thereby improving tissue regeneration in the long term [79].

A composite material based on a CNT/sodium hyaluronate complex demonstrated a high potential for the restoration of bone tissue defects in rats [80, 81]. This composite induces the expression of genes involved in bone tissue regeneration, such as osteocalcin and BMP-2 [80]. An increase in the expression of type I collagen, as well as the vascular endothelial growth factor, was also observed. When using the CNT–sodium hyaluronate composite in tibial defects, histo-morphometric analysis showed an increase in the number and organization of bone trabeculae, in comparison with the case in the control group [81].

However, carbon nanostructures raise serious concerns when used as components of biomedical devices due to the lack of data on their carcinogenicity and the accumulation of decay products in the human body [78].

Composite frameworks with metal oxides

Composite systems of PLA/metal oxide composition, including zinc oxide (ZnO), magnesium

oxide (MgO), and iron oxides (Fe_2O_3 and Fe_3O_4), have interesting and promising characteristics suitable for application in surgical osteology [82, 83]. Each of these metals has properties suitable for a variety of tissue engineering applications. Compared to clinically used PLGA materials, metal oxide composite structures can reduce inflammation and simultaneously stimulate osteogenesis and osseointegration [84].

The ZnO in the osteoplastic matrix inhibits bacterial attachment and stimulates cell differentiation in the direction of the myocyte phenotype [85]. When the oxide is integrated into the PLLA/ZnO composite system (ZnO in the form of ~40 nm nanorods), the composite slowly releases zinc ions into the environment [86]. Nanorods act as catalytic nuclei, slightly accelerating the polymer degradation. This observation is of key importance as it improves the connection between differentiated myocytes and the implant [85].

MgO is used in composite materials as an alternative to BGs to improve biomineralization and retard PLA degradation [87]. MgO particles incorporated into the polymer matrix buffer the ambient pH, thereby reducing the rate of PLA hydrolysis and weakening the autocatalytic effect of the polymer. The characteristics of the porous PLA/MgO composite framework have been studied in the field of dental bone grafting [88]. The authors reported high compressive and tensile strength, prolonged material resorption time, proliferation of bone marrow MSCs *in vitro*, and bone tissue regeneration *in vivo* in a dog model [89].

Fe_2O_3 and Fe_3O_4 have a unique property that can be used to improve the bond between tissue and biomaterial—supermagnetism [90]. The use of supermagnetic iron oxide particles, particularly in the treatment of cancer and many other drug delivery systems, is a new trend in the field of regenerative medicine [91, 92].

Studies have investigated the incorporation of superparamagnetic iron oxide nanoparticles ($\gamma\text{-Fe}_2\text{O}_3$ and $\text{FeO}\cdot\text{Fe}_2\text{O}_3$) into a PLGA matrix, followed by the application of a static magnetic field to the composite structure during cell culture. Magnetic stimulation, similar to nanoparticles obtained separately, promoted the differentiation of osteoblasts [93].

The explanation of this phenomenon consists of two aspects: first, the stimulation by the application of a static magnetic field due to the diamagnetic properties of the cell membrane changes the flow of ions through the membrane; second, iron oxide nanoparticles reduce the intracellular production of H_2O_2 , thereby accelerating the progression of the cell cycle. These two stimuli act synergistically, which leads to a significant increase in the proliferation, differentiation, and secretion of MSCs, promoting the formation of a bond between tissue and material [90, 91, 93].

COMPOSITE MATRICES FROM NATURAL POLYMERS

Since the implant used in bone tissue engineering must, to a certain extent, mimic the characteristics of cartilage and bone tissue, natural polymers appear to be an intuitive choice for the initial matrix [94]. Natural polymers can be classified according to their origin (animal, plant, or microbiological) and chemical structure (proteins, polysaccharides, polynucleotides) (Fig. 5) [95].

Porous scaffolds composed of natural polymers stimulate the osteogenic differentiation of MSCs [94]. However, the strength characteristics and resorbability of these matrices under the conditions of the recipient's organism are insufficient, and these matrices are inferior to synthetic resorbable polymer matrices [96].

Chitosan-based matrices

Chitosan is a biodegradable natural polymer obtained by the deacetylation of the natural polymer of chitin [97]. Chitosan has pronounced bactericidal properties, and due to its ability to enhance the absorption of hydrophobic macromolecules, it is used as a carrier to achieve prolonged local release of pharmaceutical substances [98].

Composite systems of the chitosan/PGA, chitosan/HAP, and chitosan/gelatin compositions can serve as effective osteoplastic carriers [99, 100]. In *in vitro* experiments, biological membranes based on chitosan nanofibrils with the addition of rhBMP-2 demonstrated a high biological activity expressed in the osteogenic differentiation of MSCs, high alkaline phosphatase activity, and calcification for 4 weeks with 50% preservation of the immobilized rhBMP-2 on the membrane [101].

Due to their mucoadhesive cationic nature, chitosan nanoparticles (NPCS) are used to reduce the toxic effect and increase the activity of drugs, since they allow the therapeutic agent to be delivered to the immediate vicinity of the injury site [102]. NPCS are usually modified to increase their effectiveness. For example, 2*N*-,6*O*-sulfated chitosan (2,6SCS) forms a polysaccharide similar in structure to heparin, which can successfully bind to the rhBMP-2 domain region (Fig. 6A). Modified NPCS retard the release of the growth factor and increase its biological activity [103, 104].

Gelatin-based matrices

Gelatin is a hydrolyzed form of collagen obtained by heat treatment. The use of gelatin as the only material in the composition of a carrier for pharmaceutical substances is complicated because it tends to undergo rapid biodegradation in the recipient's body [105]. The prolongation of the biodegradation time is achieved by chemical

“crosslinking” of collagen fibers with glutaraldehyde; however, a cytotoxic effect is noted, indicated by the retardation of the osteogenic differentiation of MSCs in *in vitro* studies [106]. A decrease in toxicity can be achieved after 4 days of washing the crosslinked matrix from glutaraldehyde [107].

A biocomposite material based on gelatin and β -TCP demonstrated improved biodegradability under the influence of collagenase with a large amount of gelatin and high osteoinduction, expressed as an increase in the level of alkaline phosphatase activity *in vitro* [108].

The photochemical process involving tris-(2,2'-bipyridine) chloride of ruthenium(II) [Ru(bpy)₃]Cl₂ and persulfate ion allows the covalent crosslinking of tyrosine-rich proteins (rubber, gelatin, and fibrinogen) because of the formation of dityrosine bonds and to obtain biopolymer materials with variable biomechanical and tissue-adhesive properties pre-set at the stage of material creation [109, 110]. The tendency of tyrosine-rich proteins to self-organize polymer fibers and interact with extracellular matrix proteins enables the application of the biopolymers crosslinked via this route as surgical sealants or drug delivery systems [111, 112].

The thus obtained photopolymerizable gelatin hydrogel (PH) possesses the porosity required to load it with modified NPCs [103, 113]. The direct introduction of growth factors into the PH does not have a significant effect, since the hydrogel swells and decomposes rapidly, and the complete release of rhBMP-2 is observed after 7 days (Fig. 6B) [103]. However, the composite PH system including 2,6SCS nanoparticles (PH/rhBMP-2/NPs) shows the best results for the stepwise release of therapeutic agents. The first intense rhBMP-2 release is recorded within the first 2 weeks after implantation, and it is associated with the swelling of the hydrogel. Thereafter, there is a gradual release over 42 days, due to the slow degradation of the PH (Fig. 6C) [103].

Collagen osteoplastic matrices

Collagen is the most abundant protein in the human body and a non-mineral biological component of the skeleton. It can be easily isolated and enzymatically purified from various types of xenogeneic matrices for use as a supporting scaffold for cell proliferation in bone tissue engineering [114, 115].

Collagen osteoplastic scaffolds are manufactured in the form of powder, membrane films, aqueous forms, gels, nanofibers, and absorbent sponges [116].

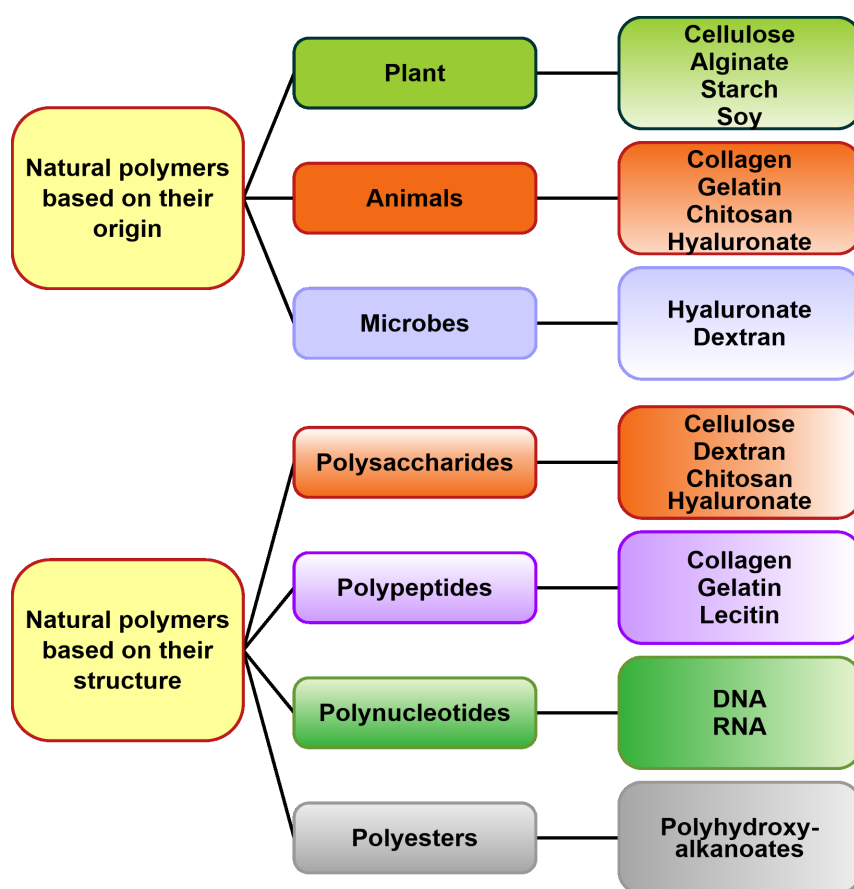


Fig. 5. Classification of natural polymers based on their origin and chemical structure.

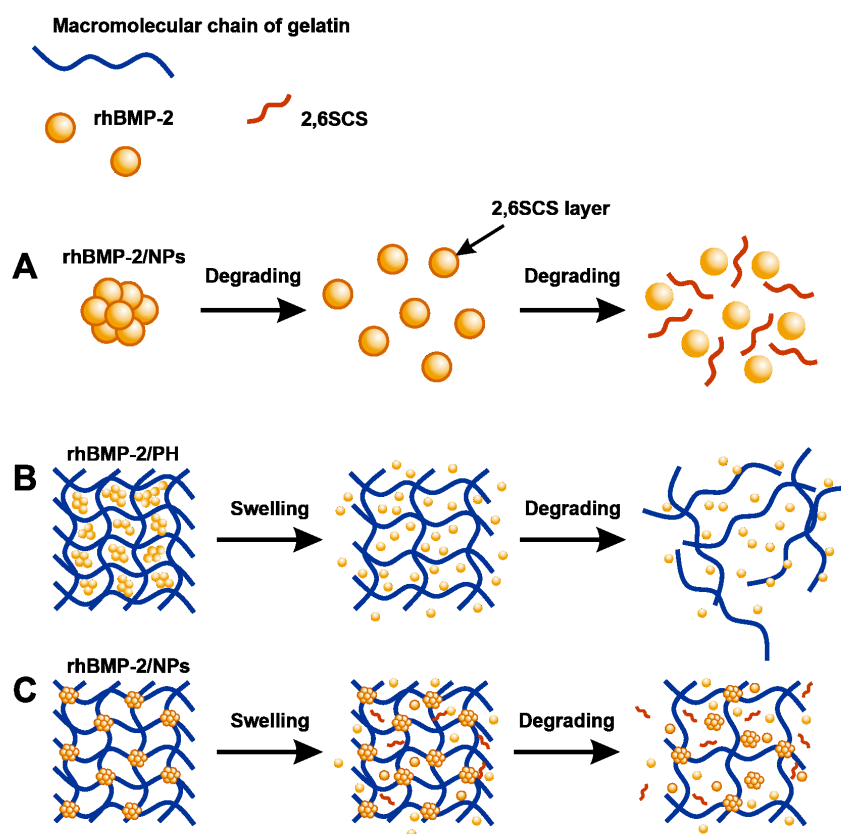


Fig. 6. Illustration of the mechanisms of rhBMP-2 release from (A) sulfated chitosan nanoparticles (NPCS), (B) photopolymerizable gelatin hydrogel, and (C) a complex of a hydrogel with NPCS.

The versatility, hygroscopicity, and ease of use of collagen sponges have led to their widespread clinical use for the localization and delivery of targeted pharmaceutical substances [117, 118]. Since 2002, the United States Food and Drug Administration has approved the commercial preparation of INFUSE with recombinant rhBMP-2 on an ACS collagen plate at a concentration of 1.5 mg/mL [119].

In surgical osteology, INFUSE is used as an alternative to the autologous iliac crest for the single-level fusion of the vertebral bodies in the lumbar spine and to accelerate the fusion of open tibial fractures with intramedullary fixation [119]. Additionally, INFUSE is widely used as an alternative to autologous bone implants for the limited enlargement of the alveolar sinus and treatment of defects associated with bone loss in dentistry [120, 121].

Despite its high biocompatibility, collagen has several disadvantages. It is mechanically unstable, and therefore, upon implantation into an environment, where the sponge is compressed by the surrounding muscles and tissues, there is a local excess release of osteoinductive proteins immobilized on the carrier [114]. Collagen resorption is unpredictable and difficult to control, which also leads to undefined kinetics of recombinant growth factor release. *In vivo*,

it was shown that after 2 weeks, only 5% of rhBMP-2 remains in the collagen sponge [122].

An increase in the collagen resorption duration can be achieved by crosslinking collagen molecular chains with chemical agents, such as glutaraldehyde, carbodiimide, and genipin, or by physical exposure, such as UV radiation or dehydrothermal treatment. However, due to cytotoxicity, chemical crosslinking agents adversely affect the biocompatibility and regenerative potential of the material [116, 123].

Additionally, collagen extracted from the xenogeneic matrix with insufficient and ineffective chemical cleaning demonstrates pronounced immunogenicity; in 20% of patients who received an implant from a collagen sponge, antibodies to type I collagen were found [114, 124].

Another disadvantage of using collagen scaffolds is the difficulty of sterilizing them, since heat sterilization causes the partial or complete, irreversible denaturation of collagen fibers [125, 126]. Thus, gas sterilization with ethylene oxide is used to sterilize collagen sponges [127]. However, with this method of sterilizing a collagen sponge with rhBMP-2 immobilized on it, an unpredictable change in the kinetics of the growth factor release and a decrease in its biological activity were noted [128, 129].

CONCLUSIONS

Despite all the advantages of an autologous bone, in the presence of cellular elements of the bone marrow, presence of growth factors, and local blood supply, synthetic and biocomposite osteoplastic matrices can be a real alternative to an autologous bone graft, particularly in the variants of transport systems for the prolonged local release of target pharmaceutical substances.

Although positive scientific and practical results have been achieved in the study of new-generation osteoplastic matrices, many unresolved issues remain, and the main ones are as follows:

- Optimization of the resorption time of the osteoplastic matrix.
- Selection of an effective technology to facilitate the resorption of the osteoplastic matrix, synchronized in time with the process of bone regeneration.
- Stabilization of the matrix to exclude a pronounced macrophage reaction of the recipient's body.
- Solving issues related to the certification and registration of new options for osteoplastic surgical implants in supervisory medical organizations.

Experimental and clinical studies on osteoplastic matrices are underway in most countries. The participation of many leading research centers, as well as the connection of significant material and financial resources, increases the possibility of achieving significant research and production success in this field of regenerative medicine.

Financial support

This study did not have any financial support from outside organizations.

Authors' contribution

D.D. Lykoshin – work idea, selection of publications, analysis and description of search results, preparation, design of the article, and writing the text of the article;

V.V. Zaitsev – selection of publications and analysis and description of search results;

M.A. Kostromina – preparation and design of the article and work with graphic materials;

R.S. Esipov – preparation and design of the article and writing the text of the article.

The authors declare no conflicts of interest.

REFERENCES

1. Henkel J., Woodruff M.A., Epari D.R., Steck R., Glatt V., Dickinson I.C., Choong P.F., Schuetz M.A., Hutmacher D.W. Bone Regeneration Based on Tissue Engineering Conceptions — A 21st Century Perspective *Bone Res.* 2013;1(3):216–248. <https://doi.org/10.4248/BR201303002>
2. Barabaschi G.D., Manoharan V., Li Q., Bertassoni L.E. Engineering Pre-vascularized Scaffolds for Bone Regeneration. *Adv. Exp. Med. Biol.* 2015;881:79–94. https://doi.org/10.1007/978-3-319-22345-2_5
3. O'Brien F.J. Biomaterials & scaffolds for tissue engineering. *Mat. Today.* 2011;14(3):88–95. [https://doi.org/10.1016/S1369-7021\(11\)70058-X](https://doi.org/10.1016/S1369-7021(11)70058-X)
4. García-Gareta E., Coathup M.J., Blunn G.W. Osteoinduction of bone grafting materials for bone repair and regeneration. *Bone.* 2015; 81:112–121. <https://doi.org/10.1016/j.bone.2015.07.007>
5. Vorobyov K.A., Bozhkova S.A., Tikhilov R.M., Cherny A.Zh. Current methods of processing and sterilization of bone allografts (review of literature). *Travmatologiya i ortopediya Rossii = Traumatology and Orthopedics of Russia.* 2017;23(3):134–147 (in Russ.). <https://doi.org/10.21823/2311-2905-2017-23-3-134-147>
6. Baldwin P., Li D.J., Auston D.A., Mir H.S., Yoon R.S., Koval K.J. Autograft, Allograft, and Bone Graft Substitutes: Clinical Evidence and Indications for Use in the Setting of Orthopaedic Trauma Surgery. *J. Orthop. Trauma.* 2019;33(4):203–213. <https://doi.org/10.1097/bot.0000000000001420>
7. Islam A., Chapin K., Moore E., Ford J., Rinnac C., Akkus O. Gamma Radiation Sterilization Reduces the High-cycle Fatigue Life of Allograft Bone. *Clin. Orthop. Relat. Res.* 2016;474(3):827–835. <https://doi.org/10.1007/s11999-015-4589-y>
8. Zamborsky R., Svec A., Bohac M., Kilian M., Kokavec M. Infection in Bone Allograft Transplants. *Exp. Clin. Transplant.* 2016;14(5):484–490. <https://doi.org/10.6002/ect.2016.0076>
9. Reddi A.H., Iwasa K. Morphogenesis, Bone Morphogenetic Proteins, and Regeneration of Bone and Articular Cartilage. In: *Principles of Regenerative Medicine* (Third Edition). Academic Press; 2019. Chapter 25. P. 405–416. <https://doi.org/10.1016/B978-0-12-809880-6.00025-4>
10. Boerckel J.D., Kolambkar Y.M., Dupont K.M., Uhrig B.A., Phelps E.A., Stevens H.Y., García A.J., Goldberg R.E. Effects of protein dose and delivery system on BMP-mediated bone regeneration. *Biomaterials.* 2011;32(22):5241–5251. <https://doi.org/10.1016/j.biomaterials.2011.03.063>

11. Damlar I., Erdoğan Ö., Tatli U., Arpağ O.F., Görmez U., Üstün Y. Comparison of osteoconductive properties of three different β -tricalcium phosphate graft materials: a pilot histomorphometric study in a pig model. *J. Craniomaxillofac. Surg.* 2015;43(1):175–180. <https://doi.org/10.1016/j.jcms.2014.11.006>
12. Tite T., Popa A.C., Balescu L.M., Bogdan I.M., Pasuk I., Ferreira J., Stan G.E. Cationic Substitutions in Hydroxyapatite: Current Status of the Derived Biofunctional Effects and Their *In Vitro* Interrogation Methods. *Materials.* 2018;11(11):2081. <https://doi.org/10.3390/ma11112081>
13. Basirun W.J., Nasiri-Tabrizi B., Baradaran S. Overview of Hydroxyapatite–Graphene Nanoplatelets Composite as Bone Graft Substitute: Mechanical Behavior and *In-vitro* Biofunctionality. *Critical reviews in solid state and material sciences.* 2018;43(3):177–212. <https://doi.org/10.1080/10408436.2017.1333951>
14. Sheikh Z., Abdallah M.N., Hanafi A.A., Misbahuddin S., Rashid H., Glogauer M. Mechanisms of *in Vivo* Degradation and Resorption of Calcium Phosphate Based Biomaterials. *Materials.* 2015;8(11):7913–7925. <https://doi.org/10.3390/ma8115430>
15. Raynaud S., Champion E., Bernache-Assollant D., Thomas P. Calcium phosphate apatites with variable Ca/P atomic ratio I. Synthesis, characterisation and thermal stability of powders. *Biomaterials.* 2002;23(4):1065–1072. [https://doi.org/10.1016/s0142-9612\(01\)00218-6](https://doi.org/10.1016/s0142-9612(01)00218-6)
16. Bose S., Tarafder S. Calcium phosphate ceramic systems in growth factor and drug delivery for bone tissue engineering: A review. *Acta Biomater.* 2012;8(4):1401–1421. <https://doi.org/10.1016/j.actbio.2011.11.017>
17. Parsamehr P.S., Zahed M., Tofighy M.A., Mohammadi T., Rezakazemi M. Preparation of novel cross-linked graphene oxide membrane for desalination applications using (EDC and NHS)-activated graphene oxide and PEI. *Desalination.* 2019;418(15):114079. <https://doi.org/10.1016/j.desal.2019.114079>
18. Poddar S., Agarwal P.S., Sahi A.K., Vajanthri K.Y., Pallawi Singh K.N., Mahto S.K. Fabrication and Cytocompatibility Evaluation of Psyllium Husk (Isabgol)/Gelatin Composite Scaffolds. *Appl. Biochem. Biotechnol.* 2019;188(3):750–768. <https://doi.org/10.1007/s12010-019-02958-7>
19. Nam K., Kimura T., Funamoto S., Kishida A. Preparation of a collagen/polymer hybrid gel designed for tissue membranes. Part I: Controlling the polymer-collagen cross-linking process using an ethanol/water co-solvent. *Acta Biomater.* 2010;6(2):403–408. <https://doi.org/10.1016/j.actbio.2009.06.021>
20. Teixeira S., Yang L., Dijkstra P.J., Ferraz M.P., Monteiro F.J. Heparinized hydroxyapatite/collagen three-dimensional scaffolds for tissue engineering. *J. Mater. Sci. Mater. Med.* 2010;21(8):2385–2392. <https://doi.org/10.1007/s10856-010-4097-2>
21. Hernigou P., Dubory A., Pariat J., Potage D., Roubineau F., Jammal S., Flouzat Lachaniette C.H. Beta-tricalcium phosphate for orthopedic reconstructions as an alternative to autogenous bone graft. *Morphologie.* 2017;101(334):173–179. <https://doi.org/10.1016/j.morpho.2017.03.005>
22. Owen G.Rh., Dard M., Larjava H. Hydroxyapatite/ β -tricalcium phosphate biphasic ceramics as regenerative material for the repair of complex bone defects. *J. Biomed. Mater. Res. B Appl. Biomater.* 2018;106(6):2493–2512. <https://doi.org/10.1002/jbm.b.34049>
23. Zhang L., Zhang Ch., Zhang R., Jiang D., Zhu Q., Wang S. Extraction and characterization of HA/ β -TCP biphasic calcium phosphate from marine fish. *Mat. Letters.* 2019;236(1):680–682. <https://doi.org/10.1016/j.matlet.2018.11.014>
24. Tanaka T., Komaki H., Chazono M., Kitasato S., Kakuta A., Akiyama S., Marumo K. Basic research and clinical application of beta-tricalcium phosphate (β -TCP). *Morphologie.* 2017;101(334):164–172. <https://doi.org/10.1016/j.morpho.2017.03.002>
25. Shishido A., Yokogawa Y. TEM Observation of Heat-Treated β -Tricalcium Phosphate Powder and its Precursor Obtained by Mechanochemical Reaction. *Key Eng. Mat.* 2017;758:184–188. <https://doi.org/10.4028/www.scientific.net/KEM.758.184>
26. Wen J., Kim I.Y., Kikuta K., Ohtsuki C. Optimization of Sintering Conditions for Improvement of Mechanical Property of α -Tricalcium Phosphate Blocks. *Glob. J. Biotechnol. Biomater. Sci.* 2016;1(1):010–016. <https://doi.org/10.17352/gjbs.000004>
27. Zhang E., Yang L., Xu J., Chen H. Microstructure, mechanical properties and bio-corrosion properties of Mg–Si(–Ca, Zn) alloy for biomedical application. *Acta Biomater.* 2010;6(5):1756–1762. <https://doi.org/10.1016/j.actbio.2009.11.024>
28. Chou J., Hao J., Kuroda S., Bishop D., Ben-Nissan B., Milthorpe B., Otsuka M. Bone Regeneration of Rat Tibial Defect by Zinc-Tricalcium Phosphate (Zn-TCP) Synthesized from Porous Foraminifera Carbonate Macrospheres. *Mar. Drugs.* 2013;11(12):5148–5158. <https://doi.org/10.3390/md1125148>
29. Hirota M., Hayakawa T., Shima T., Ametani A., Tohna I. High porous titanium scaffolds showed higher compatibility than lower porous beta-tricalcium phosphate scaffolds for regulating human osteoblast and osteoclast differentiation. *Mater. Sci. Eng. C: Mater. Biol. Appl.* 2015;49:623–631. <https://doi.org/10.1016/j.msec.2015.01.006>
30. Kaur G., Pandey O.P., Singh K., Homa D., Scott B., Pickrell G. A review of bioactive glasses: Their structure, properties, fabrication and apatite formation. *J. Biomed. Mater. Res. A.* 2014;102(1):254–274. <https://doi.org/10.1002/jbm.a.34690>
31. Fiume E., Barberi J., Vernè E., Bains F. Bioactive Glasses: From Parent 45S5 Composition to Scaffold-Assisted Tissue-Healing Therapies. *J. Funct. Biomater.* 2018;9(1):24. <https://doi.org/10.3390/jfb9010024>
32. Dittler M.L., Unalan I., Grünewald A., Beltrán A.M., Grillo C.A., Destch R., Gonzalez M.C., Boccaccini A.R. Bioactive glass (45S5)-based 3D scaffolds coated with magnesium and zinc-loaded hydroxyapatite nanoparticles for tissue engineering applications. *Colloids. Surf. B: Biointerfaces.* 2019;182:110346. <https://doi.org/10.1016/j.colsurfb.2019.110346>
33. Ferraris S., Yamaguchi S., Barbani N., Cazzola M., Cristallini C., Miola M., Vernè E., Spriano S. Bioactive materials: *In vitro* investigation of different mechanisms of hydroxyapatite precipitation. *Acta Biomater.* 2020;102:468–480. <https://doi.org/10.1016/j.actbio.2019.11.024>
34. O'Donnell M.D. Melt-Derived Bioactive Glass. In: *Bio-glasses: An introduction.* New Jersey, USA: John Wiley & Sons; 2012. P. 13–28. <https://doi.org/10.1002/9781118346457.ch2>
35. Höland W., Beall G. H. Glass-Ceramics. In: *Handbook of Advanced Ceramics: Materials, Applications, Processing and Properties.* New York, USA: Academic Press; 2013. Chapter 5.1. P. 371–381. <https://doi.org/10.1016/B978-0-12-385469-8.00021-6>
36. Nandi S.K., Mahato A., Kundu B., Mukherjee P. Doped Bioactive Glass Materials in Bone Regeneration. In: *Advanced Techniques in Bone Regeneration.* Norderstedt, Germany: BoD – Books on Demand; 2016. P. 275–328. <https://doi.org/10.5772/63266>

37. Zhang X., Zeng D., Li N., Wen J., Jiang X., Liu C., Li Y. Functionalized mesoporous bioactive glass scaffolds for enhanced bone tissue regeneration. *Sci Rep.* 2016;6:19361. <https://doi.org/10.1038/srep19361>
38. El-Rashidy A.A., Roether J.A., Harhaus L., Kneser U., Boccaccini A.R. Regenerating bone with bioactive glass scaffolds: A review of *in vivo* studies in bone defect models. *Acta Biomater.* 2017;62:1–28. <https://doi.org/10.1016/j.actbio.2017.08.030>
39. Bossard C., Granel H., Wittrant Y., Jallot É., Lao J., Vial C., Tiainen H. Polycaprolactone/bioactive glass hybrid scaffolds for bone regeneration. *Biomed. Glasses.* 2018;4(1):108–122. <https://doi.org/10.1515/bglass-2018-0010>
40. Ding Y., Souza M.T., Li W., Schubert D.W., Boccaccini A.R., Roether J.A. Bioactive Glass-Biopolymer Composites for Applications in Tissue Engineering. In: *Handbook of Bioceramics and Biocomposites*. Switzerland: Springer International Publishing; 2016. P. 325–356. https://doi.org/10.1007/978-3-319-12460-5_17
41. Meretoja V.V., Tirri T., Malin M., Seppälä J.V., Närhi T.O. Ectopic bone formation in and soft-tissue response to P(CL/DLLA)/bioactive glass composite scaffolds. *Clin. Oral. Implants Res.* 2014;25(2):159–164. <https://doi.org/10.1111/clr.12051>
42. Iqbal N., Khan A.S., Asif A., Yar M., Haycock J.W., Rehman I.U. Recent concepts in biodegradable polymers for tissue engineering paradigms: A critical review. *International Materials Reviews.* 2018. 64(2):91–126. <https://doi.org/10.1080/009506608.2018.1460943>
43. Shen Y., Tu T., Yi B., Wang X., Tang H., Liu W., Zhang Y. Electrospun acid-neutralizing fibers for the amelioration of inflammatory response. *Acta Biomater.* 2019;97:200–215. <https://doi.org/10.1016/j.actbio.2019.08.014>
44. Luo H., Xiong G., Li Q., Ma C., Zhu Y., Guo R. Preparation and properties of a novel porous poly(lactic acid) composite reinforced with bacterial cellulose nanowhiskers. *Fibers and Polym.* 2014;15(12):2591–2596. <https://doi.org/10.1007/s12221-014-2591-8>
45. Gentile P., Chiono V., Carmagnola I., Hatton P. V. An Overview of Poly(lactic-co-glycolic) Acid (PLGA)-Based Biomaterials for Bone Tissue Engineering. *Int. J. Mol. Sci.* 2014;15(3):3640–3659. <https://doi.org/10.3390/ijms15033640>
46. Elmowafy E.M., Tiboni M., Soliman M.E. Biocompatibility, biodegradation and biomedical applications of poly (lactic acid)/poly (lactic-co-glycolic acid) micro and nanoparticles. *J. Pharm. Investig.* 2019;49:347–380. <https://doi.org/10.1007/s40005-019-00439-x>
47. Anderson J.M., Shive M.S. Biodegradation and biocompatibility of PLA and PLGA microspheres. *Adv. Drug Deliv. Rev.* 2012;64:72–82. <https://doi.org/10.1016/j.addr.2012.09.004>
48. Yang F., Wang J., Hou J., Guo H., Liu C. Bone regeneration using cell-mediated responsive degradable PEG-based scaffolds incorporating with rhBMP-2. *Biomaterials.* 2013;34(5):1514–1528. <https://doi.org/10.1016/j.biomaterials.2012.10.058>
49. Ni P., Ding Q., Fan M., Liao J., Qian Z., Luo J. Injectable thermosensitive PEG-PCL-PEG hydrogel/acellular bone matrix composite for bone regeneration in cranial defects. *Biomaterials.* 2014;35(1):236–248. <https://doi.org/10.1016/j.biomaterials.2013.10.016>
50. Dorati R., DeTrizio A., Modena T., Conti B., Benazzo F., Gastaldi G. Biodegradable Scaffolds for Bone Regeneration Combined with Drug-Delivery Systems in Osteomyelitis Therapy. *Pharmaceuticals (Basel).* 2017;10(4):96. <https://doi.org/10.3390/ph10040096>
51. Buyuksungur S., Endogan Tanir T., Buyuksungur A., Bektas E.I., Torun Kose G., Yucel D. 3D printed poly-(ε-caprolactone) scaffolds modified with hydroxyapatite and poly(propylene fumarate) and their effects on the healing of rabbit femur defects. *Biomater Sci.* 2017;5(10):2144–2158. <https://doi.org/10.1039/c7bm00514h>
52. Volkmer E., Leicht U., Moritz M., Schwarz C., Wiese H., Milz S. Poloxamer-based hydrogels hardening at body core temperature as carriers for cell based therapies: *in vitro* and *in vivo* analysis. *J. Mater. Sci. Mater. Med.* 2013;24(9):2223–2234. <https://doi.org/10.1007/s10856-013-4966-6>
53. Amiryaghoubi N., Fathi M., Pesyan N.N., Samiei M., Barar J., Omid Y. Bioactive polymeric scaffolds for osteogenic repair and bone regenerative medicine. *Med. Res. Rev.* 2020;40(5):1833–1870. <https://doi.org/10.1002/med.21672>
54. Eğri S., Eczacıoğlu N. Sequential VEGF and BMP-2 releasing PLA-PEG-PLA scaffolds for bone tissue engineering: I. Design and *in vitro* tests. *Artif. Cells. Nanomed. Biotechnol.* 2017;45(2):321–329. <https://doi.org/10.3109/21691401.2016.1147454>
55. Schliephake H., Weich H., Dullin C., Gruber R., Frahse S. Mandibular bone repair by implantation of rhBMP-2 in a slow release carrier of poly(lactic acid)—An experimental study in rats. *Biomaterials.* 2008;29(1):103–110. <https://doi.org/10.1016/j.biomaterials.2007.09.019>
56. Facca S., Ferrand A., Mendoza-Palomares C., Perrin-Schmitt F., Netter P., Mainard D. Bone Formation Induced by Growth Factors Embedded into the Nanostructured Particles. *J. Biomed. Nanotechnol.* 2011;7(3):482–485. <https://doi.org/10.1166/jbn.2011.1311>
57. Wink J.D., Gerety P.A., Sherif R.D., Lim Y., Clarke N.A., Rajapakse C.S. Sustained Delivery of rhBMP-2 by Means of Poly(Lactic-co-Glycolic Acid) Microspheres: Cranial Bone Regeneration without Heterotopic Ossification or Craniosynostosis. *Plast. Reconstr. Surg.* 2014;134(1):51–59. <https://doi.org/10.1097/prs.0000000000000287>
58. Machatschek R., Schulz B., Lendlein A. The influence of pH on the molecular degradation mechanism of PLGA. *MRS Advances.* 2018;3(63):3883–3889. <https://doi.org/10.1557/adv.2018.602>
59. Liu Y., Ghassemi A.H., Hennink W.E., Schwendeman S.P. The microclimate pH in poly(D,L-lactide-co-hydroxymethyl glycolide) microspheres during biodegradation. *Biomaterials.* 2012;33(30):7584–7593. <https://doi.org/10.1016/j.biomaterials.2012.06.013>
60. Hines D.J., Kaplan D.L. Poly(lactic-co-glycolic) Acid-Controlled-Release Systems: Experimental and Modeling Insights. *Crit. Rev. Ther. Drug Carrier. Syst.* 2013;30(3):257–276. <https://doi.org/10.1615/critrevtherdrugcarrieryst.2013006475>
61. Kutikov A.B., Song J. Biodegradable PEG-Based Amphiphilic Block Copolymers for Tissue Engineering Applications. *ACS Biomater. Sci. Eng.* 2015;1(7):463–480. <https://doi.org/10.1021/acsbiomaterials.5b00122>
62. Pan H., Zheng Q., Guo X., Wu Y., Wu B. Polydopamine-assisted BMP-2-derived peptides immobilization on biomimetic copolymer scaffold for enhanced bone induction *in vitro* and *in vivo*. *Colloids Surf. B Biointerfaces.* 2016;142:1–9. <https://doi.org/10.1016/j.colsurfb.2016.01.060>
63. Majchrowicz A., Roguska A., Krawczyńska A., Lewandowska M., Marti-Muñoz J., Engel E. *In vitro* evaluation of degradable electrospun poly(lactic acid)/bioactive calcium phosphate ormoglass scaffolds. *Archiv. Civ. Mech. Eng.* 2020;20:1–11. <https://doi.org/10.1007/s43452-020-00052-y>

64. Amini A.R., Laurencin C.T., Nukavarapu S.P. Bone Tissue Engineering: Recent Advances and Challenges. *Crit. Rev. Biomed. Eng.* 2012;40(5):363–408. <https://doi.org/10.1615/critrevbiomedeng.v40.i5.10>
65. Park S.H., Park S.A., Kang Y.G., Shin J.W., Park Y.S., Gu S.R. PCL/ β -TCP Composite Scaffolds Exhibit Positive Osteogenic Differentiation with Mechanical Stimulation. *Tissue Eng. Regen. Med.* 2017;14(4):349–358. <https://doi.org/10.1007/s13770-017-0022-9>
66. Shin D.Y., Kang M.H., Kang I.G., Kim H.E., Jeong S.H. *In vitro* and *in vivo* evaluation of polylactic acid-based composite with tricalcium phosphate microsphere for enhanced biodegradability and osseointegration. *J. Biomater. Appl.* 2018;32(10):1360–1370. <https://doi.org/10.1177/0885328218763660>
67. Wang Y., Zhao Q., Han N., Bai L., Li J., Liu J., Che E., Hu L., Zhang Q., Jiang T., Wang S. Mesoporous silica nanoparticles in drug delivery and biomedical applications. *Nanomedicine.* 2015;11(2):313–327. <https://doi.org/10.1016/j.nano.2014.09.014>
68. Cheng H., Chawla A., Yang Y., Li Y., Zhang J., Jang H.L., Khademhosseini A. Development of nanomaterials for bone-targeted drug delivery. *Drug Discov. Today.* 2017;22(9):1336–1350. <https://doi.org/10.1016/j.drudis.2017.04.021>
69. Zhou Y., Quan G., Wu Q., Zhang X., Niu B., Wu B., Huang Y., Pan X., Wu C. Mesoporous silica nanoparticles for drug and gene delivery. *Acta Pharm. Sin. B.* 2017;8(2):165–177. <https://doi.org/10.1016/j.apsb.2018.01.007>
70. Vallet-Regí M. Ordered Mesoporous Materials in the Context of Drug Delivery Systems and Bone Tissue Engineering. *Chemistry.* 2006;12(23):5934–5943. <https://doi.org/10.1002/chem.200600226>
71. Ma M., Zheng S., Chen H., Yao M., Zhang K., Jia X., Mou J., Xu H., Wu R., Shi J. A combined “RAFT” and “Graft From” polymerization strategy for surface modification of mesoporous silica nanoparticles: towards enhanced tumor accumulation and cancer therapy efficacy. *J. Mater. Chem. B.* 2014;2(35):5828–5836. <https://doi.org/10.1039/C3TB21666G>
72. Motealleh A., Kehr N. S. Nanocomposite Hydrogels and Their Applications in Tissue Engineering. *Adv. Healthc. Mater.* 2017;6(1):10.1002/adhm.201600938. <https://doi.org/10.1002/adhm.201600938>
73. Xin T., Mao J., Liu L., Tang J., Wu L., Yu X., Gu Y., Cui W., Chen L. Programmed Sustained Release of Recombinant Human Bone Morphogenetic Protein-2 and Inorganic Ion Composite Hydrogel as Artificial Periosteum. *ACS Appl. Mater. Interfaces.* 2020;12(6):6840–6851. <https://doi.org/10.1021/acsami.9b18496>
74. Zhang D., Liu X., Wu G. Forming CNT-guided stereocomplex networks in polylactide-based nanocomposites. *Compos. Sci. Technol.* 2016;128:8–16. <https://doi.org/10.1016/j.compscitech.2016.03.003>
75. Kumar S.K., Jouault N., Benicewicz B., Neely T. Nanocomposites with Polymer Grafted Nanoparticles. *Macromolecules.* 2013;46(9):3199–3214. <https://doi.org/10.1021/ma4001385>
76. Mikael P.E., Amini A.R., Basu J., Josefina Arellano-Jimenez M., Laurencin C.T., Sanders M.M., Barry Carter C., Nukavarapu S.P. Functionalized carbon nanotube reinforced scaffolds for bone regenerative engineering: fabrication, *in vitro* and *in vivo* evaluation. *Biomed. Mater.* 2014;9(3):035001. <https://doi.org/10.1088/1748-6041/9/3/035001>
77. Shrestha B., DeLuna F., Anastasio M.A., Yong Ye J., Brey E.M. Photoacoustic Imaging in Tissue Engineering and Regenerative Medicine. *Tissue Eng. Part B Rev.* 2020;26(1):79–102. <https://doi.org/10.1089/ten.TEB.2019.0296>
78. Lorite G.S., Pitkänen O., Mohl M., Kordas K., Koivisto J.T., Kellomäki M., Monique Mendonça C.P., Jesus M.B. Carbon nanotube-based matrices for tissue engineering. In: *Materials for Biomedical Engineering. Bioactive Materials, Properties, and Applications.* Elsevier; 2019. Chapter 10. P. 323–353. <https://doi.org/10.1016/B978-0-12-818431-8.00003-9>
79. Zhu S., Jing W., Hu X., Huang Z., Cai Q., Ao Y., Yang X. Time-dependent effect of electrical stimulation on osteogenic differentiation of bone mesenchymal stromal cells cultured on conductive nanofibers. *J. Biomed. Mater. Res. A.* 2017;105(12):3369–3383. <https://doi.org/10.1002/jbm.a.36181>
80. Andrade V.B., Sá M.A., Mendes R.M., Martins-Júnior P.A., Silva G., Sousa B.R. Enhancement of Bone Healing by Local Administration of Carbon Nanotubes Functionalized with Sodium Hyaluronate in Rat Tibiae. *Cells Tissues Organs.* 2017;204(3–4):137–149. <https://doi.org/10.1159/000453030>
81. Sá M.A., Andrade V.B., Mendes R.M., Caliarí M.V., Ladeira L.O., Silva E.E., Silva G.A., Corrêa-Júnior J.D., Ferreira A.J. Carbon nanotubes functionalized with sodium hyaluronate restore bone repair in diabetic rat sockets. *Oral Dis.* 2013;19(5):484–493. <https://doi.org/10.1111/odi.12030>
82. Wang X., Huang Z., Wei M., Lu T., Nong D., Zhao J., Gao X., Teng L. Catalytic effect of nanosized ZnO and TiO₂ on thermal degradation of poly(lactic acid) and isoconversional kinetic analysis. *Thermochimica Acta.* 2019;672:14–24. <https://doi.org/10.1016/j.tca.2018.12.008>
83. Lebedev S.M. Manufacturing poly(lactic acid)/metal composites and their characterization. *Int. J. Adv. Manuf. Technol.* 2019;102:3213–3216. <https://doi.org/10.1007/s00170-019-03420-y>
84. Glenske K., Donkiewicz P., Köwitsch A., Milosevic-Oljaca N., Rider P., Rofall S., Franke J., Jung O., Smeets R., Schnettler R., Wenisch S., Barbeck M. Applications of Metals for Bone Regeneration. *Int. J. Mol. Sci.* 2018;19(3):826. <https://doi.org/10.3390/ijms19030826>
85. Trujillo S., Lizundia E., Vilas J.L., Salmeron-Sanchez M. PLLA/ZnO nanocomposites: Dynamic surfaces to harness cell differentiation. *Colloids Surf. B Biointerfaces.* 2016;144:152–160. <https://doi.org/10.1016/j.colsurfb.2016.04.007>
86. Pérez-Álvarez L., Lizundia E., Ruiz-Rubio L., Benito V., Moreno I., Luis J., Vilas-Vilela J.S. Hydrolysis of poly(L-lactide)/ZnO nanocomposites with antimicrobial activity. *J. Appl. Polym. Sci.* 2019;136(28):47786. <https://doi.org/10.1002/app.47786>
87. Zhao Y., Liang H., Zhang S., Qu S., Jiang Y., Chen M. Effects of Magnesium Oxide (MgO) Shapes on *In Vitro* and *In Vivo* Degradation Behaviors of PLA/MgO Composites in Long Term. *Polymers.* 2020;12(5):E1074. <https://doi.org/10.3390/polym12051074>
88. Brown A., Zaky S., Ray H. J., Sfeir C. Porous magnesium/PLGA composite scaffolds for enhanced bone regeneration following tooth extraction. *Acta Biomater.* 2015;11:543–553. <https://doi.org/10.1016/j.actbio.2014.09.008>
89. Urdzíkova L., Jendelová P., Glogarová K., Burian M., Hájek M., Syková E. Transplantation of Bone Marrow Stem Cells as well as Mobilization by Granulocyte-Colony Stimulating Factor Promotes Recovery after Spinal Cord Injury in Rats. *J. Neurotrauma.* 2016;24(9):1379–1391. <https://doi.org/10.1089/neu.2006.23.1379>

90. Li Y., Ye D., Li M., Ma M., Gu N. Adaptive Materials Based on Iron Oxide Nanoparticles for Bone Regeneration. *ChemPhysChem*. 2018;19(16):1965–1979. <https://doi.org/10.1002/cphc.201701294>
91. Sharifi S., Seyednejad H., Laurent S., Atyabi F., Saei A.A., Mahmoudi M. Superparamagnetic iron oxide nanoparticles for *in vivo* molecular and cellular imaging. *Contrast Media Mol. Imaging*. 2015;10(5):329–355. <https://doi.org/10.1002/cmml.1638>
92. Kremen T. J., Bez M., Sheyn D., Ben-David S., Da X., Tawackoli W., Wagner S., Gazit D., Pelled G. *In Vivo* Imaging of Exogenous Progenitor Cells in Tendon Regeneration via Superparamagnetic Iron Oxide Particles. *Am. J. Sports Med.* 2019;47(11):2737–2744. <https://doi.org/10.1177%2F0363546519861080>
93. Meng J., Xiao B., Zhang Y., Liu J., Xue H., Lei J., Kong H., Huang Y., Jin Z., Gu N., Xu H. Super-paramagnetic responsive nanofibrous scaffolds under static magnetic field enhance osteogenesis for bone repair *in vivo*. *Sci. Rep.* 2013;3:2655. <https://doi.org/10.1038/srep02655>
94. Ghassemi T., Shahroodi A., Ebrahimzadeh M.H., Mousavian A., Movaffagh J., Moradi A. Current Concepts in Scaffolding for Bone Tissue Engineering. *Arch. Bone Jt. Surg.* 2018;6(2):90–99. <https://dx.doi.org/10.22038/abjs.2018.26340.1713>
95. Akilbekova D., Shaimerdenova M., Adilov S., Berillo D. Biocompatible scaffolds based on natural polymers for regenerative medicine. *Int. J. Biol. Macromol.* 2018;114:324–333. <https://doi.org/10.1016/j.ijbiomac.2018.03.116>
96. Sofi H.S., Ashraf R., Beigh M.A., Sheikh F.A. Scaffolds Fabricated from Natural Polymers/Composites by Electrospinning for Bone Tissue Regeneration. *Adv. Exp. Med. Biol.* 2018;1078:49–78. https://doi.org/10.1007/978-981-13-0950-2_4
97. Islam S., Rahman Bhuiyan M.A., Islam M.N. Chitin and Chitosan: Structure, Properties and Applications in Biomedical Engineering. *J. Polym. Environ.* 2017;25:854–866. <https://doi.org/10.1007/s10924-016-0865-5>
98. Ahsan S.M., Thomas M., Reddy K.K., Sooraparaju S.G., Asthana A., Bhatnagar I. Chitosan as biomaterial in drug delivery and tissue engineering. *Int. J. Biol. Macromol.* 2018;110:97–109. <https://doi.org/10.1016/j.ijbiomac.2017.08.140>
99. Lei B., Guo B., Rambhia K.J., Ma P.X. Hybrid polymer biomaterials for bone tissue regeneration. *Front. Med.* 2019;13(2):189–201. <https://doi.org/10.1007/s11684-018-0664-6>
100. Shen R., Xu W., Xue Y., Chen L., Ye H., Zhong E., Ye Z., Gao J., Yan Y. The use of chitosan/PLA nano-fibers by emulsion eletrospinning for periodontal tissue engineering. *Artif. Cells Nanomed. Biotechnol.* 2018;46(sup2):419–430. <https://doi.org/10.1080/21691401.2018.1458233>
101. Yun Y.P., Lee S.Y., Kim H.J., Song J.J., Kim S.E. Improvement of osteoblast functions by sustained release of bone morphogenetic protein-2 (BMP-2) from heparin-coated chitosan scaffold. *Tissue Eng. Regen. Med.* 2013;10:183–191. <https://doi.org/10.1007/s13770-013-0389-1>
102. Russo E., Gaglianone N., Baldassari S., Parodi B., Cafaggi S., Zibana C., Donalisio M., Cagno V., Lembo D., Caviglioli G. Preparation, characterization and *in vitro* antiviral activity evaluation of foscarnet-chitosan nanoparticles. *Colloids Surf. B: Biointerfaces*. 2014;118:117–125. <https://doi.org/10.1016/j.colsurfb.2014.03.037>
103. Cao L., Werkmeister J.A., Wang J., Glattauer V., McLean K.M., Liu C. Bone regeneration using photocrosslinked hydrogel incorporating rhBMP-2 loaded 2-N, 6-O-sulfated chitosan nanoparticles. *Biomaterials*. 2014;35(9):2730–2742. <https://doi.org/10.1016/j.biomaterials.2013.12.028>
104. Cao L., Wang J., Hou J., Xing W., Liu C. Vascularization and bone regeneration in a critical sized defect using 2-N,6-O-sulfated chitosan nanoparticles incorporating BMP-2. *Biomaterials*. 2014;35(2):684–698. <https://doi.org/10.1016/j.biomaterials.2013.10.005>
105. Echave M.C., Saenz del Burgo L., Pedraz J.L., Orive G. Gelatin as Biomaterial for Tissue Engineering. *Curr. Pharm. Des.* 2017;23(24):3567–3584. <https://doi.org/10.2174/0929867324666170511123101>
106. Poursamar S.A., Hatami J., Lehner A.N., da Silva C.L., Ferreira F.C., Antunes A.P. Gelatin porous scaffolds fabricated using a modified gas foaming technique: Characterisation and cytotoxicity assessment. *Mater. Sci. Eng. C Mater. Biol. Appl.* 2015;48:63–70. <https://doi.org/10.1016/j.msec.2014.10.074>
107. Peng Y.Y., Glattauer V., Ramshaw J.A. Stabilisation of Collagen Sponges by Glutaraldehyde Vapour Crosslinking. *Int. J. Biomater.* 2017;2017:8947823. <https://doi.org/10.1155/2017/8947823>
108. Yokota K., Matsuno T., Tabata Y., Mataga I. Evaluation of a Porous Hydroxyapatite Granule and Gelatin Hydrogel Microsphere Composite in Bone Regeneration. *J. Hard Tissue Biol.* 2017;26(2):203–214. <https://doi.org/10.2485/jhtb.26.203>
109. Elvin C.M., Brownlee A.G., Huson M.G., Tebb T.A., Kim M., Lyons R.E., Vuocolo T., Liyou N.E., Hughes T.C., Ramshaw J.A., Werkmeister J.A. The development of photochemically crosslinked native fibrinogen as a rapidly formed and mechanically strong surgical tissue sealant. *Biomaterials*. 2009;30(11):2059–2065 <https://doi.org/10.1016/j.biomaterials.2008.12.059>
110. Monteiro N., Thirivikraman G., Athirasala A., Tahayeri A., França C.M., Ferracane J.L., Bertassoni L.E. Photopolymerization of cell-laden gelatin methacryloyl hydrogels using a dental curing light for regenerative dentistry. *Dent. Mater.* 2018;34(3):389–399. <https://doi.org/10.1016/j.dental.2017.11.020>
111. Lin C.H., Su J.J., Lee S.Y., Lin Y.M. Stiffness modification of photopolymerizable gelatin-methacrylate hydrogels influences endothelial differentiation of human mesenchymal stem cells. *J. Tissue Eng. Regen. Med.* 2018;12(10):2099–2111. <https://doi.org/10.1002/term.2745>
112. Kilic Bektas C., Hasirci V. Mimicking corneal stroma using keratocyte-loaded photopolymerizable methacrylated gelatin hydrogels. *J. Tissue Eng. Regen. Med.* 2018;12(4):e1899–e1910. <https://doi.org/10.1002/term.2621>
113. Gan Y., Li P., Wang L., Mo X., Song L., Xu Y., Zhao C., Ouyang B., Tu B., Luo L., Zhu L., Dong S., Li F., Zhou Q. An interpenetrating network-strengthened and toughened hydrogel that supports cell-based nucleus pulposus regeneration. *Biomaterials*. 2017;136:12–28. <https://doi.org/10.1016/j.biomaterials.2017.05.017>
114. Dong C., Lv Y. Application of Collagen Scaffold in Tissue Engineering: Recent Advances and New Perspectives. *Polymers*. 2016;8(2):42. <https://doi.org/10.3390/polym8020042>
115. Zhang D., Wu X., Chen J., Lin K. The development of collagen based composite scaffolds for bone regeneration. *Bioact. Mater.* 2017;3(1):129–138. <https://doi.org/10.1016/j.bioactmat.2017.08.004>

116. Gu L., Shan T., Ma Y.X., Tay F.R., Niu L. Novel Biomedical Applications of Crosslinked Collagen. *Trends Biotechnol.* 2019;37(5):464–491. <https://doi.org/10.1016/j.tibtech.2018.10.007>
117. Badiyan Z.S., Berezanskyy T., Utzinger M., Aneja M.K., Emrich D., Erben R., Schüler C., Altpeter P., Ferizi M., Hasenpusch G., Rudolph C., Plank C. Transcript-activated collagen matrix as sustained mRNA delivery system for bone regeneration. *J. Control Release.* 2016;239:137–148. <https://doi.org/10.1016/j.jconrel.2016.08.037>
118. Hettiaratchi M.H., Krishnan L., Rouse T., Chou C., McDevitt T.C., Gulberg R.E. Heparin-mediated delivery of bone morphogenetic protein-2 improves spatial localization of bone regeneration. *Sci. Adv.* 2020;6(1):eaay1240. <https://doi.org/10.1126/sciadv.aay1240>
119. Peckman S., Zanella J.M., McKay W.F. Infuse® Bone Graft. In: *Drug-Device Combinations for Chronic Diseases*. New Jersey, USA: John Wiley & Sons; 2015;241–260. <https://doi.org/10.1002/9781119002956.ch09>
120. Scalzone A., Flores-Mir C., Carozza D., d'Apuzzo F., Grassia V., Perillo L. Secondary alveolar bone grafting using autologous versus alloplastic material in the treatment of cleft lip and palate patients: systematic review and meta-analysis. *Prog. Orthod.* 2019;20(1):6. <https://doi.org/10.1186/s40510-018-0252-y>
121. Bowler D., Dym H. Bone Morphogenetic Protein: Application in Implant Dentistry. *Dent. Clin. North. Am.* 2015;59(2):493–503. <https://doi.org/10.1016/j.cden.2014.10.006>
122. Geiger M., Li R.H., Friess W. Collagen sponges for bone regeneration with rhBMP-2. *Adv. Drug Deliv. Rev.* 2003;55(12):1613–1629. <https://doi.org/10.1016/j.addr.2003.08.010>
123. Oryan A., Kamali A., Moshiri A., Baharvand H., Daemi H. Chemical crosslinking of biopolymeric scaffolds: Current knowledge and future directions of crosslinked engineered bone scaffolds. *Int. J. Biol. Macromol.* 2018;107(Pt A):678–688. <https://doi.org/10.1016/j.ijbiomac.2017.08.184>
124. Dai M., Liu X., Wang N., Sun J. Squid type II collagen as a novel biomaterial: Isolation, characterization, immunogenicity and relieving effect on degenerative osteoarthritis via inhibiting STAT1 signaling in pro-inflammatory macrophages. *Mater. Sci. Eng. C Mater. Biol. Appl.* 2018;89:283–294. <https://doi.org/10.1016/j.msec.2018.04.021>
125. Monaco G., Cholas R., Salvatore L., Madaghiale M., Sannino A. Sterilization of collagen scaffolds designed for peripheral nerve regeneration: Effect on microstructure, degradation and cellular colonization. *Mater. Sci. Eng. C Mater. Biol. Appl.* 2017;71:335–344. <https://doi.org/10.1016/j.msec.2016.10.030>
126. Delgado L.M., Fuller K., Zeugolis D.I. Influence of Cross-Linking Method and Disinfection/Sterilization Treatment on the Structural, Biophysical, Biochemical, and Biological Properties of Collagen-Based Devices. *ACS Biomater. Sci. Eng.* 2018;4(8):2739–2747. <https://doi.org/10.1021/acsbiomaterials.8b00052>
127. Dai Z., Ronholm J., Tian Y., Sethi B., Cao X. Sterilization techniques for biodegradable scaffolds in tissue engineering applications. *J. Tissue Eng.* 2016;7:2041731416648810. <https://doi.org/10.1177/2041731416648810>
128. Nune K.C., Misra R., Bai Y., Li S., Yang R. Interplay of topographical and biochemical cues in regulating osteoblast cellular activity in BMP-2 eluting three-dimensional cellular titanium alloy mesh structures. *J. Biomed. Mater. Res. A.* 2019;107(1):49–60. <https://doi.org/10.1002/jbm.a.36520>
129. Cha J.K., Song Y.W., Kim S., Thoma D.S., Jung U.W., Jung R.E. Core Ossification of Bone Morphogenetic Protein-2-Loaded Collagenated Bone Mineral in the Sinus. *Tissue Eng. Part A.* 2020;10.1089/ten.TEA.2020.0151. <https://doi.org/10.1089/ten.tea.2020.0151>

About the authors:

Dmitry D. Lykoshin, Engineer-Researcher, Laboratory of Biopharmaceutical Technologies, Shemyakin and Ovchinnikov Institute of Bioorganic Chemistry, Russian Academy of Sciences (16/10, Miklukho-Maklaya ul., Moscow, 117997, Russia). E-mail: ldd-94@ya.ru. Scopus Author ID 57219992166, ResearcherID AAB-1166-2021, <https://orcid.org/0000-0003-1612-1643>

Vladimir V. Zaitsev, Cand. Sci. (Med.), Leading Researcher, Team Leader of osteoplastic materials, N.N. Priorov National Medical Research Center of Traumatology and Orthopedics, Ministry of Health of the Russian Federation, (10, Priorova ul., Moscow, 127299, Russia). E-mail: zaitsev-cito@mail.ru. Scopus Author ID 56648236900, ResearcherID AAI-4110-2020, <https://orcid.org/0000-0003-1109-5642>

Maria A. Kostromina, Junior Researcher, Laboratory of Biopharmaceutical Technologies, Shemyakin and Ovchinnikov Institute of Bioorganic Chemistry, Russian Academy of Sciences (16/10, Miklukho-Maklaya ul., Moscow, 117997, Russia). E-mail: kostromasha@mail.ru. Scopus Author ID 55123242300 ResearcherID R-9418-2016, <https://orcid.org/0000-0001-6768-8995>

Roman S. Esipov, Dr. Sci. (Chem.), Principal Researcher, Head of the Laboratory of Biopharmaceutical Technologies, Shemyakin and Ovchinnikov Institute of Bioorganic Chemistry, Russian Academy of Sciences, (16/10, Miklukho-Maklaya ul., Moscow, 117997, Russia). E-mail: refolding@mail.ru. Scopus Author ID 6701850033, Researcher ID G-4950-2017, <https://orcid.org/0000-0002-3231-5838>

Об авторах:

Лыкошин Дмитрий Дмитриевич, инженер лаборатории биофармацевтических технологий Федерального государственного бюджетного учреждения науки Институт биоорганической химии им. академиков М.М. Шемякина и Ю.А. Овчинникова Российской академии наук (Россия, 117997, Москва, ул. Миклухо-Маклая, д. 16/10, к. 1). E-mail: ldd-94@yandex.ru. Scopus Author ID 57219992166, ResearcherID AAB-1166-2021, <https://orcid.org/0000-0003-1612-1643>

Зайцев Владимир Валентинович, к.м.н., ведущий научный сотрудник, руководитель группы остеопластических материалов, Национальный медицинский исследовательский центр травматологии и ортопедии им. Н.Н. Приорова, Министерство здравоохранения Российской Федерации. (Россия, 127299, Москва, ул. Приорова, д. 10). E-mail: zaitsev-cito@mail.ru. Scopus Author ID 56648236900, ResearcherID AAI-4110-2020, <https://orcid.org/0000-0003-1109-5642>

Костромина Мария Андреевна, младший научный сотрудник лаборатории биофармацевтических технологий Федерального государственного бюджетного учреждения науки Институт биоорганической химии им. академиков М.М. Шемякина и Ю.А. Овчинникова Российской академии наук (Россия, 117997, Москва, ул. Миклухо-Маклая, д. 16/10, к. 1). E-mail: kostromasha@mail.ru. Scopus Author ID 55123242300 ResearcherID R-9418-2016, <https://orcid.org/0000-0001-6768-8995>

Есилов Роман Станиславович, д.х.н., старший научный сотрудник, заведующий лабораторией биофармацевтических технологий Федерального государственного бюджетного учреждения науки Институт биоорганической химии им. академиков М.М. Шемякина и Ю.А. Овчинникова Российской академии наук (Россия, 117997, Москва, ул. Миклухо-Маклая, д. 16/10, к. 1). E-mail: refolding@mail.ru. Scopus Author ID 6701850033, Researcher ID G-4950-2017, <https://orcid.org/0000-0002-3231-5838>

The article was submitted: November 20, 2020; approved after reviewing: December 19, 2020; accepted for publication: January 30, 2021.

Translated from Russian into English by H. Moshkov

Edited for English language and spelling by Enago, an editing brand of Crimson Interactive Inc.

ISSN 2686-7575 (Online)

<https://doi.org/10.32362/2410-6593-2021-16-2-xx-yy>



UDC 548.736

RESEARCH ARTICLE

Neutron-diffraction study of the cubic-tetragonal phase structural transition in the single crystals of the solid solutions of zirconium and yttrium oxides

Viktor A. Sarin, Alexander A. Bush[@]

MIREA – Russian Technological University, Moscow, 119454 Russia

[@]Corresponding author, e-mail: aabush@yandex.ru

Abstract

Objectives. The determination of the phase relations, crystallographic characteristics, microstructure features, and atomic crystal structure of zirconium oxide crystals that are partially and completely stabilized by yttrium oxide additives, and the identification of the crystallographic and crystal-chemical correlations with the physicochemical properties of single crystals.

Methods. The neutron structure of the crystals was studied using the neutron time-of-flight and constant wavelength methods using a high-resolution Fourier diffractometer on the IBR-2 pulsed fast reactor and a four-circle neutron diffractometer “Syntex.” Single crystals were grown by directed crystallization from the melts of mixtures $(1 - x)\text{ZrO}_2 \cdot x\text{Y}_2\text{O}_3$, $x = 0.03$ and $x = 0.12$ with different growth rates (10 and 40 mm/h).

Results. It was observed that when growing single crystals with $x = 0.03$ – 0.05 , the crystal was stratified into cubic and tetragonal phases, and the ratio between the phases depended on the growth rate. At a growth rate of 40 mm/h, the content of the cubic phase was insignificant. In the crystals of partially stabilized zirconium dioxide (ZrO_2) with the additions of 3 mol % Y_2O_3 , the coherent coexistence of cubic and tetragonal phases was established, and the twin law for a tetragonal component (rotation of unit cell axis by 90° around the **a** (**b**) axis) that was observed during the phase transition from high-temperature cubic phase to tetragonal phase was determined. For the fully stabilized zirconium oxide of the cubic symmetry (with 12 mol % Y_2O_3), the 0.3 Å displacements of oxygen atoms from their partial structural positions in the directions [100] and [111] were determined. These displacements correlated with the directions of the ion transport.

Conclusions. Previous studies have shown that the ratio between the cubic and tetragonal phases of the single crystals of the ZrO_2 – Y_2O_3 system depends on the growth rate of the single crystals. The content of Y_2O_3 in the cubic and tetragonal phases of a single crystal was determined using the non-destructive neutronography method on the same volume sample of a solid solution of this system. Moreover, the displacements of oxygen atoms from the main position of the crystal were determined.

Keywords: yttrium oxide-stabilized ZrO_2 crystals, neutron structure analysis, crystal microstructure, atomic crystal structure

For citation: Sarin V.A., Bush A.A. Neutron-diffraction study of the cubic-tetragonal phase structural transition in the single crystals of the solid solutions of zirconium and yttrium oxides. *Tonk. Khim. Tekhnol. = Fine Chem. Technol.* 2021;16(2):xx–yy (Russ., Eng.). <https://doi.org/10.32362/2410-6593-2021-16-2-xx-yy>

НАУЧНАЯ СТАТЬЯ

Нейтроннографическое исследование структурного перехода кубическая–тетрагональная фаза в монокристаллах твердых растворов оксида циркония с оксидом иттрия

В.А. Сарин, А.А. Буш[@]

МИРЭА – Российский технологический университет, Москва, 119454 Россия

[@]Автор для переписки, e-mail: aabush@yandex.ru

Аннотация

Цели. Определение фазовых соотношений, кристаллографических характеристик, особенностей микроструктуры и атомно-кристаллической структуры кристаллов оксида циркония, частично и полностью стабилизированных добавками оксида иттрия, выявление кристаллографических и кристаллохимических корреляций с физико-химическими свойствами монокристаллов.

Методы. Нейтронноструктурные исследования кристаллов проведены методами времени пролета нейтронов и постоянной длины волны с использованием Фурье дифрактометра высокого разрешения на импульсном быстром реакторе ИБР-2 и четырехкружного нейтронного дифрактометра «Синтекс». Монокристаллы были выращены направленной кристаллизацией из расплавов смесей $(1-x)ZrO_2 \cdot xY_2O_3$, $x = 0.03$ и 0.12 с разными скоростями роста (10 и 40 мм/ч).

Результаты. Установлено, что при выращивании монокристаллов с $x = 0.03–0.05$ происходит расслоение кристалла на кубическую и тетрагональную фазы, соотношение между которыми зависит от скорости выращивания. При скорости роста 40 мм/ч содержание кубической фазы незначительно. В кристаллах частично стабилизированного диоксида циркония ZrO_2 (с добавками 3 mol % Y_2O_3) установлено когерентное сосуществование кубической и тетрагональной фаз и определен закон двойникования для тетрагональной компоненты (вращение осей элементарной ячейки на 90° вокруг осей **a** (**b**)), возникающего при фазовом переходе из высокотемпературной кубической фазы в тетрагональную. Для полностью стабилизированного диоксида циркония кубической симметрии (с 12 mol % Y_2O_3) определены смещения атомов кислорода на 0.3 \AA из их частных структурных позиций в направлениях $[100]$ и $[111]$. Эти смещения коррелирует с направлениями ионного транспорта.

Выводы. Исследования показали, что соотношение между кубической фазой и тетрагональной фазой монокристаллов системы $ZrO_2–Y_2O_3$ зависит от скорости выращивания монокристаллов. На одном и том же объемном образце твердого раствора этой системы неразрушающим методом нейтроннографии определено содержание Y_2O_3 и в кубической, и в тетрагональной фазе монокристалла. Определены смещения атомов кислорода из основной позиции кристалла.

Ключевые слова: стабилизированные оксидом иттрия кристаллы ZrO_2 , нейтронноструктурный анализ, микроструктура кристаллов, атомно-кристаллическая структура

Для цитирования: Сарин В.А., Буш А.А. Нейтроннографическое исследование структурного перехода кубическая–тетрагональная фаза в монокристаллах твердых растворов оксида циркония с оксидом иттрия. *Тонкие химические технологии.* 2021;16(1):55–66. <https://doi.org/10.32362/2410-6593-2021-16-1-55-66>

INTRODUCTION

The first practical application of a solid electrolyte based on the ceramics comprising yttrium-stabilized zirconium oxide was described in the patent of the famous German physicochemist, Walter Nernst, in the autumn of 1897 [1]. The patent was concerned with the description of the design of an incandescent lamp, where an oxygen-containing solid electrolyte was first used as an incandescent element. This was the so-called Nernst lamp, which worked in open air without vacuuming the bulb. Materials based on stabilized zirconium oxide are now widely used in applications such as to create oxide fuel cells, solids, and chemically resistant electrolytes for the sensors of oxygen content in liquid and gaseous media in high-temperature ranges. An important advantage for the design development is the presence of high mechanical and strength properties, which are possessed by materials based on stabilized zirconium oxide.

However, ceramic materials based on zirconium oxide still have certain mechanical drawbacks, such as low cracking resistance, poor antifricationality, and brittleness. Therefore, a fundamentally new step in the materials science of the composite materials based on zirconium oxide was the development of a method for producing zirconium oxide single crystals by the directional crystallization of the melt in a "cold container." This was performed at the Institute of General Physics of the Russian Academy of Sciences using direct high-frequency heating, and fully stabilized zirconium dioxide was produced using this method with high ionic conductivity. Further, a relatively new material, i.e., partially stabilized zirconium dioxide (PSZD), which has high mechanical and tribological characteristics, was afforded [2].

CRYSTALLOGRAPHY OF THE PHASES OF ZIRCONIUM OXIDE

Pure zirconium dioxide has three polymorphic phases [3]: cubic ($Fm\bar{3}m$) at $T > 2640$ K, tetragonal ($P4_2/nmc$) at $T = 1440\text{--}2640$ K, and monoclinic ($P2_1/c$) at $T < 1440$ K. The monoclinic and tetragonal phases are the distorted modifications of the cubic structure of the fluorite type. The phases with a cubic structure can be obtained at room temperature by adding stabilizing oxides, such as MgO, CaO, CeO₂, and Y₂O₃, to ZrO₂. The phase diagram of the ZrO₂-Y₂O₃ system is shown in Fig. 1. In the ZrO₂-Y₂O₃ system, the areas of the phase diagram are of interest wherein a tetragonal phase (~ 3 mol % Y₂O₃) and a cubic phase (> 8 mol % Y₂O₃) are present. In the 3 mol % region, the phase transition with a decrease in temperature was performed through

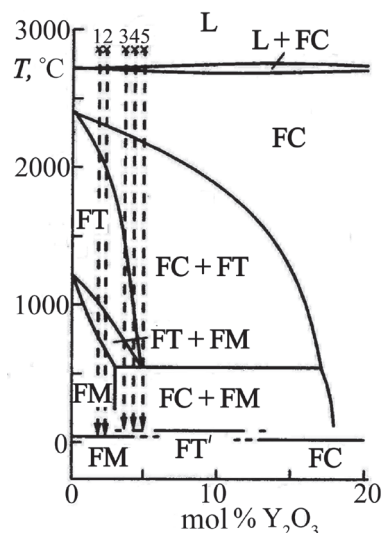


Fig. 1. Phase diagram of the ZrO₂-Y₂O₃ system in the region rich in zirconium dioxide; dotted lines are the cooling lines of the initial compositions: $(1-x)\text{ZrO}_2 \cdot x\text{Y}_2\text{O}_3$ with $x = 0.0086$ (1), 0.0100 (2), 0.0178 (3), 0.0200 (4), and 0.0234 (5) [3] (L – liquid phase, FC, FT, and FM – fluorite cubic, tetragonal, and monoclinic phases, respectively).

the region of coexistence of the cubic and tetragonal phases. The resulting tetragonal phase is commonly referred to as the metastable t -phase. It is believed that the resulting compressive stresses improve the mechanical properties of tetragonal zirconium dioxide compared to fully stabilized (cubic) zirconium dioxide. In the literature on the study of systems based on zirconium oxide, two tetragonal phases t' and t'' have been considered [4–6].

In the mechanical properties of single crystals compared to that of ceramics, some features are present that are not solely associated with the absence of grain boundaries inherent in ceramics. The fundamental fact is that the tetragonal phase forms a domain microstructure in a single crystal [7].

The formation of the microstructure of single crystals depends on the type and concentration of the stabilizing oxides as well as on the residual temperature stresses that occur during the growth and cooling of the single crystal. However, the main studies on the materials based on zirconium dioxide have been conducted on polycrystalline samples. To the best of our knowledge, no extensive study has been conducted on the microstructure of the single crystals of tetragonal zirconium dioxide from the crystallographic point of view. Several questions remain unclear. For example, how do the cubic and tetragonal phases relate to each other in terms of symmetry in the region of their coexistence after the

phase transition; what is the law of symmetry among the domains in the tetragonal phase. This study was undertaken to obtain additional information about the microstructure of the tetragonal phase based on zirconium dioxide. The use of neutron diffraction, on the one hand, was due to the comparable scattering power of the elements that make up the crystal, and consequently, the structural parameters of oxygen atoms were accurately determined. On the other hand, the large penetrating power of neutrons allowed us to study relatively large samples with linear dimensions up to several millimeters.

OBJECTIVES OF THE STUDY

1. To determine phase relations and crystallographic characteristics for the microstructure of single crystals grown by directed crystallization from the melts of mixtures $97\text{ZrO}_2 \cdot 3\text{Y}_2\text{O}_3$ and $88\text{ZrO}_2 \cdot 12\text{Y}_2\text{O}_3$ with different growth rates (10 and 40 mm/h).
2. To determine the oxygen content in samples with 3 mol % Y_2O_3 and samples grown from the region with 12 mol % Y_2O_3 , depending on the unit cell parameters of the concentration.
3. To identify the crystallographic and crystal-chemical correlations with the physicochemical properties of single crystals.

EXPERIMENTAL

Growth of oxide single crystals by directed crystallization using direct high-frequency melting in a cold container

The crystals of partially and fully stabilized ZrO_2 (3 and 12 mol % Y_2O_3) were grown by directed melt crystallization in a cold container through direct high-frequency heating using the Kristall-407 apparatus (Physical Institute of the Russian Academy of Sciences, Moscow, Russia) [2]. The growth rates varied from 10 to 40 mm/h. Moreover, the obtained crystals were 5–20 mm in cross section and 40 mm in height. When the melt was crystallized, the single crystals of ZrO_2 PSZD (3 mol % Y_2O_3) at high temperature had a cubic structure of the fluorite type, and as the temperature decreased, they experienced polymorphic transformations according to the phase diagram (Fig. 1). Furthermore, the external shape of the crystal was preserved, similar to the shape of a single crystal of a single-phase cubic solid solution based on zirconium dioxide; however, unlike that of the latter, which are optically transparent, the crystals of the PSZD were opaque.

The composition of the crystals of the present work was determined by the composition of the initial charge. The variable parameter for single crystals with 3 mol % Y_2O_3 was the growth rate, which was 10 and 40 mm/h. For the structural study, crystals with a diameter of 5 mm were cut from large columnar crystals.

Neutron-diffraction installations

In the present work, using a high-resolution neutron-diffraction setup for the interplanar distance was necessary. This was caused by the need for the precise measurement of the lattice parameters, a confident separation of the phases formed in the system after the phase transition during the growth of crystals according to the measured parameters of the unit cell, and the determination of the change in their ratio with varying growth rates. Conversely, the knowledge of the unit cell parameters with high accuracy enables the use of their known dependence on the concentration to determine the concentrations of the elements in the system and, first of all, oxygen.

For high-resolution experiments, a high-resolution Fourier diffractometer (HRFD) was used at the IBR-2 pulsed reactor in Dubna (Russia), and accordingly, the neutron time-of-flight method [8, 9]. Previously, the main axis was derived for the crystals on the neutron-diffraction spectrometer, NPMS (neutron pulsed magnetic spectrometer, Joint Institute for Nuclear Research, Dubna, Russia) [10]. For the diffraction studies of single crystals, a three-circle goniometer was placed on the central table of the spectrometer, which comprised a χ -ring with a Euler saddle and the axes φ and ω . Thus, the crystal could be freely moved to any reflecting position. The software enabled to search on a crystal with an unknown crystallographic direction at a given interplanar distance d [11]. The samples were further processed on the goniometer of the HRFD installation.

The distribution of atoms in the unit cell and the distances among them are significantly important characteristics that are associated with the basic properties of the crystal. This problem was solved using the constant wavelength method, and the experiment was conducted on a neutronography unit for the study of single crystals at the stationary water–water nuclear reactor VVR-c in Obninsk (Russia) [12].

Microstructure, unit cell parameters, and phase composition of the single crystals of the zirconium oxide–yttrium oxide system

To understand the “crystallographic” state of the crystals and microstructure (the phase ratio and the model of crystal twinning after the phase transition), the inverse lattice of the single crystals was initially studied employing a copper-based photomethod on an X-ray Weissenberg installation (Fig. 2), and then, to achieve a better resolution, on the neutron photomethod installation (neutron Weissenberg installation, Hahn and Meitner Institute, Berlin, Germany), and on the “flat cone (E2)” installation (Hahn and Meitner Institute, Berlin, Germany) on the constant power reactor at the Berlin Neutron Center [13]. The geometry of the diffraction reflection arrangement and the lattice

parameters determined from the rotation neutronogram as well as the “0” layer scan for a crystal with 12 mol % Y_2O_3 allowed us to establish that the studied crystals had cubic symmetry, the lattice parameter $a = 5.15 \text{ \AA}$, and the reflection extinction law corresponded to the $Fm\bar{3}m$ space group. The rotation neutronogram and the “0” layer scan (Fig. 3a and 3b) showed diffuse scattering, which was caused by the defect structure of the crystal.

The neutron diagram of the rotation and the zero layer of the 3 mol % Y_2O_3 crystal around the axis [110] are shown in Fig. 3b and 3d. The calculation showed that the period along this direction is doubled with respect to the cubic cell. Also, the period along the direction of the “ a ” axis on the zero-layer scan was doubled for the cubic crystal when rotating along the axis [110]. The observed geometry of the location of reflexes in the back of the grid was suggested to be due to a possible twinning in the expected tetragonal phase after the phase transition from the cubic phase, and the proposed twinning law is the rotation of the axis of the direct lattice of a crystal by 90° around the axis “ a ” and/or the axis “ b .” The twinning scheme is shown in Fig. 4.

No reflexes that could belong to the monoclinic phase were observed. Based on the twinning law, we expect a characteristic splitting of the reflexes along the direction $[h00]$. Notably, the splitting of reflexes can only be observed on the high-resolution neutron-diffraction patterns.

For this purpose, the diffraction spectra of $(h00)$ and $(hh0)$ reflections from the single crystals with a 3% Y_2O_3 content grown at a growth rate of 10 and 40 mm/h, as well as from a single crystal with a 12% Y_2O_3 content, were measured on the HRFD neutronography unit.

In the diffractograms for the tetragonal samples (Fig. 5a and 5b), a splitting of the reflexes occurred. However, the most intense peak (400) showed splitting, not into the expected two, but three peaks. The data on the interplanar distances calculated from the diffraction spectrum along the direction $[h00]$ and the corresponding unit cell parameters are shown in Table 1. Based on the phase diagram and the measured values of the parameters, we propose a model for the coexistence of the tetragonal and cubic phases in the sample under study. It is advisable to compare the diffraction spectra for two samples with 3 mol % Y_2O_3 (tetragonal + cubic phase) and samples with 12 mol % Y_2O_3 . Notably, according to the values of the structural factors, a pure cubic sample with 12 mol % Y_2O_3 lacked reflex 600. In the tetragonal samples with 3 mol % Y_2O_3 with an admixture of the cubic phase, only reflexes 600 and 006 belonging to the tetragonal phase were present, and no reflex 600 from the cubic phase was present. Further, in a tetragonal sample with an admixture of the cubic phase, the diffraction spectrum in the reflection region 400 comprised three reflexes, of which two extreme reflexes corresponded to the tetragonal reflexes 400 and 004, and one reflex in the center corresponded to the position of the reflex 400 of the cubic phase.

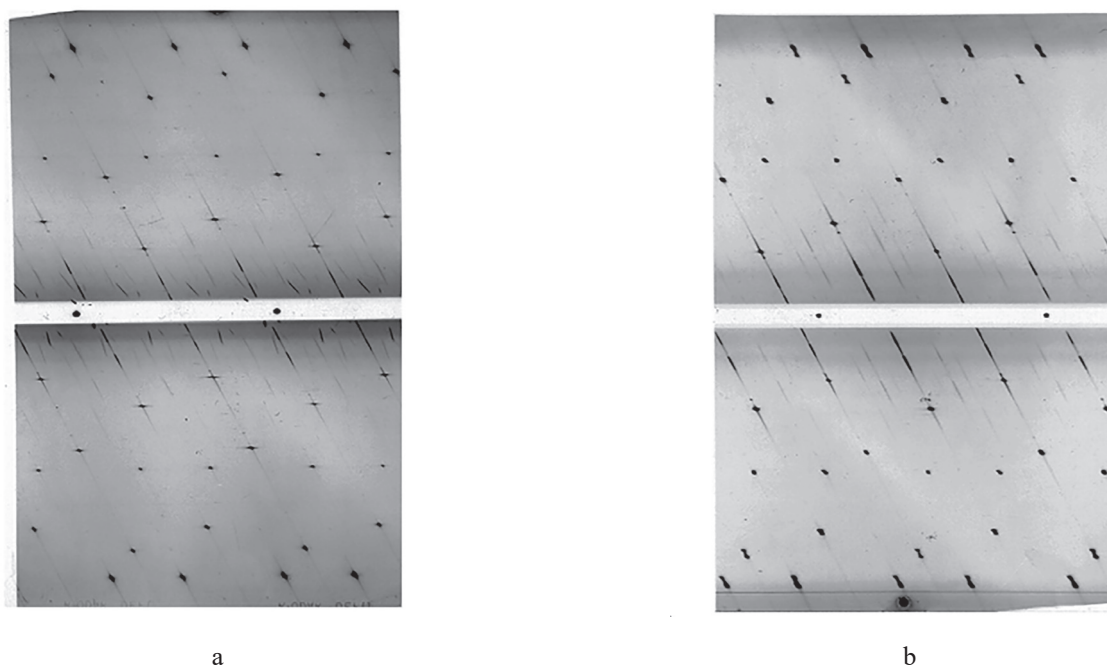


Fig. 2. Weissenberg film of the layers $(0hl)$ of the $(1-x)ZrO_2 \cdot xY_2O_3$ crystal: (a) $x = 0.12$, cubic phase; (b) $x = 0.03$, tetragonal phase.

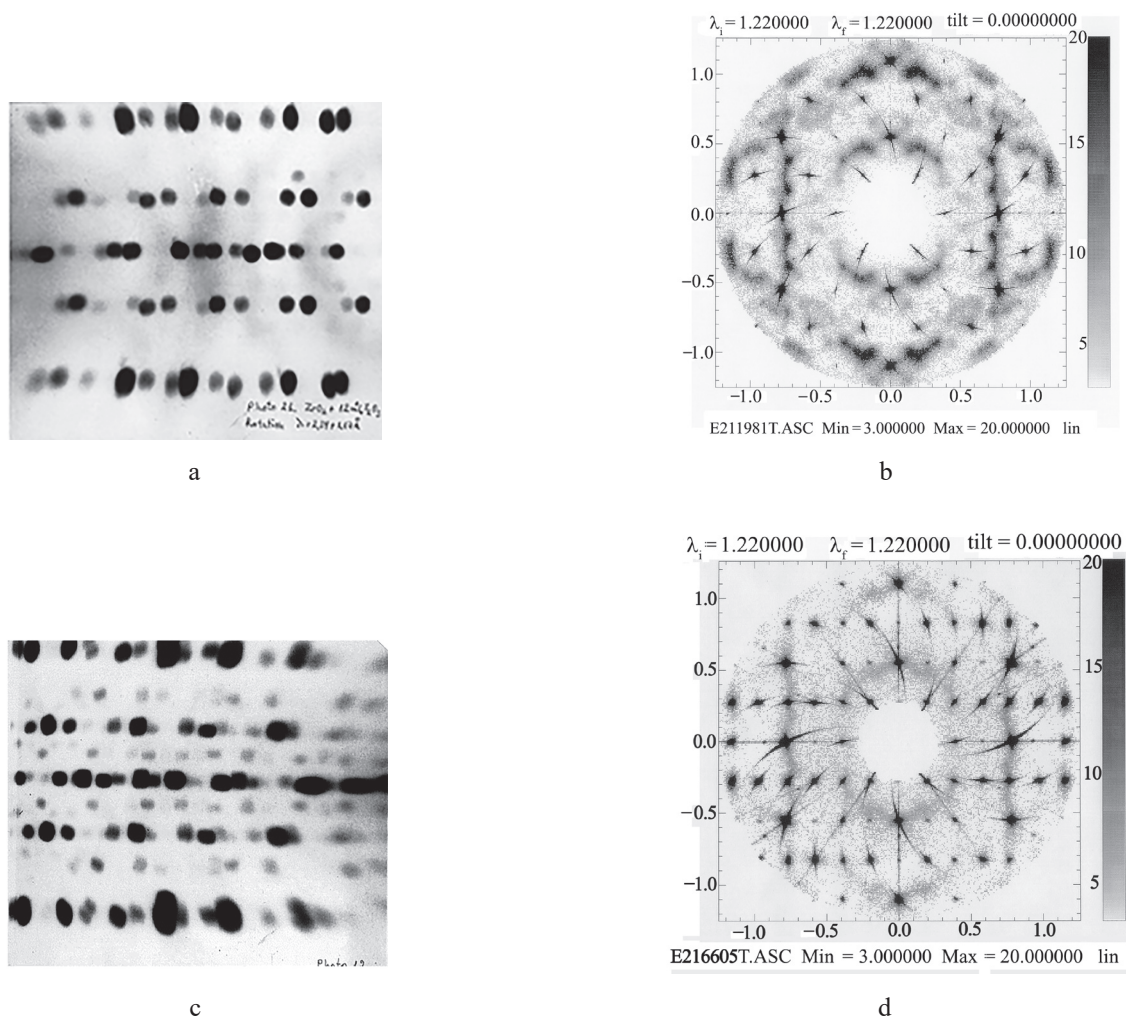


Fig. 3. Reciprocal lattice of $(1-x)\text{ZrO}_2 \cdot x\text{Y}_2\text{O}_3$ single crystals:
 (a, c) the neutronograms of the rotation of crystals with $x = 0.12$ (a) and 0.03 (c).
 The axis of rotation $[110]$. Weissenberg neutron installation.
 (b, d) scan “0” layer with $x = 0.12$ (b) and 0.03 (d). The axis of rotation $[110]$.
 The installation of E2. Flat cone neutron diffractometer.

The diffraction spectra showed that the content of the cubic phase in the PSZD crystals with 3 mol % Y_2O_3 , with the simultaneous presence of the tetragonal and cubic phases, is noticeably high in crystals having the growth rate of 10 mm/h. Notably, a special material science study has shown that the growth rate of 10 mm/h is optimal for obtaining PSZD crystals that have the necessary functional and operational characteristics, which should be, for example, a structural material for an electrosurgical instrument [14].

According to the parameters of the unit cell obtained in the present work (Table 1) using the ratio $a_{\text{cub}} = 5.1063 + 0.200x$, Å, where x is the content of Y_2O_3 according to the formula $(1-x)\text{ZrO}_2 \cdot x\text{YO}_{1.5}$ [15], the concentration of yttrium oxide for the cubic phase was determined. To determine the content of yttrium oxide in the tetragonal phase $(1-x)\text{ZrO}_2 \cdot x\text{Y}_2\text{O}_3$, the following relations were proposed in [16]: $a_{\text{tet}} = 5.060 + 0.6980x$, Å;

$c_{\text{tet}} = 5.195 - 0.6180x$, Å. According to Table 1, calculations based on these ratios afforded ~3 mol % Y_2O_3 for the cubic phase, and ~4 mol % Y_2O_3 for the tetragonal phase. Given the approximate nature of the formulas, the contents of Y_2O_3 in the two phases of the samples under study were similar.

In general, during cooling, in the region of 3–5 mol % Y_2O_3 , the crystal was stratified into cubic and tetragonal phases with almost the same content of yttrium oxide, ~3 mol % Y_2O_3 . No traces of the monoclinic phase were observed. Thus, the data of this study are consistent with the data of [17], according to which the monoclinic phase in the single crystals grown from the melt appears only when the Y_2O_3 content is below 2.5 mol %. Further, as the present study shows, the cubic and tetragonal phases are strictly crystallographically oriented and coherently connected by the planes of the $\{100\}$ type.

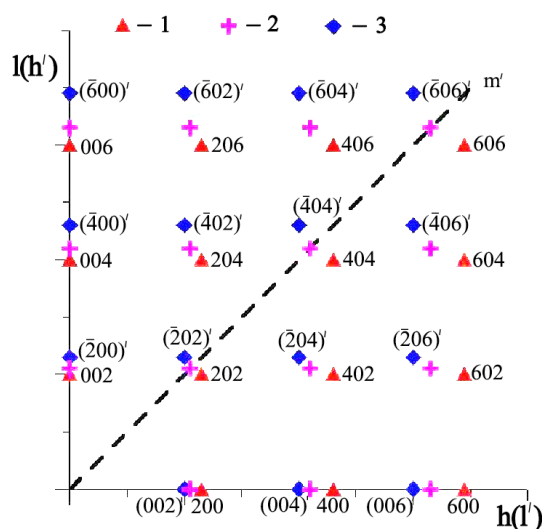


Fig. 4. Reciprocal lattice of the $(1-x)\text{ZrO}_2:x\text{Y}_2\text{O}_3$ single crystal with $x = 0.03$. Section $h0l$. Coherent coexistence of tetragonal and cubic phases. The twinning law in the tetragonal phase: rotation around the axis $a (=b)$ by 90° . Equivalent to the plane of symmetry $m' = (110)$ in the cubic phase. (1) The first component of the twin of the tetragonal phase; (2) the cubic phase; and (3) the second component of the twin of the tetragonal phase.

Displacements of oxygen atoms from the main position in the cubic phase

For a detailed study on the structural features of the solid solution of the zirconium oxide–yttrium oxide system in the cubic phase, a neutron-structural study of a single crystal with 12 mol % Y_2O_3 was carried out. The experiment was conducted on a stationary reactor at the branch of the L.Y. Karpov Research Institute of

Physics and Chemistry in Obninsk, Russia. A set of integral intensities of Bragg reflexes was obtained using a four-circle neutron diffractometer “Syntex” from Syntex, USA. The monochromatic wavelength was $\lambda = 1.167 \text{ \AA}$. After the refinement of the positional and thermal parameters of the structure by the least-squares method, the Fourier difference syntheses of the nuclear density were performed. In the Fourier difference syntheses of the nuclear density (Fig. 6a and 6b) from a single crystal of the cubic phase in the region of the main position of the oxygen atom O1, additional peaks are noted with the coordinates given in Tables 2a and 2b. That is, for oxygen, not only a vacancy is present in its main position $8c$ but also embedded oxygen atoms O2, which were displaced from the main position and located statistically at position $48g$ and O3 at position $32f$. A general view of the structure with basic and displaced atoms is shown in Fig. 7a. The 0.3 \AA displacements of O3 oxygen atoms from the main position in the tetragonal phase along the direction $[100]$ (Fig. 7b and Table 3) were also observed in the studies on polycrystals [18].

In [19], in addition to the displacement of oxygen atoms, the displacement of zirconium atoms from their main positions was also noted, and the short-range order with displaced atoms in the averaged unit cell was interpreted by the authors [19] as a solid solution crystal memory of the equilibrium configuration of the initial zirconium and yttrium oxides. The presence of the statistical positions of oxygen atoms along the direction $[100]$ and $[111]$ can be considered as the domain structure of the anionic sublattice, which is usually associated with the lighter direction of ion transport. In this case, these displacements, established in the present work, assume a two-dimensional grid of the movement of oxygen ions from position $8c$ in the direction of position $48g$

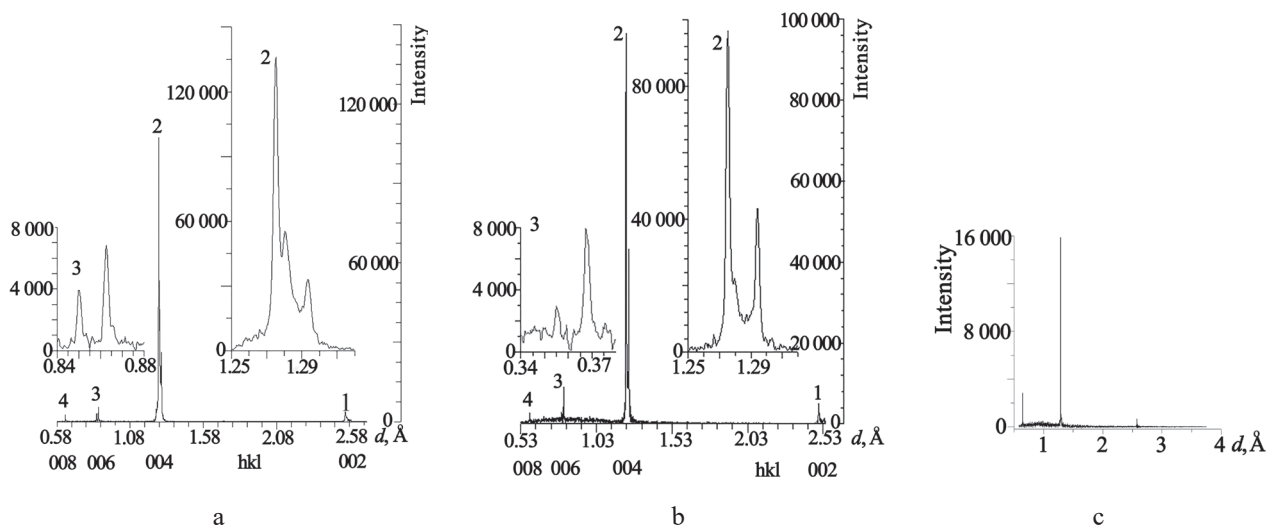


Fig. 5. High-resolution diffraction spectra in the direction of $[h00]$ for the $(1-x)\text{ZrO}_2:x\text{Y}_2\text{O}_3$ single crystals: (a) $x = 0.03$, 10 mm/h; (b) $x = 0.03$, 40 mm/h; and (c) $x = 0.12$ mol.

Table 1. Data on interplanar distances d and I_{\max} intensity maxima on diffraction reflexes, which were obtained from the time-of-flight diffraction spectrum from the $(1-x)\text{ZrO}_2 \cdot x\text{Y}_2\text{O}_3$ single crystal with $x = 0.03$. HRFD. The direction of the $\langle h00 \rangle$. hkl indexes are given for the tetragonal setting

hkl	$d, \text{Å}$	I_{\max}	$a, \text{Å}$
200	2.5498	3.385	5.0996
300	1.7134	0.500	5.1402
400	1.2934	19.439	5.1736
	1.2795	31.287	5.1180
	1.2745	75.891	5.0980
600	0.8623	2.650	5.1738
	0.8499	1.442	5.0994
800	0.6375	3.565	5.1000
020	2.5491	2.858	5.0982
040	1.2927	33.530	5.1708
	1.2799	32.471	5.1196
	1.2745	74.292	5.0980
060	0.8619	10.074	5.1714
	0.8496	3.759	5.0976
080	0.6375	5.601	5.1000
002	2.5475	1.335	5.0950
004	1.2919	28.905	5.1676
	1.2792	25.943	5.1168
	1.2738	60.040	5.0952
006	0.8619	6.993	5.1714
	0.8492	2.181	5.0952
008	0.6371	6.118	5.0968

Table 2a. The coordinates x/a , y/b , and z/c of the atoms in the crystal structure of the $(1-x)\text{ZrO}_2 \cdot x\text{Y}_2\text{O}_3$ crystal, $x = 0.12$

Atom	x/a	y/b	z/c	$B(\text{is/eq}), \text{Å}^2$	q	N
Zr1	0	0	0	0.80(9)	0.8(14) Zr/0,2(13) (Y)	4a
O1	1/4	1/4	1/4	2.72(7)	0.80(2) (O)	8c
O2	0.122(24)	1/4	1/4	2.50(4)	0.008 (O)	48g
O3	0.298(13)	$-x + 1/2$	$-x + 1/2$	2.52(4)	0.01 (O)	32f

Note: $B(\text{is/eq})$ is the factor of the isotropic thermal vibrations of the atom, q is the population of the position of the atom, and N is the designation and multiplicity of the position of the atom according to international tables.

Table 2b. The distance between the atoms in the crystal structure of $(1-x)\text{ZrO}_2 \cdot x\text{Y}_2\text{O}_3$, $x = 0.12$, Å

Atom	O1	O2	O3
Zr(Y)	2.14; 2.23; 2.30	1.93; 2.67	2.13; 2.66

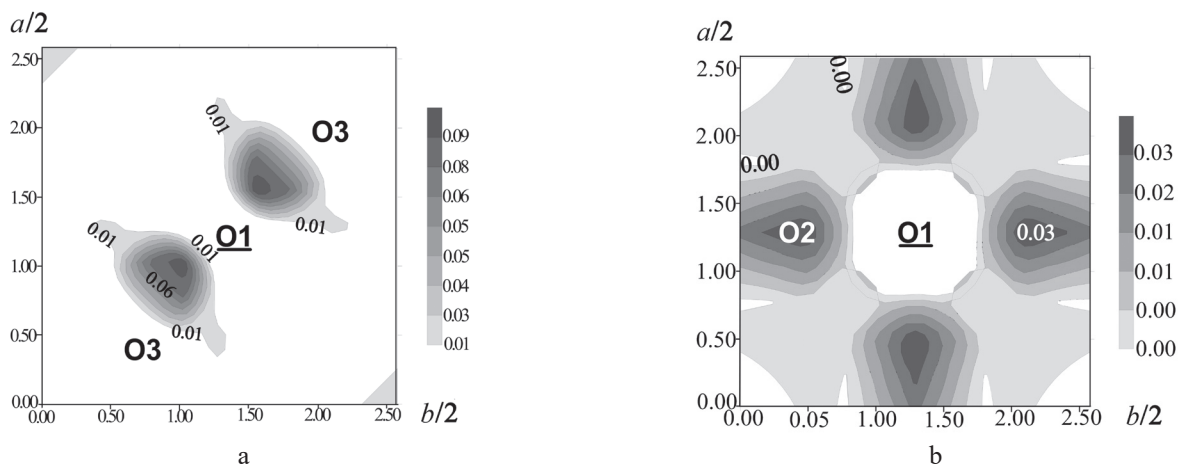


Fig. 6. Crystal $(1-x)\text{ZrO}_2 \cdot x\text{Y}_2\text{O}_3$ with $x = 0.12$: (a) the difference Fourier synthesis of the nuclear density. The cross section of the unit cell $z/c = 0.20$; (b) the difference Fourier synthesis of the nuclear density. The cross section of the unit cell $z/c = 0.25$.

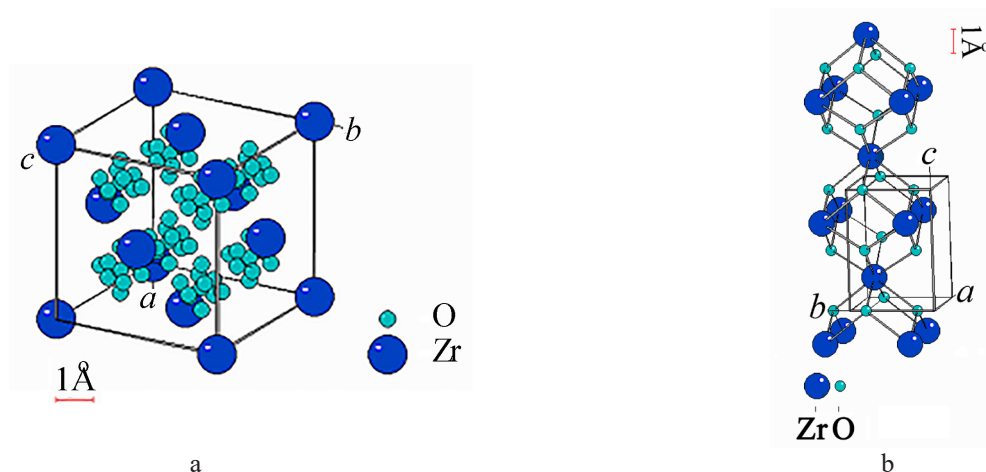


Fig. 7. (a) Crystal structure of the $(1-x)\text{ZrO}_2 \cdot x\text{Y}_2\text{O}_3$ with $x = 0.12$. Averaged unit cell (space group $Fm\bar{3}m$, $a = 5.143$ Å). Disorder in the oxygen subcell: the main positions and embedded oxygen atoms are shown (the scale of the size of oxygen atoms is especially reduced to show disordering in the oxygen subcell).
 (b) Crystal structure of $(1-x)\text{ZrO}_2 \cdot x\text{Y}_2\text{O}_3$ $c x = 0.03$. ($P4_2/nmc$, $a = 5.09$, $c = 5.17$ Å). Averaged unit cell. The main positions and embedded oxygen atoms are shown (the scale of the size of oxygen atoms is especially reduced to show the atoms in the oxygen subcell).

Table 3. The coordinates x/a , y/b , and z/c of the atoms in the crystal structure of the $(1-x)\text{ZrO}_2 \cdot x\text{Y}_2\text{O}_3$ crystal, $x = 0.03$. Space group $P4_2/nmc$

Atom	x/a	y/b	z/c	$B(\text{is/eq}), \text{Å}^2$	N
Zr1	3/4	1/4	3/4	0.52(9)	2
O1	1/4	1/4	0.4731(13)	2.2(2)	4

Note: $B(\text{is/eq})$ is the factor of the isotropic thermal vibrations of the atom; N is the designation and multiplicity of the position of the atom according to international tables.

and position $32f$. However, this reasoning applies only to single atoms; for example, to one of the 8 basic oxygen atoms in the independent part of the unit cell, or one of the 48 or 32 embedded oxygen atoms. As shown in the structure of the unit cell shown in Fig. 6, all possible directions of the general type $\langle 100 \rangle$ and $\langle 111 \rangle$ should be considered.

MAIN RESULTS AND CONCLUSIONS

1. It was observed that when growing the single crystals of the ZrO_2 - Y_2O_3 system from the region of the phase diagram with 3–5 mol % Y_2O_3 at a growth rate of 10 and 40 mm/h, the crystal stratified into cubic and tetragonal phases. The ratio between the cubic and tetragonal phases depends on the growth rate of single crystals. At a growth rate of 40 mm/h, the content of the cubic phase was insignificant.

2. It was observed that the microstructure of the samples was characterized by the presence of a composite structure comprising a micro-double structure of tetragonal phases and coherently connected to it along the planes of $\{100\}$ cubic phases. The law of the twinning of the tetragonal phase was the rotation of the axis of the unit cell by 90° around the axis a (b).

3. According to the precision measured parameters of the unit cell, it was found that the content of Y_2O_3 in the cubic and tetragonal phases of the single crystal was 3–4 mol %. This determination was performed on the same bulk sample using the non-destructive neutronography method.

4. In the unit cell of a cubic crystal, the 0.3 Å displacement of oxygen atoms from the main position of the crystal was determined. Moreover, the displacement of oxygen atoms in the directions $[100]$ and $[111]$ correlated with the directions of ion transport.

Acknowledgments

The study was supported by the Ministry of Science and Higher Education of the Russian Federation: project FSFZ-0706-2020-0022.

Authors' contribution

V.A. Sarin – conducting X-ray and neutron structural experiments, processing results, and writing the text of the article;

A.A. Bush – conducting X-ray structural experiments, processing experimental results, and writing the text of the article.

The authors declare no conflicts of interest.

REFERENCES

1. Nerst W. Electrical glow light: US Patent 623.811. Appl. 02.10.1897.
2. Kuz'minov Yu.S., Lomonova E.E., Osiko V.V. *Tugoplavkie materialy iz kholodnogo tiglya (Refractory Materials from Cold Crucible)*. Moscow: Nauka; 2004. 372 p. (in Russ.). ISBN 5-02-002820-7
3. Scott H.G. Phase relationships in the yttria-rich part of the yttria-zirconia system. *J. Mater. Sci.* 1977;12(2):311–316. <https://doi.org/10.1007/BF00566272>
4. Yashima M., Ishizawa N., Yoshimura M. In: *Science and Technology of Zirconia. Conference Proceedings*. Vol. V. Badwal S.P.S., Bannister M.J., Hannink R.H. (Eds.). Lancaster: Technomic Publishing; 1993. P.125–135. ISBN 1566760739.
5. Swain M.V. Grain-size dependence of toughness and transformability of 2 mol % Y-TZP ceramics. *J. Mater. Sci. Lett.* 1986;5(11):1159–1162. <https://doi.org/10.1007/BF01742233>
6. Borik M.A., Bublik V.T., Vishnyakova M.A., Lomonova E.E., Myzina V.A., Tabachkova N.Yu., Timofeev A.A. Structure and Phase Composition Studies of Partially Stabilized Zirconia. *J. Surface Investig. X-ray, Synch. Neutron Tech.* 2011;5(1):166–171. <https://doi.org/10.1134/S1027451011020042>

СПИСОК ЛИТЕРАТУРЫ

1. Nerst W. Electrical glow light: US Patent 623.811. Appl. 02.10.1897.
2. Кузьминов Ю.С., Ломонова Е.Е., Осико В.В. *Тугоплавкие материалы из холодного тигля*. М: Наука; 2004. 372 с. ISBN 5-02-002820-7
3. Scott H.G. Phase relationships in the yttria-rich part of the yttria-zirconia system. *J. Mater. Sci.* 1977;12(2):311–316. <https://doi.org/10.1007/BF00566272>
4. Yashima M., Ishizawa N., Yoshimura M. In: *Science and Technology of Zirconia. Conference Proceedings*. Vol. V. Badwal S.P.S., Bannister M.J., Hannink R.H. (Eds.). Lancaster: Technomic Publishing. 1993. P.125–135. ISBN 1566760739.
5. Swain M.V. Grain-size dependence of toughness and transformability of 2 mol % Y-TZP ceramics. *J. Mater. Sci. Lett.* 1986;5(11):1159–1162. <https://doi.org/10.1007/BF01742233>
6. Borik M.A., Bublik V.T., Vishnyakova M.A., Lomonova E.E., Myzina V.A., Tabachkova N.Yu., Timofeev A.A. Structure and Phase Composition Studies of Partially Stabilized Zirconia. *J. Surface Investig. X-ray, Synch. Neutron Tech.* 2011;5(1):166–171. <https://doi.org/10.1134/S1027451011020042>

7. Chan C.-J., Lange F.F., Ruhle M., Jue J.-F., Virkar A.V. Ferroelastic Domain Switching in Tetragonal Zirconia Single Crystals—Microstructural Aspects. *J. Am. Ceram. Soc.* 1991;74(4):807–813. <https://doi.org/10.1111/j.1151-2916.1991.tb06929.x>
8. Aksenov V.L., Balagurov A.M., Simkin V.G., Bulkin A.P., Kudrjashev V.A., Trounov V.A., Antson O., Hiismaki P., Tiitta A. Performance of the High Resolution Fourier Diffractometer at the IBR-2 Pulsed Reactor. *J. Neutron Res.* 1997;5(4):181–200. <https://doi.org/10.1080/10238169708200223>
9. Balagurov A.M., Bobrikov I.A., Bokuchava G.D., Zhuravlev V.V., Simkin V.G. Correlation Fourier Diffractometry: 20 Years of Experience at the IBR-2 reactor. *Fizika elementarnykh chastits i atomnogo yadra = Physics of Elementary Particles and Atomic Nuclei.* 2015;46(3):454–501 (in Russ.).
10. Georgiev D., Nietz V.V., Petukhova T.B., Sirotnin A.P., Yakovlev A.A. Spectrometer for Neutron Studies of Condensed Matter with a Pulsed Magnetic Field. *J. Neutron Research.* 1997;5(3):109–122. <https://doi.org/10.1080/10238169708200217>
11. Georgiev D., Petukhova T.B., Sarin V.A., Dudka A.P. A system for controlling a three-circle goniometer and recording neutron spectra in the study of single crystals by time-of-flight diffraction. In: *Proceedings Second National Conference of RSNE-99, Moscow, May 23–27, 1999.* P. 430 (in Russ.).
12. Kodess B.N., Sarin V.A. A Neutron diffractometer for determining the structural characteristics of single crystals. *Meas. Tech.* 2015;57(11):1299–1303. <https://doi.org/10.1007/s11018-015-0624-3>
- [Kodess B.N., Sarin V.A. A Neutron diffractometer for determining the structural characteristics of single crystals. *Izmerit. Tekh. = Meas. Tech.* 2014;(11):51–54 (in Russ.).]
13. Robertson T., Graf H.A., Michaelsen R., Vorderwisch (Eds.) *Neutron-scattering. Instrumentation at the Research Reactor BER II.* Berlin Neutron Scattering Center (BENSC); 1996. 55 p. Available from: https://inis.iaea.org/search/search.aspx?orig_q=RN:28021933
14. Belov S.V., Borik M.A., Danileiko Ju.K., Shulutko A.M., Lomonova E.E., Osiko V.V., Salyuk V.A. New Bipolar Electrosurgical Tools Based on Zirconia. *Biomed. Eng.* 2013;47(2):78–82. <https://doi.org/10.1007/s10527-013-9339-4>
- [Belov S.V., Borik M.A., Danileiko Ju.K., Shulutko A.M., Lomonova E.E., Osiko V.V., Salyuk V.A. New Bipolar Electrosurgical Tools Based on Zirconia. *Med. Tekh. = Biomed. Eng.* 2013;2(278):20–24 (in Russ.).]
15. Yashima M., Ishizava N., Yoshimura M. Application of an Ion-Packing Model Based on Defect Clusters to Zirconia Solid Solutions: II, Applicability of Vegard's Law. *J. Am. Ceram. Soc.* 1992;75(6):1550–1557. <https://doi.org/10.1111/j.1151-2916.1992.tb04223.x>
16. Ingel R.P., Lewis D. Lattice Parameters and Density for Y_2O_3 -Stabilized ZrO_2 . *J. Am. Ceram. Soc.* 1986;69(4):325–332. <https://doi.org/10.1111/j.1151-2916.1986.tb04741.x>
17. Aboimov M.A., Borik M.A., Gogotsi G.A., Kalabukhova V.F., Lomonova E.E., Myzina V.A. Phase transformations in crystals of partially stabilized zirconia. *Inorg. Mater.* 1997;33(3):285–291.
- [Aboimov M.A., Borik M.A., Gogotsi G.A., Kalabukhova V.F., Lomonova E.E., Myzina V.A. Phase transformations in crystals of partially stabilized zirconia. *Neorgan. Mater. = Inorg. Mater.* 1997;33(3):344–351 (in Russ.).]
7. Chan C.-J., Lange F.F., Ruhle M., Jue J.-F., Virkar A.V. Ferroelastic Domain Switching in Tetragonal Zirconia Single Crystals—Microstructural Aspects. *J. Am. Ceram. Soc.* 1991;74(4):807–813. <https://doi.org/10.1111/j.1151-2916.1991.tb06929.x>
8. Aksenov V.L., Balagurov A.M., Simkin V.G., Bulkin A.P., Kudrjashev V.A., Trounov V.A., Antson O., Hiismaki P., Tiitta A. Performance of the High Resolution Fourier Diffractometer at the IBR-2 Pulsed Reactor. *J. Neutron Res.* 1997;5(4):181–200. <https://doi.org/10.1080/10238169708200223>
9. Балагуров А.М., Бобриков И.А., Бокучава Г.Д., Журавлёв В.В., Симкин В.Г. Корреляционная фурье-дифрактометрия: 20-летний опыт эксплуатации на реакторе ИБР-2. *Физика элементарных частиц и атомного ядра.* 2015;46(3):454–501.
10. Georgiev D., Nietz V.V., Petukhova T.B., Sirotnin A.P., Yakovlev A.A. Spectrometer for Neutron Studies of Condensed Matter with a Pulsed Magnetic Field. *J. Neutron Research.* 1997;5(3):109–122. <https://doi.org/10.1080/10238169708200217>
11. Георгиев Д., Петухова Т.Б., Сарин В.А., Дудка А. П. Система управления трехкружным гониометром и регистрации нейтронных спектров при исследовании монокристаллов методом дифракции по времени пролета. В сб.: *Тезисы докладов 2-й национальной конференции РСНЭ-99.* Москва, 23–27 мая 1999 г. М.: Изд-во ИК РАН; 1999. С. 430.
12. Кодесс Б.Н., Сарин В.А. Нейтронный дифрактометр для определения структурных характеристик монокристаллов. *Измерительная техника.* 2014;(11):51–54.
13. Robertson T., Graf H.A., Michaelsen R., Vorderwisch (Eds.) *Neutron-scattering. Instrumentation at the Research Reactor BER II.* Berlin Neutron Scattering Center (BENSC); 1996. 55 p. Available from: https://inis.iaea.org/search/search.aspx?orig_q=RN:28021933
14. Белов С.В., Борик М.А., Данилейко Ю.К., Шулютко А.М., Ломонова Е.Е., Осико В.В., Салюк В.А. Новый биполярный электрохирургический инструментарий на основе диоксида циркония. *Мед. техника.* 2013;2(278):20–24.
15. Yashima M., Ishizava N., Yoshimura M. Application of an Ion-Packing Model Based on Defect Clusters to Zirconia Solid Solutions: II, Applicability of Vegard's Law. *J. Am. Ceram. Soc.* 1992;75(6):1550–1557. <https://doi.org/10.1111/j.1151-2916.1992.tb04223.x>
16. Ingel R.P., Lewis D. Lattice Parameters and Density for Y_2O_3 -Stabilized ZrO_2 . *J. Am. Ceram. Soc.* 1986;69(4):325–332. <https://doi.org/10.1111/j.1151-2916.1986.tb04741.x>
17. Абоимов М.А., Борик М.А., Гогоци Г.А., Калабухова В.Ф., Ломонова Е.Е., Мызина В.А. Исследование фазовых переходов в кристаллах частично стабилизированного диоксида циркония. *Неорган. материалы.* 1997;33(3):344–351.
18. Steele D. and Fender B.E.F. The Structure of Cubic $ZrO_2:YO_{1.5}$ Solid Solutions by Neutron Scattering. *J. Phys. C.: Solid State Phys.* 1974;7(1):1–11. <https://doi.org/10.1088/0022-3719/7/1/009>
19. Ishizawa N., Matsushima Y., Hayashi M., Ueki M. Synchrotron radiation study of yttria-stabilized zirconia, $Zr_{0.758}Y_{0.242}O_{1.879}$. *Acta Cryst.* 1999;B55(5):726–735. <https://doi.org/10.1107/s0108768199005108>

18. Steele D., Fender B.E.F. The Structure of Cubic $ZrO_2:YO_{1.5}$ Solid Solutions by Neutron Scattering. *J. Phys. C.: Solid State Phys.* 1974;7(1):1–11. <https://doi.org/10.1088/0022-3719/7/1/009>

19. Ishizawa N., Matsushima Y., Hayashi M., Ueki M. Synchrotron radiation study of yttria-stabilized zirconia, $Zr_{0.758}Y_{0.242}O_{1.879}$. *Acta Cryst.* 1999;B55(5):726–735. <https://doi.org/10.1107/s0108768199005108>

About the authors:

Viktor A. Sarin, Cand. Sci. (Phys.–Math.), Leading Engineer, Research Institute of Solid-State Electronics Materials, MIREA – Russian Technological University (78, Vernadskogo pr., Moscow, 119454, Russia). E-mail: vic.fet@yandex.com. Scopus Author ID 7005455400.

Alexander A. Bush, Dr. Sci. (Eng.), Professor, Director of the Research Institute of Solid-State Electronics Materials, MIREA – Russian Technological University (78, Vernadskogo pr., Moscow, 119454, Russia). E-mail: aabush@yandex.ru. Scopus Author ID 7201882802, Researcher ID R-2287-2016, <https://orcid.org/0000-0003-3990-9847>

Об авторах:

Сарин Виктор Анатольевич, к.ф.-м.н., ведущий инженер НИИ материалов твердотельной электроники ФГБОУ ВО «МИРЭА – Российский технологический университет» (119454, Россия, Москва, пр-т Вернадского, д. 78). E-mail: vic.fet@yandex.com. Scopus Author ID 7005455400.

Буш Александр Андреевич, д.т.н., профессор, директор НИИ материалов твердотельной электроники ФГБОУ ВО «МИРЭА – Российский технологический университет» (119454, Россия, Москва, пр-т Вернадского, д. 78). E-mail: aabush@yandex.ru. Scopus Author ID 7201882802, Researcher ID R-2287-2016, <https://orcid.org/0000-0003-3990-9847>

The article was submitted: November 25, 2020; approved after reviewing: December 09, 2020; accepted for publication: February 04, 2021.

Translated from Russian into English by N. Isaeva

Edited for English language and spelling by Enago, an editing brand of Crimson Interactive Inc.

CHEMISTRY AND TECHNOLOGY OF INORGANIC MATERIALS
ХИМИЯ И ТЕХНОЛОГИЯ НЕОРГАНИЧЕСКИХ МАТЕРИАЛОВ

ISSN 2686-7575 (Online)

<https://doi.org/10.32362/2410-6593-2021-16-1-67-75>



UDC 666.3/.7

RESEARCH ARTICLE

Chemical and technological aspects of increasing the functional characteristics of hard piezoceramics

Mikhail V. Talanov^{1,@}, Mikhail A. Marakhovskiy²

¹Research Institute of Physics, Southern Federal University, Rostov-on-Don, 344090 Russia

²NKTB Piezopribor, Southern Federal University, Rostov-on-Don, 344090 Russia

@Corresponding author, e-mail: mvtalanov@gmail.com

Abstract

Objectives. Ferroelectrically hard piezoelectric ceramics are in demand for high-power applications in piezotransformers, ultrasonic emitters, and piezo motors, which requires a combination of high piezoelectric characteristics and mechanical quality factors in it. The aim of this research was to reveal the main regularities in the microstructure and functional characteristic formation of ferroelectrically hard piezoceramics based on two widespread chemical systems, $Pb(Zr_xTi_{1-x})O_3$ and $(Na_{1-x}K_x)NbO_3$, through various technological modes of production. In this study, two fundamentally different technological ways of forming a dense microstructure on the example of above systems have been employed to obtain the best set of dielectric, piezoelectric, and mechanical parameters for practical applications. In the case of lead-containing ceramics, various sintering technologies have been used, including conventional ceramic, hot pressing, and spark plasma sintering.

Methods. The microstructure of the piezoelectric ceramics was investigated using electron microscopy, and the functional characteristics were assessed in terms of mechanical and piezoelectric properties. The density values were determined by hydrostatic weighing in octane, the relative dielectric permittivity was measured using an LCR meter, and the values of the piezoelectric coefficient and mechanical quality factor were gathered using the resonance–antiresonance method.

Results. This research has identified that spark plasma sintering technology makes it possible to obtain high-density samples, which contain a homogeneous microstructure and double the figure-of-merit values, for use in high-power piezoelectric devices that operate at piezoresonance frequencies. It also found that the addition of a small amount of $CuNb_2O_6$ ($x = 0.025$) to lead-free solid solutions leads to the formation of a liquid phase during sintering, thereby creating a compacted microstructure with relative density values (96%) that have practical limitations in conventional ceramic technology. An increase in both the piezoelectric and mechanical properties, which leads to a twofold increase in the values of the quality indicator, was also observed.

Conclusions. It is possible to increase, and even to double, the functional characteristics of both lead-containing and lead-free ferroelectrically hard piezoceramics by varying the technology used in the manufacturing process. By using spark plasma sintering technology with lead-containing ceramics, it is possible to reduce the optimum sintering temperature by 200°C and the sintering time by more than 20 times, thus reducing production costs.

Keywords: piezoceramics, sintering technology, spark plasma sintering, microstructure, piezoelectric properties, mechanical quality factor, liquid phases, figure-of-merit

For citation: Talanov M.V., Marakhovsky M.A. Chemical and technological aspects of increasing the functional characteristics of hard piezoceramics. *Tonk. Khim. Tekhnol. = Fine Chem. Technol.* 2021;16(1):67–75 (Russ., Eng.). <https://doi.org/10.32362/2410-6593-2021-16-1-67-75>

НАУЧНАЯ СТАТЬЯ

Химико-технологические аспекты повышения функциональных характеристик сегнетожесткой пьезокерамики

М.В. Таланов^{1,@}, М.А. Мараховский²

¹НИИ физики, Южный федеральный университет, Ростов-на-Дону, 344090 Россия

²НКТБ Пьезоприбор, Южный федеральный университет, Ростов-на-Дону, 344090 Россия

@Автор для переписки, e-mail: mvtalanov@gmail.com

Аннотация

Цели. Сегнетожесткая пьезоэлектрическая керамика востребована при создании устройств, работающих в силовых режимах: пьезотрансформаторах, ультразвуковых излучателях и пьезодвигателях, что требует сочетания в ней высоких пьезоэлектрических характеристик и механической добротности. В этой работе на примере двух широко распространенных химических систем $Pb(Zr_xTi_{1-x})O_3$ и $(Na_{1-x}K_x)NbO_3$ продемонстрированы принципиально различные химико-технологические пути формирования плотной микроструктуры и достижения наилучших, с точки зрения практических применений, наборов диэлектрических, пьезоэлектрических и механических параметров. В случае свинецсодержащей керамики были использованы различные технологии спекания: обычная керамическая, горячее прессование и искровое плазменное спекание. Для повышения функциональных характеристик бессвинцовой керамики был выбран путь, связанный с добавлением медьсодержащего компонента $CuNb_2O_6$ (x) к исходной системе ниобата натрия-калия. Целью настоящей работы стало выявление основных закономерностей формирования микроструктуры и функциональных характеристик сегнетожесткой керамики на основе систем $Pb(Zr_xTi_{1-x})O_3$ и $(Na_{1-x}K_x)NbO_3$, при вариации технологических режимов их изготовления.

Материалы. Микроструктура пьезоэлектрической керамики исследовалась методом электронной микроскопии, а функциональные характеристики оценивались по показателям механических и пьезоэлектрических свойств. Значения плотности определялись методом гидростатического взвешивания в октане, относительная диэлектрическая проницаемость была измерена с помощью LCR-метра, а значения пьезоэлектрического коэффициента и механической добротности установлены на основании резонансно-антирезонансного метода.

Результаты. Установлено, что применение технологии искрового плазменного спекания позволяет получить высокоплотные образцы свинецсодержащей керамики с однородной микроструктурой и более чем в два раза возросшими значениями показателя качества (figure-of-merit) для ее использования в устройствах силовой пьезотехники, работающих на частотах пьезорезонанса. Обнаружено, что добавка небольшого количества $CuNb_2O_6$ ($x = 0.025$) к бессвинцовым твердым растворам приводит к образованию в процессе спекания жидкой фазы, в результате чего формируется уплотненная микроструктура с практически предельными для обычной керамической технологии значениями относительной плотности (96%). Наблюдается возрастание как пьезоэлектрических, так и механических свойств, что приводит к двукратному повышению значений показателя качества.

Выводы. Вариация технологических режимов изготовления как свинецсодержащей, так и бессвинцовой сегнетожесткой пьезокерамики позволяет существенно (в два раза) повысить ее функциональные характеристики. Использование метода искрового плазменного спекания при изготовлении свинецсодержащей керамики способствует сокращению как оптимальной температуры процесса на 200 °С, так и продолжительности изотермической выдержки более чем в 20 раз. Такой прием существенно снижает производственные затраты.

Ключевые слова: пьезокерамика, технология спекания, искровое плазменное спекание, микроструктура, пьезоэлектрические свойства, механическая добротность, жидкие фазы, показатель качества

Для цитирования: Таланов М.В., Мараховский М.А. Химико-технологические аспекты повышения функциональных характеристик сегнетожесткой пьезокерамики. *Тонкие химические технологии*. 2021;16(1):67–75. <https://doi.org/10.32362/2410-6593-2021-16-1-67-75>

INTRODUCTION

In recent decades, ceramics based on the $\text{Pb}(\text{Zr}_x\text{Ti}_{1-x})\text{O}_3$ (PZT) system have become the most popular piezoelectric materials in industry and technology [1]. Through chemical modification of the PZT system, it has been possible to obtain a large number of solid solutions that demonstrate a variety of physical properties. Depending on the chosen modifier, ceramic solid solutions can have both ferroelectrically soft and hard properties. The former are observed in solid solutions in which the Zr^{4+} and Ti^{4+} ions have been partially replaced by ions with a higher formal valence (e.g., Nb^{5+} , Sb^{5+} , or W^{6+}), while in the latter, they are replaced by ions with a lower valence (e.g., Fe^{2+} or Mn^{2+}) [1–4]. Cardinal differences in the physical properties of piezomaterials determine the range of their practical applications. Thus, the creation of high-voltage equipment (such as ultrasonic emitters, piezotransformers, and piezomotors), requires ferroelectrically hard piezoceramics that combine high piezoelectric parameters (piezoelectric coefficients d_{33} and d_{31} , planar and thickness coefficients of electromechanical coupling K_p and K_t) with a mechanical quality factor (Q_m) and low values for the tangent of the dielectric loss angle ($\text{tg}\delta$) [5, 6]. However, the role of technological factors in the formation of the microstructure and the functional characteristics of ferroelectrically hard ceramics has been researched to a much lesser extent than in the case of ferroelectrically soft materials. This is largely on account of differences in the influence of the defect subsystem on the growth of crystallites during sintering. In ferroelectrically hard ceramics based on PZT, a slow grain growth is observed [1]; however, the

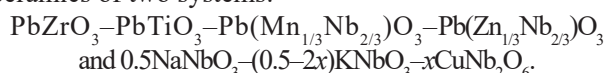
choice of sintering technology and modes can affect the functional characteristics of ferroelectrically hard ceramics based on PZT [7].

The study of lead-free solid solutions with properties similar to PZT ceramics is an important area of research regarding the creation of ferroelectrically hard piezomaterials, given that PZT ceramics contain a substantial amount of lead, an extremely toxic element. One of the most promising lead-free systems is the solid solution of $(\text{Na}_{1-x}\text{K}_x)\text{NbO}_3$ (KNN) [1], which is characterized by its relatively high values of piezoelectric response ($d_{33} \sim 80$ pC/N, $K_p \sim 0.36$) [8]. To increase the hardness of KNN-based ceramics, Cu^{2+} ions are introduced into the perovskite structure in the form of various compounds (CuO , $\text{K}_{5.4}\text{Cu}_{1.3}\text{Ta}_{10}\text{O}_{29}$, $\text{K}_4\text{CuNb}_8\text{O}_{23}$, and CuNb_2O_6) [9–11], which form liquid phases during sintering. This results in a significant decrease in the optimal sintering temperatures, the preservation of the stoichiometry of a given composition, and an increase in the relative densities of ceramics. It also produces a significant increase in the mechanical quality factor Q_m , which favors the use of KNN systems in ultrasonic emitters for medical devices and high-power piezotechnics.

Analysis of the literature demonstrates that there are fundamental differences in the most common technological approaches to improving the functional characteristics of lead-containing (based on PZT) and lead-free (based on KNN) ferroelectrically hard ceramics. Thus, the purpose of this study is to identify the main regularities involved in the formation of the microstructure of ferroelectrically hard ceramics, based on both the PZT and KNN systems, through variations in the technological modes of their manufacture.

EXPERIMENTAL

The study investigates the ferroelectrically hard ceramics of two systems:



In the lead-free ceramics, the concentration of CuNb_2O_6 (x) varied: $x = 0.025, 0.050, \text{ and } 0.075$. The details of the solid-phase synthesis of PZT and KNN-based compounds are described in [12] and [13], respectively.

The sintering of lead-containing samples was carried out in accordance with the following technologies:

- sintering in the chamber furnace Nabertherm L5/13/P330 (*Nabertherm GmbH*, Germany) at atmospheric pressure (ATM) and sintering temperatures $T_{\text{sint}} = 1150\text{--}1200^\circ\text{C}$;
- sintering by hot pressing (HP) with uniaxial pressure on the USSK-1 installation (*Piezopribor SBDT*, Southern Federal University, Russia) at sintering temperatures $T_{\text{sint}} = 1125\text{--}1175^\circ\text{C}$;
- spark plasma sintering (SPS) in a vacuum at uniaxial pressure and current pulses on the SPS515S unit (*Fuji Electronic Industrial Co., Ltd.*, Japan) at sintering temperatures $T_{\text{sint}} = 930\text{--}970^\circ\text{C}$.

Sintering of lead-free samples with different concentrations of CuNb_2O_6 (x) was carried out using conventional ceramic technology at $T_{\text{sint}} = 1100\text{--}1170^\circ\text{C}$.

The control of the completeness of the sintering process of the studied ceramics was carried out according to the results of X-ray phase analysis (ARL X'TRA diffractometers (*Thermo Fisher Scientific*, Switzerland) and DRON-3.0 (*RPE Burevestnik*, Russia)), microstructure images (JEOL JSM-6390LA scanning electron microscopes (*JEOL*, Japan) and Hitachi TM1000 (*HITACHI*, Japan)), and by the values of the density of sintered piezoelectric ceramics, determined by hydrostatic weighing in octane. In the lead-containing samples, X-ray patterns identified a tetragonal crystal structure and showed no trace of impurity phases [12]. Lead-free solid solutions have orthorhombic symmetry with a monoclinic perovskite subcell, and the content of the low-melting impurity phase depends on the concentration of CuNb_2O_6 [13].

Disks with a diameter of 10 mm and a thickness of 1 mm, with silver-containing electrodes applied to the end parts, were used as measuring samples. The main electrophysical characteristics (d_{31} , K_p , Q_m) of the pre-polarized samples were determined at room temperature using a precision impedance meter, Wayne Kerr 6500V (*Wayne Kerr Electronics*, UK), in accordance with OST 11 0444 87. The values of the relative permittivity of the polarized samples ($\epsilon_{33}^T/\epsilon_0$) and $\text{tg}\delta$ were measured using a bench that included the LCR-meter Agilent E4980A (*Agilent Technologies*, USA). The piezoelectric coefficient d_{33} was measured using the APC d_{33} -meter system (*APC International, Ltd.*, USA).

RESULTS AND DISCUSSION

Ferroelectrically hard ceramics based on PZT system

Figure 1 contains images of the microstructure of ferroelectrically hard ceramics based on the PZT system that have been sintered in various ways. A polydisperse grain structure with pore-like inclusions was observed in the ceramic samples sintered at 1150°C (Fig. 1a). When sintering is undertaken using conventional ceramic technology, a strongly pronounced secondary recrystallization, which increases with higher T_{sint} values, is observed (Fig. 1b). In samples sintered at 1200°C (Fig. 1c), a significant amount of the glass phase is observed. The formation of this glass phase leads to a decrease in the experimental density and piezoelectric characteristics (Table 1); at the same time, the values of the mechanical quality factor increase by more than 15% relative to the values observed in the samples with the maximum density (at $T_{\text{sint}} = 1170^\circ\text{C}$). Note that residual porosity is observed throughout the entire temperature range of ceramic sintering.

Ceramic samples obtained by the HP method (Fig. 1d–f) do not contain visible residual pores and have a dense structure on account of the mechanical pressure applied during sintering. However, secondary recrystallization is produced as a result of the high temperature (above 1100°C) and the long duration of the sintering process (12 h). Note that this process causes the growth of large crystallites (Fig. 1f), which can reach the size of about 20 μm , on the surface of which small shells are visible—places of local melting of the liquid phase. The formation of an inhomogeneous large-crystal microstructure leads to a decrease in the experimental density and in all the main functional characteristics (Table 1).

All of the ceramic samples sintered by the SPS method had a homogeneous microstructure, with grain sizes not exceeding 5 μm and no visible glass phase inclusions (Fig. 1g–i). It would appear that such a fine-grained microstructure of ceramics is the result of the mechanical pressure applied during the sintering process and its short duration. Note that an increase in the sintering temperature to 970°C did not lead to a significant increase in the average grain size, but rather an increase in the degree of perfection of the crystallites' shape; at the same time, there was an increase in the experimental density value and in all the main functional characteristics (Table 1). An increase in the sintering temperature was seen to have the greatest effect on the increase in the dielectric properties; there was an increase of more than 30% when the T_{sint} changed from 930 to 970°C . This may be due to a change in the electrical conductivity of the grain boundaries, but this requires further investigation using dielectric spectroscopy.

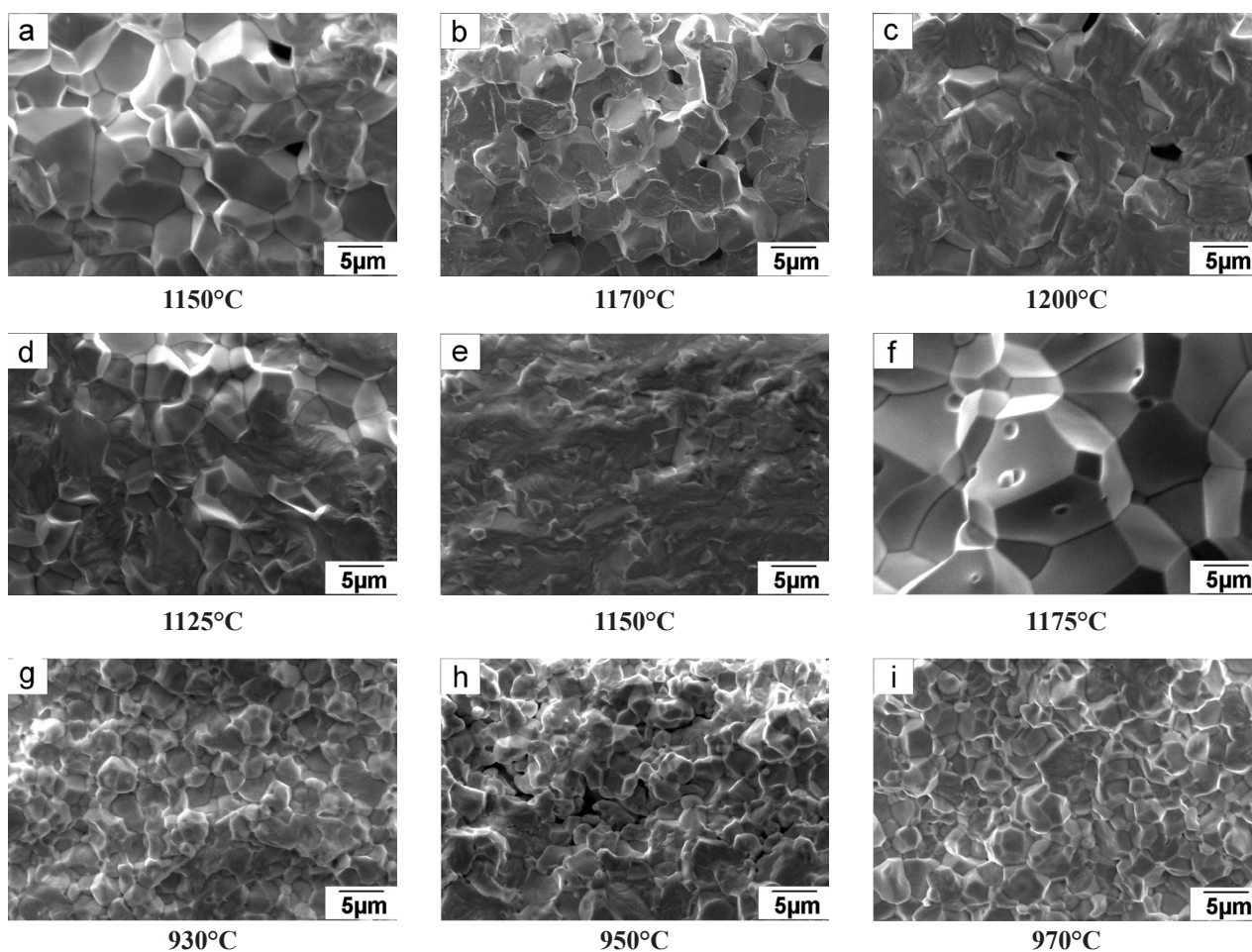


Fig. 1. Fragments of the microstructure of PZT-based ceramics sintered using various technologies: ATM (a–c), HP (d–f), and SPS (g–i).

Table 1. Experimental density and main dielectric, piezoelectric, and mechanical characteristics of ferroelectrically hard ceramics based on PZT sintered using various technologies

Sintering technology	Sintering temperature, °C	Density, g/cm ³	$\epsilon_{33}^T/\epsilon_0$	d_{31} , pC/N	Q_m
ATM	1150	7.73	1292	115	449
	1170	7.80	1307	125	538
	1200	7.78	1297	119	624
HP	1125	7.67	1399	122	545
	1150	7.72	1415	130	644
	1175	7.70	1387	127	576
SPS	930	7.91	1153	119	912
	950	7.94	1349	127	1012
	970	7.98	1514	129	1090

The choice of sintering technology and mode had the greatest impact on the mechanical quality factor values: in the case of ceramics sintered by the SPS method, Q_m exceeds 1000, which is 70–140% more than the values typically found in the other samples (Table 1). At the same time, the differences in the d_{31} values of samples sintered using different technologies (but with optimal T_{sint}) do not exceed the experimental error. When compared with ceramics sintered using conventional ceramic technology, those sintered by the SPS method are characterized by more than twice the figure-of-merit values, $\text{FOM} = K^2 \cdot Q_m$ (where, K is one of the coefficients of electromechanical coupling, depending on the type of device) [14].

The most significant factors that affect the manifestation of physical properties were identified through analysis of data published in literature that is devoted to the establishment of correlations between the technology of ceramic manufacturing, the average size of crystallites, and the macroscopic responses (dielectric, piezoelectric, mechanical) of piezoceramics [15–17]. These include changes in the configuration and size of domains and in the pinning effect of domain walls, which can be enhanced both by increasing the concentration of oxygen vacancies and by reducing the size of crystallites, thus increasing the area of intercrystalline boundaries that can also act as pinning centers [17]. However, in this case, a sharp increase in Q_m did not result in a decrease in the d_{31} values. The ceramics sintered by the SPS and ATM methods were characterized by the very close parameters of the dielectric hysteresis loops [18], which indicates the absence of any significant rearrangement of the domain structure. It is possible that a change in sintering modes can

lead to the development of several processes that affect macroscopic responses in different ways, for example, to an increase in the density of the boundaries of 90° domains [15] and to an increase in pinning by intercrystalline boundaries with a decrease in the average grain size. Note that, to date, there is no unambiguous understanding of the relationship between the size of the crystallites and the behavior of their dielectric and piezoelectric properties, while the established correlations even within a single PZT chemical system are contradictory [19].

Ferroelectrically hard ceramics based on the KNN system

Figure 2 shows images of the microstructure of ferroelectrically hard ceramics based on the KNN system that contain different concentrations of CuNb_2O_6 (x). It can be seen that the addition of even a small amount of CuNb_2O_6 (Fig. 2a and 2b) leads to the formation of a compacted microstructure that includes a significant glass phase content and large individual crystallites. As shown in [13], the addition of CuNb_2O_6 to the KNN system leads to the appearance of the impurity phase $\text{K}_4\text{CuNb}_8\text{O}_{23}$. This compound has a low melting point (1050°C), which contributes to the formation of liquid phases during sintering, and as a result, it increases the density of ceramics [20]. The relative density of samples with $x = 0.025$ reaches 96%, which is almost the limit result for unmodified KNN ceramics, even when using SPS [21]. As a result, it is possible to obtain an increase of $\sim 10\%$ in the dielectric and piezoelectric characteristics and an increase of 60% in the mechanical quality factor (see Table 2) when compared to unmodified KNN ceramics sintered using conventional ceramic technology [8]).

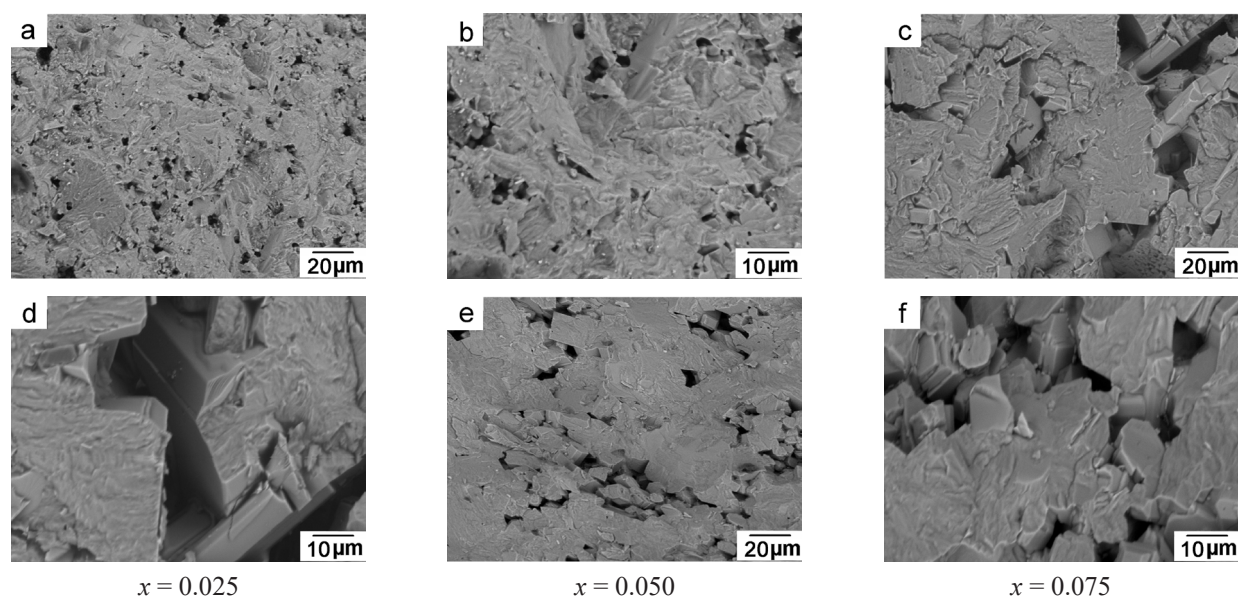


Fig. 2. Fragments of the microstructure of KNN-based ceramics with different concentrations of CuNb_2O_6 (x).

Table 2. Experimental density and main dielectric, piezoelectric, and mechanical characteristics of ferroelectrically hard ceramics based on KNN with different concentrations of CuNb_2O_6 (x)

x	Density, g/cm^3	$\epsilon_{33}^T/\epsilon_0$	d_{33} , pC/N	Q_m
0.025	4.36	343	88	211
0.050	3.65	253	43	314
0.075	3.55	332	26	290

Further increases in the concentration of CuNb_2O_6 , to $x = 0.050$ (Fig. 2c and 2d) and 0.075 (Fig. 2e and 2f), led to a spur increase in the content of the impurity phase [13] and a significant decrease in the relative density of ceramics to values below 80%. At the same time, individual cubic-shaped crystallites, with sizes exceeding 20 μm , were observed (Fig. 2c and 2d); this is typically seen in KNN ceramics with Cu-containing additives that form liquid phases [10, 11, 22]. The ceramics of both compositions are characterized by the accumulation of pores around large crystallites, which is likely to be the result of excessive growth that occurred due to the liquid phase, in place of which numerous voids were subsequently formed. As shown in [23], which uses the example of Al_2O_3 with CaO and TiO_2 additives that provoke the formation of liquid phases during sintering, an increase in the content of the TiO_2 additives leads to a sharp increase in the number of crystallites, which prevents their excessive growth and contributes to the formation of a more homogeneous microstructure (Fig. 2e and 2f). When x increases, there is a sharp drop in the values of the piezoelectric parameters, while the value of Q_m increases by 50% (Table 2).

Note that in this paper, KNN-based ceramics are made by solid-phase synthesis and are sintered using conventional ceramic technology. However, the use of HP and SPS technologies makes it possible to significantly increase the values of the main piezoelectric characteristics of unmodified KNN ceramics, with the value of d_{33} doubling. For this reason, further study is required with regard to the effect of sintering modes on the properties of ferroelectrically hard ceramics that are based on KNN with CuNb_2O_6 additives.

CONCLUSIONS

This paper studies the microstructure features of ferroelectrically hard piezoceramics based on PZT and KNN systems with variations in the chemical and technological modes of their manufacture. In the case of lead-containing ceramics, three different

sintering technologies were used: ATM, HP, and SPS. Within each of these, the production modes were optimized in order to obtain samples that had the maximum density and best combinations of functional characteristics. It has been established that SPS is the optimal technology for the application of the studied ferroelectrically hard ceramics in high-power piezotechnics devices operating at piezoresonance frequencies. Ceramics sintered by this method are characterized by a high density, a homogeneous microstructure, and an increase of more than twice the amount of FOM values in comparison with those sintered by conventional ceramic technology. In addition, the use of SPS allowed a reduction of 200°C in the optimal sintering temperature and reduced the sintering time by more than 20 times, which reduces production costs. This technology can also be used in the manufacture of multilayer converters with a low-voltage control, in which the sintering of ceramic layers and the burning of conductive electrodes are combined in one technological operation.

This paper takes a new approach to studying improvements in the functional characteristics of lead-free ceramics, by adding a copper-containing additive CuNb_2O_6 (x) to the base KNN system, which contributes to the appearance of liquid phases during sintering. It was found that, at $x = 0.025$, a compacted microstructure is formed with relative density values (96%) that have practical limitations in conventional ceramic technology. As a result, there is an increase in both the piezoelectric and mechanical properties, which leads to a twofold increase in the values of the FOM when compared to KNN ceramics. This offers an opportunity for further research on the choice of technology and modes of sintering lead-free ceramics based on the system considered in this paper.

Thus, on the basis of the performed research, it has been established that the choice of chemical and technological modes of manufacturing both lead-containing and lead-free ferroelectrically hard piezoceramics can significantly (twice) increase its functional characteristics.

Acknowledgments

The authors are grateful to G.M. Konstantinov for obtaining microstructure images of lead-free ceramics. The study was carried out with the financial support of the Ministry of Science and Higher Education of the Russian Federation (State task in the field of scientific activity, scientific project No. 0852-2020-0032), (BAZ0110/20-3-07IF).

Authors' contribution

M.V. Talanov – production and experimental study of dielectric and piezoelectric properties of ceramic samples, interpretation of experimental results, writing the text of the article;

M.A. Marakhovsky – production and experimental study of the dielectric and piezoelectric properties of ceramic samples, study, and description of the microstructure of ceramics based on the lead zirconate–titanate system, discussion of measurement results.

The authors declare no conflicts of interest.

REFERENCES

- Jaffe B., Cook W.R., Jaffe H. *Piezoelectric Ceramics*. New York: Academic Press; 1971. 317 p.
- Tan Q., Li J., Viehland D. Role of lower valent substituent-oxygen vacancy complexes in polarization pinning in potassium-modified lead zirconate titanate. *Appl. Phys. Lett.* 1999;75(3):418–420. <https://doi.org/10.1063/1.124394>
- Feng Y., Wu J., Chi Q., Li W., Yu Y., Fei W. Defects and Aliovalent Doping Engineering in Electroceramics. *Chem. Rev.* 2020;120(3):1710–1787. <https://doi.org/10.1021/acs.chemrev.9b00507>
- Fesenko E.G., Dantsiger A.Ya., Razumovskaya O.N. *Novye p'ezokeramicheskie materialy (New piezoceramic materials)*. Rostov-on-Don: Rostov University; 1983.160 p. (in Russ.).
- Zhang S., Xia R., Lebrun L., Anderson D., ShROUT T.R. Piezoelectric materials for high power, high temperature applications. *Mater. Lett.* 2005;59(27):3471–3475. <https://doi.org/10.1016/j.matlet.2005.06.016>
- Lee H.J., Zhang S., Bar-Cohen Y., Sherrit S. High Temperature, High Power Piezoelectric Composite Transducers. *Sensors.* 2014;14(8):14526–14552. <https://doi.org/10.3390/s140814526>
- Kamel T.M., de With G. Poling of hard ferroelectric PZT ceramics. *J. Europ. Ceram. Soc.* 2008;28(9):1827–1838. <https://doi.org/10.1016/j.jeurceramsoc.2007.11.023>
- Egerton L., Dillon D. M. Piezoelectric and Dielectric Properties of Ceramics in the System Potassium Sodium Niobate. *J. Am. Ceram. Soc.* 1959;42(9):438–442. <https://doi.org/10.1111/j.1151-2916.1959.tb12971.x>
- Yang M.-R., Tsai C.-C., Hong C.-S., Chu S.-Y., Yang S.-L. Piezoelectric and ferroelectric properties of CN-doped (K_{0.5}Na_{0.5})NbO₃ lead-free ceramics. *J. Appl. Phys.* 2010;108(9):094103. <https://doi.org/10.1063/1.3493732>
- Park B.C., Hong I.K., Jang H.D., Tran V.D.N., Tai W.P., Lee J.-S. Highly enhanced mechanical quality factor in lead-free (K_{0.5}Na_{0.5})NbO₃ piezoelectric ceramics by co-doping with K_{5/4}Cu_{1/3}Ta₁₀O₂₉ and CuO. *Mater. Lett.* 2010;64(14):1577–1579. <https://doi.org/10.1016/j.matlet.2010.04.031>
- Park H.-Y., Choi J.-Y., Choi M.-K., Cho K.-H., Nahm S., Lee H.-G., Kang H.-W. Effect of CuO on the Sintering Temperature and Piezoelectric Properties of (Na_{0.5}K_{0.5})NbO₃ Lead-Free Piezoelectric Ceramics. *J. Am. Ceram. Soc.* 2008;91(7):2374–2377. <https://doi.org/10.1111/j.1551-2916.2008.02408.x>
- Marakhovsky M.A., Panich A.A., Talanov M.V., Marakhovskiy V.A. Study of the influence of technological factors on improving the efficiency of ferroelectrically hard piezoceramic material PCR-8. *Ferroelectrics.* 2020;560(1):1–6. <https://doi.org/10.1080/00150193.2020.1722875>
- Talanov M.V., Shikina L.A., Reznichenko L.A. Synthesis and properties of Na_{1-x}K_xNbO₃-based solid solutions in the CuNb₂O₆-NaNbO₃-KNbO₃ system. *Inorg. Mater.* 2016;52(10):1063–1069. <https://doi.org/10.1134/S0020168516100186>
[Original Russian Text: Talanov M.V., Shikina L.A., Reznichenko L.A. Synthesis and properties of Na_{1-x}K_xNbO₃-based solid solutions in the CuNb₂O₆-NaNbO₃-KNbO₃ system. *Neorgan. Materialy.* 2016;52(10):1134–1140 (in Russ.). <https://doi.org/10.7868/S0002337X16100183>
- Rödel J., Webber K.G., Dittmer R., Jo W., Kimura M., Damjanovic D. Transferring lead-free piezoelectric ceramics into application. *J. Europ. Ceram. Soc.* 2015;35(6):1659–1681. <https://doi.org/10.1016/j.jeurceramsoc.2014.12.013>
- Zheng P., Zhang J.L., Tan Y.Q., Wang C.L. Grain-size effects on dielectric and piezoelectric properties of poled BaTiO₃ ceramics. *Acta Materialia.* 2012;60(13–14):5022–5033. <https://doi.org/10.1016/j.actamat.2012.06.015>
- Huan Y., Wang X., Fang J., Li L. Grain size effect on piezoelectric and ferroelectric properties of BaTiO₃ ceramics. *J. Europ. Ceram. Soc.* 2014;34(5):1445–1448. <https://doi.org/10.1016/j.jeurceramsoc.2013.11.030>
- Sakaki C., Newalkar B.L., Komarneni S., Uchino K. Grain Size Dependence of High Power Piezoelectric Characteristics in Nb Doped Lead Zirconate Titanate Oxide Ceramics. *Jpn. J. Appl. Phys.* 2001;40(12R):6907–6910. <https://doi.org/10.1143/JJAP.40.6907>

18. Marakhovskiy M.A., Panich A.A., Talanov M.V., Marakhovskiy V.A. Effect of the Type of Sintering on the Dielectric Hysteresis of a Hard Piezoceramic Material based on Lead Zirconate Titanate. *Bull. Russ. RAS. Sciences: Physics*. 2020;84(11):1419–1421. <https://doi.org/10.3103/S1062873820110179>

[Original Russian Text: Marakhovskiy M.A., Panich A.A., Talanov M.V., Marakhovskiy V.A. Effect of the Type of Sintering on the Dielectric Hysteresis of a Hard Piezoceramic Material based on Lead Zirconate Titanate. *Izv. RAN. Seriya Fizicheskaya*. 2020;84(11):1667–1669. <https://doi.org/10.31857/S0367676520110186>]

19. Randall C.A., Kim N., Kucera J.-P., Cao W., Shrout T.R. Intrinsic and Extrinsic Size Effects in Fine-Grained Morphotropic-Phase-Boundary Lead Zirconate Titanate Ceramics. *J. Am. Ceram. Soc.* 1998;81(3):677–688. <https://doi.org/10.1111/j.1151-2916.1998.tb02389.x>

20. Matsubara M., Yamaguchi T., Sakamoto W., Kikuta K., Yogo T., Hirano S. Processing and Piezoelectric Properties of Lead-Free (K,Na)(Nb,Ta) O₃ Ceramics. *J. Am. Ceram. Soc.* 2005;88(5):1190–1196. <https://doi.org/10.1111/j.1551-2916.2005.00229.x>

21. Zhang B.P., Li J.-F., Wang K., Zhang H. Compositional Dependence of Piezoelectric Properties in NaK_{1-x}NbO₃ Lead-Free Ceramics Prepared by Spark Plasma Sintering. *J. Am. Ceram. Soc.* 2006;89(5):1605–1609. <https://doi.org/10.1111/j.1551-2916.2006.00960.x>

22. Ahn C.-W., Lee H.-Y., Han G., Zhang S., Choi S.-Y., Choi J.-J., Kim J.-W., Yoon W.-H., Choi J.-H., Park D.-S., Hahn B.-D., Ryu J. Self-Growth of Centimeter-Scale Single Crystals by Normal Sintering Process in Modified Potassium Sodium Niobate Ceramics. *Sci. Rep.* 2015;5:17656. <https://doi.org/10.1038/srep17656>

23. Hong S.H., Kim D.Y. Effect of Liquid Content on the Abnormal Grain Growth of Alumina. *J. Am. Ceram. Soc.* 2001;84(7):1597–1600. <https://doi.org/10.1111/j.1151-2916.2001.tb00883.x>

About the authors:

Mikhail V. Talanov, Cand. Sci. (Phys.–Math.), Leading Researcher, Research Institute of Physics, Southern Federal University (194, Stachki pr., Rostov-on-Don, 344090, Russia). E-mail: mvtalanov@gmail.com. Scopus Author ID 53164920700, Researcher ID P-8971-2019, <https://orcid.org/0000-0002-5416-9579>

Mikhail A. Marakhovskiy, Cand. Sci. (Eng.), Head of Sector, Scientific Design and Technological Bureau Piezopribor, Southern Federal University (10, Milchakova ul, Rostov-on-Don, 344090, Russia). E-mail: marmisha@mail.ru. Scopus Author ID 57210826910.

Об авторах:

Таланов Михаил Валерьевич, к.ф.-м.н., ведущий научный сотрудник Научно-исследовательского института физики Южного федерального университета (344090, Россия, г. Ростов-на-Дону, пр-т Стачки, д. 194). E-mail: mvtalanov@gmail.com. Scopus Author ID 53164920700, Researcher ID P-8971-2019, <https://orcid.org/0000-0002-5416-9579>

Мараховский Михаил Алексеевич, к.т.н., начальник сектора Научного конструкторско-технологического бюро «Пьезоприбор» Южного федерального университета (344090, Россия, г. Ростов-на-Дону, ул. Мильчакова, д. 10). E-mail: marmisha@mail.ru. Scopus Author ID 57210826910.

The article was submitted: October 28, 2020; approved after reviewing: January 06, 2021; accepted for publication: February 03, 2021.

Translated from Russian into English by N. Isaeva

Edited for English language and spelling by Enago, an editing brand of Crimson Interactive Inc.

**ANALYTICAL METHODS IN CHEMISTRY
AND CHEMICAL TECHNOLOGY**

**АНАЛИТИЧЕСКИЕ МЕТОДЫ
В ХИМИИ И ХИМИЧЕСКОЙ ТЕХНОЛОГИИ**

ISSN 2686-7575 (Online)

<https://doi.org/10.32362/2410-6593-2021-16-1-76-87>



UDC 543.51:543.544.53

RESEARCH ARTICLE

Comparing the original and biosimilar biotherapeutics of the monoclonal antibody eculizumab by intact mass measurement and middle-up mass spectrometry analysis

Maksim B. Degterev[@], Rakhim R. Shukurov

International Biotechnology Center Generium, Volginskiy, Vladimir oblast, 601125 Russia
[@]Corresponding author, e-mail: degterev@ibcgenerium.ru

Abstract

Objectives. In this biosimilar research, we compare the monoclonal antibody eculizumab obtained from different drugs [original Soliris[®] (Alexion Pharmaceuticals) and candidate Elizaria[®] (Generium)] by intact mass measurement and middle-up mass spectrometry analysis to enhance the role of mass spectrometry methods in biopharmaceutical development processes.

Methods. The intact mass measurement is performed using a high-resolution ESI-MS. The middle-up analysis is performed by reversed-phase high-performance liquid chromatography with ESI-MS detection, subsequent IdeS treatment of antibodies, and disulfide bond reduction.

Results. We have shown some small differences between the original and candidate drugs in the minor glycans level. Man5 glycan is only found in the original Soliris, and G0 is only found in the Elizaria. Glycation sites are also found in the light chain and Fd subunits of the original Soliris. The glycation level does not exceed 4.4%. The non-clipped C-end lysine level and G0F glycan levels are slightly lower in the original Soliris. All registered differences are not crucial for eculizumab's quality and do not affect its effectiveness and preclinical safety. Generally, the results show a high level of similarity between the original and candidate drugs.

Conclusions. The comparative mass spectrometry analysis of eculizumab in the original Soliris and Elizaria allows us to estimate their high degree of similarity by molecular masses and major modification profiles.

Keywords: Eculizumab, mass spectrometry, posttranslational modifications, biosimilar drugs, glycosylation, high-performance liquid chromatography-mass spectrometry, intact mass measurement, middle-up analysis, monoclonal antibody

For citation: Degterev M.B., Shukurov R.R. Comparing the original and biosimilar biotherapeutics of the monoclonal antibody eculizumab by intact mass measurement and middle-up mass spectrometry analysis. *Tonk. Khim. Tekhnol. = Fine Chem. Technol.* 2021;16(1):76–87 (Russ., Eng.). <https://doi.org/10.32362/2410-6593-2021-16-1-76-87>

НАУЧНАЯ СТАТЬЯ

Сравнение оригинального и биоаналогичного препаратов моноклонального антитела экулизумаб методами масс-спектрометрии интактного белка и «с середины вверх»

М.Б. Дегтерев[@], Р.Р. Шукуров

Международный биотехнологический центр «Генериум», Владимирская область, Петушинский район, пос. Вольгинский, 601125 Россия

[@]Автор для переписки, e-mail: degterev@ibcgenerium.ru

Аннотация

Цели. В целях исследования биоаналогичности, а также внедрения масс-спектрометрии в процессы биофармацевтической разработки было необходимо провести сравнительное масс-спектрометрическое исследование моноклонального антитела экулизумаб из оригинального лекарственного препарата «Солирис»[®] и кандидатного «Элизария»[®] производства АО «ГЕНЕРИУМ» методами измерения молекулярных масс интактных молекул (intact mass measurement) и их субъединиц (middle-up).

Методы. Измерение масс интактных белков и оценку долей их модификаций проводили при помощи инфузионной масс-спектрометрии высокого разрешения с электрораспылительной ионизацией. Измерение молекулярных масс субъединиц и оценку долей их модификаций проводили методом обращенно-фазовой ВЭЖХ, совмещенной с масс-спектрометрией высокого разрешения с электрораспылительной ионизацией после предварительного расщепления антител ферментом IdeS и разрыва дисульфидных связей.

Результаты. Нами был зарегистрирован ряд небольших отличий в содержании некоторых минорных гликанов: олигосахарид Man5 был обнаружен только в белке оригинального препарата, а G0 – только в кандидатном белке; в субъединицах LC и Fd оригинального белка были зарегистрированы сайты гликирования с содержанием данной модификации не выше 4.4%. Также доли неотщепленного C-концевого лизина и гликана G0F в оригинальном белке были несколько ниже, чем в кандидатном. Однако зарегистрированные отличия не являлись критическими параметрами качества экулизумаба и не влияли на активность молекул и их безопасность в доклинических испытаниях, и, в целом, сравниваемые молекулы продемонстрировали высокое сходство.

Выводы. Сравнительный хромато-масс-спектрометрический анализ экулизумаба из оригинального и кандидатного препаратов позволил установить высокую степень сопоставимости сравниваемых молекул по молекулярным массам и по профилям мажорных модификаций.

Ключевые слова: экулизумаб, масс-спектрометрия, посттрансляционные модификации, биоаналогичность, гликозилирование, ВЭЖХ-МС, intact mass measurement, middle-up

Для цитирования: Дегтерев М.Б., Шукуров Р.Р. Сравнение оригинального и биоаналогичного препаратов моноклонального антитела экулизумаб методами масс-спектрометрии интактного белка и «с середины вверх». *Тонкие химические технологии.* 2021;16(1):76–87. <https://doi.org/10.32362/2410-6593-2021-16-1-76-87>

INTRODUCTION

One of the most promising areas in the pharmaceutical industry is biopharmaceuticals (e.g., therapeutic proteins). Therapeutic proteins exhibit much higher specificity and activity than chemically synthesized low-molecular-weight drugs. Since their development, they are found effective in treating many acute diseases previously inaccessible to therapy, increasing the patients' duration and quality of life. For the last five years, the US Food and Drug Administration¹ (FDA) has approved 213 drugs, of which 44 are monoclonal antibodies.²

One of the main driving forces for the development of biopharmaceuticals is the development of biosimilar drugs due to several reasons. The biosimilar drug's cost is typically lower than the original drug's cost; hence its release is attractive for pharmaceutical companies. Stringent requirements for the comprehensive characterization of a promising biosimilar molecule developed by leading regulatory bodies such as the FDA and the European Medicines Evaluation Agency (EMA) minimize the risk of an ineffective or hazardous product entering the market. They also stimulate research by developing new analysis methods and deepening understanding of the structures and functions of therapeutic proteins, their targets, and the pathogenesis of various diseases.

Monoclonal antibodies account for most developed biosimilar drugs. Monoclonal antibodies are successfully used in treating serious diseases, including hereditary diseases. The potential of some monoclonal antibodies to expand indications for therapeutic use is also a stimulus for the development of biosimilar drugs. A striking example is eculizumab. It is a recombinant humanized monoclonal antibody (IgG2/4k) used for treating paroxysmal nocturnal hemoglobinuria, atypical hemolytic uremic syndrome, myasthenia gravis, and

optic neuromyelitis. The development of biosimilar eculizumab requires a comprehensive, in-depth study of its physicochemical properties. Currently, an important method for studying proteins has become the method of mass spectrometry (MS). Hence, it is possible to determine the molecular mass of an intact molecule (by intact mass measurement) and its subunits (by middle-up analysis).

Intact mass measurement of a protein molecule for the comparison of biological products makes it possible to establish its authenticity by the correspondence of the measured value to the expected one, measure the content of some modified forms, and evaluate the purity of the drug by the number of proteoforms found with a polypeptide chain cleavage [1–3]. Suppose the measurement is carried out in the mode of native MS. In that case, the list of characteristics to be determined can also be supplemented with information on the molecule's spatial organization, on the content of proteins with different conformations and their aggregates in the sample [4, 5]. Intact mass measurement involves preliminary purification and fractionation of the protein before it is enter to the ion source of the mass spectrometer using offline (ultrafiltration, dialysis, and size exclusion purification) or online (high-performance liquid chromatography (HPLC) and capillary electrophoresis) methods followed by collecting mass spectra for a sample or its fractions, their mathematical processing (deconvolution), and interpreting obtained data [6, 7]. The method's main advantages are achieving high-speed research and obtaining a picture of the structure and shape of whole protein molecules [3, 4].

However, the high complexity and heterogeneity of therapeutic proteins limit intact molecule applicability for in-depth comparability studies. The method does not yet allow identifying minor modifications and establishing their positions in the molecule, interpreting and annotating the spectra of proteins with ultrahigh heterogeneity [8]. A significant part of these problems is solved by middle-up analysis, slightly reducing the analysis performance and minimizing the risk of losing data about the molecule under study. Its essence lies in the limited chemical or enzymatic cleavage of the protein molecule under the study of obtaining large fragments. Then, these fragments are separated using HPLC or capillary electrophoresis and entered to the mass spectrometer. The obtained mass spectra are interpreted, taking into account theoretical data on the molecule's structure, allowing a deeper characterization of the profile of modifications, degradant forms, and interpreting the results of an analysis of proteins characterized by high heterogeneity of forms [9].

¹ Guidance, Compliance & Regulatory Information (Biologics). <https://www.fda.gov/vaccines-blood-biologics/guidance-compliance-regulatory-information-biologics> (accessed 21.10.2020).

² Global Therapeutic Proteins Market Report 2020: Market was Valued at \$93.14 Billion in 2018 and is Expected to Grow to \$172.87 Billion through 2022. <https://www.businesswire.com/news/home/20191223005228/en/Global-Therapeutic-Proteins-Market-Report-2020-Market-was-Valued-at-93.14-Billion-in-2018-and-is-Expected-to-Grow-to-172.87-Billion-through-2022---ResearchAndMarkets.com> (accessed 21.10.2020).

³ Biological guidelines. <https://www.ema.europa.eu/en/human-regulatory/research-development/scientific-guidelines/biological-guidelines> (accessed 21.10.2020).

⁴ ASSESSMENT REPORT FOR Soliris. International Nonproprietary Name: ECULIZUMAB. Procedure No. EMEA/H/C/000791/II/0050. European Medicines Agency, Committee for Medicinal Products for Human Use (CHMP). March 21, 2013. EMA/CHMP/126714/2013

In this study, we evaluate the comparability of eculizumab from different sources by infusion MS after purification of the protein by size-exclusion filtration. To perform middle-up analyses, we have ensured that the antibody is cleaved in the hinge region with the IdeS protease before analysis. Then, the fragments' disulfide bridges are disrupted with TCEP-HCl. Before entering the mass spectrometer, the resulting antibody subunits (light chain (LC), Fc/2, and Fd: light chain and monoclonal antibody fragments located in the region from the hinge region to the C-terminus of the heavy chain and from the N-terminus of the heavy chain to the hinge region, respectively) are separated and purified from impurities using reverse-phase HPLC.

The results of mass spectrometric comparison of eculizumab from the original and candidate drugs show their similarity in the main quality parameters: the molecular masses of the main protein proteoforms coincide with each other and with the expected values; the glycosylation profiles of the compared samples turned out to be close with each other, as well as the content of some modified variants: oxidized forms of the Fc/2 subunit and forms with uncleaved C-terminal lysine. Significant differences are recorded in the content of high-mannose and fucosylated glycans and glycosylated variants of LC and Fd subunits: Man5 glycan and glycosylated variants are found in the eculizumab from the original drug, and G0 (fucosylated) glycan is found in Elizaria® drug. The content of these proteoforms does not exceed 4.4%. All reported differences are expected because of using different host cell lines. The differences are not significant in the effectiveness and safety of eculizumab. The data obtained have become the basis for further, deeper comparison of molecules by other methods.

MATERIALS AND METHODS

The candidate Elizaria drug was produced from *Generium JSC* (Moscow, Russia); the original drug was purchased as part of the Soliris® drug (*Alexion Pharmaceuticals*, Zürich, Switzerland). Deionized water was obtained using a MilliQ IQ 7000 system (*Merck*, Darmstadt, Germany). Acetonitrile (LC-MS grade) was also purchased from *Merck*. We use the IdeS protease manufactured by *Promega* (Madison, WI, USA). HPLC column BioResolve RP mAb Polyphenyl and difluoroacetic acid (DFA, LC-MS grade) were purchased from *Waters* (Finglas, Dublin, Ireland). Zeba Spin Desalting Columns (7K MWCO, 0.5 mL) and tris-(2-carboxyethyl)phosphine hydrochloride (TCEP-HCl) were purchased from *Thermo Scientific* (Dreieich, Germany). The rest of the reagents and materials (Na_2HPO_4 , NaH_2PO_4 , NaCl,

guanidine hydrochloride, ethylenediaminetetraacetic acid (EDTA), and trisaminomethane hydrochloride (Tris-HCl)) were purchased from *Sigma-Aldrich* (St. Louis, MO, USA). All studies were performed using a Nexera X2 HPLC system (*Shimadzu Co.*, Tokyo, Japan) connected to a 6550 QTOF mass spectrometer (*Agilent Technologies*, Santa Clara, CA, USA).

EXPERIMENTAL

Sample preparation for intact mass measurement

In this experiment, we use three series of original and candidate drugs. The antibody concentration in the solution is adjusted to 1.0 mg/mL. The buffer is replaced with a 0.15% solution of difluoroacetic acid by size exclusion filtration through Zeba Spin columns according to the instructions.

Sample preparation for middle-up analysis

The antibody concentration in the solution is adjusted to 2.0 mg/mL by dilution with 50-mM phosphate buffer with 150-mM NaCl (pH 6.6). Then, to 25- μL sample solutions, 2- μL IdeS solution (1 U/ μL) is added and incubated at 37°C for 1.5 h. The samples are diluted twice with denaturing buffer containing 6-M guanidine-HCl, 1-mM EDTA, and 0.1-M Tris-HCl (pH 7.8); 2.5 μL of 1-M TCEP-HCl solution is added. The incubation periods last for 18 h at 4°C.

The mechanism of action of the IdeS enzyme comprises cutting the antibody molecule in the hinge region, resulting in the formation of two subunits [F(ab')₂ and Fc/2] (Fig. 1). Subsequent chemical cleavage of the disulfide bridges divided the F(ab')₂ subunit into two fragments: LC and the Fd subunit.

Intact mass measurement

We have performed the test in the infusion MS mode. The injection rate of the sample solution is 10 $\mu\text{L}/\text{min}$. Before ionization, it is mixed with a 0.15% DFA solution flow supplied at a rate of 100 $\mu\text{L}/\text{min}$. The device operated under the following conditions: positive ionization mode and high mass range with boundaries of 700–8000 Th with signal detection in the frontal scanning mode. The linear data collection rate is 1 Hz, and the evaporator pressure is 22 psi. We analyze each sample in three technical replicas. We process the experimental results using the MassHunter Qualitative Analysis B.09.00 (*Agilent Technologies*) and UniDec v.4.1.2 [10].

Middle-up analysis

We have performed the linear gradient reversed-phase HPLC-MS mode test using a BioResolve RP mAb Polyphenyl column (1.0 \times 150 mm). Mobile phase A: 0.15% DFA in water; mobile phase B: 0.15% DFA in acetonitrile. Gradient scheme: 0 min (26% B), 22 min (41.5% B), 22.1 min (98% B), 24 min (98% B), 24.1 min (26% B),

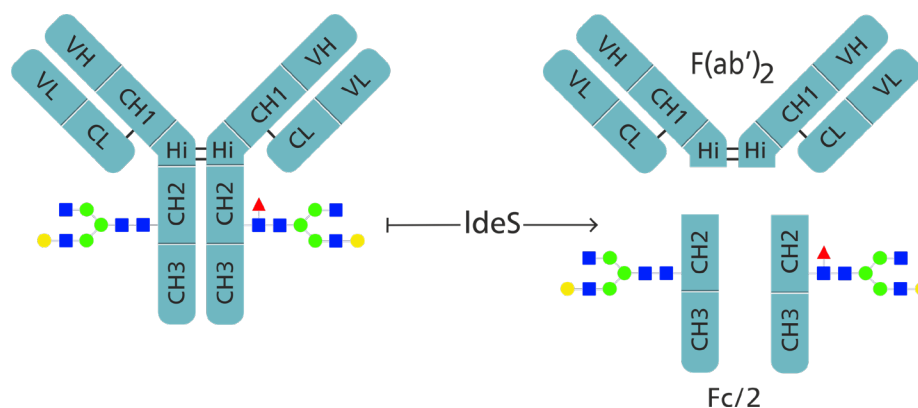


Fig. 1. Mechanism of action of the IdeS protease.

30 min (26% B) at 80°C and flow rate of 0.1 mL/min. We process the obtained mass spectra using MassHunter Qualitative Analysis B.09.00 and UniDec v.4.1.2 [10].

Statistical comparison of results

The analysis methods used for comparison are qualitative to establish the equivalence of the results, according to the currently accepted standards [11, 12]; the concept of a quality range is introduced. Its boundaries are determined by a threefold increase in the standard deviation of the measured parameters of the original samples from their mean values.

RESULTS AND DISCUSSION

Measuring the molecular mass of intact antibodies

The average molecular mass of the major proteoform of eculizumab, taking into account its amino acid sequence and main modifications (a pair of G0F glycans, a pair of cleaved C-terminal lysines, a pair of pyroglutamates at the N-termini of heavy chains, and 17 disulfide bonds) is 147874 Da. Comparative analysis of the raw mass spectra of eculizumab from samples

of various manufacturers shows that the distribution of the protein’s charge states in all cases ranges from 35+ to 65+, with the most intense states in the range from approximately 40+ to 50+ (Fig. 2).

We perform the deconvolution of mass spectra using UniDec software with the following settings: *m/z* range of 2250–4300 Th, automatic noise subtraction, range of charge states at 35–65, automatic smoothing of mass spectra, peak width at half-height of 0.8 Th, and normalized peak detection limit at 1%. It shows the presence in all studied samples of glycoforms’ molecular mass distribution, monoclonal antibodies’ characteristic, in the region expected for eculizumab. The molecular mass of the major glycoform G0F/G0F in all samples corresponds to the expected value of 148874 Da, and the deviation of its mass from the expected did not exceed 1 Da (7 ppm). Eight proteoforms are found in the original Soliris, and seven proteoforms in Elizaria, of which six and five, respectively, differed in the glycan profile; the remaining two differ in the content of uncleaved C-terminal lysine (Fig. 3 and Table 1).

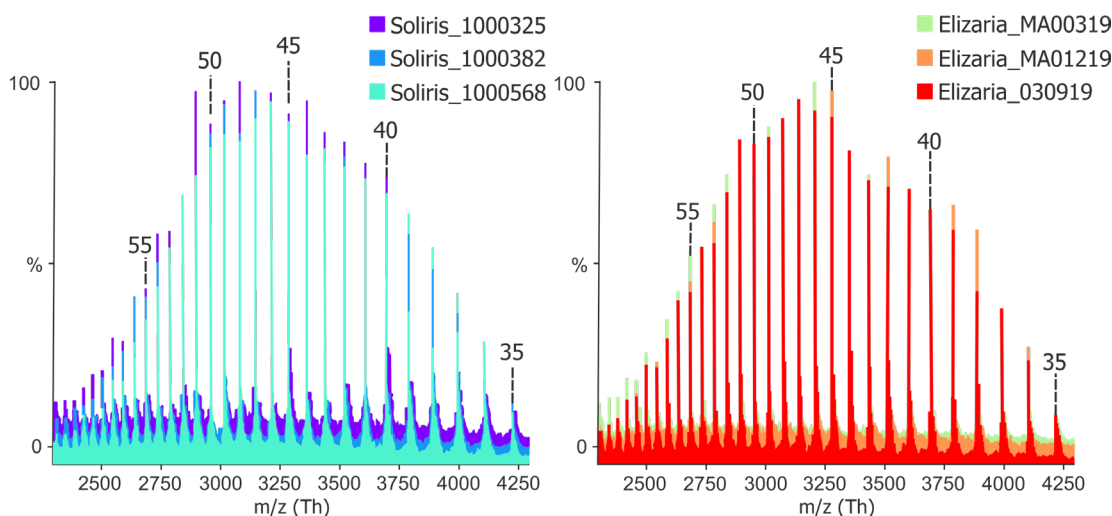


Fig. 2. Mass spectra of the original Soliris and Elizaria drugs before deconvolution. Individual charge states are annotated.

The content of the major glycoforms of eculizumab in the compared samples is similar. G0F/G0F, G1F/G0F, and G1F/G1F occupy the first, second, and third places, respectively. Glycoforms with smaller proportions are distributed more variably. Therefore, in the samples of the original Soliris, the variant G0F/G0F-GN is in fourth place, and in the drug Elizaria, the variant G0F/G0 is in fourth place.

The fifth places in all cases are represented by the glycoform G2F/G1F, and the sixth place is registered only in the samples of the original Soliris, G2F/G2F. The content of galactosylated glycans of the main functional group of oligosaccharides in the samples of the original Soliris and Elizaria are 25.7–26.4% and 11.9–14.7%, respectively. The proportions of forms of antibodies with uncleaved C-terminal

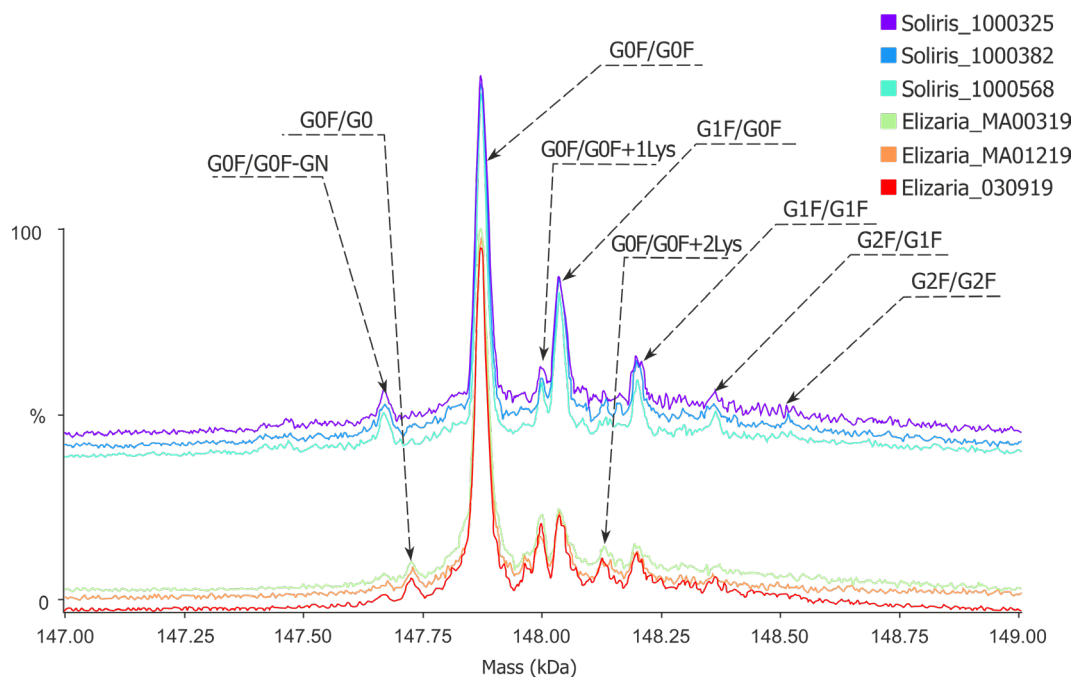


Fig. 3. Mass spectra of the original Soliris and Elizaria drugs after deconvolution. The identified proteoforms are annotated.

Table 1. Results of measuring the molecular masses of eculizumab proteoforms from the compared samples

Eculizumab proteoforms	Theoretical mass, Da	Measured mass			
		Original Soliris		Elizaria	
		Average \pm SD, Da	Error, ppm	Average \pm SD, Da	Error, ppm
G0F/G0	147728	–	–	147727 \pm 2	–5
G0F/G0F-GN	147671	147669 \pm 1	–11	–	–
G0F/G0F	147874	147873 \pm 1	–5	147874 \pm 0	0
G0F/G0F+1Lys	148002	147999 \pm 3	–23	148000 \pm 1	–16
G1F/G0F	148036	148036 \pm 3	0	148036 \pm 2	2
G0F/G0F+2Lys	148130	148130 \pm 3	2	148128 \pm 2	–14
G1F/G1F	148198	148197 \pm 2	–7	148198 \pm 2	–2
G2F/G1F	148360	148360 \pm 2	0	148363 \pm 1	20
G2F/G2F	148522	148513 \pm 13	–61	–	–

Note: SD, standard deviation.

lysine, both one and two, are slightly higher in the samples of Elizaria (Fig. 4 and Table 2). All observed differences could be explained using different cell lines to produce the original Soliris and Elizaria. The original Soliris is produced using NS0 rodent myeloma cells; Elizaria is produced using a line of Chinese hamster ovary cells that produces more galactosylated forms [13, 14]. However, the proportion of galactosylated glycans is important only for antibodies that implement a therapeutic function through the mechanism of complement-dependent cytotoxicity. In eculizumab, this mechanism is deliberately inhibited [13–15]. Similar to the previous ones, differences in uncleaved C-terminal lysine content are due to different producers and usually do not significantly affect the antibody’s therapeutic efficacy and safety.

Therefore, the samples of the original Soliris and Elizaria can be considered comparable in molecular masses and spectrum of the presented proteoforms, despite some differences in their content.

Middle-up analysis

Treating the samples with IdeS protease followed by destructing disulfide bonds using TCEP makes it possible to obtain from the eculizumab molecule three well chromatographically separated subunits, Fc/2, LC, and Fd. Figure 5 shows the recorded chromatographic peak of the coeluting oxidized form and the form with uncleaved C-terminal lysine of the Fc/2 subunit and a peak of the Fd subunit with one unbroken internal disulfide bond.

The molecular masses of all subunits coincide with the calculated ones; the maximum discrepancy from the expected value does not exceed 0.6 Da (40 ppm, Table 3).

The proportion of glycosylated forms in the compared samples slightly changes compared to the intact molecule analysis (Fig. 6 and Table 4). Thus, the difference between the content of the major glycan G0F decreases: its average levels in the original Soliris and Elizaria are 58.2 and 60.8%, respectively. The contents of G1F and G2F are approximately 14.0 and 2.5%, respectively, in all samples; no reliable difference is established for this parameter. In the middle-up analysis, we have confirmed the data on the uniqueness of oligosaccharides G0F-GN in the composition of the original Soliris and G0 in the composition of Elizaria, and another glycan, unique for the original Soliris, is discovered—Man5. Studying LC and Fd subunits makes it possible to understand why the difference in the content of G1F and G2F glycans in intact molecules. In the middle-up analysis, we have found minor proteoforms in LC and Fd subunits in the original Soliris by identifying by a characteristic mass shift of 162 Da as glycosylated variants. Their content ranges from 2.8 to 4.6%. The contribution of these forms overestimates the levels of G1F/G1F, G2F/G1F, and G2F/G2F in the analysis of intact molecule from the original Soliris. The content of galactosylated glycans in the samples of Elizaria fully corresponds to the original Soliris quality range. In the C-terminal lysine content of the compared samples, a rather close similarity is observed: compliance with the quality range is demonstrated by two out of three series of Elizaria medicinal products. The oxidation of the Fc/2 subunit becomes a new modification, which is established using the middle-up analysis. Its content in all candidate drug batches also corresponds to the quality range of the original Soliris.

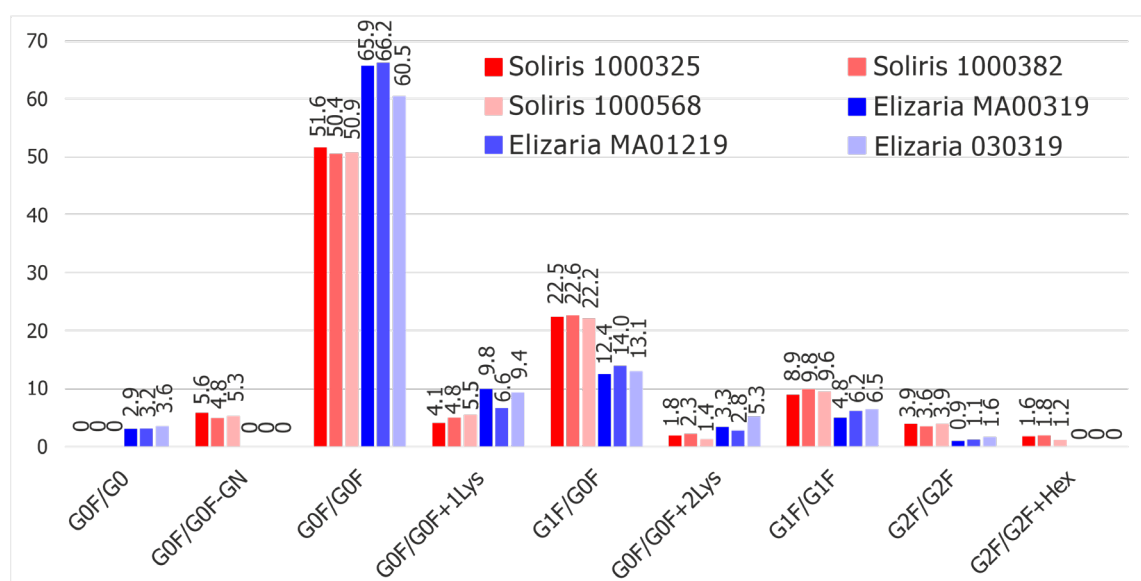
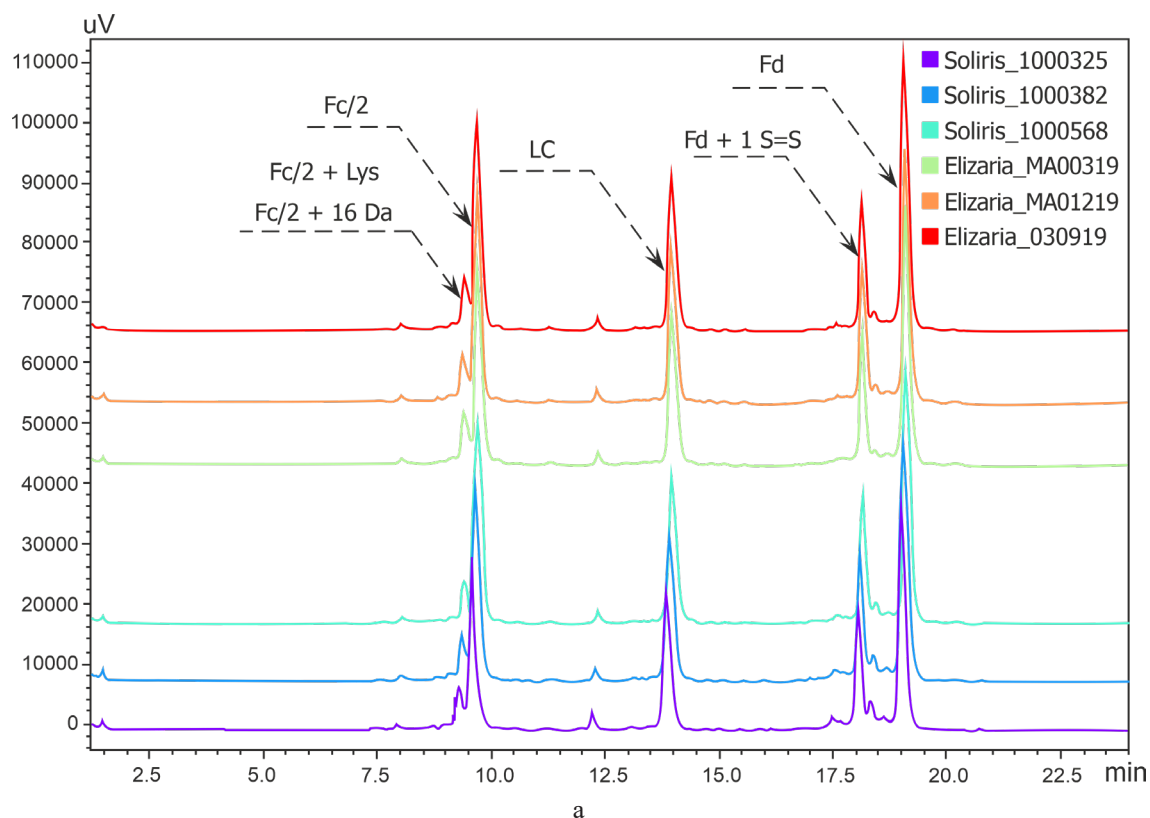


Fig. 4. The content of proteoforms in individual series of the original Soliris and Elizaria drugs.

Table 2. Comparison of the proportions of eculizumab proteoforms in the analyzed intact molecules

Eculizumab proteoforms	Original Soliris		Elizaria		Quality range, % (Average \pm 3SD)	Compliance of Elizaria with the quality range, %
	Average	SD, %	Average	SD, %		
G0F/G0	–	–	3.2	0.3	–	None
G0F/G0F-GN	5.2	0.4	–	–	4.0–6.4	None
G0F/G0F	51.0	0.6	64.2	3.2	49.2–52.8	None
G0F/G0F+1Lys	4.8	0.7	8.6	1.7	2.7–6.9	33
G1F/G0F	22.4	0.2	13.2	0.8	21.8–23.0	None
G0F/G0F+2Lys	1.8	0.4	3.8	1.3	0.6–3.0	33
G1F/G1F	9.4	0.5	5.8	0.9	7.9–10.9	None
G2F/G1F	3.8	0.2	1.2	0.4	3.2–4.4	None
G2F/G2F	1.5	0.3	–	–	0.6–2.4	None
Galactosylated glycans, sum ($0.5 \times \text{G0F/G1F} + \text{G1F/G1F} + \text{G2F/G1F} + \text{G2F/G2F}$)	26.0	0.4	13.6	1.5	24.8–27.2	None

Note: SD, standard deviation.



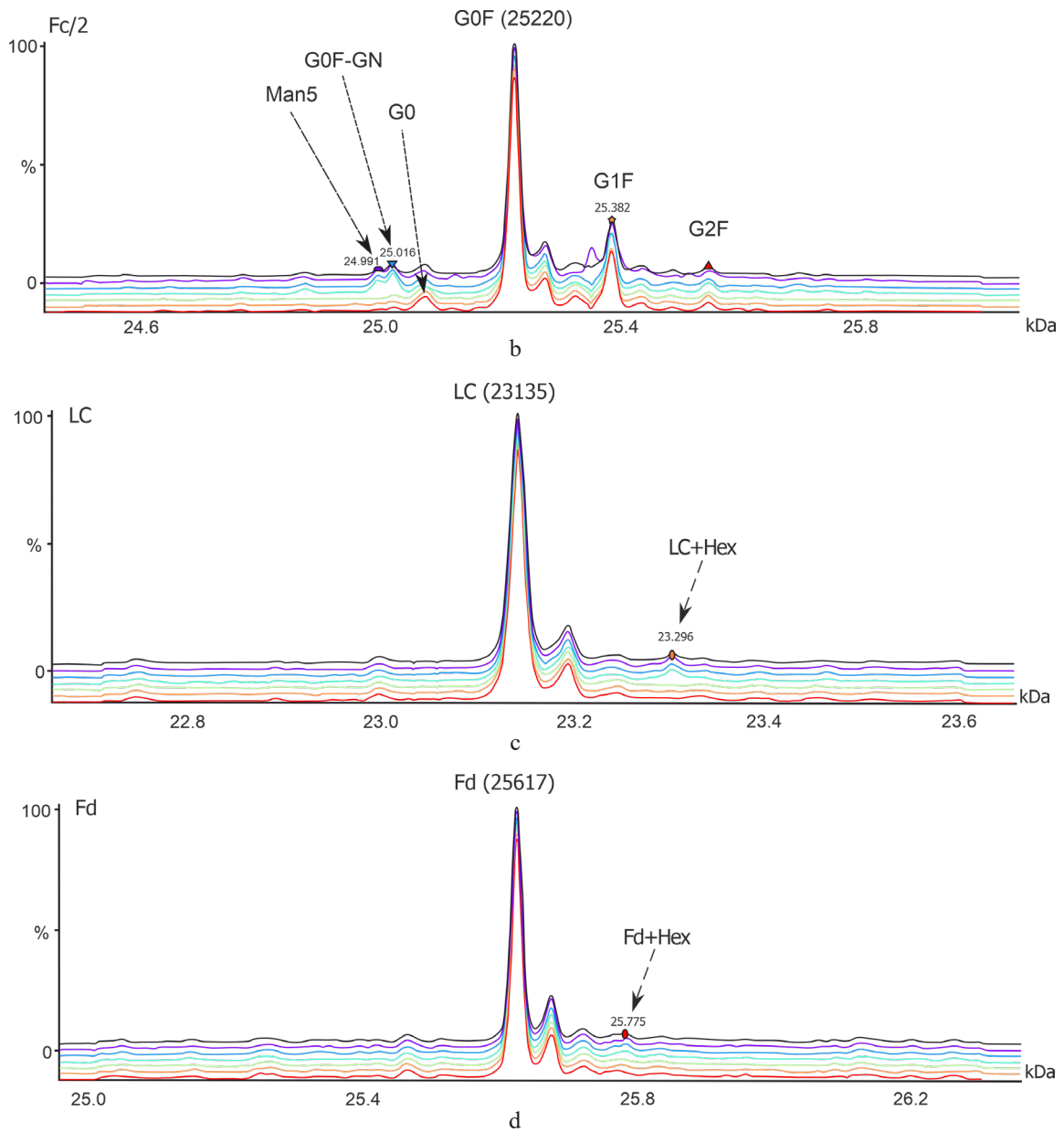


Fig. 5. Annotated chromatograms (a) and mass spectra (b–d) of eculizumab subunits of the original Soliris and Elizaria drugs.

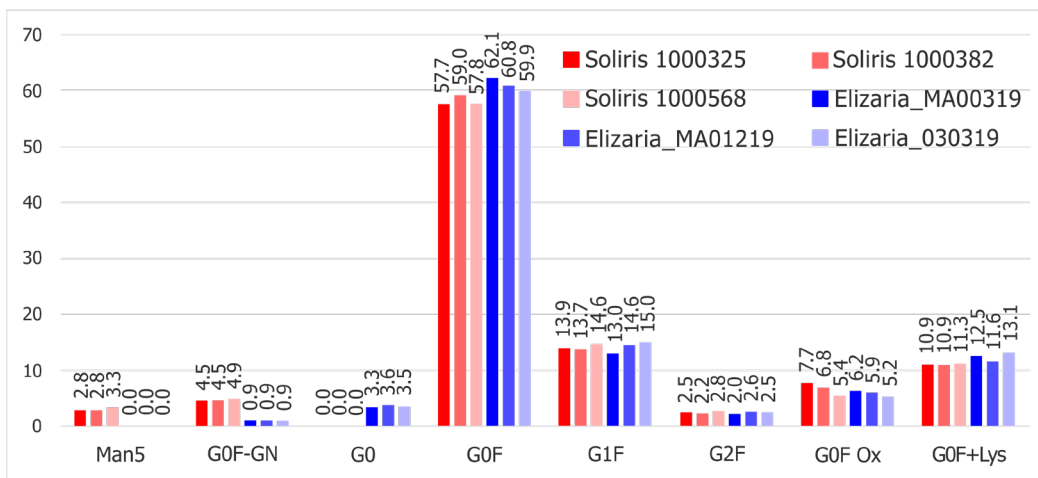


Fig. 6. The content of proteoforms in the Fc/2 subunit of separate series of the original Soliris and Elizaria drugs.

Table 3. Results of measuring the molecular masses of eculizumab subunits from the compared samples

Eculizumab proteoforms	Theoretical mass, Da	Measured mass			
		Original Soliris		Elizaria	
		Average \pm SD, Da	Error, ppm	Average \pm SD, Da	Error, ppm
Fc/2+Man5	24992	24992 \pm 0.3	7	–	–
Fc/2+G0F-GN	25017	25017 \pm 0.6	–13	25016	–40
Fc/2+G0	25074	–	–	25073	–40
Fc/2+G0F	25220	25220	0	25220	0
Fc/2+G1F	25382	25382 \pm 0.3	–7	25382	0
Fc/2+G2F	25544	25544 \pm 0.6	13	25544 \pm 0.6	13
Fc/2 + 16 Da (oxidation)	148198	148197 \pm 2	–7	148198 \pm 2	–2
Fc/2+Lys	25348	25349	39	25349	39
LC	23135	23135	0	23135	0
Fd	25617	25617 \pm 0.6	–13	25617 \pm 0.6	–13

Note: SD, standard deviation.

Table 4. Comparison of the proportions of eculizumab proteoforms in the subunits of the analyzed samples

Eculizumab proteoforms	Original Soliris		Elizaria		Quality range, % (Average \pm 3SD)	Compliance of Elizaria with the quality range, %
	Average	SD, %	Average	SD, %		
Man5	3.0	0.3	–	–	2.1–3.9	None
G0F-GN	4.6	0.2	0.9	0	4.0–5.2	None
G0	–	–	3.5	0.2	–	None
G0F	58.2	0.8	60.9	1.1	55.8–60.6	33
G1F	14.1	0.5	14.2	1.0	12.6–15.6	100
G2F	2.5	0.3	2.4	0.3	1.6–3.4	100
G0F Ox	6.6	1.2	5.8	0.5	2.0–10.2	100
G0F+Lys	11.1	0.2	12.4	0.8	10.5–11.7	67
LC+Hex	4.4	0.2	–	–	3.8–5.0	None
Fd+Hex	2.9	0.1	–	–	2.6–3.2	None
Galactosylated glycans, sum (G1F + G2F)	16.6	0.7	16.5	1.3	14.5–18.7	100

CONCLUSIONS

The development and registration of biosimilar therapeutic proteins require their comprehensive characterization, in the physicochemical part of which HPLC-MS occupies one of the leading positions. The options for this analysis are quite diverse because of the goals of the researchers. However, both in biopharmaceutical comparability studies and in developing a molecule, the entire protein molecule must be described. The results of this analysis become the basis for a deeper characterization of objects of comparison or development.

The study of the monoclonal antibody eculizumab in the original Soliris and Elizaria by mass spectrometric intact mass measurement shows the identity of the molecular masses of most of the proteoforms found in the samples. However, it demonstrates differences in their content, which consisted in a lower content of the major glycoform G0F/G0F and larger—glycoforms G1F/G0F, G1F/G1F, G2F/G1F, and G2F/G2F as part of the original Soliris. However, a detailed study of the antibody subunits by an HPLC-MS middle-up analysis allowed explaining the increased content of heavier glycoforms by glycation sites in the LC and Fd subunits of eculizumab from the original Soliris. As expected, the comparison of oligosaccharides attached to the canonical glycosylation site on the Fc/2 subunit establishes high comparability of the compared samples. Significant differences are observed in the content of the major glycoform G0F;

however, the difference in the content of this glycan averaged 2.7%. In the intact molecule analysis, the analogous parameter for the G0F/G0F variant between the original and candidate drugs is at the level of 13.2%. The content of minor oligosaccharides Man5, G0F-GN, and G0 also differ, but their share does not exceed 4.6%.

This work becomes part of the report on the comprehensive comparative characterization of eculizumab of the original and candidate drugs and allowed obtaining Russian marketing authorization for the world's first biosimilar drug based on eculizumab. Mass spectrometric study of intact molecules and subunits of eculizumab from various sources shows the samples' fundamental comparability, which has become the basis for further and deeper HPLC-MS characterization, acting as an orthogonal analysis method for "classical" chromatographic and electrophoretic studies of the comparability of eculizumab.

Acknowledgments

The authors thank S. Taran, Lead Expert of the Department of Analytical Methods, and M. Smolov, Head of the Laboratory of Physicochemical Methods of IBC Generium, for their help with preparing the manuscript.

Authors' contribution

All authors equally contributed to the research work.

Potential Conflict of Interest Statement

The authors are employees of the Generium International Biotechnological Center, an organization that develops a biosimilar drug to eculizumab.

REFERENCES

- Dillon T.M., Bondarenko P.V., Rehder D.S., Pipes G.D., Kleemann G.R., Ricci M.S. Optimization of a reversed-phase high-performance liquid chromatography/mass spectrometry method for characterizing recombinant antibody heterogeneity and stability. *J. Chromatogr. A.* 2006;1120(1–2):112–120. <https://doi.org/10.1016/j.chroma.2006.01.016>
- Ren D., Pipes G., Xiao G., Kleemann G.R., Bondarenko P.V., Treuheit M.J., Gadgil H.S. Reversed-phase liquid chromatography–mass spectrometry of site-specific chemical modifications in intact immunoglobulin molecules and their fragments. *J. Chromatogr. A.* 2008;1179(2):198–204. <https://doi.org/10.1016/j.chroma.2007.11.088>
- Sawyer W.S., Srikumar N., Carver J., Chu P.Y., Shen A., Xu A., Williams A.J., Spiess C., Wu C., Liu Y., Tran J.C. High-throughput antibody screening from complex matrices using intact protein electrospray mass spectrometry. *Proc. Natl. Acad. Sci. USA.* 2020;117(18):9851–9856. <https://doi.org/10.1073/pnas.1917383117>
- Haberger M., Leiss M., Heidenreich A-K., Pester O., Hafenmair G., Hook M., Bonnington L., Wegele H., Haindl M., Reusch D., Bulau P. Rapid characterization of biotherapeutic proteins by size-exclusion chromatography coupled to native mass spectrometry. *MAbs.* 2015;8(2):331–33. <https://doi.org/10.1080/19420862.2015.1122150>
- Leney A.C., Heck A.J. Native Mass Spectrometry: What is in the Name? *J. Am. Soc. Mass Spectrom.* 2017;28(1):5–13. <https://doi.org/10.1007/s13361-016-1545-3>
- Wehofsky M., Hoffmann R. Automated deconvolution and deisotoping of electrospray mass spectra. *J. Mass Spectrom.* 2002;37(2):223–229. <https://doi.org/10.1002/jms.278>
- Lu J., Trnka M.J., Roh S.H., et al. Improved Peak Detection and Deconvolution of Native Electrospray Mass Spectra from Large Protein Complexes. *J. Am. Soc. Mass Spectrom.* 2015;26(12):2141–2151. <https://doi.org/10.1007/s13361-015-1235-6>
- Wohlschlager T., Scheffler K., Forstenlehner I.C. et al. Native mass spectrometry combined with enzymatic dissection unravels glycoform heterogeneity of biopharmaceuticals. *Nat. Commun.* 2018;9:1713. <https://doi.org/10.1038/s41467-018-04061-7>

9. Lermyte F., Tsybin Y.O., O'Connor P.B., Loo J.A. Top or Middle? Up or Down? Toward a Standard Lexicon for Protein Top-Down and Allied Mass Spectrometry Approaches. *J. Am. Soc. Mass Spectrom.* 2019;30(7):1149-1157. <https://doi.org/10.1007/s13361-019-02201-x>

10. Marty M.T., Baldwin A.J., Marklund E.G., Hochberg G.R.A., Benesch J.L.P., Robinson C.V. Bayesian deconvolution of mass and ion mobility spectra: from binary interactions to polydisperse ensembles. *Anal. Chem.* 2015;87(8):4370-4376. <https://doi.org/10.1021/acs.analchem.5b00140>

11. Tsong Y., Dong X., Shen M. Development of statistical methods for analytical similarity assessment. *J. Biopharm. Stat.* 2017;27(2):197-205. <https://doi.org/10.1080/10543406.2016.1272606>

12. Chow S.-C. Challenging issues in assessing analytical similarity in biosimilar studies. *Biosimilars.* 2015;5:33-39. <https://doi.org/10.2147/BS.S84141>

13. Raju T.S., Jordan R.E. Galactosylation variations in marketed therapeutic antibodies. *MAbs.* 2012;4(3):385-391. <https://doi.org/10.4161/mabs.19868>

14. Bruce A., Hunter J., Malanson H.F. Recombinant glycosylated eculizumab and eculizumab variants: US Patent US20170073399A1. Priority 11.09.2015.

15. Reusch D., Tejada M.L. Fc glycans of therapeutic antibodies as critical quality attributes. *Glycobiology.* 2015;25(12):1325-1334. <https://doi.org/10.1093/glycob/cwv065>

About the authors:

Maksim B. Degterev, Research Scientist, Physico-Chemical Methods Laboratory, International Biotechnology Center Generium (14, Vladimirskaia ul., Volginskiy, Vladimir oblast, 601125, Russia). E-mail: degterev@ibcgenerium.ru. <https://orcid.org/0000-0002-5541-5575>

Rakhim R. Shukurov, Head of the Analytical Methods Department, International Biotechnology Center Generium (14, Vladimirskaia ul., Volginskiy, Vladimir oblast, 601125, Russia). E-mail: shukurov@ibcgenerium.ru. <https://orcid.org/0000-0002-6532-7835>

Об авторах:

Дегтерев Максим Борисович, научный сотрудник лаборатории физико-химических методов ООО «МБЦ «Генериум» (601125, Россия, Владимирская обл., Петушинский район, пос. Вольгинский, ул. Владимирская, д. 14). E-mail: degterev@ibcgenerium.ru. <https://orcid.org/0000-0002-5541-5575>

Шукуров Рахим Рахманкулович, начальник отдела аналитических методов ООО «МБЦ «Генериум» (601125, Россия, Владимирская обл., Петушинский район, пос. Вольгинский, ул. Владимирская, д. 14). E-mail: shukurov@ibcgenerium.ru. <https://orcid.org/0000-0002-6532-7835>

The article was submitted: November 19, 2020; approved after reviewing: December 08, 2020; accepted for publication: February 06, 2021.

Translated from Russian into English by H. Moshkov

Edited for English language and spelling by Enago, an editing brand of Crimson Interactive Inc.

**ANALYTICAL METHODS IN CHEMISTRY
AND CHEMICAL TECHNOLOGY**

**АНАЛИТИЧЕСКИЕ МЕТОДЫ
В ХИМИИ И ХИМИЧЕСКОЙ ТЕХНОЛОГИИ**

ISSN 2686-7575 (Online)

<https://doi.org/10.32362/2410-6593-2021-16-1-88-98>



UDC 541.64:542.954:547.582

RESEARCH ARTICLE

Development of the technique for quality control of 1,3-bis(3,4-dicyanophenoxy)benzene by HPLC

Zinaida N. Shchekoldina^{1,*}, Alexey A. Bogolyubov¹, Alexander Yu. Zakharov², Boris A. Bulgakov¹, Alexander V. Babkin¹, Alexey V. Kepman¹

¹Moscow State University, Moscow, 119991 Russia

²Kurnakov Institute of General and Inorganic Chemistry, Russian Academy of Sciences, Moscow, 119991 Russia

*Corresponding author, e-mail: z.shchekoldina@gmail.com

Abstract

Objectives. Determination of target products and byproducts is necessary for the quality control of phthalonitrile monomer synthesis as well as production scaling and performing related kinetic studies. High-performance liquid chromatography (HPLC) is a simple and affordable method for quantitative chemical analysis, which also verifies the quality of raw materials. The objective of this study was to develop an HPLC technique for determining the composition of the reaction mixture in the synthesis of 1,3-bis(3,4-dicyanophenoxy)benzene (DPB).

Methods. Reversed-phase HPLC was used to quantitatively analyze the reaction mixture.

Results. A simple and rapid method for the quantitative HPLC analysis of phthalonitrile monomers and their mixtures with reagents was developed. Reaction times and the accumulation of byproducts were also studied.

Conclusions. The successful performance of the developed technique allows us to recommend it for practical applications. The results obtained for reactors of different sizes have good convergence, and DPB synthesis was successfully scaled up to intermediate scale equipment.

Keywords: 1,3-bis(3,4-dicyanophenoxy)benzene, high-performance liquid chromatography, quantitative analysis, scaling up, phthalonitrile resins

For citation: Shchekoldina Z.N., Bogolyubov A.A., Zakharov A.Yu., Bulgakov B.A., Babkin A.V., Kepman A.V. Development of the technique for quality control of 1,3-bis(3,4-dicyanophenoxy)benzene by HPLC. *Tonk. Khim. Tekhnol. = Fine Chem. Technol.* 2021;16(1):88–98 (Russ., Eng.). <https://doi.org/10.32362/2410-6593-2021-16-1-88-98>

НАУЧНАЯ СТАТЬЯ

Разработка методики количественного анализа целевого и побочных продуктов синтеза 1,3-бис(3,4-дицианофенокси)бензола методом ВЭЖХ

З.Н. Щеколдина^{1,*}, А.А. Боголюбов¹, А.Ю. Захаров², Б.А. Булгаков¹,
А.В. Бабкин¹, А.В. Кепман¹

¹Московский государственный университет им. М.В. Ломоносова, Москва, 119991 Россия

²Институт общей и неорганической химии им. Н.С. Курнакова РАН, Москва, 119991 Россия

*Автор для переписки, e-mail: z.shchekoldina@gmail.com

Аннотация

Цели. Для аналитического контроля производства фталонитрильных мономеров, изучения масштабирования технологии их получения и проведения кинетических исследований актуальна задача по разработке способа определения концентрации целевого и побочных продуктов в присутствии реагентов. Наиболее простым и доступным методом количественного анализа рассматриваемых соединений является высокоэффективная жидкостная хроматография (ВЭЖХ), позволяющая также проводить верификацию сырья и контроль качества готовой продукции. Цель данной работы заключалась в разработке методики количественного анализа компонентов реакционной смеси при синтезе 1,3-бис(3,4-дицианофенокси)бензола (ДФБ) методом ВЭЖХ.

Методы. Для количественного анализа компонентов реакционной смеси использовали метод ВЭЖХ в обращенно-фазовом режиме.

Результаты. Разработана простая и быстрая методика количественного анализа фталонитрильных мономеров и их смесей с реагентами методом ВЭЖХ. По данным исследования конверсии компонентов реакционной смеси сделан вывод о продолжительности реакции и накоплении побочных продуктов.

Выводы. Успешная апробация позволяет рекомендовать разработанную методику для применения в аналитической практике. Результаты, полученные при переходе от реакции в колбе к реактору объемом 15 л, характеризуются хорошей сходимостью. Синтез ДФБ успешно масштабируется на оборудование промежуточного масштаба.

Ключевые слова: 1,3-бис(3,4-дицианофенокси)бензол, высокоэффективная жидкостная хроматография, количественный анализ, масштабирование, фталонитрильные связующие

Для цитирования: Щеколдина З.Н., Боголюбов А.А., Захаров А.Ю., Булгаков Б.А., Бабкин А.В., Кепман А.В. Разработка методики количественного анализа целевого и побочных продуктов синтеза 1,3-бис(3,4-дицианофенокси)-бензола методом ВЭЖХ. *Тонкие химические технологии*. 2021;16(1):88–98. <https://doi.org/10.32362/2410-6593-2021-16-1-88-98>

INTRODUCTION

Phthalonitriles are promising compounds to produce highly heat-resistant resins and polymer composite materials (PCMs), which are widely utilized in the space and aviation industries. Phthalonitrile matrices have good mechanical characteristics, low moisture absorption, high heat resistance, and are currently the most thermally and oxidatively stable polymers [1–7].

Along with low-melting phosphorus containing monomers [8–10], an important component of

phthalonitrile resin compositions for PCMs [11–14] is 1,3-bis(3,4-dicyanophenoxy)benzene (DPB) (**3**), a product of the reaction between 4-nitrophthalonitrile (4NPN) (**1**) and resorcinol (**2**) [15]. The thermal properties of DPB and a corresponding polymer¹ are presented in Table 1 [15]. This data demonstrates the high heat-resistance of the thermoset plastic derived from DPB.

¹ The authors used 2.4 mol % 1,3-bis(3-aminophenoxy)benzene for curing DPB. The process was conducted in a nitrogen atmosphere according to the following temperature regime: 2 h at 250°C, 2 h at 325°C, 4 h at 350°C, and 8 h at 375°C.

Table 1. Thermal properties of 1,3-bis(3,4-dicyanophenoxy)benzene (DPB) and a DPB-based polymer

Monomer	Cured matrix		
mp*, °C	T _g ** , °C	T _{5%} ***, N ₂ , °C	Char yield (at 900°C), N ₂ , %
185–190	>400	527	70

* Melting point;

** Glass transition temperature;

*** Temperature at 5% mass loss.

DPB is synthesized in an aprotic dipolar solvent in the presence of a base (potassium carbonate), forming 4-(3-hydroxyphenoxy)phthalonitrile (HPPN) (**4**) and 3,3',4,4'-tetracyanodiphenyl ether (PN2O) (**5**) as byproducts. The reaction scheme and byproduct structures are shown in Fig. 1.

An effective way to quantify target compounds and byproducts in the presence of reagents is required for the analytical control of the phthalonitrile resins production and for performing relevant kinetic studies during production process optimization. High-performance liquid chromatography (HPLC) is the simplest and most accessible method of quantitative analysis for the compounds under consideration, and it also allows to carry out quality control of the raw materials and products.

Scaling up the synthesis of phthalonitrile monomer DPB is an important step in producing high heat resistant resins at industrial level, which also requires precise analysis of the composition of the reaction mixture for the technical control of the synthesis.

This study aimed to develop an HPLC protocol for the quantitative analysis of the target products and byproducts of DPB synthesis in order to effectively scale up the reaction from laboratory to intermediate scale equipment.

EXPERIMENTAL

Equipment and reagents

Equipment: Agilent 1260 Infinity LC with a diode array detector (Agilent Technologies, USA) and an ultrasonic bath.

Column: Zorbax C18 Eclipse Plus 4.6 × 100 mm, 3.5 μm phase (Agilent Technologies).

Reagents: Resorcinol (99%, Sumitomo Chemical Co., Japan); 4NPN (99.5%, CDH Chemicals, India); acetonitrile (A) (used without further purification) (HPLC, CHIMMED, Russia); and degassed water (B) (Werner UP60B ultrafine cleaning system).

DPB for constructing calibration curves was obtained as described in [15], purified by extraction chromatography (chloroform eluent and silica gel phase), and recrystallized from dimethylacetamide.

HPPN for constructing calibration curves was obtained as described in [16] and purified by extraction chromatography (chloroform eluent and silica gel phase).

PN2O for constructing calibration curves was obtained as described in [17] and purified by recrystallization from dimethylacetamide.

HPLC analysis of the components of the reaction mixture

A test sample weighing 100 ± 3 mg was added to 10 mL of acetonitrile and left in an ultrasonic bath for 10 min. Insoluble impurities were removed using a 0.45 μm pore syringe filter. In chromatographic vials, 900 μL of acetonitrile was added to 100 μL of the filtrate solution, and HPLC analysis was carried out according to the parameters listed in Table 2.

Method for DPB synthesis in a 2-L flask

A 2 L three-necked flask, equipped with a reflux condenser and mechanical paddle stirrer, was

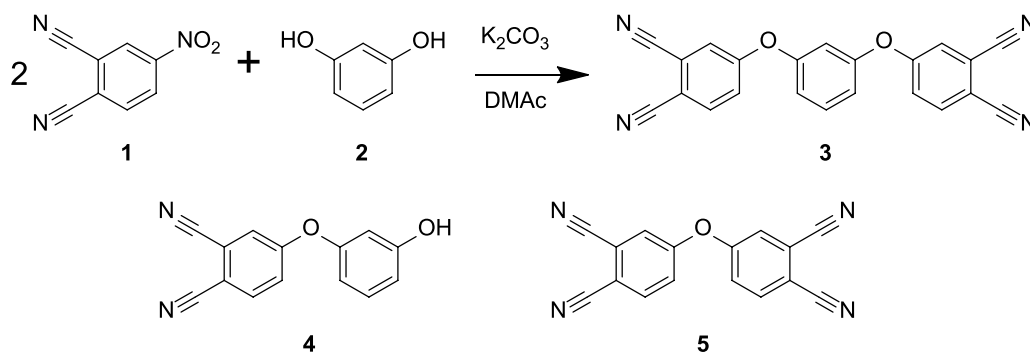
**Fig. 1.** 1,3-bis(3,4-dicyanophenoxy)benzene synthesis scheme.

Table 2. Parameters of the HPLC system

Chromatographic system parameters	Value
Elution mode	Isocratic
Flow rate	1.0 mL/min
Analysis time	10 min
Eluent composition	Acetonitrile and water
Solvent ratio (acetonitrile : water, v:v)	55 : 45
Injected sample volume	3 μ L
Column temperature	30.0°C
Detection wavelengths	258 nm, 276 nm

loaded with 138.7 g (1.260 mol, 1 equiv) of resorcinol and 836 mL of dimethylacetamide. After degassing at 70°C with a residual pressure of 20 mbar and stirring at 300 rpm for 1 h, the system was filled with argon. To the resulting solution, 382.5 g (2.768 mol, 2.2 equiv) of powdered potassium carbonate was added and stirred, the degassing was repeated, and the system was again filled with argon. Then, 436.0 g (2.518 mol, 2 equiv) of 4NPN was added in a weak argon counterflow. The synthesis was carried out at 70°C with constant stirring for 24 h, and samples were collected at specified time intervals (Fig. 7). The reaction mass was then poured into 3010 mL of water and stirred for 1 h. The precipitate was filtered, washed on the filter three times with 93 mL of hot water for each wash, and dried at 80°C for 24 h. The obtained product was a light yellow powder with a yield of 388.1 g (85%).

The ^1H and ^{13}C nuclear magnetic resonance (NMR) spectra were recorded on a Bruker Avance III spectrometer (Bruker, USA) with operating frequencies of 600 and 151 MHz, respectively.

^1H NMR (600 MHz, $\text{DMSO-}d_6$) δ ppm, 7.05–7.24 (m, 3 H), 7.55 (dd, $J = 8.70, 2.17$ Hz, 2 H), 7.60 (t, $J = 7.70$ Hz, 1 H), 7.92 (d, $J = 2.17$ Hz, 2 H), 8.13 (d, $J = 8.70$ Hz, 2 H).

^{13}C NMR (151 MHz, $\text{DMSO-}d_6$) δ ppm, 108.63 (3 C), 112.72 (4 C), 115.35 (4 C), 115.84 (5 C), 116.73 (3 C), 117.41 (7 C), 122.23–123.36 (14 C), 132.25 (4 C), 136.25 (8 C).

The NMR spectra of the target product corresponded with previously reported data [18].

Method for DPB synthesis in a 15-L reactor

A glass reactor with a 15 L volume was loaded with 1040.2 g (9.447 mol, 1 equiv) of resorcinol and 6240 mL of dimethylacetamide. The solution

was stirred at 120 rpm, heated to 70°C, and degassed for around 1 h at a residual pressure of 20 mbar. The apparatus was then filled with argon.

In a weak argon countercurrent, 2872.3 g (20.782 mol, 2.2 equiv) of dry powdered potassium carbonate was added. The degassing process was repeated without stirring, and the system was refilled with argon while cooling to 20°C. In a weak argon counterflow, 3271.1 g (18.894 mol, 2 equiv) of 4NPH was added in four to five doses with periodic stirring. The synthesis was performed at 70°C with constant stirring for 24 h.² The suspension was poured from the reactor into an intermediate vessel, then water (22500 mL) was quickly added and stirred with a spatula until the product solidified. The suspension was then filtered using the same suction filter, keeping all of the collected filter cake solids on the filter. The reactor was then heated to 100°C and rinsed with water in portions and stirred for around 10 min. The filter cake was washed using this water at 95°C in the filter jacket by transferring it through an intermediate vessel and stirring the filter cake after each wash, requiring a total of 8300 mL of water for three washes. The substance from the suction filter was transferred onto trays and dried for 48 h at 80°C, giving a yield of 2909.6 g (85%) of the product in the form of a light yellow to yellow powder.

Reaction mixture sample preparation for HPLC analysis

Distilled water was added to approximately 3 mL of the reaction mixture and acidified at a ratio of 1.0 : 3.6 with glacial acetic acid. The resulting suspension was filtered through a glass filter, leaving a precipitate that was washed with ~12 mL of distilled water three times and then dried at 80°C.

² During composition analysis, the reaction mixture was mixed for 54 h and samples were collected after predetermined periods of time.

RESULTS AND DISCUSSION

Development of a procedure for analyzing the components of the reaction mixture by HPLC

Determination of the maximum working concentration. Portions of resorcinol, 4NPN, HPPN, and DPB each weighing 100 ± 3 mg were mixed with 10 mL of acetonitrile, and the resulting solutions were placed in an ultrasonic bath for 10 min.

Reference solutions with concentrations of 0.25, 0.50, 0.75, 1.00, 1.25, 1.50, and 1.75 mg/mL of each component were diluted with acetonitrile from the initial solutions in chromatographic vials.

Chromatographic separation was performed in the gradient mode, as outlined in Table 3.

A section of the resulting chromatogram containing the peaks of the test substances is shown in Fig. 2.

As can be seen from the chromatogram, at the same analyte concentrations the maximum peak height (H) is typical for HPPN. It is also clear that baseline resolution of the peaks corresponding to 4NPN and HPPN will be most critical for the success of the method. Table 4 shows the HPPN peak height H dependence on its concentration C in the model solution.

Table 4 shows that the maximum concentration with acceptable detector response is 1.25 mg/mL. Further tests were conducted at this concentration.

The substance PN2O is characterized by low solubility in acetonitrile. To prepare a reference solution,

10 ± 3 mg PN2O and 10 mL acetonitrile were kept in an ultrasonic bath for 10 min, which achieved complete solubilization.

Because the proportion of PN2O in the target product does not exceed 5%, the maximum concentration was chosen to be 0.10 mg/mL (10% of 1.00 mg/mL).

Determination of working wavelengths. Figure 3 shows the absorbance spectra of the analytes.

The substances 4NPN, HPPN, DPB, and PN2O have three characteristic absorption maxima in the UV-Vis range. Usually, they are analyzed at a wavelength of 258 nm; however, in this region of the spectrum, resorcinol has a much lower absorption and its maximum absorption is observed at 276 nm. Therefore, for the sensitive chromatographic analysis of their mixture, using two wavelengths is advisable, i.e., 258 and 276 nm.

Eluent composition. To determine the optimal composition of the eluent, analysis was conducted in isocratic mode with acetonitrile to water ratios of 40 : 60, 50 : 50, and 60 : 40.

The isocratic mode was chosen because it is more stable than the gradient mode and allows recycling of the solvent, which contributes to significant savings in acetonitrile.

When the composition of the eluent was 40 : 60 acetonitrile to water, the DPB peak was not observed for more than 40 min before the analysis was interrupted.

Table 3. Gradient mode for determining the maximum concentration with acceptable detector response

Time, min	0–26	26–31	31–34	34–38	38–40
A, %	55	55–98	98	98–55	55

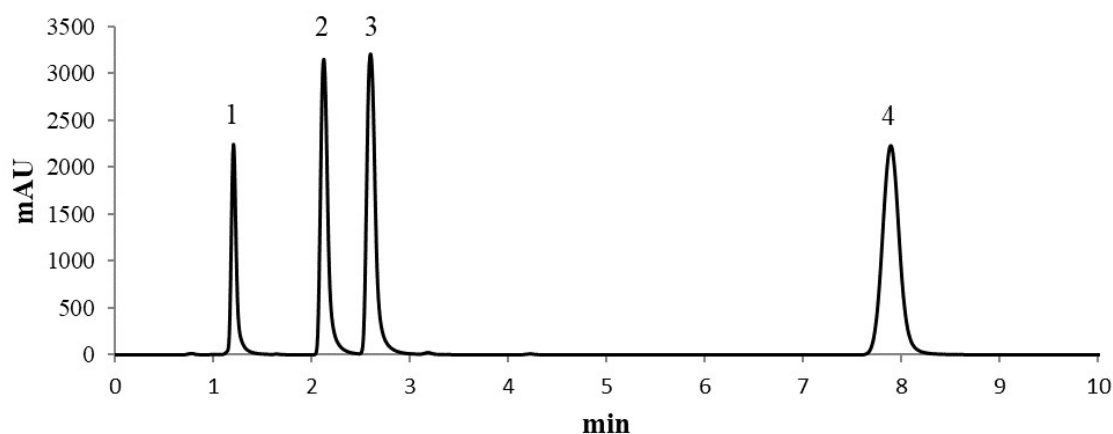
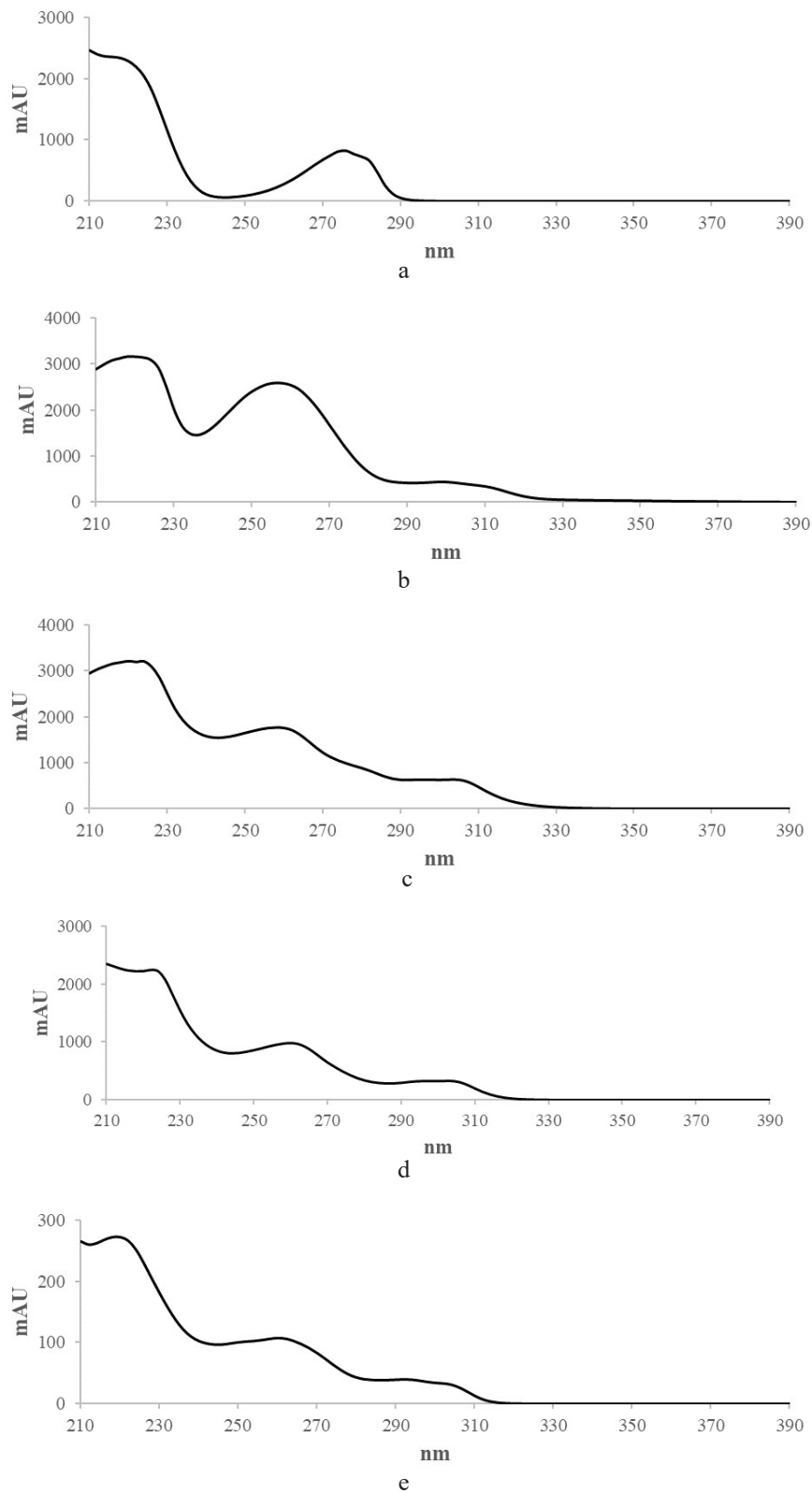


Fig. 2. Chromatogram of the reference solutions at 224 nm: (1) resorcinol, (2) 4-nitrophthalonitrile (4NPN), (3) 4-(3-hydroxyphenoxy)phthalonitrile (HPPN), and (4) 1,3-bis(3,4-dicyanophenoxy)benzene (DBP).

Table 4. HPPN peak height at different concentrations, signal recorded at 224 nm

<i>H</i> , mAU	1112	2219	2879	3149	3250	3277	3308
<i>C</i> , mg/mL	0.25	0.50	0.75	1.00	1.25	1.50	1.75

**Fig. 3.** Absorbance spectra of (a) resorcinol, (b) 4NPN, (c) HPPN, (d) DPB, and (e) 3,3',4,4'-tetracyano diphenyl ether (PN2O).

At a solvent ratio of 50 : 50, the separation time of the components was 15 min, and at 60 : 40, it was 7 min; however, in the latter case, the peaks were not sufficiently resolved.

Further tests were conducted at various solvent ratios ranging from 50 : 50 to 60 : 40. The results for 4NPN, the compound from the critical pair which elutes first, at a wavelength of 258 nm, are presented in Table 5.

Based on the time taken and the resolution of the critical pair, the acetonitrile to water ratio of 55 : 45 was considered optimal for the separation. Notably, the chromatogram obtained after washing the system does not show peaks of the analytes, and the change in the absorption of the baseline is only because of the contribution of the acetonitrile. The three-dimensional (3D) spectrum that demonstrates this is shown in Fig. 4.

Determination of the linearity range of the calibration curves. Figure 5 shows the dependence of the peak area on the concentration of the analytes.

These graphs show that the dependences are linear throughout the studied mass percent concentration range.

Conversion of reagents in the synthesis of DPB. DPB was synthesized in both a 2-L flask and a 15-L reactor (Fig. 6).

The quantity of analytes in samples of the reaction mixture was determined by the optimized HPLC protocol above, and averages were calculated from the results of two parallel analyses of each sample.

Then, the ratio of molar fractions (α) of the analytes was calculated, and the same reaction conditions were maintained in the scaled up 15-L reactor.

Figure 7 charts the conversion of the analytes, with $t = 0$ as the moment 4NPN was added.

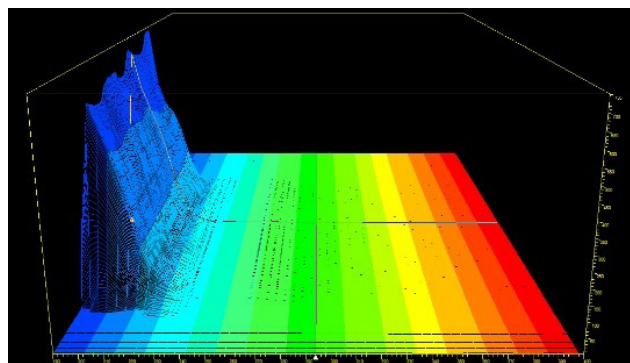


Fig. 4. 3D spectrum plotted during column washing.

The reaction proceeds via the intermediate HPPN that reacts with 4NPN to obtain the target product. The quantity of HPPN in the samples initially decreases gradually and then remains constant.

The DPB content reaches a plateau approximately 20 h after the start of the reaction, and the degree of 4NPN conversion reaches a maximum approximately 45.5 h.

A sharp increase in the amount of PN2O is observed in the initial section but then reaches a plateau approximately 20 h after the start of the reaction.

The data obtained for the 2-L and 15-L syntheses are roughly the same, indicating that the scaling up of the synthesis of DPB is achievable and effective.

CONCLUSIONS

This study developed a rapid and simple method for the quantitative analysis of phthalonitrile monomers (HPPN and DPB), resorcinol, 4NPN, and

Table 5. Chromatographic parameters of the 4NPN peak at various solvent ratios

A, %	Total run time, min	Resolution to HPPN peak	Symmetry	Efficiency
50	15	6.20	0.73	6580
52	12	5.18	0.72	6149
54	11	4.38	0.72	5726
55	10	3.88	0.71	5250
56	9	3.66	0.70	5280
58	8	3.01	0.70	5139
60	7	2.51	0.70	4640

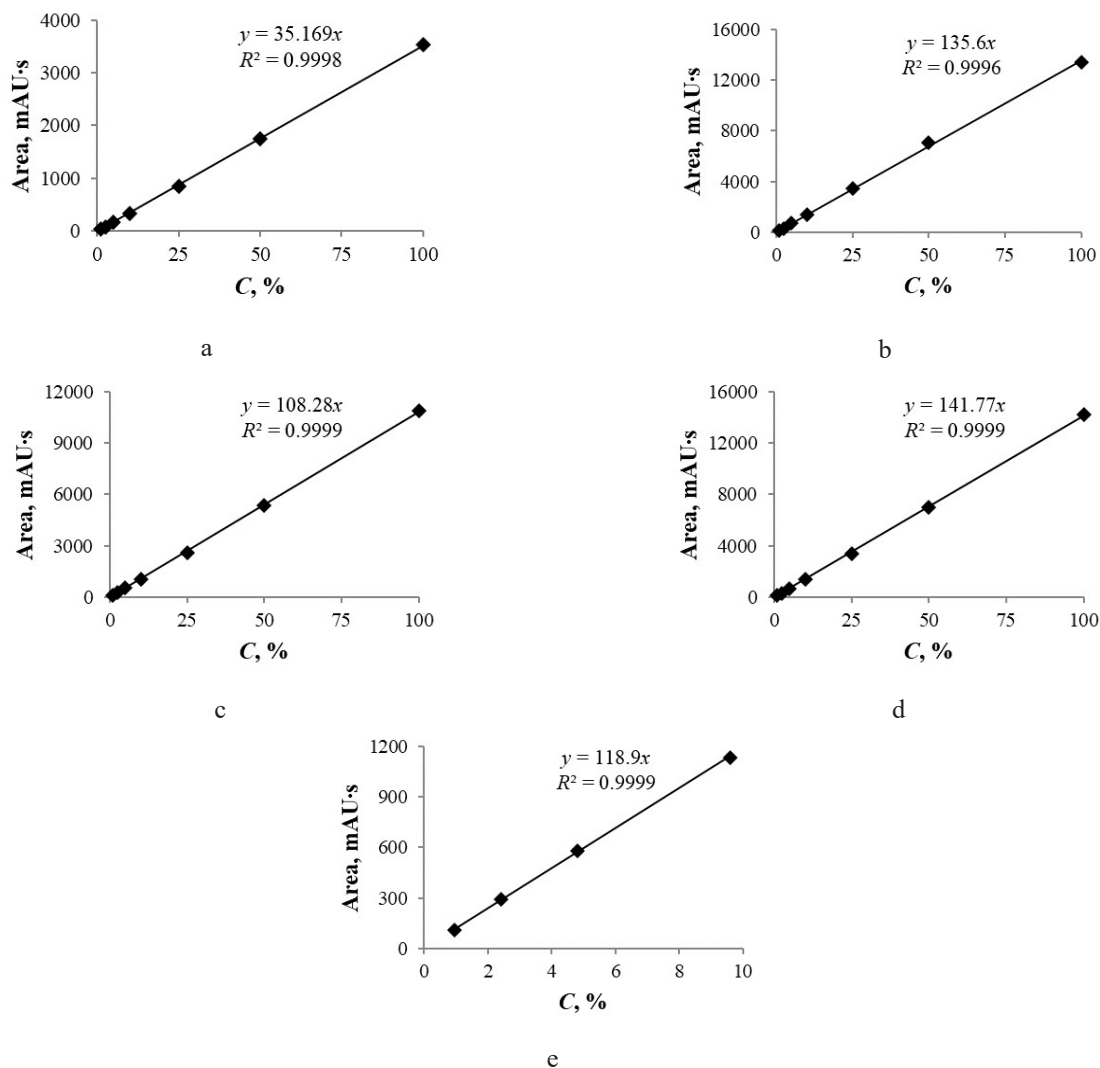


Fig. 5. Calibration curves for (a) resorcinol 276 nm, (b) 4NPN 258 nm, (c) HPPN 258 nm, (d) DPB 258 nm, and (e) PN2O 258 nm. C, % corresponds to mass percent.



Fig. 6. 15-L reactor.

PN2O by reversed-phase HPLC. Our technique is effective for a wide range of analyte concentrations and can determine impurities as low as 0.5% of the content of each compound.

Through our analysis of the composition of the reaction mixture, we were able to determine both the reaction time and related byproducts of the synthesis. Finally, from our successful syntheses in both 2-L and 15-L reaction volumes, we conclude that phthalonitrile monomer DPB synthesis can be effectively scaled up from the laboratory scale to the intermediate scale equipment with no changes in reaction conditions.

Acknowledgments

This work was conducted in the framework of the state assignment of the Chemistry Department of Moscow State University (Agreement No. AAAA-A21-121011590086-0).

This research was performed according to the Development Program of the Interdisciplinary Scientific and Educational School of Moscow State University "The future of the planet and global environmental change."

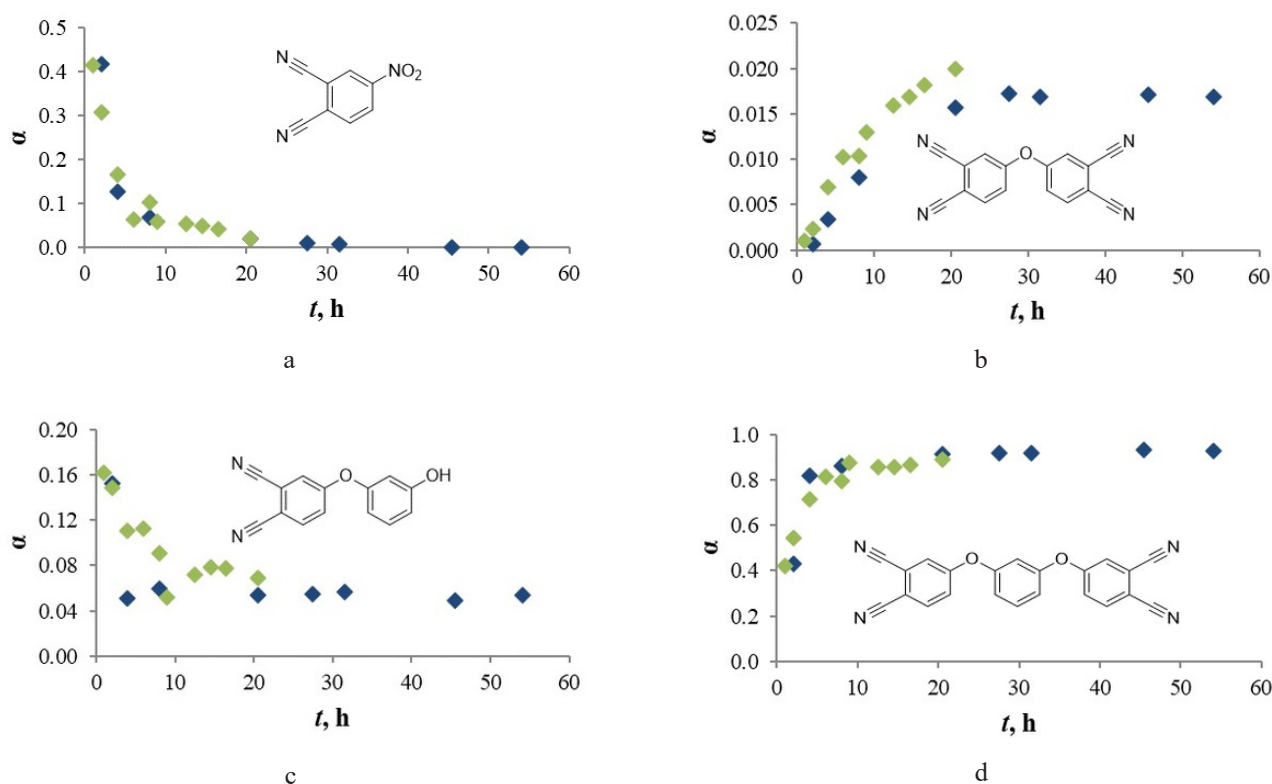


Fig. 7. Conversion of (a) 4NPN, (b) PN2O, (c) HPPN, and (d) DPB. Green is the synthesis in a 2-L flask, and blue is the synthesis in a 15-L reactor.

Authors' contribution

Z.N. Shchekoldina – synthesis in a 2-L flask, literature data collection and analysis, graphic design, and drafting a manuscript;

A.A. Bogolyubov – synthesis in a 15-L reactor and collection and systematization of experimental data on synthesis scaling;

A.Yu. Zakharov – instrumental research and collection and systematization of experimental data on the development of HPLC methods;

B.A. Bulgakov – substantiation of the research concept, planning of the main stages, experimental data analysis, formulation of conclusions, generalization of research results, and editing and revision of the manuscript;

A.V. Babkin – substantiation of the research concept, interpretation of research results, obtaining pure substances for HPLC calibration, and performing NMR;

A.V. Kepman – substantiation of the research concept, interpretation of research results, and group leadership.

The authors declare no conflicts of interest.

REFERENCES

- Laskoski M., Neal A., Schear M.B., Keller T.M., Ricks-Laskovski H.L., Saab A.P. Oligomeric aliphatic-aromatic ether containing phthalonitrile resins. *J. Polym. Sci. Part A Polym. Chem.* 2015;53(18):2186–2191. <https://doi.org/10.1002/pola.27659>
- Babkin A.V., Zodbinov E.B., Bulgakov B.A., Kepman A.V., Avdeev V.V. Low-melting siloxane-bridged phthalonitriles for heat-resistant matrices. *Eur. Polym. J.* 2015;66:452–457. <https://doi.org/10.1016/j.eurpolymj.2015.03.015>
- Derradji M., Jun W., Wenbin L. *Phthalonitrile resins and composites: properties and applications*. 1st Edition. Elsevier; 2018. 404 p. ISBN: 9780128129661
- Wang G., Guo Y., Han Y., Li Z., Ding J., Jiang H., Zhou H., Zhao T. Enhanced properties of phthalonitrile resins reinforced by novel phthalonitrile-terminated polyaryl ether nitrile containing fluorene group. *High Perform. Polym. SAGE Publications Ltd.* 2020;32(1):3–11. <https://doi.org/10.1177/0954008319847259>
- Li Z., Guo Y., Wang G., Xu S., Yan Y., Liu X., Luo Z., Ye L., Zhou H., Zhao T. Preparation and characterization of a self-catalyzed fluorinated novolac-phthalonitrile resin. *Polym. Adv. Technol.* 2018;29(12):2936–2942. <https://doi.org/10.1002/pat.4413>
- Ren D., Lei Y., Pan H., Yan L., Xu M., Liu X. Design of the phthalonitrile-based composite laminates by improving the interfacial compatibility and their enhanced properties. *J. Appl. Polym. Sci.* 2018;135(7):45881. <https://doi.org/10.1002/app.45881>
- Sastri S.B., Armistead J.P., Keller T.M. Phthalonitrile-carbon fiber composites. *Polym. Compos.* 1996;17(6):816–822. <https://doi.org/10.1002/pc.10674>
- Bulgakov B.A., Babkin A.V., Dzhevakov P.B., Bogolyubov A.A., Sulimov A.V., Kepman A.V. Low-melting phthalonitrile thermosetting monomers with siloxane- and phosphate bridges. *Eur. Polym. J.* 2016;84:205–217. <https://doi.org/10.1016/j.eurpolymj.2016.09.013>

9. Yakovlev M.V., Morozov O.S., Afanasieva E.S., Bulgakov B.A., Babkin A.V., Kepman A.V. Tri-functional phthalonitrile monomer as stiffness increasing additive for easy processable high performance resins. *React. Funct. Polym.* 2020;146:104409. <https://doi.org/10.1016/j.reactfunctpolym.2019.104409>
10. Terekhov V.E., Aleshkevich V.V., Afanasieva E.S., Nechausov S. Bis(4-cyanophenyl) phenyl phosphate as viscosity reducing comonomer for phthalonitrile resins. *React. Funct. Polym.* 2019;139:34–41. <https://doi.org/10.1016/j.reactfunctpolym.2019.03.010>
11. Bulgakov B.A., Sulimov A.V., Babkin A.V., Timoshkin I.A., Solopchenko A.V., Kepman A.V. Phthalonitrile-carbon fiber composites produced by vacuum infusion process. *J. Compos. Mater.* 2017;51(30):4157–4164. <https://doi.org/10.1177/0021998317699452>
12. Timoshkin I.A., Aleshkevich V.V., Afanas'eva E.S., Bulgakov B.A., Babkin A.V., Kepman A.V. Heat-Resistant Carbon Fiber Reinforced Plastics Based on a Copolymer of Bisphthalonitriles and Bisbenzotrile. *Polym. Sci. Ser. C.* 2020;62(2):172–182. <http://doi.org/10.1134/S1811238220020150>
[Original Russian Text: Timoshkin I.A., Aleshkevich V.V., Afanas'eva E.S., Bulgakov B.A., Babkin A.V., Kepman A.V. Heat-Resistant Carbon Fiber Reinforced Plastics Based on a Copolymer of Bisphthalonitriles and Bisbenzotrile. *Vysokomol. Soed. Ser. C.* 2020;62(2):174–185. (in Russ.). <https://doi.org/10.31857/S2308114720020156>]
13. Bulgakov B.A., Sulimov A.V., Babkin A.V., Afanasiev D.V., Solopchenko A.V., Kepman A.V. et al. Flame-retardant carbon fiber reinforced phthalonitrile composite for high-temperature applications obtained by resin transfer molding. *Mendeleev Commun.* 2017;27(3):257–259. <https://doi.org/10.1016/j.mencom.2017.05.013>
14. Bulgakov B.A., Belsky K.S., Nechausov S.S., Afanasieva E.S., Babkin A.V., Kepman A.V. Carbon fabric reinforced propargyl ether/phthalonitrile composites produced by vacuum infusion. *Mendeleev Commun.* 2018;28(1):44–46. <https://doi.org/10.1016/j.mencom.2018.01.014>
15. Keller T.M., Dominguez D.D. High temperature resorcinol-based phthalonitrile polymer. *Polymer.* 2005;46(13):4614–4618. <https://doi.org/10.1016/j.polymer.2005.03.068>
16. Lyubimtsev A., Vagin S., Syrbu S., Hanack M. Synthesis of Novel Covalently Linked Dimeric Phthalocyanines. *European J. Org. Chem.* 2007;2007(12):2000–2005. <https://doi.org/10.1002/ejoc.200600733>
17. Ryoichi F., Fumio O. Method for manufacturing 4,4'-oxydiphthalic acid and method for manufacturing 4,4'-oxydiphthalic dianhydride: pat. PCT/JP2012/057040. Japan. 26.09.2013.
18. Chen X., Shan S., Liu J., Quab X., Zhang Q. Synthesis and properties of high temperature phthalonitrile polymers based on *o*, *m*, *p*-dihydroxybenzene isomers. *RSC Adv.* 2015;5(98):80749–80755. <https://doi.org/10.1039/C5RA15321B>

About the authors:

Zinaida N. Shchekoldina, Postgraduate Student, Department of Chemical Technology and New Materials, Lomonosov Moscow State University (1–11, Leninskie Gory, Moscow, 119991, Russia). E-mail: z.shchekoldina@gmail.com. <https://orcid.org/0000-0002-6096-8123>

Alexey A. Bogolyubov, Cand. Sci. (Chem.), Engineer, Department of Chemical Technology and New Materials, Lomonosov Moscow State University (1–11, Leninskie Gory, Moscow, 119991, Russia). E-mail: astralpyre@gmail.com. <https://orcid.org/0000-0002-0193-1750>

Alexander Yu. Zakharov, Postgraduate Student, Laboratories of Crystal Chemistry and X-Ray Structural Analysis, Kurnakov Institute of General and Inorganic Chemistry, Russian Academy of Sciences (31, Leninsky prospect, Moscow, 119991, Russia). E-mail: alexan.zakharov@ya.ru. <https://orcid.org/0000-0003-4893-3857>

Boris A. Bulgakov, Cand. Sci. (Chem.), Senior Science Master, Department of Chemical Technology and New Materials, Lomonosov Moscow State University (1–11, Leninskie Gory, Moscow, 119991, Russia). E-mail: bbulgakov@gmail.com. <https://orcid.org/0000-0001-6208-3962>

Alexander V. Babkin, Cand. Sci. (Chem.), Senior Science Master, Department of Chemical Technology and New Materials, Lomonosov Moscow State University (1–11, Leninskie Gory, Moscow, 119991, Russia). E-mail: alexandr.babkin@gmail.com. Scopus Author ID 56258683200, <https://orcid.org/0000-0003-2309-4524>

Alexey V. Kepman, Cand. Sci. (Chem.), Head Scientist Researcher, Department of Chemical Technology and New Materials, Lomonosov Moscow State University (1–11, Leninskie Gory, Moscow, 119991, Russia). E-mail: alexkep@inunit.com.

Об авторах:

Щеколдина Зинаида Николаевна, аспирант кафедры химической технологии и новых материалов Московского государственного университета им. М.В. Ломоносова (119991, Россия, Москва, ул. Ленинские Горы, д. 1, стр. 11). E-mail: z.shchekoldina@gmail.com. <https://orcid.org/0000-0002-6096-8123>

Боголюбов Алексей Алексеевич, к.х.н., инженер 1 кат. кафедры химической технологии и новых материалов Московского государственного университета им. М.В. Ломоносова (119991, Россия, Москва, ул. Ленинские Горы, д. 1, стр. 11). E-mail: astralpyre@gmail.com. <https://orcid.org/0000-0002-0193-1750>

Захаров Александр Юрьевич, аспирант лаборатории кристаллохимии и рентгеноструктурного анализа Института общей и неорганической химии им. Н.С. Курнакова РАН (119991, Россия, Москва, Ленинский проспект, д. 31). E-mail: alexan.zakharov@ya.ru. <https://orcid.org/0000-0003-4893-3857>

Булгаков Борис Анатольевич, к.х.н., старший научный сотрудник кафедры химической технологии и новых материалов Московского государственного университета им. М.В. Ломоносова (119991, Россия, Москва, ул. Ленинские Горы, д. 1, стр. 11). E-mail: bbulgakov@gmail.com. <https://orcid.org/0000-0001-6208-3962>

Бабкин Александр Владимирович, к.х.н., старший научный сотрудник кафедры химической технологии и новых материалов Московского государственного университета им. М.В. Ломоносова (119991, Россия, Москва, ул. Ленинские Горы, д. 1, стр. 11). E-mail: alexandr.babkin@gmail.com. Scopus Author ID 56258683200, <https://orcid.org/0000-0003-2309-4524>

Кепман Алексей Валерьевич, к.х.н., ведущий научный сотрудник кафедры химической технологии и новых материалов Московского государственного университета им. М.В. Ломоносова (119991, Россия, Москва, ул. Ленинские Горы, д. 1, стр. 11). E-mail: alexkep@inumit.com.

The article was submitted: October 17, 2020; approved after reviewing: November 03, 2020; accepted for publication: January 18, 2021.

Translated from Russian into English by H. Moshkov

Edited for English language and spelling by Enago, an editing brand of Crimson Interactive Inc.

MIREA – Russian Technological University
78, Vernadskogo pr., Moscow, 119454, Russian Federation.

Publication date *February 26, 2021.*

Not for sale

МИРЭА – Российский технологический университет
119454, РФ, Москва, пр-кт Вернадского, д. 78.

Дата опубликования *26.02.2021*

Не для продажи

